Establishing the Quality of Molecular Coatings on Gold Nanoparticles

by

Idah C. Pekcevik

M.Sc., Mendeleyev University of Chemical Technology of Russia, 2008
B.Sc., Mendeleyev University of Chemical Technology of Russia, 2006

Thesis Submitted in Partial Fulfillment of the

Requirements for the Degree of

Doctor of Philosophy

in the

Department of Chemistry

Faculty of Science

© Idah Chebet Pekcevik 2014

SIMON FRASER UNIVERSITY

Fall 2014

Approval

Name:	**Idah C. Pekcevik**
Degree:	**Doctor of Philosophy**
Title:	***Establishing the Quality of Molecular Coatings on Gold Nanoparticles***
Examining Committee:	**Chair:** Dr. Michael Eikerling Professor

Dr. Byron D. Gates
Senior Supervisor
Associate Professor

_____

Dr. George Agnes
Supervisor
Professor

_____

Dr. Dipankar Sen
Supervisor
Professor

_____

Dr. Bingyun Sun
Internal Examiner
Assistant Professor

_____

Dr. Robert W. J. Scott
External Examiner
Associate Professor
Department of Chemistry
University of Saskatchewan

_____

Date Defended/Approved: December 16, 2014

Partial Copyright Licence

SFU

Abstract

The surface chemistry of nanoparticles imparts colloidal stability to nanoparticles by acting as barriers between their surrounding environment and the nanoparticles. Gold nanoparticles (AuNPs) are an ideal platform for many studies because of localized surface plasmon resonant properties, chemical stability, and the relative ease of modifying their surfaces with a wide variety of molecular coatings (e.g., alkanethiolates). Understanding and improving the physicochemical stability of these surface-modified nanoparticles is essential for their reproducible use in each application. The long-term colloidal stability of AuNPs relies on the resistance of their surface modifications to thermal degradation, chemical attack and oxidizing conditions. For this purpose, my research has been focused on determining the quality of molecular coatings on gold nanoparticles, and developing techniques, which are complementary to each other, to assess the quality factor of these coatings. Gold nanoparticles with varied qualities of molecular coatings were prepared and tested for their relative stabilities under various physical (e.g., temperature, time, laser irradiation) and chemical (e.g., in presence of metal etchants) conditions. We found that the quality of molecular coatings on AuNPs depends on the process conditions such as solution composition (e.g., the presence of co-surfactants, concentration of excess surfactants), density of capping molecules, and process time, used to form these coatings. We found that higher quality molecular coatings on the gold colloids increased the chances that the particles would remain stable over the over the duration of their intended use. Those colloids modified with relatively higher quality self-assembled monolayers were also more resistant to cyanide etching. These results highlight the importance of methodology for preparing high quality monolayers on nanoparticles and testing their ability to remain stable over the duration of their intended use, for example, during photothermal processes. In addition, the loading of DNA molecules onto AuNPs was tuned to achieve varying densities of DNA, and through this work, achieved the highest reported loading of single-stranded DNA (ss-DNA) molecules on gold nanorods. These high loadings of DNA oligonucleotides could enable a high loading of therapeutics onto the nanorods, which could translate into a higher or more prolonged delivery of therapeutic doses when actived by photothermal or other processes.

Keywords: Gold nanoparticles; quality of molecular coatings; self-assembled monolayers; physicochemical stability; photothermal; alkanethiolates

Dedication

To my beloved family. Thank you mum and dad for always encouraging me to do the best I could. Thank you for supporting me and reminding me that I am great. For not giving up on me. I love you so much. Cheru, Cheboo, and Georgy, thanks for being patient with me as your big sister went through her studies. Thank you for your love, texts and calls.

Thank you Daddy Abraham and mommy Joshabelle for pushing me to trust in God. Daddy you were always so proud of my work, and it gave me confidence to finish my studies. Mommy you took time to talk with me and encourage me, and talk to Daddy on my behalf. I love you both.

Grandma Clydene, thank you so much for always believing in me.

Acknowledgements

I would like to sincerely thank my senior supervisor, Dr. Byron Gates for his dedicated supervision throughout my graduate studies. Thank you for being very understanding of personal challenges and helpful too. Thank you for all the interesting projects that you let me get involved with, both at SFU and at the BC Cancer Agencies. Thank you for letting me train and work with undergraduate students. I couldn't have asked for a better supervisor.

Thanks to my committee members, Dr. Dipankar Sen and Dr. George Agnes. Thank you for invaluable advice for my research and about my presentation skills.

Thanks to Dr. Donald Yapp at the BC Cancer Agency for collaborating with Byron and myself.

Thanks to the Gates' group members. In particular, I would like to thank Michael Wang for training me on TEM (Hitachi and Tecnai) and XPS, as well as several other characterization techniques within our lab. Thanks also to Dennis Hsiao for training me on nanoparticle synthesis and photothermal experiments. I greatly enjoyed working collaboratively with Michael Wang, Iris Guo, Shakiba Mahmoudi and Sonia Raboun, among other students.

Thanks to Li Yang and Dr. Xin Zhang for training me on the TEMs. Thanks also to Prof. Karen Kavanagh for invaluable advice while I was using the TEMs.

Thanks to Saied for his patience in setting up laser experiments together with me. Thank you also for letting me use the LASIR facility very flexibly as need arose.

I would also like to thank Dr. Vincent Semetey for letting me use his lab when I visited the Marie Curie Institute in France. Thank you for the opportunity to learn about biofunctionalization of gold nanoparticles, which has been very useful in my research.

Finally, my sincere thanks to Sister Carol for giving me a quiet place to focus on writing my thesis. Thank you so much for all the sisterly advice and for being such a blessing throughout the writing process.

Table of Contents

List of Tables

List of Figures

List of Acronyms

AFM   Atomic force microscopy

AuNPs   Gold nanoparticles

AuNRs   Gold nanorods

CTAB   Cetylrimethylammonium bromide

CTAC   Cetyltrimethylammonium chloride

DLS   Dynamic light scattering

DMAP   4-(Dimethylamino) pyridine

DNA   Deoxyribonucleic acid

EDTA   Ethylenediaminetetraacetic acid

KCN   Potassium cyanide

LSPR   Localized Surface Plasmon Resonance

MHA   6-Mercaptohexanoic acid

MHDA   16-mercaptohexadecanoic acid

MUDA   11-Mercaptoundecanoic acid

P20   Polysorbate 20

PEG   Polyethylene glycol

PTE   Photothermal effect

PVP   Polyvinylpyrrolidone

SAMs   Self-assembled monolayers

SDS   Sodium dodecylsulfate

STM   Scanning tunneling microscopy

TA   Thioctic acid

TBE   Tris borate EDTA

TCEP   Tris (2-carboxyethyl) phosphine hydrochloride

TEM   Transmission electron microscopy

TOAB   Tetraoctylammonium bromide

XPS   X-ray photoelectron spectroscopy

Glossary

Dynamic Light Scattering

A sample being analyzed is exposed to a laser beam, which results in light scattering. The intensity of light scattering depends on the size of particles in the sample. The intensity of the scattered light is then measured by detectors placed at fixed angles to the laser beam. A mathematical model (Mie theory) is used to get a particle size distribution of the given sample.

Extinction Spectroscopy

Light interacts with particles, causing the promotion of electrons from the ground state to an excited state. When the incoming light matches an electronic transition within the particles, some of the light is absorbed simultaneous to the promotion of an electron to a higher energy orbital. A spectrometer records the wavelength at which absorption occurs, as well as the intensity of absorption at each wavelength. Extinction spectra can be used to calculate the concentration of a solution of plasmonic nanoparticles using Beer-Lambert's law.

Surface Plasmon Resonance

Gold nanoparticles can strongly absorb and scatter light due to the collective oscillation of surface conduction electrons. Conduction band electrons interact with photons, leading to oscillations of the free electrons. When the frequency of oscillations of the surface conduction electrons is the same as the frequency of the incident light, there is an intense absorption of light at a given wavelength of light and this is known as the surface plasmon resonance. The surface plasmon resonance band of plasmonic nanoparticles is sensitive to their size, shape and local environment.

Surface Potential

When an electric field is applied to a solution, charged particles suspended in this solution move toward the oppositely charged electrode. The measured electrophoretic mobility of these particles in an electric field is its surface potential. Surface potential influences the colloidal stability of nanoparticles. The higher the potential, the higher the electrostatic repulsion between colloids, and the greater their colloidal stability.

Transmission Electron Microscopy	High energy beam of electrons illuminate a thin sample (of <100 nm thickness). The beam of electrons is focused into a small, coherent beam by a condenser lens.The focused beam of electrons are then transmitted through the sample. These transmitted electrons are focused by the objective lens into an image on a screen or charge coupled device (CCD). In addition, the image contrast can be enhanced by the objective aperture, which blocks diffracted or scattered electrons from reaching the viewing screen. Dark regions and lighter regions within the sample represent relatively thick and thin (or relative differences in electron density of the material within) regions of the sample, respectively. The light regions have more electrons transmitted through them; while the dark regions have less electrons transmitted through them.
X-ray Photoelectron Spectroscopy	It is a surface sensitive technique (only photoelectrons generated to a depth of ~10 nm from the surface can be detected). This technique of surface analysis can be used to probe the chemical environment and the elemental composition of a surface. Irradiation of the surface of a sample with X-rays leads to the generation of photoelectrons, with binding energies that are characteristic of the element and core level from which the photoelectron was ejected.

Chapter 1.

Surface Chemistry of Gold Nanoparticles

Ever since the first report of colloidal gold by Faraday in 1857,[1] gold nanoparticles have been widely pursued as a platform for multiple applications. There are numerous advantages of using gold-based nanoparticles. Gold is more resistant to oxidation than many other metals, making it relatively easier to handle these nanoparticles under atmospheric conditions and within biological systems due to its biocompatibility.[2-4] Nanoscale gold particles also exhibit many other useful properties. The localized surface plasmon resonant properties of gold nanoparticles are useful for monitoring binding and/or release of molecules from receptive ligands bound to the surfaces of these particles.[5] The surface plasmon band of gold nanoparticles depends on the particle size and shape, as well as the dielectric layer around the nanoparticles. These particles can also be used as imaging agents in biological systems.[6-9] In addition, energy released by photothermal processes from these particles can activate chemical processes (e.g., molecular release) associated with molecules bound to their surfaces,[10-13] or lead to the thermally stimulated destruction of cancerous cells.[2,14,15] Understanding and controlling the surface chemistry of these nanoparticles is, therefore, of utmost importance when preparing nanoparticles for their intended use in each of these specific applications.

Gold nanoparticles are easily decorated with coatings that are terminated with a wide range of chemistries, such as peptides and strands of DNA.[16-18] The preparation of molecular coatings on gold nanoparticles is a simple method to modify their surface chemistry and to protect these nanoparticles from unwanted aggregation. Aggregation of nanoparticles results from particle-particle interactions due to the high surface energies of these nanoscale particles. The nanoparticles could remain partially unprotected if the molecular coatings are desorbed from their surfaces during exposure of these

nanoparticles to various oxidative,[19] chemical[20-22] and physiological environments.[23] This desorption of coating molecules could further lead to destabilization of the nanoparticles, precipitation from solution, and potentially a loss of the desired properties of the nanoparticles. Therefore, the environment surrounding the particles (such as solvent composition and solution pH), as well as the nature of the interaction between molecular coatings and the nanoparticles are all factors to be carefully considered when preparing these nanoparticles for their intended applications. For example, thiolated polyethylene glycol (PEG) is commonly used as a molecular coating on gold nanoparticles to impart solubility and minimize the rate of clearance of these PEG-modified particles from biological systems.[24-26] However, PEG degrades at high temperatures[27,28] and it is, therefore, logical to choose alternative coatings for these nanoparticles, when using the particles in applications that require high temperatures. Thus, analyzing the surface chemistry of both the as-synthesized nanoparticles, as well as the surfaces of these particles post-modification, is useful for reproducibly preparing robust nanoparticles with uniform surface chemistries and long-term stability. Changes to the properties of gold surfaces can be easily controlled by tuning the composition of these molecular coatings.[29-31] A common approach to modifying the surfaces of gold colloids is through ligand exchange. This and other approaches to modifying the surfaces of gold nanoparticles will be discussed in further detail below.

My thesis will focus on understanding the surface chemistry of gold nanoparticles modified with various thiol-based coatings, and how the surface chemistry of these particles affects their colloidal stability under changes to their physical (e.g., increased temperature) and chemical (e.g., gold etchants) environments. This work focuses on preparing nanoparticles with high quality molecular coatings, which has an impact on the colloidal and thermal stabilities of the resulting monolayer-protected gold nanoparticles. In this chapter, a literature review of different approaches to gold nanoparticle synthesis and methods for their surface modification will be discussed.

1.1. Surfactant-Mediated Synthesis of Gold Nanoparticles

Gold nanoparticles with various interesting shapes such as spheres, rods, stars, nanopods, cubes, nanocages, wires, triangular prisms and other branched nanoparticles

have been prepared by solution-phase methods.[32-42] Examples of methods of preparing gold colloids include the citrate reduction approach[43-50], the Brust-Schiffrin method[51-56] and the template-assisted synthesis.[57-59] Each of these methods has their benefits and drawbacks, which will be discussed in further detail below. Control over shapes of the as-synthesized nanoparticles is most commonly achieved using structure-directing surfactants, to form complex shapes of gold nanostructures.[32] For example, cetyltrimethylammonium bromide (CTAB) is commonly used to direct the growth of small gold nanoparticles into gold nanorods. However, changing the surfactant to cetyltrimethylammonium chloride (CTAC) has been shown to result into the growth of cubic and trisoctahedral-shaped gold nanoparticles.[33] In another study, the addition of iodide ions into a growth solution of gold nanoparticles containing CTAB resulted in the formation of triangular nanoprisms.[36] A careful choice of surfactants is, therefore, important for the synthesis of gold nanoparticles with a particular shape. Other reaction conditions including the pH of the solution, reaction temperature and concentration of reactants also can influence the shapes of resulting nanoparticles.[39,60,61] Establishing control over the size and shape of nanoparticles requires a detailed understanding of the effects of each of these reaction parameters. The following discussion focuses on the preparation of spherical and rod-shaped gold nanoparticles and their surface modification with alkanethiol-based molecular coatings.

1.1.1. Citrate reduction method for preparation of gold nanoparticles

The citrate reduction method is one of the most commonly used approaches for the preparation of spherical gold nanoparticles with diameters in the range 10 to 150 nm.[43,44,46] This method was originally introduced in 1951 by Turkevich et al.[45] and has been modified over the years.[62] The modification has resulted in better control over particle size and dispersity. This method is, therefore, commonly referred to as the Turkevich method of gold synthesis. In a typical synthesis, an aqueous solution of hydrogen tetrachloroaurate is reduced in the presence of aqueous trisodium citrate with heat, resulting in the formation of spherical gold colloids (Figure 1.1). Trisodium citrate is both the reducing agent to convert Au(III) to Au(0), as well as the stabilizer of the resulting gold spheres. Dimensions of the synthesized nanoparticles can be tuned by

varying the ratio of citrate to gold salt, choice of solvent and solution pH.[48] Recently, a seeded approach has been explored for the synthesis of ~200-nm diameter monodisperse gold nanoparticles.[48]

Citrate molecules stabilize gold nanoparticles by coordination of the carboxylates from trisodium citrate with the surfaces of the as-synthesized gold nanoparticles, and by additional intermolecular interactions (hydrogen bonding and weak van der Waals forces) between adjacent citrate molecules.[47] The resulting nanoparticles have a weakly bound coating of citrate and a negative surface potential.[48,63] The mechanism behind this synthesis of gold nanoparticles can be divided into 3 stages: 1) rapid reduction of Au(III) into atoms of Au(0), which form nuclei. Note that there might still be some Au(III) remaining in solution[49]; 2) aggregation of nuclei; and 3) further growth of nuclei into nanoparticles through Ostwald ripening.[49] The reduction of Au(III) is outlined in Equations 1.1 to 1.4 below, and can be summarized as follows: i) tetrachloroauric acid dissociates in aqueous solutions into $AuCl_4^-$ ions; ii) some of the Cl^- is substituted with OH^- at pH 6, forming an OH^- containing metallocomplex as illustrated in Equation 1.1; iii) gold (III) molecules then coordinate with a carboxylate group of the citrate (Equation 1.2); iv) there is a decarboxylation of the coordinated complex according to Equation 1.3, with a release of CO_2, along with the formation of dicarboxyacetone, unassociated Cl^- and a Au(I) complex;[50,64,65] and v) reduction of the Au(I) complex by the formed dicarboxyacetone according to Equation 1.4.[65] These steps lead to the reduction of the gold salt along with the oxidation of the coordinating ligand.

$$HAuCl_4 + 2H_2O \rightleftharpoons [AuCl_2(OH)_2]^- + 3H^+ + 2Cl^- \qquad \text{(Eq. 1.1)}$$

$$[AuCl_2(OH)_2]^- + [C_6H_5O_7]^{3-} \rightarrow [Au(Cl)(OH)_2(C_6H_5O_7)]^{3-} + Cl^- \qquad \text{(Eq. 1.2)}$$

$$[Au(Cl)(OH)_2(C_6H_5O_7)]^{3-} \rightarrow [Au(OH)_2]^- + [C_5H_4O_5]^- + CO_2 + Cl^- \qquad \text{(Eq. 1.3)}$$

$$[Au(OH)_2]^- + [C_5H_4O_5]^- \rightarrow Au^0 + 2OH^- + 2\,CO_2 + [C_3H_4O]^- \qquad \text{(Eq. 1.4)}$$
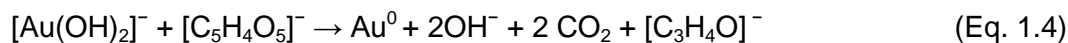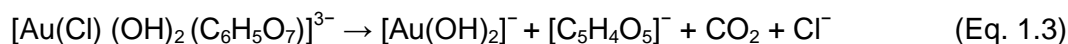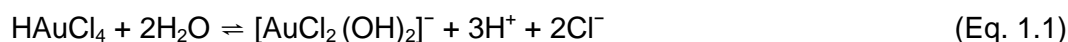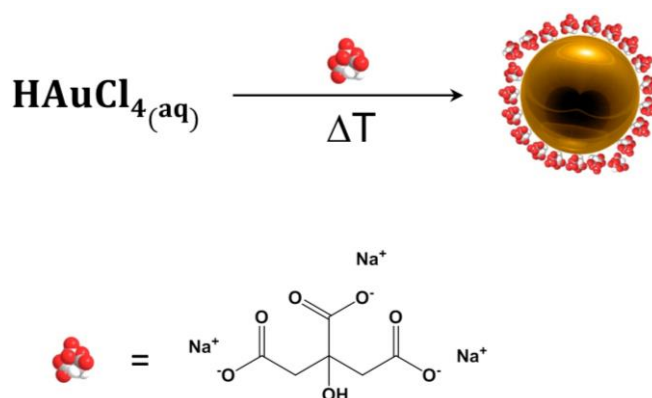
Figure 1.1. **Schematic depiction of citrate-stabilized gold nanoparticles.**

Because of the weak interaction between adsorbed citrate molecules and gold nanoparticle surfaces, the gold nanoparticles can be further modified with molecules that bind more strongly to gold (such as alkanethiols) through the displacement of the citrate coatings.[23,66] This weak interaction between the capping layers and the nanoparticle surfaces could, however, lead to an instability during the subsequent modification steps of these citrate-capped nanoparticles.[67-69] To circumvent this problem, additional surfactants can be adsorbed onto citrate-capped gold nanoparticles prior to the addition of alkanethiols to these solutions of gold nanoparticles.[67-69]

1.1.2.   Brust-Schiffrin method for preparation of gold nanoparticles

The Brust–Schiffrin method involves a two-phase (water-to-toluene) transfer and is used to prepare small spherical gold nanoparticles (diameters below 5 nm). This method of gold nanoparticle synthesis was pioneered by Brust, Schiffrin and colleagues in 1994.[52] In a typical synthesis, an aqueous solution of hydrogen tetrachloroaurate is transferred to an organic phase using tetraoctylammonium bromide (TOAB) as the phase transfer agent. The TOAB complexes with gold, encapsulating gold inside TOAB micelles, which are then transferred into the organic layer (Figure 1.2). The gold salt is then reduced by sodium borohydride in the presence of an alkanethiol leading to the formation of spherical gold nanoparticles commonly referred to as monolayer protected clusters.[51-56,70] The resulting gold spheres in the organic phase are stabilized by the alkanethiols, which displace weakly bound TOAB. An advantage of this technique is that the as-synthesized gold nanoparticles can be isolated, stored as a powder, and

redispersed in non-polar solvents without irreversible aggregation.[52,55] The ability to dry the nanoparticles (into a powder) can be used to prepare solutions of very high concentrations.[71] However, further modification of these as-synthesized nanoparticles with pre-formed thiolated coatings (that strongly bind to the gold surfaces) could restrict the possibility of further functionalization of the same when there is an incomplete displacement of the pre-formed alkanethiolate layers, making it difficult to fully control the composition of the resulting nanoparticle coating. The requirement of an additional purification step to purify the sample of TOAB from the synthesized nanoparticles is also a disadvantage of this synthetic approach. It is also important to understand the surface chemistry of these as-synthesized alkanethiol-stabilized gold nanoparticles for their reproducible post-synthesis modification.

$$HAu(III)Cl_{4(aq)} + TOAB_{(toluene\ layer)} + RSH \longrightarrow TOA-Au(I)\ complex + RSSR$$
$$TOAB = [CH_3(CH_2)_7]_4NBr$$

$$TOA-Au(I)\ complex \xrightarrow[RSH]{NaBH_4}$$

monolayer-protected cluster
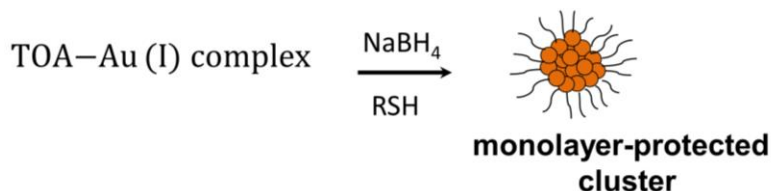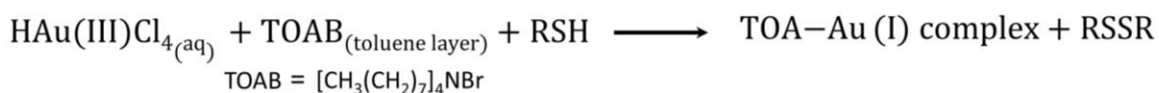
Figure 1.2.   **Mechanism of the formation of gold nanoparticles through the 2-phase Brust-Schiffrin method. (R in RSH represents an alkyl group of a thiol molecule).**

Gold nanoparticles can also be synthesized in the presence of other surfactants that include oleylamine[72], phosphines[73] and polyvinylpyrrolidone[74,75]. Some other surfactant molecules added to gold nanoparticles can also be used as templates to direct anisotropic growth of the nanostructures as described in more detail below.

1.1.3.   Template-assisted synthesis of gold nanorods

Template-assisted synthesis is a method in which surfactants act as soft templates to direct the growth of gold nanoparticles, usually with a non-spherical shape. A template here implies high concentration of surfactants. The first synthesis of rod-

shaped gold nanoparticles was reported in 1989 by Wiesner and Wokaun, using phosphorus as reducing agents for the formation of gold seeds and hydrogen peroxide for the growth of gold nanorods.[76] This seed-mediated synthesis was further modified by Murphy's group in 2001 by introducing a cetyltrimethylammonium bromide (CTAB) surfactant and silver ions into the growth solution of gold nanorods.[77] In this method, citrate-modified gold nanoparticles were added into a growth solution containing CTAB, Au(I) and silver ions. The gold seeds acted as nucleation centers during the growth of the nanorods. Au(III) was reduced to Au(I) by the addition of a relatively weak reducing agent, ascorbic acid (Figure 1.3), into the growth solution. The silver is believed to bind to the {100} crystal facets, inhibiting nucleation on that crystal facet and promoting growth on the {111} facets of the gold nanoparticles.[78-80] The aspect ratio of synthesized gold nanorods can be tuned by varying the amount of silver added during the synthesis of these nanorods.[79] Some studies report that silver also assists in the packing of CTAB molecules by decreasing repulsion between the positively charged ammonium headgroups of CTAB.[59,79] The exact mechanism of silver binding to the gold is, however, still not clearly understood in the literature.[78,80] The introduction of silver into the synthesis of gold nanorods is also reported to greatly improve the yield of nanorods (up to ~99%).[32,79] Growth of gold nanorods in the absence of silver results in the formation of a mixture of rods, spheres, and triangles.[32] Cetyltrimethylammonium bromide (CTAB) is the most frequently used surfactant for the synthesis of anisotropic gold nanoparticles in aqueous solutions.[57-59,78-81] CTAB is reported to preferentially bind to the {100} facets of gold nanorods due to the relatively high surface energy at this facet compared to the other crystal planes of the gold seeds, lowering its surface energy and stabilizing the {100} facet. CTAB makes rod-like micelles, which direct axial growth at the ends of the nanorods at the same time inhibiting lateral growth during synthesis of the gold nanorods. Further longitudinal growth continues through the addition of gold atoms to the ends of the nanorods, resulting in elongation of the rods.[57,58] It has also been proposed that an oriented attachment of gold particles might lead to the elongation of nanorods during the growth processes.[58] CTAB forms a bilayer on gold nanorods. The resulting CTAB-coated nanorods have a positive surface potential.[82,83] This bilayer of CTAB formed is, however, difficult to displace from the surfaces of the gold nanorods.[81,84] Its displacement can be achieved through several approaches, including

ligand exchange, which displaces this bilayer with other molecular coatings, or by encapsulating the bilayer-coated gold nanorods with a layer of silica.[83,85,86]
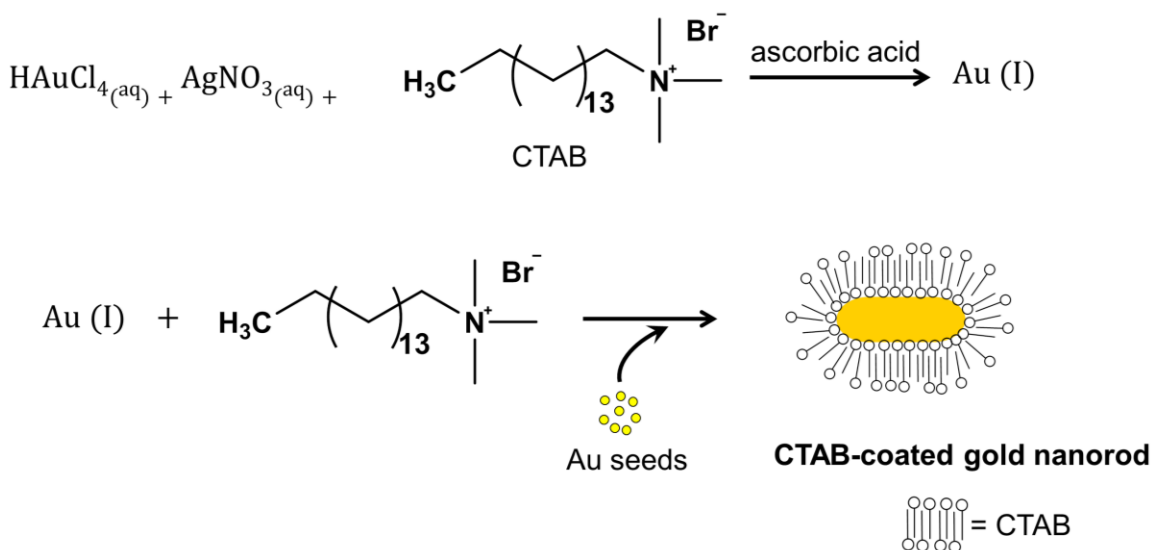
Figure 1.3. **Mechanism of the formation of gold nanorods through a template-assisted growth**

1.2. Ligand Exchange on Gold Nanoparticles

1.2.1. Displacement of non-covalently bound coatings

This method of surface chemistry modification provides a way to prepare gold nanoparticles with a variety of surface properties or functionalities by displacement of the surfactants that originally coat these nanoparticles. For example, citrate coated gold nanoparticles can be functionalized with carboxylate-terminated alkanethiols by ligand exchange between citrate and the desired alkanethiol coatings.[23,66,87,88] In one example, the citrate coating on gold nanoparticles was exchanged for 2-mercaptosuccinic acid (MSA). These MSA functionalized gold nanoparticles were more stable against changes in pH and better resisted cyanide etching when compared to those nanoparticles capped with citrate coatings.[23] A recent study by Xia et al. showed varied efficiencies of ligand exchange on nanoparticles capped with citrate, polyvinylpyrrolidone (PVP), cetyltrimethylammonium chloride (CTAC), and cetyltrimethylammonium bromide

(CTAB). The efficiency of ligand exchange was quantified by determining the surface coverage of an amine functionalized poly(ethylene glycol) or PEG. The surface coverage, and hence efficiency of PEGylation, was determined from either amine-based assays or from the reactions of the terminal amine groups with molecular labels (e.g., fluorescamine dye or Cu^{2+} label). PEGylation efficiency was highest for citrate-coated nanoparticles in comparison to those nanoparticles coated with PVP, CTAC, and CTAB. The PEG coverage density following ligand exchange on each of these gold particle was 1.63, 0.61, 0.41, and 0.052 molecules/nm^2 for the nanoparticles originally coated with citrate, PVP, CTAC, and CTAB, respectively. The relatively high PEG density formed on those particles that were originally coated with citrate is attributed to the ease of displacement of the citrate molecules, in comparison to the CTAB capping which has a stronger binding to gold particles.[66] In another example, citrate coatings on gold nanoparticles were exchanged for 11-mercaptoundecanoic acid (MUDA), 6-mercaptohexanoic acid (MHA), or thioctic acid (TA). Each of these had slightly varying packing densities, dependent on the alkanethiol chain lengths and the footprint of these alkanethiols. The surface density of MUDA, MHA and TA on these nanoparticles, following the displacement of citrate was 4.97, 4.58 and 2.20 molecules/nm^2, respectively.[87] The effect of ligand composition, such as ligand footprint, on the packing densities of the ligands on nanoparticles will be discussed in section 1.3.2.

Ligand exchange is routinely performed on anisotropic gold nanoparticles by displacing CTAB for other more strongly binding coatings such as thiolated polyethylene glycol[81,89], and MUDA[84]. Weaker binding amphiphilic ligands were unable to completely displace CTAB from the surfaces of gold nanorods. These amphiphilic molecules included positively charged (Oligofectamine), negatively charged (phosphatidylserine) and neutral (Brij 56) ligands.[90] These amphiphile-coated nanorods demonstrated greater stability against repeated centrifugal wash steps, when compared to those nanorods stabilized with CTAB only. These amphiphile-coated nanorods were also more stable over a wider range of pH values, higher salt concentrations (up to 400 mM NaCl), higher temperatures and during pulsed laser irradiation in comparison to those nanorods coated with CTAB, which aggregated under similar conditions.[90]

1.2.2. Co-surfactant stabilized nanoparticles

Ligand exchange can also be performed in the presence of co-surfactant molecules, which improve the stability of gold nanoparticles during the exchange step. These co-surfactants loosely bind to the surfaces of the gold nanoparticles (AuNPs) and are slowly displaced over time during formation of monolayers of more strongly binding molecules. Co-surfactants are normally added into solutions of gold nanoparticles preceding the addition of molecules that have a higher affinity to the gold surface. These co-surfactants improve the colloidal stability of the nanoparticles by slowing the rate of exchange of coatings. Examples of commonly used surfactants are polysorbates (e.g., Tween 20, 40 or 80).[67-69] For such nanoparticles functionalized in the presence of a co-surfactant, it is crucial to analyze (either directly or indirectly) the surfaces for any trace amounts of surfactants remaining on their surfaces following ligand exchange processes. These could otherwise create defects on surfaces of nanoparticle, which can lead to instability when the particles are exposed to harsh environmental conditions. For example, the loosely adsorbed surfactants could be desorbed from the nanoparticle surfaces when nanoparticle solutions are heated at elevated temperatures, exposing vacancies on the surfaces of the nanoparticles.[91]

1.2.3. Two-phase extraction

Another approach to modifying the surfaces of gold nanoparticles by ligand exchange is through phase extraction of the nanoparticles. This approach to surface functionalization is versatile for changing surface chemistries of nanoparticles, and can be used to prepare nanoparticles that are either soluble in water or in organic solvents.[92-96] This approach has been particularly useful in modifying the solubility of quantum dots for their use in biological applications.[92] However, the technique, suffers from the inability to prepare nanoparticles with capping layers of a uniform composition due to the incomplete displacement of one ligand with another. In this approach, nanoparticles undergo phase transfer from polar to non-polar solvents and vice versa, following exchange of capping layers on the nanoparticle surfaces. For example, when excess 4-(dimethylamino) pyridine (DMAP) was added to tetraoctylammonium bromide (TOAB)-capped gold nanoparticles, which were suspended in toluene, there was an

immediate transfer of the particles from the organic layer to an aqueous layer as seen by the subsequent ruby red color of the aqueous layer.[97] The displacement of TOAB with DMAP created hydrophilic AuNPs. In this study, DMAP readily adsorbed onto the gold surfaces, displacing the weakly bound TOAB. These DMAP capped gold nanoparticles had a surface potential of +32 mV from zeta potential measurements, and were stable at 4°C for several weeks. There was, however, ~6 to 16 molar % of TOAB remaining in solution with the DMAP capped gold nanoparticles as detected by ion chromatrography. A sufficient amount of DMAP was also required for a successful phase transfer of the nanoparticles into the aqueous layer. It is, therefore, important to analyze the surface chemistry of the nanoparticles following the ligand exchange processes in order to ensure that the initial surfactants present before exchange have been mostly removed and that those remaining would not significantly influence the surface chemistry and stability of the nanoparticles.

1.3. Quality of Alkanethiol-Based Molecular Coatings on Gold Nanoparticles

Alkanethiolate coated gold substrates can be prepared by immersing the substrate (either thin films of gold or colloidal gold nanoparticles) into a solution of alkanethiols. These molecules spontaneously assemble on the surfaces of gold forming self-assembled monolayers (SAMs) of alkanethiolates. The driving forces for this assembly process are substrate-molecular interactions, as well as intermolecular forces.[98] The resulting monolayer constitutes a dative bond formed between the gold substrate and the alkanethiolates, which will be reviewed in more detail below. In this section, the quality of alkanethiol-based molecular coatings will be discussed as a function of the packing of these coatings on the surfaces of gold. The quality of capping layers has important implications in cell targeting, drug delivery and gene therapy, where ligand densities directly affect the targeting efficiency and amounts of drug deliverable from nanoparticle carriers. In most of these applications, a higher density of functional ligands (such as DNA) is desirable. In addition, the quality of capping layers affects their ability to protect the underlying nanoparticles against changes from the surrounding environment, including solvent-particle interactions or interactions with other dissolved

species. Investigation of the packing density, orientation and conformation of molecular coatings on the surfaces of gold is important in understanding the structure-function relationship of the modified surfaces.

The most commonly used techniques to characterize the composition, and integrity of molecular coatings on gold include: i) contact angle measurements, which indicates the wetting ability of the monolayers on thin films of gold; ii) X-ray photoelectron spectroscopy (XPS) that provides information on the oxidation states and chemical environments of molecular coatings, as well as monolayer coverage[99,100]; iii) infrared and Raman spectroscopies that can be used to assess the chain orientation, the conformation and packing of molecules within monolayers[20,98,100]; and iv) atomic force microscopy (AFM) and scanning tunneling microscopy (STM) that provide direct molecular level information about the monolayer structures (size of domains and their spatial distribution). Pinhole defects within molecular coating layers have been studied by AFM and STM imaging techniques.[109,128] The quality of molecular coatings on colloidal gold particles can also be probed indirectly using chemical methods. Examples of such methods include cyanide etching of gold cores, as well as other oxidizing conditions, with the rate of etching directly related to the quality of the capping layers on the gold particles.[101,102] Defects within the molecular coatings have also been studied by cyclic voltammetry.[103] The current required to desorb thiolates from gold surfaces is measured and the amount of current passed can be used as a measure of the degree of coverage (or presence of defects within the coatings) of alkanethiolates on gold substrates. Desorption of thiolates from gold surfaces proceeds at the defect sites of the molecular coatings.[98] The surface coverage is obtained by integrating the desorption peak. In addition, Raman bands attributed to C-S stretching vibrations (with either a trans or gauche C-S stretching bands) around ~700 cm^{-1} are used to assess the conformation of alkanethiolate monolayers on gold surfaces.[98] Water contact angle measurements are a relatively fast method for assessing quality of monolayers, but it is a macroscopic technique. It only provides information about the molecular coatings over large areas, such as the wettability of the coating layer. Hydrophobic films are expected to have high water contact angles due to the poor wettability of the coatings. XPS is an ultrahigh vacuum technique that is highly surface sensitive. It can be used to analyze the nature of molecular coatings on a surface (e.g., bound, unbound or oxidized coatings),

providing information about chemical states as well as the integrity of molecular coatings.

1.3.1. Lattice, Tilt and Rotation of the Molecular Coatings

The spacing between adjacent alkanethiolates is dictated by the underlying substrate (such as a curved vs flat surface), as well as the structure of the alkanethiol molecules. STM studies of alkanethiolates on Au (111) surfaces have shown that the sulfur headgroups are arranged in a hexagonal array with spacings between adjacent headgroups of 0.499 nm and with a surface coverage, θ, of 0.33 (out of 1).[104,105] These molecules adopt and average tilt (α) of 33° away from the surface normal, as depicted in Figure 1.4. The ordering within a full monolayer of alkanethiolates on a Au (111) surface of gold is anticipated to adopt a structure of (√3 × √3)R30° (R refers to the rotation of the unit cell of the alkanethiolates relative to the unit cell of the gold atoms) with a secondary ordering of the chains corresponding to a c(4 x 2) superlattice.[98,104-106] This geometry results in adsorption of one thiolate molecule between 3 gold atoms and an overall 1/3 coverage of thiolates on the Au(111) planes (Figure 1.5), with the alkanethiolate chains tilting away at an angle of 33° from the surface normal.[107,108] This translates into intermolecular spacings in the SAMs (√3 x 0.288 = 0.499 nm) that are √3 times larger than the spacing of the gold atoms (0.288 nm), and that the molecules in the monolayer are tilted 30° with respect to the normal to the Au(111) lattice.[109] By comparison, the S to S spacing between alkanethiolates adsorbed on Au(110) surfaces is 0.576 nm, with the sulfur atoms bound in a rectangular pattern (Figure 1.6) corresponding to the atomic structure of the Au(110) surface (or a c(2 x 2) structure).[105] The alkanethiolates are tilted at an angle of 40° from the surface normal on the Au(110) surfaces. Alkanethiolates on Au(100) similarly adopt a structure of c(2 x 2) with a S to S spacing of 0.416 nm and a molecular tilt of 30° from the surface normal (Figure 1.7).[110,111]
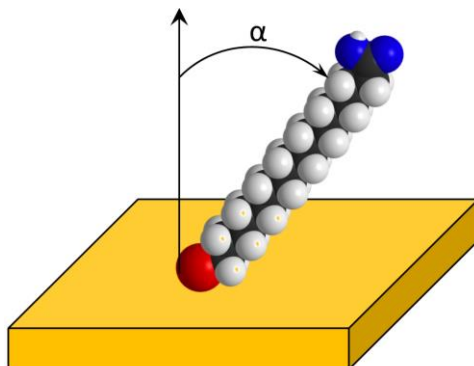
Figure 1.4. The tilt angle (α) is used to describe the molecular tilt away from the normal on a surface of gold.[104,106]
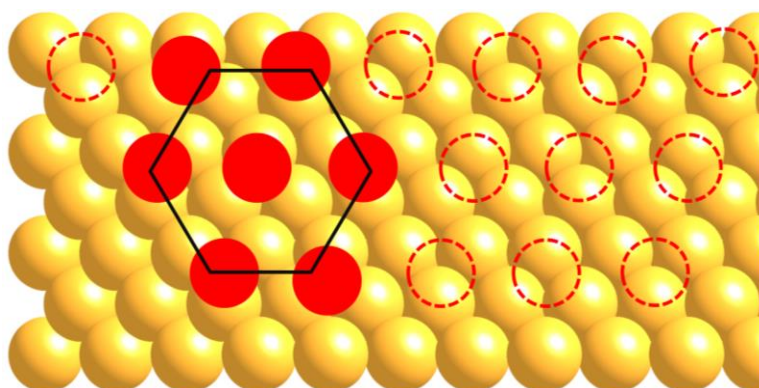
Figure 1.5. Adsorbed alkanethiolates on a Au (111) surface. The adsorbate structure is described as ($\sqrt{3} \times \sqrt{3}$)R30°. Both the filled and dashed circles represent alkanethiolates adsorbed on a Au (111) surface. Some circles are dashed to allow for a clear view of the underlying gold substrate.
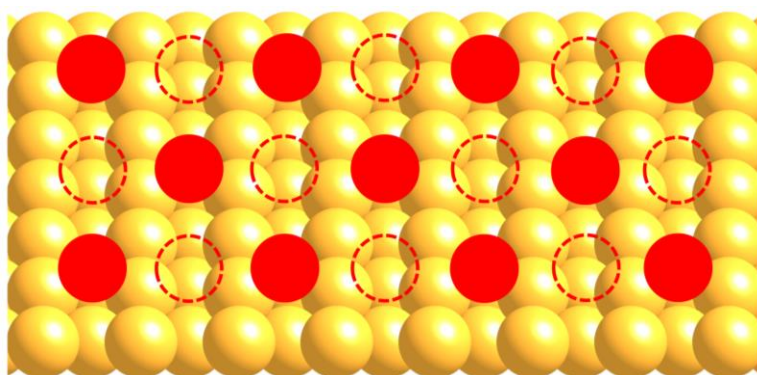
Figure 1.6.   **Adsorbed alkanethiolates on a Au (110) surface. The adsorbate structure of thiolates bound to the rectangular hollow sites of the Au (110) surface is c(2 x 2)R40°. Both the filled and dashed circles represent alkanethiolates adsorbed on a Au (110) surface.**
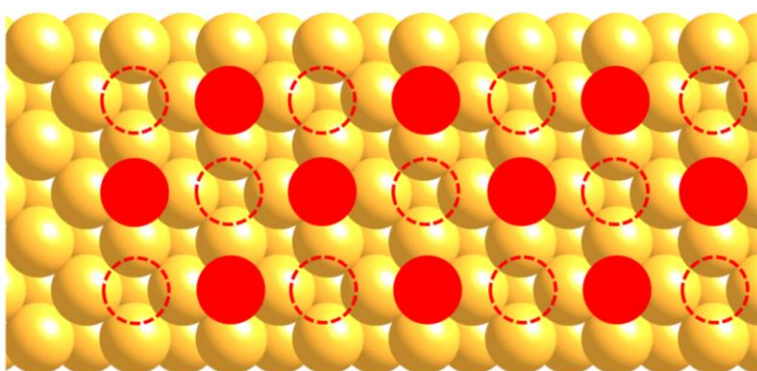
Figure 1.7.   **Adsorbed alkanethiolates on a Au (100) substrate. These alkanethiolates adopt a c(2 x 2)R30°. The dashed cirles are left unfilled for a clear view of the position each thiolate occupies on the substrate. Both the filled and dashed circles represent alkanethiolates adsorbed on a Au (100) surface.**

Surfaces of small gold nanoparticles have a high surface curvature in comparison to planar gold substrates. This difference in curvature is expected to affect the packing of alkanethiols on both types of surfaces.[112] A decreased chain density and enhanced mobility of the terminal methyl chains is expected for increasing diameters of the gold cores.[98] Small sized AuNPs (<4 nm) have a relatively high surface coverage of alkanethiolates, versus planar surfaces. The former have θ values higher than 0.33.[113] In addition, a nanoparticle coated with a well-packed monolayer of alkanethiolates is

expected to have a hydrodynamic radius equal to the sum of the radius of the gold core and approximately the length of a fully extended alkanethiol chain. A smaller hydrodynamic diameter would otherwise indicate loosely packed monolayers.[87,98]

1.3.2. Impact of the footprint and structural composition on quality (packing) of alkanethiol-based capping layers

The nature of molecular interactions, such as bidentate versus multidentate headgroups, length of alkyl chains and structure of the spacer (branched versus linear) directly affects the ordering and packing density of molecules coating the gold surfaces.[87,114,115] The ordering and packing of molecules within these coatings directly affects the quality of resulting coatings. These are important considerations for functionalizing nanoparticles for use in biosensing, drug delivery or catalysis. It is, therefore, necessary to determine the quality of these coatings on the surfaces of nanoparticles when preparing particles that need to remain stable under a variety of environmental conditions. In a study by Ivanov and colleagues, the packing densities of monolayers prepared from 6-carbon chain and 11-carbon chain alkanethiols were 4.58 molecules/nm^2 and 4.97 molecules/nm^2, respectively. This observation that the packing density increased with increasing chain length of the alkanethiols could be attributed to enhanced intermolecular interactions of the alkanethiolates as the chain length increased.[116,117] The same authors demonstrated that multidentate-binding of alkanethiols (with a disulfide headgroup) resulted in poor ligand ordering and a relatively low loading of alkanethiolates (2.20 molecules/nm^2) on similar sized gold nanoparticles.[87] Lanterna and colleagues similarly demonstrated that the packing density of heterocyclic thiol-based molecules depends on these length of the molecules. This study showed that coverage of thiones on gold nanoparticles increased as the length of the thiones increased from 1.2 nm to 2 nm. Nanoparticles modified with relatively long chains of thiones were also more resistant towards cyanide etching.[117] Although interstrand van der Waals interactions can increase surface coverage of thiol-based coatings on AuNPs, molecular geometry also plays an important role in the packing of these molecules on surfaces of gold. Hinterwirth and co-workers demonstrated that the surface density of a short chain 3-mercaptopropionic acid (spacer length 0.68 nm) and a thiolated polyethylene glycol or PEG (spacer length 3.52 nm)

resulted in capping layers with densities of 6.26 molecules/nm^2 and 4.29 molecules/nm^2, respectively.[118] In the latter example, the reversed trend of packing densities and chain length was attributable to steric hindrance of the PEG molecules, which are more flexible and would probably pack less tightly on nanoparticles.[118] Zhang and co-workers modified gold nanoparticles with monodentate and multidentate thiols (bi- and tridentate) and compared the stabilities of the modified nanoparticles in organic solvents.[119] They illustrated that tridentate binding thiols provided the most stability against aggregation of gold nanoparticles due to their chelating effect on the surfaces of the nanoparticles. The particle stability was assessed by changes in the position of the extinction spectra, as well as the hydrodynamic diameters of the modified nanoparticles.[119] Other studies have also shown improved stabilities for nanoparticles coated with multidentate thiols versus monodentate thiols at high salt concentrations[102,120], as well as against ligand detachment at high temperatures[121] and ligand displacement by other thiols (e.g., dithiothreitol).[102,122] The improved stability of multidentate-thiol coatings under these harsh conditions could be attributed to the fact that desorption of these molecules requires simultaneous breaking of multiple Au-S bonds, which is energetically disfavored relative to the monodentate alkanethiolates.[121] Another study showed that dithiolate-coated AuNPs were less protected against cyanide etching when compared to monothiolate coated particles due to the poorer packing efficiency of the former coatings.[101] Taken together, these studies suggest that packing efficiencies on metal surfaces are an important consideration, which directly affects the physicochemical stability of thiol coated nanoparticles.

1.3.3. Strength of interactions between nanoparticles and molecular coatings

Thiol-based coatings stabilize gold nanoparticles through formation of a strong dative bond between the nanoparticles and the sulfur headgroups, as well as intermolecular forces between the alkyl chains of neighboring thiols. Each of these interactions stabilizes the nanoparticles and prevents interparticle interactions. The Au-S bond formed between alkanethiols and gold substrates has been measured to be 45-50 kcal mol^{-1}.[98,100,107,118,123] Intermolecular forces between between the capping alkanethiolates are reported have values between 1-2 kcal mol^{-1} per methylene groups

in the hydrocarbon chains.[104] For example, the intermolecular force between hexanethiol chains is ~6 kcal mol^{-1} and is ~12 kcal mol^{-1} for benzenethiol chains.[123] The kinetics and thermodynamics of adsorption and desorption of thiolated coatings on surfaces of gold enables an assessment of the energetics of interaction between headgoups-metal surfaces as well as intermolecular interactions between adjacent thiolates. For example, the Gibb's free energy of adsorption (ΔG_{ads}) was determined to be −5.5 kcal/mol and −4.4 kcal/mol for 18-carbon chain and 8-carbon chain alkanethiols, respectively, at 293K.[124] Schessler and colleagues investigated the kinetics of alkanethiol adsorption on gold using quartz crystal microbalance to monitor the rate of reaction.[125] They demonstrated that dynamics of the self-assembly process is an interplay between thiolate interactions with the metal substrate, as well as the thiol-solvent interactions. Rates of adsorption of thiols onto gold varied depending on the concentration of thiol in solution. These authors also showed that the adsorption enthalpy (ΔH_{ads}) constitutes a solvation enthalpy (that depends on the type of solvent) and a monolayer formation enthalpy (dominated by the Au-S bond formation). The adsorption of thiols, van der Waals interactions, hydrophilic/hydrophobic interactions, hydrogen bonding, and solvent-solute interactions can all contribute to the value of ΔH.[126] The entropy of adsorption (ΔS_{ads}) is dominated by the change in order within the system associated with the organization of the molecular coatings on the gold surfaces. Thiol molecules lose some degree of translational freedom as they bind to the gold surfaces, which results in a decrease in the system's entropy. The ΔS at a particular temperature can also be affected by solvation/desolvation of bound thiolates, as well as the process of expulsion of water molecules from a surface.[126] The calculated ΔG_{ads}, ΔH_{ads}, and ΔS_{ads} values for 1-octadecanethiol monolayers formed from n-hexane onto Au(111) are −5.5 kcal/mol, −20 kcal/mol, and −48 cal/(mol.K) respectively at 303 K.[125] These thermodynamic parameters largely drive molecular self-assembly at the interface between the gold and the thiols and/or solvent molecules. The thermodynamics and kinetics of these interactions are, however, temperature dependent.[126]

1.3.4.   Thermal annealing of defects within molecular coatings

A common way of re-organizing molecules within SAMs (to enhance their ordering and uniformity) on planar gold surfaces is by thermally annealing these films

18

(Figure 1.8).[127] Thermal annealing at higher temperatures (such as those >70°C) is also used to eliminate defects on the gold substrates, which increases grain sizes.[98] Annealing results in the formation of large ordered domains of SAMs due to the coalescence of domain boundaries and vacancy islands (gold pits).[109,128] For example, octanethiol SAMs formed on gold nanoplates displayed disordered phases as observed by STM. There was, however, a structural transition of these SAMs following annealing at 70°C for 30 min to form long-range ordered domains of these alkanethiol-based SAMs. This ordering was attributed to an optimization of van der Waals forces between alkyl chains due to a rearrangement of alkanethiolates on the gold nanoplates during the annealing process.[128] This process of re-organizing SAMs is, however, limited to the thermal stability of these films on gold surfaces. Heating the films to high temperatures (e.g., 130°C) for a prolonged time could lead to oxidation and desorption of thiolates from gold surfaces.[129] Delamarche and colleagues annealed dodecanethiol SAMs in air at 85°C to 130°C over a period of 10 h. In their study, gold terraces and depressions (2.4 Å deep) coalesced into larger features with average sizes of ~11 nm in width following annealing of the samples at 100°C for 2 h, and the terraces disappeared completely following annealing of the samples at 100°C for 10 h. Increasing the annealing temperature to 115°C led to a distortion of the monolayer topography due to a desorption of the SAMs in the form of disulfides (via oxidation of the alkanethiolates to disulfides), and a complete removal of the SAMs from the gold surfaces after annealing in air at 130°C over a period of 10 h.[129] Improving the quality of molecular coatings can include post-assembly thermal treatment of the monolayers to minimize pre-formed domain boundaries and defects in the molecular coatings. This thermal treatment has to be performed within the constraints of the system under study to avoid oxidative or structural damage to the monolayers and gold nanoparticles.
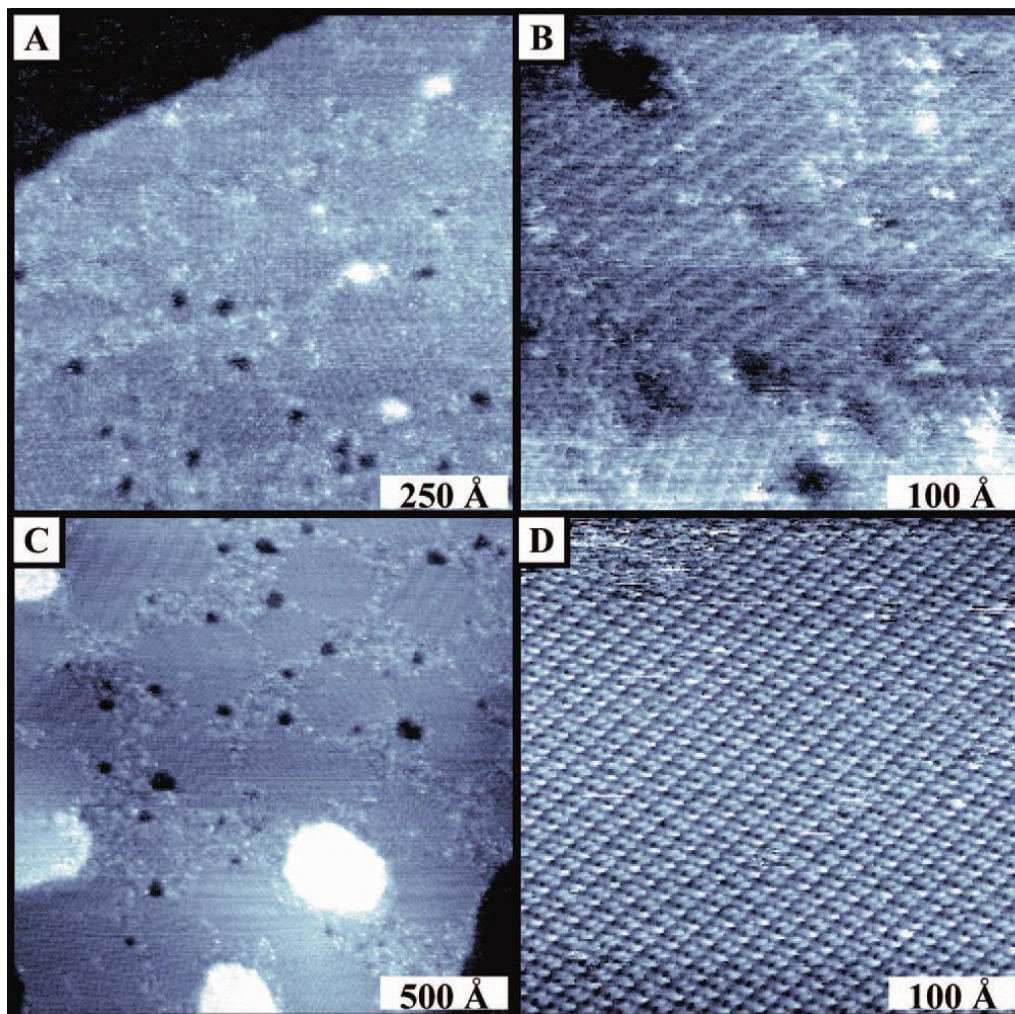
Figure 1.8. Scanning tunneling microscopy images of 2-adamantanethiol SAMs on Au{111}. These SAMs were prepared by either: (a and b) immersing substrates into 1 mM thiol solution at room temperature for 24 h; or (c and d) immersion of substrates into the thiol solution at 70°C for 2 h, followed by dry-annealing of the samples at 78°C over a period of 17 h. Those SAMs prepared at 70°C form large domains with lower defect densities. Thermal annealing of these SAMs further allows the formation highly ordered monolayers with long-range order. Sample bias 0.80 V, tunnelling current 2.0 pA. Reprinted with permission from Kim, M.; Hohman, J. N.; Morin, E. I.; Daniel, T. A.; Weiss, P. S. *J. Phys. Chem. A.* 2009, *113*, 3895. Copyright 2009 American Chemical Society.[127]

1.3.5. Uniformity of molecular coatings on different facets of gold nanoparticles

Gold nanoparticles have been widely pursued for their unique properties relative to their bulk counter parts. For example, the relatively high surface area to volume ratio of these particles is desirable for their increased catalytic activity.[130,131] This increased activity can be attributed to the increased density of the edge and corner sites on the faceted surfaces of the crystalline nanoparticles.[132-134] The catalytically active sites are potential weak points in any molecular coatings, and must be capped with surfactants to stabilize the particles against unwanted interactions with their surrounding environment. These less desirable interactions include aggregation of the particles when dispersed in solution. The assembled surfactant molecules protect the particles from aggregation by creating a dense molecular packing that covers the crystalline facets. Defects in these self-assembled molecular coatings can expose the highly active surfaces of the particles. Physicochemical stability is, however, desired in bio-relevant solutions as opposed to catalytic properties for many sought after applications for gold nanoparticles.

Cetyltrimethylammonium bromide (CTAB) plays two major roles in the synthesis of gold nanorods as discussed in more detail above: i) it forms a complex with the gold ions; and ii) binds preferentially to the sides of the growing nanorods. The Au (III)-CTAB complex slows the reduction of the Au(III) precursor and regulates nanorod growth processes. The preferential binding of CTAB to the {100} side facets of gold nanorods promotes elongated growth of these anisotropic structures with gold atoms being deposited at their end facets.[135] The {110} and {111} end facets, therefore, have a lower density of CTAB molecules. The different reactivities of the side and end facets of these nanorods allow the selective binding of molecules to the specific facets. This selectivity has been demonstrated by end functionalization of gold nanorods and formation of end-to-end tethered gold nanorods.[136-139] Because the end facets have fewer CTAB molecules compared to the sides of the as-synthesized gold nanorods, relatively low concentrations of molecular additives preferentially bind to the ends of the nanorods. The resulting assemblies of gold nanorods could also be useful as surface enhanced Raman spectroscopy substrates and in the fabrication of plasmonic devices.[136,139] Understanding the reactivity of the gold nanoparticles will help guide coating of any

21

potential weakly protected regions of the surfaces on the nanoparticles, and thereby, improve the physicochemical stability of the particles.

1.3.6. Electrochemical reactions for the formation of thiol-based SAMs

The formation of a Au-S bond occurs by a redox reaction between thiol coatings and the surface gold atoms. The proton from alkanethiols (RSH) is reportedly lost in the form of a dihydrogen and might be converted into water in the presence of oxygen.[98] The adsorption of thiols on a gold surface can generally be written as:[96,97]

$$Au^0 + SR^- \rightarrow Au{-}SR + e^-$$ (Eq. 1.5)

Bound alkanethiolates can be electrochemically desorbed from a surface of gold through the reaction:[103,140,141]

$$Au{-}SR + e^- \rightarrow Au^0 + SR^-$$ (Eq. 1.6)

Dias and colleagues studied the electrochemical behavior of ethanethiol monolayers formed on gold electrodes by cyclic voltammetry (Figure 1.9).[103] The gold electrodes were characterized in 0.5 M NaOH electrolyte over a potential region of −1.5 V to 0.7 V, recorded at a scan rate of 600 mV s^{-1}.The study described above explained the formation of a thiolate bond and its desorption from gold surfaces in terms of oxidation and reduction processes. The oxidation of gold (as in equation 1.5) was characterized by a peak at -0.93 V (position #1 as indicated in Figure 1.9), while the reductive desorption of bound alkanethiolates (as in equation 1.6) was characterized by a peak at -1.15 V (positions #7, Figure 1.9). Additional peaks at 0.12 V and 0.62 V (positions #3 and 4, Figure 1.9) were attributed to the formation of dithiol species.[103] The desorbed thiols could also be oxidatively re-adsorbed onto gold surfaces by changing the electrode potential to the positive direction following the reductive desorption process.[142]
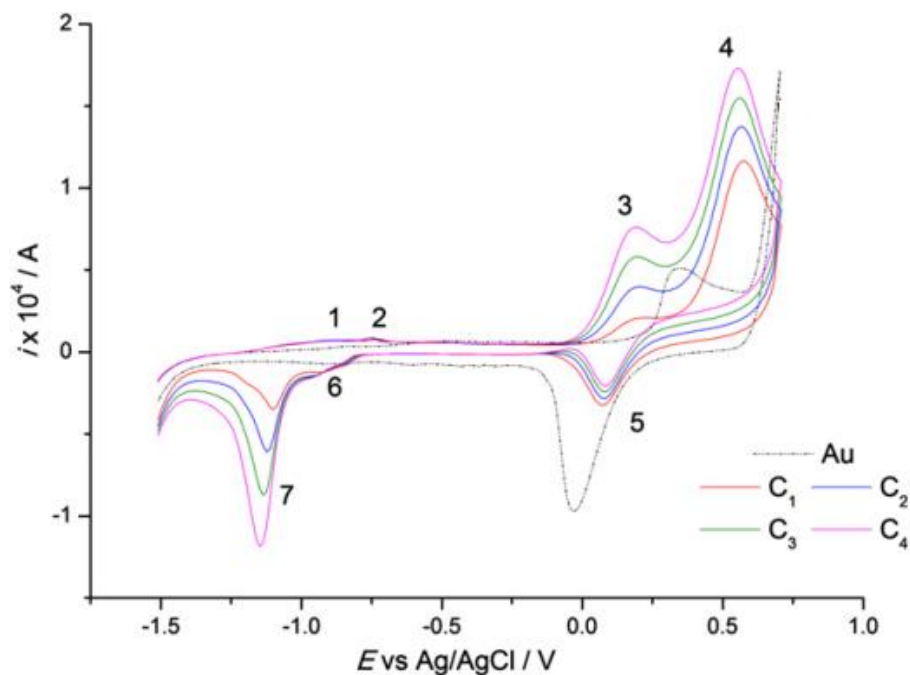
Figure 1.9 **Cyclic voltammograms of a bare gold electrode (- -) in 0.5 mol L^{-1} NaOH and with ethanethiol (C$_1$ = 1.61 mmol L^{-1} , C$_2$ = 3.22 mmol L^{-1} , C$_3$ = 4.83 mmol L^{-1} , C$_4$ = 6.44 mmol L^{-1}). Experimental conditions: t$_{pt}$ = 30 s, E$_{pt}$ = −1.5 V, E$_{start}$ = − 1.5 V, E$_{end}$ = 0.7 V, scan rate = 600 mV s^{-1}. The oxidation peaks at −0.93 V, −0.77 V, 0.12 V and 0.62 V are represented by the numbers 1 to 4, respectively. The reduction peaks at 0.08 V, −0.93 V, and −1.15 V are represented by the numbers 5 to 7, respectively. Reprinted with permission from Dias, D.; Hasse, U.; Fricke, K.; do Nascimento, P. C.; Scholz, F. *J. Electroanal. Chem.* 2013, *690*, 121. Copyright 2012 Elsevier.[103]**

In addition, applied electric potentials can affect the protonation state of acid-terminated alkanethiolates. For example, Rosendahl and co-workers demonstrated that COOH terminal groups of 4-mercaptobenzoic acid can either be protonated or deprotonated when the gold substrates are subjected to different electrochemical potentials.[143] The monolayers of 4-mercaptobenzoic acid had voltammetric peaks at −200 mV, which was attributed to the protonation and deprotonation of these carboxylic acid-terminated SAMs. These authors also showed that the voltammetric peaks are sensitive to the presence of ions, with the peak intensities decreasing as the concentration of cations increased.[143] The formation of thiol-based SAMs is, therefore, electrochemical in nature, involving the transfer of electrons resulting from the interaction of the gold surfaces and the alkanethiol coatings. Electrochemistry plays a role in the

overall quality of the SAMs formed on planar surfaces, but recent work is underway to understand the electrochemistry as it applies to nanoparticles in suspensions.[144]

1.3.7. Further challenges to preparing ideal coatings on nanoparticles

The local environment (e.g., ions in solution, surfactants, salts, buffer solution, solvents) of nanoparticles can directly affect the physicochemical properties of the particles. Some examples include the influence of solution pH, surface potential (or charge), and hydrodynamic diameter on physicochemical stability of the particles. Physically adsorbed molecules affect the hydrodynamic diameter of the nanoparticles. Interactions of the solvent, surfactants and salts with surfaces of nanoparticles during the formation of coating layers can improve stability or destabilize the colloids. For example, interactions between gold nanoparticles and high concentrations of phosphate ions is known to destabilize the particles.[145] Proteins can adsorb onto gold nanoparticles, depending on the surface potential of the particles, leading to the formation of protein coronas, which are mostly undesired when these particles are used within biological media.[146-149] Interactions between gold nanoparticles and salts could lead to charge shielding on surfaces of the particles. The magnitude of surface potential of nanoparticles is also important for their colloidal stability. When added to solutions of nanoparticles, high concentrations of salts screen the charge on the particle surfaces and could lead to agglomeration and precipitation of the nanoparticles.[150-152] An optimal ionic strength has, however, been shown to improve the packing of some molecules onto the surfaces of gold nanoparticles.[153-154] The influence of pH is clearly demonstrated for carboxylate terminated coatings, where the coatings are protonated (COOH) at low pH values and deprotonated (COO$^-$) at high pH values.[152,155,156] The deprotonated particles have a negative charge, which stabilizes these particles through electrostatic repulsion between particles. In the case of amino terminated coatings, the coated nanoparticles are charged at low pH values (NH$_3^+$) and the particles are uncharged at high pH values (NH$_2$). The stability of nanoparticles can thus be improved by carefully assessing and tuning variables such as solution pH, ionic strength, and the surface charge of these particles.

24

A summary of some methods used for the preparation of thiol-based molecular coatings on gold nanoparticles and associated stability tests of the nanoparticles is provided in Table 1.1.

Table 1.1.   Summary of Nanoparticle Coating Procedures

AuNPs	molecular coating	time allowed for the formation of SAMs	stability	Ref
10 nm spherical AuNPs	2-mercaptosuccinic acid	8-12 h	1) HCl titration-AuNPs were stable for several additions of HCl, as assessed by extinction at 600 nm 2) cyanide etching – smaller shift in SPR peaks compared to citrate stabilized AuNPs	23
4 nm spherical AuNPs	zwitterionic disulfide	12 h	1) stable against aggregation in 3 M NaCl for 3 months as assessed by extinction spectroscopy 2) no visible aggregation in polyelectrolytes, and in the presence of BSA protein	157
20 nm spherical AuNPs	1) 11-mercaproundecanoic acid plus Tween 20 2) 16-mercaptohexadecanoic acid plus Tween 20	4 h	1) change in extinction spectra (600-800 nm) used to assess flocculation as a function of pH 2) particles prepared in the absence of Tween 20 were more destabilized with pH change	67

AuNPs	molecular coating	time allowed for the formation of SAMs	stability	Ref
3.25 nm and 15 nm spherical AuNPs	thiolated polymer bearing diacetylene groups	overnight at 4°C	1) stable in 2 M NaCl, as assessed by extinction spectroscopy 2) stable in a high concentration of BSA, as assessed by extinction spectroscopy 3) stable in water/isopropanol mixture, as assessed by extinction spectroscopy 4) stable at pH 1.2-14, as assessed by extinction spectroscopy 5) stable at 100°C; stable with 5 repeated cycles of freezing (−20°C) and thawing 6) stable against competitive displacement with mercaptoethanol, dithiothreitol, cysteamine, cysteine, α-lipoic acid, and 11-amino-1-undecanethiol following incubation with each respective thiol for 72 h	31
17 nm spherical AuNPs	glutathione (GSH), mercaptopropionic acid (MPA), cysteine, dihydrolipoic acid (DHLA), thiolated PEG (PEG-SH)	overnight at 4°C	1) PEG-coated nanoparticles were most stable against change of pH between 5.4-9.4, as assessed by extinction spectroscopy 2) PEGylated particles did not aggregate at salt concentrations of up to 1 M NaCl, as assessed by extinction spectroscopy	158

AuNPs	molecular coating	time allowed for the formation of SAMs	stability	Ref
12 nm and 30 nm spherical AuNPs	1) α-methoxypoly- (ethylene glycol)-ω-(11-mercaptoundecanoate) (PEGMUA) 2) α-methoxypoly(ethylene glycol)-ω-(3-mercaptopropionate) (PEGMPA) 3) α-methoxypoly(ethylene glycol)-ω-(4-mercaptophenylethanoate) (PEGMPAA)	30 min	1) stable in 400 nM NaCl for 6 h, whereas citrate capped AuNPs aggregated within <1 min of addition of the same concentration of salt, as assessed by extinction spectroscopy 2) cyanide etching- stability against KCN etchant decreased in the order: AuNP@PEGMUA >> AuNP@PEGMPAA > AuNP@PEGMPA. AuNP@PEGMUA was etched completely within ~23 h, whereas PEGMPA and PEGMUA capped nanoparticles were etched within 4 min in 100 mM KCN. This difference in stabilities was correlated with the lengths and structures of spacers within the capping molecules. 3) PEGMUA capped nanoparticles were most stable against competitive displacement with dithiothreitol (DTT)	21

AuNPs	molecular coating	time allowed for the formation of SAMs	stability	Ref
15 nm spherical AuNPs	1) HS-PEG-OCH$_3$ 2) thioctic acid-PEG-OCH$_3$ 3) bis(thioctic acid)-PEG-OCH$_3$	overnight at room temperature	1) nanoparticles capped with bis(TA)-PEG-OCH$_3$ were stable at pH 1.1-13.9 over a period of 7 months, as assessed by extinction spectroscopy 2) stable in 2 M NaCl for 7 months, as assessed by extinction spectroscopy 3) nanoparticles capped with bis(TA)-PEG- OCH$_3$ remained stable in a solution of 1.5 M DTT + 400 mM NaCl for 60 min; HS-PEG-OCH$_3$ capped nanoparticles aggregated after only 10 min Bis(TA)-PEG-OCH$_3$ provided enhanced stability compared to the monothiol- and dithiol-PEG coatings. The multidentate binding to AuNPs provided stability at the above mentioned harsh conditions	159

AuNPs	molecular coating	time allowed for the formation of SAMs	stability	Ref
20-50 nm spherical AuNPs	1) 2-tetradecylpropane-1,3-dithiol (C16C2) 2) 2-methyl-2-tetradecylpropane-1,3-dithiol (C16C3) 3) 1,1,1-tris(mercaptomethyl)-pentadecane (t-C16) 4) hexadecanethiol (n-C16) 5) 2,2-dimethylhexadecane-1-thiol (DMC16)	24 h	The multidentate coatings $C_{16}C_2$, $C_{16}C_3$ and, t-C_{16} stabilized gold nanoparticles better than monodentate n-C_{16} and DMC_{16}, as assessed by extinction spectroscopy. The multidentate cappings also enabled phase transfer of nanoparticles, and those particles remained stable in an organic phase for at least 1 month	119
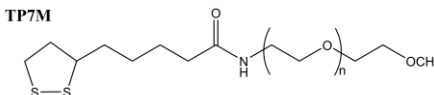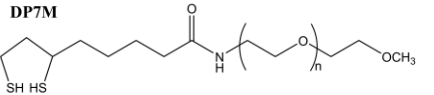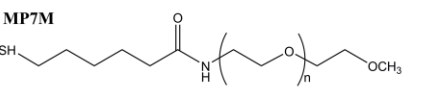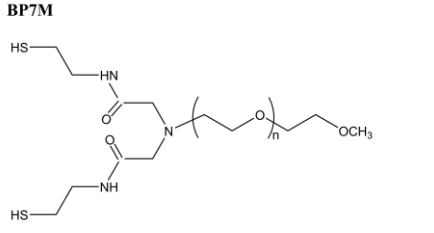
AuNPs	molecular coating	time allowed for the formation of SAMs	stability	Ref
15 nm spherical AuNPs	TP7M has a disulfide headgroup DP7M has a dithiol headgroup and is more structurally constrained MP7M has a monothiol headgroup BP7M has a dithiol headgroup and a relatively flexible structure TP7M DP7M MP7M BP7M	8 h	1) MP7M capped nanoparticles were destabilized within 5 min of heating to 100°C in a 2 M solution of NaCl; TP7M aggregated at a slower rate-solution turned light-pink colored after 15 min under similar conditions (these were destabilized after 24 h at room temperature), as assessed by extinction spectroscopy 2) 1.5 M DTT + 0.8 M NaCl + 10 mM NaOH: AuNP-MP7M particles immediately precipitated and completely lost the original red colloidal color in less than 20 min; AuNP-BP7M and AuNP-DP7M were relatively stable for 20 min; AuNP-TP7M showed very little change even after 90 min in DTT solution, as assessed by extinction spectroscopy.	102

Table 1.1 summarizes some methods used to prepare thiol-based molecular coatings on gold nanoparticles and reveals inconsistencies in how molecular coatings are prepared on the nanoparticles. For example, the time allowed for the formation of SAMs widely varies, and those would likely result in varying qualities of coatings. The work in this thesis aims to address such inconsistencies by preparing coatings of varying

qualities on AuNPs and assessing the relative stabilities of the nanoparticles. The quality of molecular coatings on AuNPs will be varied by tuning the time allowed for the formation of SAMs, or by varying the initial concentration of thiol-based coatings added to gold nanoparticles. In addition, the stability of AuNPs will also be assessed as a function of known concentrations of excess stabilizing surfactants in solutions of nanoparticles.

1.4. Thesis Overview

The molecular coatings on nanoparticles form the interface between the particle and its surrounding environment. The ability to fine tune compositions of molecular coatings opens up a wide variety of possibilities for uses of the capped particles. These coatings protect the nanoparticles from unwanted changes and are used to improve the physicochemical stability of nanoparticles (e.g., in physiological media). However, understanding and improving the quality of their molecular coatings is important for reproducibly using the modified particles in each specific application. In this dissertation, an evaluation of gold nanoparticle stability is performed and correlated with quality of their molecular coatings. Chapter 1 introduces the quality factor of molecular coatings on as-synthesized nanoparticles, as well as looking into literature methods on modifying the surfaces of the as-synthesized nanoparticles. Chapter 2 focuses on the method of preparation of molecular coatings, with an aim of preparing gold nanoparticles with high quality coatings. The long-term stability of these modified nanoparticles is assessed using a series of complementary techniques to correlate stability of nanoparticles with the quality of their molecular coatings. Chapter 3 studies the photothermal stability of gold nanoparticles as a function of their surface chemistry (e.g., covalent versus non-covalent coatings). The ability of nanoparticles to 'self-repair' during photothermal processes is probed through the addition of excess surfactants into the suspensions of gold nanoparticles. Chapter 4 focuses on the quantitative loading of DNA onto gold nanoparticles. This technique is useful for the preparation of multifunctional nanoparticles, where a specific number of molecules in a coating can be controllably loaded onto nanoparticles for a predictable biological stability and specificity in targeting.

Chapter 5 will present conclusions and future directions proposed for further improvements and analysis to the molecular coatings on gold nanoparticles.

1.5. References

(1)   Faraday, M. *Philosophical Transactions of the Royal Society of London.* **1857**, 147, 145-181.

(2)   Cai, W.; Gao, T.; Hong, H.; Sun, J. *Nanotechnology, Science and Applications*, **2008**, 17-32.

(3)   Vigderman, L.; Zubarev, E. R. *Advanced Drug Delivery Reviews* **2013**, *65*, 663-676.

(4)   Shukla, R.; Bansal, V.; Chaudhary, M.; Basu, A.; Bhonde, R. R.; Sastry, M. *Langmuir* **2005**, *21*, 10644-10654.

(5)   Eustis, S.; El-Sayed, M. A. *Chemical Society Reviews* **2006**, *35*, 209-217.

(6)   Huang, P.; Bao, L.; Zhang, C. L.; Lin, J.; Luo, T.; Yang, D. P.; He, M.; Li, Z. M.; Gao, G.; Gao, B.; Fu, S.; Cui, D. X. *Biomaterials* **2011**, *32*, 9796-9809.

(7)   Chen, H. Y.; Li, B. W.; Ren, X. Y.; Li, S. N.; Ma, Y. X.; Cui, S. S.; Gu, Y. Q. *Biomaterials* **2012**, *33*, 8461-8476.

(8)   von Maltzahn, G.; Park, J.-H.; Agrawal, A.; Bandaru, N. K.; Das, S. K.; Sailor, M. J.; Bhatia, S. N. *Cancer Research* **2009**, *69*, 3892-3900.

(9)   Eghtedari, M.; Oraevsky, A.; Copland, J. A.; Kotov, N. A.; Conjusteau, A.; Motamedi, M. *Nano Letters* **2007**, *7*, 1914-1918.

(10)   Huschka, R.; Neumann, O.; Barhoumi, A.; Halas, N. J. *Nano Letters* **2010**, *10*, 4117-4122.

(11)   Poon, L.; Zandberg, W.; Hsiao, D.; Erno, Z.; Sen, D.; Gates, B. D.; Branda, N. R. *ACS Nano* **2010**, *4*, 6395-6403.

(12)   Bakhtiari, A. B. S.; Hsiao, D.; Jin, G. X.; Gates, B. D.; Branda, N. R. *Angewandte Chemie-International Edition* **2009**, *48*, 4166-4169.

(13)   An, X. Q.; Zhan, F.; Zhu, Y. Y. *Langmuir* **2013**, *29*, 1061-1068.

(14)   Tong, L.; Zhao, Y.; Huff, T. B.; Hansen, M. N.; Wei, A.; Cheng, J. X. *Advanced Materials* **2007**, *19*, 3136-3141.

(15)   Takahashi, H.; Niidome, T.; Nariai, A.; Niidome, Y.; Yamada, S. *Chemistry Letters* **2006**, *35*, 500-501.

(16)   Giljohann, D. A.; Seferos, D. S.; Daniel, W. L.; Massich, M. D.; Patel, P. C.; Mirkin, C. A. *Angewandte Chemie-International Edition* **2010**, *49*, 3280-3294.

(17)   Levy, R.; Thanh, N. T. K.; Doty, R. C.; Hussain, I.; Nichols, R. J.; Schiffrin, D. J.; Brust, M.; Fernig, D. G. *Journal of the American Chemical Society* **2004**, *126*, 10076-10084.

(18)   Niemeyer, C. M. Angewandte Chemie-International Edition **2001**, 40, 4128-4158.

(19)   Lee, M. T.; Hsueh, C. C.; Freund, M. S.; Ferguson, G. S. *Langmuir* **1998**, *14*, 6419-6423.

(20)   Kudelski, A. Journal of Raman Spectroscopy **2003**, 34, 853-862.

(21)   Schulz, F.; Vossmeyer, T.; Bastus, N. G.; Weller, H. *Langmuir* **2013**, *29*, 9897-9908.

(22)   Ansar, S. M.; Arneer, F. S.; Hu, W. F.; Zou, S. L.; Pittman, C. U.; Zhang, D. M. *Nano Letters* **2013**, *13*, 1226-1229.

(23)   Zhu, T.; Vasilev, K.; Kreiter, M.; Mittler, S.; Knoll, W. *Langmuir* **2003**, *19*, 9518-9525.

(24)   Storm, G.; Belliot, S. O.; Daemen, T.; Lasic, D. D. *Advanced Drug Delivery Reviews* **1995**, *17*, 31-48.

(25)   Liu, J. B.; Yu, M. X.; Ning, X. H.; Zhou, C.; Yang, S. Y.; Zheng, J. *Angewandte Chemie-International Edition* **2013**, *52*, 12572-12576.

(26)   Lankveld, D. P. K.; Rayavarapu, R. G.; Krystek, P.; Oomen, A. G.; Verharen, H. W.; van Leeuwen, T. G.; De Jong, W. H.; Manohar, S. *Nanomedicine* **2011**, *6*, 339-349.

(27)   Boughen, L.; Liggat, J.; Ellis, G. *Clinical Biochemistry* **2010**, *43*, 750-753.

(28)   Donbrow, M.; Azaz, E.; Pillersdorf, A. *Journal of Pharmaceutical Sciences* **1978**, *67*, 1676-1681.

(29)   Witt, D.; Klajn, R.; Barski, P.; Grzybowski, B. A. *Current Organic Chemistry* **2004**, *8*, 1763-1797.

(30)   Wang, H.; Chen, S. F.; Li, L. Y.; Jiang, S. Y. *Langmuir* **2005**, *21*, 2633-2636.

(31)   Bartczak, D.; Kanaras, A. G. *Langmuir* **2010**, *26*, 7072-7077.

(32)   Grzelczak, M.; Perez-Juste, J.; Mulvaney, P.; Liz-Marzan, L. M. *Chemical Society Reviews* **2008**, *37*, 1783-1791.

(33)   Zhang, J. H.; Xi, C. X.; Feng, C.; Xia, H. B.; Wang, D. Y.; Tao, X. T. *Langmuir* **2014**, *30*, 2480-2489.

(34)   Ye, E. Y.; Win, K. Y.; Tan, H. R.; Lin, M.; Teng, C. P.; Mlayah, A.; Han, M. Y. *Journal of the American Chemical Society* **2011**, *133*, 8506-8509.

(35)   Dertli, E.; Coskun, S.; Esenturk, E. N. *Journal of Materials Research* **2013**, *28,* 250-260.

(36)   Ha, T. H.; Koo, H. J.; Chung, B. H. *Journal of Physical Chemistry C* **2007**, *111*, 1123-1130.

(37)   Nehl, C. L.; Liao, H. W.; Hafner, J. H. *Nano Letter*s **2006**, *6*, 683-688.

(38)   Cobley, C. M.; Au, L.; Chen, J. Y.; Xia, Y. N. *Expert Opinion on Drug Delivery* **2010**, *7*, 577-587.

(39)   Chu, H. C.; Kuo, C. H.; Huang, M. H. *Inorganic Chemistry* **2006**, *45*, 808-813.

(40)   O'Brien, M. N.; Jones, M. R.; Brown, K. A.; Mirkin, C. A. *Journal of the American Chemical Society* **2014**, *136*, 7603-7606.

(41)   Xia, Y. N.; Xiong, Y. J.; Lim, B.; Skrabalak, S. E. *Angewandte Chemie-International Edition* **2009**, *48,* 60-103.

(42)   M. S. Zhu, B. Lei, F. F. Ren, P. L. Chen, Y. F. Shen, B. Guan, Y. K. Du, T. S. Li, M. H. Liu *Scientific Reports.* **2014**, *4*, 5259. **DOI:** 10.1038/srep05259.

(43)   Zabetakis, K.; Ghann, W. E.; Kumar, S.; Daniel, M. C. *Gold Bulletin* **2012**, *45*, 203-211.

(44)   Horovitz, O.; Tomoaia, G.; Mocanu, A.; Yupsanis, T.; Tomoaia-Cotisel, M. *Gold Bulletin* **2007**, *40*, 213-218.

(45)   Turkevich, J.; Stevenson, P. C.; Hillier, J. *Discussions of the Faraday Society* **1951**, *11*, 55-75.

(46)   Kimling, J.; Maier, M.; Okenve, B.; Kotaidis, V.; Ballot, H.; Plech, A. *Journal of Physical Chemistry B* **2006**, *110*, 15700-15707.

(47)   Park, J. W.; Shumaker-Parry, J. S. *Journal of the American Chemical Society* **2014**, *136*, 1907-1921.

(48)   Bastus, N. G.; Comenge, J.; Puntes, V. *Langmuir* **2011**, *27*, 11098-11105.

(49)   Polte, J.; Ahner, T. T.; Delissen, F.; Sokolov, S.; Emmerling, F.; Thunemann, A. F.; Kraehnert, R. *Journal of the American Chemical Society* **2010**, *132*, 1296-1301.

(50)   Ojea-Jimenez, I.; Campanera, J. M. *Journal of Physical Chemistry C* **2012**, *116*, 23682-23691.

(51)   Li, Y.; Zaluzhna, O.; Xu, B. L.; Gao, Y. A.; Modest, J. M.; Tong, Y. J. *Journal of the American Chemical Society* **2011**, *133*, 2092-2095.

(52)   Brust, M.; Walker, M.; Bethell, D.; Schiffrin, D. J.; Whyman, R. *Journal of the Chemical Society-Chemical Communications* **1994**, *7*, 801-802.

(53)   Li, Y.; Zaluzhna, O.; Tong, Y. Y. J. *Chemical Communications* **2011**, *47*, 6033-6035.

(54)   Zhu, L. L.; Zhang, C.; Guo, C. C.; Wang, X. L.; Sun, P. C.; Zhou, D. S.; Chen, W.; Xue, G. *Journal of Physical Chemistry C* **2013**, *117*, 11399-11404.

(55)   Perala, S. R. K.; Kumar, S. *Langmuir* **2013**, *29*, 9863-9873.

(56)   Goulet, P. J. G.; Lennox, R. B. *Journal of the American Chemical Society* **2010**, *132*, 9582-9584.

(57)   Li, N.; Zhao, P. X.; Astruc, D. *Angewandte Chemie-International Edition* **2014**, *53*, 1756-1789.

(58)   Xiao, J. Y.; Qi, L. M. *Nanoscale* **2011**, *3*, 1383-1396.

(59)   Park, K.; Drummy, L. F.; Wadams, R. C.; Koerner, H.; Nepal, D.; Fabris, L.; Vaia, R. A. *Chemistry of Materials* **2013**, *25*, 555-563.

(60)   Dasog, M.; Hou, W.; Scott, R. W. J. *Chemical Communications* **2011**, *47*, 8569-8571.

(61)   Zhao, P. X.; Li, N.; Astruc, D. *Coordination Chemistry Reviews* **2013**, *257*, 638-665.

(62)   Frens, G. *Nature-Physical Science.* **1973**, *241*, 20-22.

(63)   Majzik, A.; Patakfalvi, R.; Hornok, V.; Dekany, I. *Gold Bulletin* **2009**, *42*, 113-123.

(64)   Ji, X. H.; Song, X. N.; Li, J.; Bai, Y. B.; Yang, W. S.; Peng, X. G. *Journal of the American Chemical Society* **2007**, *129*, 13939-13948.

(65)   Doyen, M.; Bartik, K.; Bruylants, G. *Journal of Colloid and Interface Science* **2013**, *399*, 1-5.

(66)   Xia, X. H.; Yang, M. X.; Wang, Y. C.; Zheng, Y. Q.; Li, Q. G.; Chen, J. Y.; Xia, Y. N. *ACS Nano* **2012**, *6*, 512-522.

(67)   Aslan, K.; Perez-Luna, V. H. *Langmuir* **2002**, *18*, 6059-6065.

(68)   Zhao, Y.; Wang, Z.; Zhang, W.; Jiang, X. *Nanoscale* **2010**, *2*, 2114-2119.

(69)   Duy, J.; Connell, L. B.; Eck, W.; Collins, S. D.; Smith, R. L. *Journal of Nanoparticle Research* **2010**, *12*, 2363-2369.

(70)   Li, Y.; Zaluzhna, O.; Tong, Y. Y. J. *Langmuir* **2011**, *27*, 7366-7370.

(71)   Goulet, P. J. G.; Bourret, G. R.; Lennox, R. B. *Langmuir* **2012**, *28*, 2909-2913.

(72)   Mourdikoudis, S.; Liz-Marzan, L. M. *Chemistry of Materials* **2013**, *25*, 1465-1476.

(73)   Daniel, M. C.; Astruc, D. *Chemical Reviews* **2004**, *104*, 293-346.

(74)   Lim, B.; Camargo, P. H. C.; Xia, Y. N. *Langmuir* **2008**, *24*, 10437-10442.

(75)   Hoppe, C. E.; Lazzari, M.; Pardinas-Blanco, I.; Lopez-Quintela, M. A. *Langmuir* **2006**, *22*, 7027-7034.

(76)   Wiesner, J.; Wokaun, A. *Chemical Physics Letters* **1989**, *157*, 569-582.

(77)   Jana, N. R.; Gearheart, L.; Murphy, C. J. *Advanced Materials*. **2001**, *13*, 1389-1393.

(78)   Jackson, S. R.; McBride, J. R.; Rosenthal, S. J.; Wright, D. W. *Journal of the American Chemical Society* **2014**, *136*, 5261-5263.

(79)   Almora-Barrios, N.; Novell-Leruth, G.; Whiting, P.; Liz-Marzan, L. M.; Lopez, N. *Nano Letters* **2014**, *14*, 871-875.

(80)   Placido, T.; Comparelli, R.; Giannici, F.; Cozzoli, P. D.; Capitani, G.; Striccoli, M.; Agostiano, A.; Curri, M. L. *Chemistry of Materials* **2009**, *21*, 4192-4202.

(81)   Kinnear, C.; Dietsch, H.; Clift, M. J. D.; Endes, C.; Rothen-Rutishauser, B.; Petri-Fink, A. *Angewandte Chemie-International Edition* **2013**, *52*, 1934-1938.

(82)   Hu, X. G.; Gao, X. H. *Physical Chemistry Chemical Physics* **2011**, *13*, 10028-10035.

(83)   Gole, A.; Murphy, C. J. *Chemistry of Materials* **2005**, *17*, 1325-1330.

(84)   Thierry, B.; Ng, J.; Krieg, T.; Griesser, H. J. *Chemical Communications* **2009**, *13*, 1724-1726.

(85)   Pekcevik, I. C.; Poon, L. C. H.; Wang, M. C. P.; Gates, B. D. *Analytical Chemistry* **2013**, *85*, 9960-9967.

(86)   Pastoriza-Santos, I.; Perez-Juste, J.; Liz-Marzan, L. M. *Chemistry of Materials* **2006**, *18*, 2465-2467.

(87)   Ivanov, M. R.; Haes, A. J. *Analytical Chemistry* **2012**, *84*, 1320-1326.

(88)   Sperling, R. A.; Parak, W. J. Philosophical Transactions of the Royal Society a-Mathematical Physical and Engineering Sciences **2010**, *368*, 1333-1383.

(89)   Niidome, T.; Yamagata, M.; Okamoto, Y.; Akiyama, Y.; Takahashi, H.; Kawano, T.; Katayama, Y.; Niidome, Y. *Journal of Controlled Release* **2006**, *114*, 343-347.

(90)   Kah, J. C. Y.; Zubieta, A.; Saavedra, R. A.; Hamad-Schifferli, K. *Langmuir* **2012**, *28*, 8834-8844.

(91)   Dederichs, T.; Moller, M.; Weichold, O. *Langmuir* **2009**, *25*, 10501-10506.

(92)   Yang, J.; Lee, J. Y.; Ying, J. Y. *Chemical Society Reviews* **2011**, *40*, 1672-1696.

(93)   Lista, M.; Liu, D. Z.; Mulvaney, P. *Langmuir* **2014**, *30*, 1932-1938.

(94)   Cheng, W. L.; Wang, E. *Journal of Physical Chemistry B* **2004**, *108*, 24-26.

(95)   McMahon, J. M.; Emory, S. R. *Langmuir* **2007**, *23*, 1414-1418.

(96)   Brinas, R. P.; Maetani, M.; Barchi, J. J. *Journal of Colloid and Interface Science* **2013**, *392*, 415-421.

(97)   Gandubert, V. J.; Lennox, R. B. *Langmuir* **2005**, *21*, 6532-6539.

(98)   Love, J. C.; Estroff, L. A.; Kriebel, J. K.; Nuzzo, R. G.; Whitesides, G. M. *Chemical Reviews* **2005**, *105*, 1103-1169.

(99)   Snow, A. W.; Jernigan, G. G.; Ancona, M. G. *Analyst* **2011**, *136*, 4935-4949.

(100)   Nuzzo, R. G.; Dubois, L. H.; Allara, D. L. *Journal of the American Chemical Society* **1990**, *112*, 558-569.

(101)   Mei, B. C.; Oh, E.; Susumu, K.; Farrell, D.; Mountziaris, T. J.; Mattoussi, H. *Langmuir* **2009**, *25*, 10604-10611.

(102)   Oh, E.; Susumu, K.; Maekinen, A. J.; Deschamps, J. R.; Huston, A. L.; Medintz, I. L. *Journal of Physical Chemistry C* **2013**, *117*, 18947-18956.

(103)   Dias, D.; Hasse, U.; Fricke, K.; do Nascimento, P. C.; Scholz, F. *Journal of Electroanalytical Chemistry* **2013**, *690*, 121-126.

(104)   Vericat, C.; Vela, M. E.; Salvarezza, R. C. *Physical Chemistry Chemical Physics* **2005**, *7*, 3258-3268.

(105)   Camillone, N.; Chidsey, C. E. D.; Liu, G.; Scoles, G. *Journal of Chemical Physics* **1993**, *98*, 4234-4245.

(106)   Vericat, C.; Vela, M. E.; Benitez, G. A.; Gago, J. A. M.; Torrelles, X.; Salvarezza, R. C. *Journal of Physics-Condensed Matter* **2006**, *18*, R867-R900.

(107)   Nuzzo, R. G.; Zegarski, B. R.; Dubois, L. H. *Journal of the American Chemical Society* **1987**, *109*, 733-740.

(108)   Schonenberger, C.; Jorritsma, J.; Sondaghuethorst, J. A. M.; Fokkink, L. G. J. *Journal of Physical Chemistry* **1995**, *99*, 3259-3271.

(109)   Delamarche, E.; Michel, B.; Biebuyck, H. A.; Gerber, C. *Advanced Materials* **1996**, *8*, 719-729.

(110)   Vericat, C.; Vela, M. E.; Corthey, G.; Pensa, E.; Cortes, E.; Fonticelli, M. H.; Ibanez, F.; Benitez, G. E.; Carro, P.; Salvarezza, R. C. *RSC Advances* **2014**, *4*, 27730-27754.

(111)   Azcarate, J. C.; Corthey, G.; Pensa, E.; Vericat, C.; Fonticelli, M. H.; Salvarezza, R. C.; Carro, P. *Journal of Physical Chemistry Letters* **2013**, *4*, 3127-3138.

(112)   Browne, K. P.; Grzybowski, B. A. *Langmuir* **2011**, *27*, 1246-1250.

(113)   Cheng, H.; Yang, L. N.; Jiang, Y.; Huang, Y. Y.; Sun, Z. H.; Zhang, J.; Hu, T. D.; Pan, Z. Y.; Pan, G. Q.; Yao, T.; Bian, Q.; Wei, S. Q. *Nanoscale* **2013**, *5*, 11795-11800.

(114)   Ansar, S. M.; Haputhanthri, R.; Edmonds, B.; Liu, D.; Yu, L. Y.; Sygula, A.; Zhang, D. M. *Journal of Physical Chemistry C.* **2011**, *115*, 653-660.

(115)   Chinwangso, P.; Jamison, A. C.; Lee, T. R. *Accounts of Chemical Research* **2011**, *44*, 511-519.

(116)   Techane, S. D.; Gamble, L. J.; Castner, D. G. *Journal of Physical Chemistry C* **2011**, *115*, 9432-9441.

(117)   Lanterna, A. E.; Coronado, E. A.; Granados, A. M. *Journal of Physical Chemistry C* **2012**, *116*, 6520-6529.

(118)   Hinterwirth, H.; Kappel, S.; Waitz, T.; Prohaska, T.; Lindner, W.; Lammerhofer, M. *ACS Nano* **2013**, *7*, 1129-1136.

(119)   Zhang, S. S.; Leem, G.; Srisombat, L.-O.; Lee, T. R. *Journal of the American Chemical Society* **2008**, *130*, 113-120.

(120)   Mei, B. C.; Susumu, K.; Medintz, I. L.; Mattoussi, H. *Nature Protocols* **2009**, *4*, 412-423.

(121)   Shon, Y. S.; Lee, T. R. *Journal of Physical Chemistry B* **2000**, *104*, 8192-8200.

(122)   Roux, S.; Garcia, B.; Bridot, J. L.; Salome, M.; Marquette, C.; Lemelle, L.; Gillet, P.; Blum, L.; Perriat, P.; Tillement, O. *Langmuir* **2005**, *21*, 2526-2536.

(123)   Pensa, E.; Cortes, E.; Corthey, G.; Carro, P.; Vericat, C.; Fonticelli, M. H.; Benitez, G.; Rubert, A. A.; Salvarezza, R. C. *Accounts of Chemical Research* **2012**, *45*, 1183-1192.

(124)   Karpovich, D. S.; Blanchard, G. J. *Langmuir* **1994**, *10*, 3315-3322.

(125)   Schessler, H. M.; Karpovich, D. S.; Blanchard, G. J. *Journal of the American Chemical Society* **1996**, *118*, 9645-9651.

(126)   Ravi, V.; Binz, J. M.; Rioux, R. M. *Nano Letters* **2013**, *13*, 4442-4448.

(127)   Kim, M.; Hohman, J. N.; Morin, E. I.; Daniel, T. A.; Weiss, P. S. *Journal of Physical Chemistry A* **2009**, *113*, 3895-3903.

(128) Lee, N. S.; Kim, D.; Kang, H.; Park, D. K.; Han, S. W.; Noh, J. *Journal of Physical Chemistry C* **2011**, *115*, 5868-5874.

(129) Delamarche, E.; Michel, B.; Kang, H.; Gerber, C. *Langmuir* **1994**, *10*, 4103-4108.

(130) Liu, Y. P.; Wang, C. W.; Cai, N.; Long, S. H.; Yu, F. Q. *Journal of Materials Science* **2014**, *49*, 7143-7150.

(131) Chen, M. S.; Goodman, D. W. *Science* **2004**, *306*, 252-255.

(132) Lopez, N.; Janssens, T. V. W.; Clausen, B. S.; Xu, Y.; Mavrikakis, M.; Bligaard, T.; Norskov, J. K. *Journal of Catalysis* **2004**, *223*, 232-235.

(133) Aiken, J. D.; Finke, R. G. Journal of Molecular Catalysis A: Chemical **1999**, 145, 1-44.

(134) Hvolbaek, B.; Janssens, T. V. W.; Clausen, B. S.; Falsig, H.; Christensen, C. H.; Norskov, J. K. *Nano Today* **2007**, *2*, 14-18.

(135) Ortiz, N.; Skrabalak, S. E. *Langmuir* **2014**, *30*, 6649-6659.

(136) Zhen, S. J.; Huang, C. Z.; Wang, J.; Li, Y. F. *Journal of Physical Chemistry C* **2009**, *113*, 21543-21547.

(137) Liu, K.; Resetco, C.; Kumacheva, E. *Nanoscale* **2012**, *4*, 6574-6580.

(138) Ferrier, R. C.; Lee, H. S.; Hore, M. J. A.; Caporizzo, M.; Eckmann, D. M.; Composto, R. J. *Langmuir* **2014**, *30*, 1906-1914.

(139) Selvakannan, P. R.; Dumas, E.; Dumur, F.; Pechoux, C.; Beaunier, P.; Etcheberry, A.; Secheresse, F.; Remita, H.; Mayer, C. R. *Journal of Colloid and Interface Science* **2010**, *349*, 93-97.

(140) Novakova, Z.; Orinakova, R.; Fedorkova, A. S.; Orinak, A. *Journal of Solid State Electrochemistry* **2014**, *18*, 2289-2295.

(141) Pensa, E.; Vericat, C.; Grumelli, D.; Salvarezza, R. C.; Park, S. H.; Longo, G. S.; Szleifer, I.; De Leo, L. P. M. *Physical Chemistry Chemical Physics* **2012**, *14*, 12355-12367.

(142) Pesika, N. S.; Stebe, K. J.; Searson, P. C. *Langmuir* **2006**, *22*, 3474-3476.

(143) Rosendahl, S. M.; Burgess, I. J. *Electrochimica Acta*, **2008**, *53*, 6759-6767.

(144) Vivek, J. P.; Burgess, I. J. *Journal of Physical Chemistry C* **2008**, *112*, 2872−2880.

(145) Du, S. F.; Kendall, K.; Toloueinia, P.; Mehrabadi, Y.; Gupta, G.; Newton, J. *Journal of Nanoparticle Research* **2012**, *14*, 758.

(146) Nel, A. E.; Madler, L.; Velegol, D.; Xia, T.; Hoek, E. M. V.; Somasundaran, P.; Klaessig, F.; Castranova, V.; Thompson, M. *Nature Materials* **2009**, *8*, 543-557.

(147) Chakraborty, S.; Joshi, P.; Shanker, V.; Ansari, Z. A.; Singh, S. P.; Chakrabarti, P. *Langmuir* **2011**, *27*, 7722-7731.

(148) Khan, S.; Gupta, A.; Nandi, C. K. *Journal of Physical Chemistry Letters* **2013**, *4*, 3747-3752.

(149) Tsai, D.-H.; DelRio, F. W.; Keene, A. M.; Tyner, K. M.; MacCuspie, R. I.; Cho, T. J.; Zachariah, M. R.; Hackley, V. A. *Langmuir.* **2011**, *27*, 2464-2477.

(150) Gebauer, J. S.; Treuel, L. *Journal of Colloid and Interface Science* **2011**, *354*, 546-554.

(151) Pellegrino, T.; Kudera, S.; Liedl, T.; Javier, A. M.; Manna, L.; Parak, W. J. *Small* **2005**, *1*, 48-63.

(152) Pfeiffer, C.; Rehbock, C.; Huhn, D.; Carrillo-Carrion, C.; de Aberasturi, D. J.; Merk, V.; Barcikowski, S.; Parak, W. J. *Journal of the Royal Society Interface.* **2014**, *11*, 20130931.

(153) Volkert, A. A.; Subramaniam, V.; Ivanov, M. R.; Goodman, A. M.; Haes, A. J. *ACS Nano* **2011**, *5*, 4570-4580.

(154) Petrovykh, D. Y.; Kimura-Suda, H.; Whitman, L. J.; Tarlov, M. J. *Journal of the American Chemical Society* **2003**, *125*, 5219-5226.

(155) Li, G. T.; Wang, T. Y.; Bhosale, S.; Zhang, Y.; Fuhrhop, J. H. *Colloid and Polymer Science* **2003**, *281*, 1099-1103.

(156) Mayya, K. S.; Patil, V.; Sastry, M. *Langmuir* **1997**, *13*, 3944-3947.

(157) Rouhana, L. L.; Jaber, J. A.; Schlenoff, J. B. *Langmuir* **2007**, *23*, 12799-12801.

(158) Gao, J.; Huang, X. Y.; Liu, H.; Zan, F.; Ren, J. C. *Langmuir* **2012**, *28*, 4464-4471.

(159)   Stewart, M. H.; Susumu, K.; Mei, B. C.; Medintz, I. L.; Delehanty, J. B.; Blanco-Canosa, J. B.; Dawson, P. E.; Mattoussi, H. *Journal of the American Chemical Society* **2010**, *132*, 9804-9813.

Chapter 2.

Long Term Stability of Gold Nanoparticles

2.1. Introduction

The molecular coatings decorating the surfaces of nanoparticles determine, for the most part, the colloidal stability of these particles. These coatings, a single-molecule in thickness, form a barrier between a nanoparticle and its surroundings.[1,2] This barrier protects against the interactions with other particles in solution or various components of the suspending medium (e.g., solvent molecules and dissolved ions). The long-term colloidal stability of nanoparticles depends on the properties of these molecular coatings, such their functionality, uniformity and integrity.[3-5] Degradation of these coatings or non-uniformities therein could lead to a loss of colloidal stability, which is manifest by aggregation and/or precipitation of the nanoparticles.[6,7] Damage to molecular coatings could result from either chemical attack and/or dissolution of these molecules from the surfaces of the nanoparticles.[7-9] Although composition of these molecular coatings can be fine-tuned to improve the stability of nanoparticles,[10-12] their ability to resist degradation will ultimately depend on the uniformity of these coatings. Uniformity of molecular coatings on surfaces is determined by the interactions between and the arrangement of these molecules,[5,11-14] as well as defects therein.[11,15] We demonstrate herein that the methods used to decorate nanoparticles with molecular coatings determine the uniformity of the capping layer and, ultimately, the long-term colloidal stability of the nanoparticles.

An important aspect of preparing nanoparticles with long-term colloidal stability is the choice of their molecular coatings. The composition of these molecules will influence both uniformity of the coating and colloidal stability of the nanoparticle. The structure of these molecules can be classified as three main components that includes a headgroup attaching to the surfaces of the nanoparticle, a functional group interacting with the solution, and a spacer separating this functional group from the headgroup.[1,11,16] Each of these components plays an important role in stabilizing the nanoparticles. The headgroup largely defines the strength of the interactions between the molecular coating and the surfaces of the nanoparticles. These interactions can be covalent or non-covalent in nature. Non-covalent interactions can suffer from an equilibrium between molecules associated with the particle surfaces and those free in solution.[17-19] The dynamics of this process can lead to instabilities in the capping layers, which can be influenced by temperature and composition of the solvent. The spacer can have a variety of molecular lengths and compositions.[20,21] Linear alkyl chains have favorable intermolecular interactions through van der Waals forces that stabilize adjacent molecules within these coatings.[1,11,14] The terminal functional groups interact with the solvent molecules and play a significant role in determining the colloidal properties of the nanoparticles. This terminal group can have a variety of compositions depending on the desired use of the nanoparticles.[16,22] Each component of these molecular coatings plays an integral part in stabilizing the nanoparticles. Non-uniformities within these capping layers could, however, lead to instabilities for the nanoparticles.

Irregularities in the layers capping nanoparticles can be attributed to a number of sources. The source of these irregularities can include non-covalent attachment of molecules that block surface reactive sites (e.g., surfactant molecules that compete for surface sites or misoriented surface reactive molecules),[23-26] as well as defects that are attributed to the relative organization of molecules and/or atoms on the surfaces of the nanoparticles.[16,27] These defects within the molecular coatings could lead to the destabilization of the nanoparticles when exposed to harsh environments, such as elevated temperatures, chemical oxidizers, and/or etchants. Oxidative damage, for example, can lead to the loss of covalently linked molecules from the nanoparticle's surfaces.[28,29] Elevated solution temperatures can induce dissociation of non-covalent molecular coatings from nanoparticles.[14,17,30,31] Damage to molecular coatings on the

45

surfaces of the particles by any of these processes could lead to a loss of colloidal stability. The quality of the molecular coating determines nanoparticle solubility, resistance to aggregation, and ability to resist chemical attack. It is, therefore, essential to understand these molecular-scale coatings. This detailed analysis should include an assessment of both the quality and temperature stability of the molecular coatings, which will determine the long-term stability of the nanoparticles.

In this study, we assess the quality of coatings that stabilize nanoparticles. These studies utilize gold nanoparticles (AuNPs) as a relatively stable platform onto which we assembled molecular coatings of mercaptohexadecanoic acid (MHDA). Mercaptohexadecanoic acid (MHDA) is a long-chain alkanethiol with a terminal carboxylic acid group and was chosen for the preparation of AuNPs with enhanced stability. In addition, the MHDA capped AuNPs were assessed for their colloidal stability, and ultimately the quality of these coatings, when prepared in the presence or absence of a co-surfactant. The addition of a co-surfactant to solutions of AuNPs helps to stabilize the nanoparticles during ligand exchange processes.[32-34] These co-surfactants are ultimately outcompeted for surface sites as Au-S bonds form between the alkanethiol coatings and the surfaces of the AuNPs.[32,33] A series of AuNPs were prepared by varying the time allowed for the formation of MHDA based capping layers, such as for periods from 30 min to 2 days (Figure 2.1). Colloidal stability was compared for MHDA capped nanoparticles prepared either in the presence or absence of polysorbate 20. The goal of these studies was to elucidate the quality of the MHDA coatings on the AuNPs.

We used a set of complementary techniques to assess the quality of the surface coatings on AuNPs. The colloidal solutions of AuNPs were monitored for changes in both their chemical and physical properties. In addition, a complementary study was performed to probe the ability of the capping layers on these AuNPs to resist the attack of a chemical etchant. Potassium cyanide, a gold etchant, was added in excess to suspensions of colloidal AuNPs.[9,29,35-38] Our hypothesis was that the rate of destabilization and dissolution of the AuNPs should be proportional to the quantity and type of defects in their capping layers. Insights from this study create a picture of defects within these molecular layers. Methods presented herein form a set of simple techniques to probe long-term stability of nanoparticles and the quality of their molecular coatings.

46
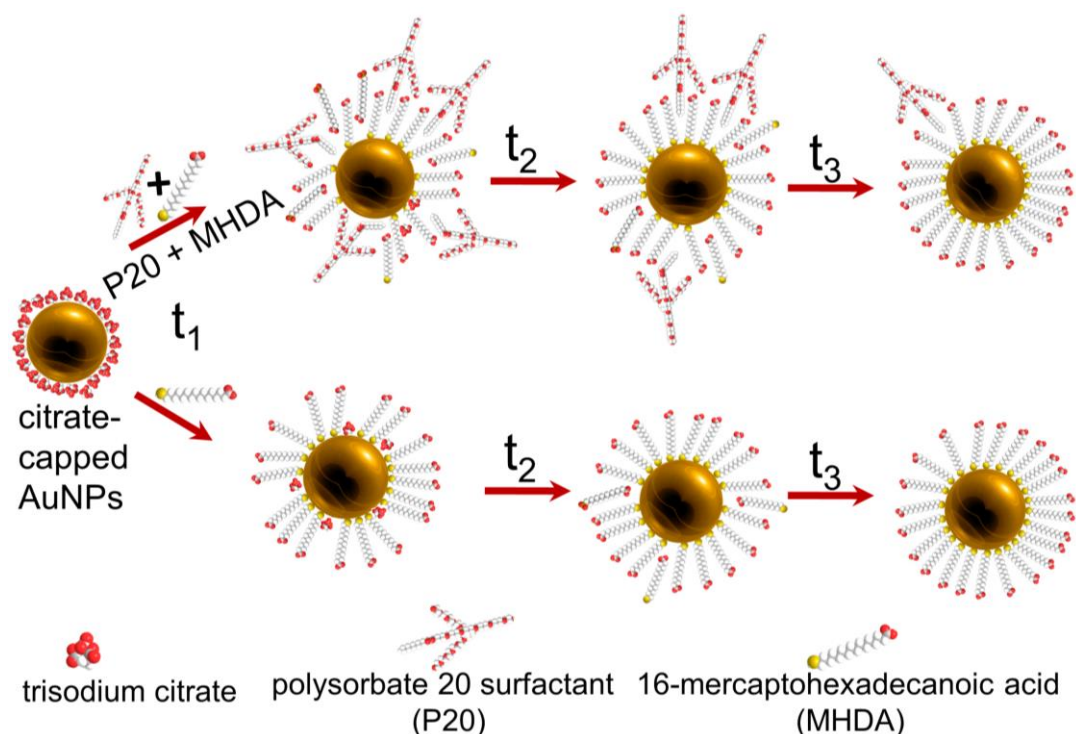
Figure 2.1. **Gold nanoparticles (AuNPs) capped with MHDA and adsorbed P20 co-surfactants (or only with MHDA) as formed by a progressive displacement of a citrate coating as a function of increasing time (t_1 to t_2 to t_3). The quality of each molecular coating varies as a function of the time period allowed for the formation of the new capping layers.**

2.2. Experimental Methods

Synthesis and Characterization of Gold Nanoparticles. Solutions of sodium citrate capped gold nanoparticles were prepared with modifications to a previously published procedure.[1] Glass flasks and Teflon® coated stir bars used in this synthesis were soaked for ~15 min with a 15 mL solution of aqua regia [3:1 (v/v) solution of 37% hydrochloric acid and 70% nitric acid]. *CAUTION: Aqua regia solutions are extremely corrosive. This solution should be handled with extreme care.* The aqua regia soaked flasks and stir bars were rinsed with more than 500 mL of 18 MΩ•cm deionized water

47

produced using a Barnstead NANOpure DIamond Life Science water filtration system. The rinsed flasks and stir bars were further cleaned for 15 min with a ~15 mL of piranha solution [7:2 (v/v) mixture of concentrated 97% sulfuric acid and a 30% hydrogen peroxide]. *CAUTION: Piranha solution is a strong oxidizing agent and reacts violently with organic compounds. This solution should be handled with extreme care.* These flasks and stir bars were subsequently rinsed with >500 mL of 18 MΩ•cm water, and dried at 120°C.

Gold nanoparticles were synthesized from a solution of tetrachloroauric (III) acid ($HAuCl_4•3H_2O$). This solution was prepared by dissolving 100 mg of $HAuCl_4•3H_2O$ (99.9% pure; Sigma-Aldrich, St. Louis, MO, USA) in 50 mL 18 MΩ•cm water to prepare a stock solution of 5.11 mM gold salt. Stock solutions of the gold salt were prepared at least 24 h prior to use. A solution of 0.022 mM sodium citrate tribasic dihydrate (99.0% pure; Sigma-Aldrich, St. Louis, MO, USA) was also prepared by dissolving 6.58 mg of the citrate in 5 mL of 18 MΩ•cm water. For the synthesis of gold nanoparticles, a 1.45 mL aliquot of the gold salt stock solution was diluted to 50 mL in a volumetric flask with 18 MΩ•cm water. The diluted salt solution was transferred to a 250 mL round bottom flask and brought to reflux. Meanwhile, the 5 mL solution of sodium citrate was heated to 60°C and then quickly added to the boiling solution of gold salt. The combined solutions were refluxed for another 10 min. The resulting solutions of gold nanoparticles had a characteristic extinction maximum at 521 nm. Beer's law was used to calculate the concentration of gold nanoparticles using an extinction coefficient of $\varepsilon=8.78\times10^8$ M^{-1} cm^{-1} at the maximum absorbance of the nanoparticles.[2] Extinction spectra were recorded between 300 to 900 nm on a Cary 300-Bio UV-Visible spectrophotometer for solutions contained in polystyrene cuvettes with a 1 cm path length (Starna Cells Inc., Atascadero, CA, USA). These measurements were recorded at room temperature. Ten microliter aliquots of these solutions were also drop cast onto copper transmission electron microscopy (TEM) grids coated with carbon and Formvar (300 mesh; Electron Microscopy Sciences, Hatfield, PA, USA) then dried under vacuum in a desiccator. Diameter of these particles (21±2 nm) was measured from micrographs (Figure 2.2) acquired using a Hitachi H-8000 STEM operating at 200 kV.

Preparation of Gold Nanoparticles Coated with 16-Mercaptohexadecanoic Acid in the Presence of Polysorbate 20 Surfactants. The MHDA was purchased from Sigma-Aldrich (St. Louis, MO, USA) at 90% purity and was used upon receipt without further purification. To prepare the MHDA coated gold nanoparticles, 25 mL of a solution containing the citrate-capped particles (optical density or OD of 0.5; 0.58 nM gold nanoparticles) was mixed with 25 mL of 0.32 M polysorbate 20 (Sigma-Aldrich, St. Louis, MO, USA). This solution was prepared by dissolving 8.32 g polysorbate 20 into 25 mL of a 10 mM phosphate buffered solution at pH 7.2 (sodium phosphate monobasic and sodium phosphate dibasic; Caledon Laboratories Ltd., Georgetown, ON, Canada). This mixture was allowed to sit, undisturbed in a round-bottom flask for 30 min. Then 1.5 mL of freshly prepared 1 mM MHDA (2.89 mg MHDA dissolved in 10 mL of 95% ethanol) was added to the round-bottom flask containing the gold nanoparticles and polysorbate 20 surfactants. The reaction mixture was stirred at 22°C for 30 min, 4 h or 2 days. When the designated period of time for exchange of the capping groups was complete, the MHDA capped gold nanoparticles were transferred to 1.5 mL volume Eppendorf tubes for purification. An aliquot of 1 mL was transferred into each Eppendorf. The alkanethiolate modified gold nanoparticles were purified of excess alkanethiols and polysorbates 20 with 3 steps of centrifugation (13,200 rpm for 10 min), decantation of supernatants, and re-suspension in 10 mM phosphate buffer at pH 7.2. Purified solutions contained 0.45 nM gold nanoparticles.

Preparation of Gold Nanoparticles Coated with 16-Mercaptohexadecanoic Acid without using Polysorbate 20 Surfactants. The gold nanoparticles were also modified with MHDA without the addition of polysorbate 20 (or P20) using the methods described above. The purified solutions contained 0.45 nM gold nanoparticles.

Preparation of Gold Nanoparticles Coated with 16-Mercaptohexadecanoic Acid without using Polysorbate 20 Surfactants, Suspended in a 1 x TBE. A 10 X TBE (TBE: Tris base, boric acid and EDTA) solution at pH 8.0. was prepared using 108 g tris base, 55 g boric acid, and 40 mL of EDTA solution (0.5 M) mixed in 1 L of water, and diluted 10 times. A 1 x TBE running buffer contains 89 mM Tris-base, 89 mM boric acid and 2 mM EDTA. The gold nanoparticles were also modified with MHDA without the

addition of polysorbate 20 (or P20), purified using the methods described above, and suspended in a 1 x TBE buffer.

Monitoring the Colloidal Stability of Monolayer Protected Gold Nanoparticles as a Function of Temperature. The stability of MHDA modified gold nanoparticles with and without the addition of polysorbate 20 surfactants were separately tested at different temperatures over the period of ~1 month (or 672 h). These solutions were maintained at either 22.0±0.3°C, 37.0±0.5°C, or 45.0±0.5°C using microprocessor controlled Precision 280 water baths from ThermoScientific. For consistency between the experiments, each synthesis of gold nanoparticles was divided into 3 equal portions. All of these portions were evaluated in parallel, but each portion was tested at a different incubation temperatures. The study discussed in detail below focuses on data collected over time starting with an initial gold nanoparticle concentration of ~0.5 nM dispersed in phosphate buffer at pH 7.2. All solutions were held in 20 mL liquid scintillation vials (VWR, Edmonton, AB, Canada) at the set temperature without agitation and in the absence of light during the course of the experiments. The monolayer capped gold nanoparticles were monitored during the month-long studies by a combination of extinction spectroscopy, zeta potential (ZP) measurements and dynamic light scattering (DLS) based particle size analysis (PSA) measurements (Malvern Zetasizer Nano-ZS). Each measurement was taken at regular intervals (0, 24, 48, 72, 168, 336, and 672 h) during these studies. Extinction spectra were recorded (300 to 900 nm on a Cary 300-Bio UV-Visible spectrophotometer) for every solution of gold nanoparticles held at different temperatures (22, 37, or 45°C) after each interval of time. All solutions were shaken prior to the acquisition of each extinction spectrum. This agitation dispersed particles that had settled from solution. A portion of these suspended particles were transferred to a cuvette to measure their extinction spectra. Minimal changes in the scattering of light at wavelengths higher than 600 nm suggests that there are very few changes to the concentration of suspended aggregates throughout these experiments. The peak intensity at 523 nm correlates with concentration of nanoparticles in solution; a decreased intensity indicated precipitation of nanoparticles.

At the same time intervals, we also acquired the PSA and ZP measurements on each of these solutions using folded capillary cells (Malvern, Westborough, MA, USA. Part number DTS 1060). The volume of the cells is 0.75 mL. The capillary cells were cleaned by injection of 0.6 mL of ethanol through the cell using a 10 mL syringe. Ethanol solution was flushed through the cells 3 times. These cleaned capillary cells were rinsed with 10 mM phosphate buffer at pH 8.0. The rinsing solutions were removed prior to loading solutions of nanoparticles. Intensity of the back-scattered light was measured at an angle of 173° from the incident He-Ne laser (633 nm).

Aside from the influence of temperature, the pH and composition of the buffer solution can also influence the stability of the monolayer protected gold nanoparticles. For these studies, the gold nanoparticles stabilized either with or without polysorbates and MHDA coatings prepared over a period of 2 days were suspended in a series of different buffers. These buffers, each at an ionic strength of 10 mM, included: i) phosphoric acid/sodium phosphate monobasic (pH 3.0); ii) acetic acid/sodium acetate (pH 5.0); iii) sodium phosphate monobasic/sodium phosphate dibasic (pH 7.2); iv) sodium phosphate dibasic (pH 9.1); and v) sodium carbonate (pH 11.2). The primary discussion in this study focuses on solutions with a pH of 7.2. Further data is included for results pertaining to nanoparticles dispersed in each of the buffered solutions mentioned above (Figure 2.23).

X-ray Photoelectron Spectroscopy (XPS) Analysis of Gold Nanoparticles. Solutions of gold nanoparticles (MHDA-capped with and without the addition of polysorbate 20) were prepared as outlined above. These solutions were divided into two portions for XPS analyses. For one portion, freshly prepared and purified solutions were centrifuged at 13,200 rpm for 10 min, their supernatants decanted and the samples drop-cast onto polished Si substrates (Silicon Sense Inc.) for XPS analysis. The second portion of the solutions were purified of excess thiol and surfactants by centrifugation at 13,200 rpm for 10 min and a subsequent decantation of supernatants, and then stored at 22°C for 1 month (without agitation and in the absence of light) prior to XPS analysis.These XPS analyses were performed using a Kratos Analytical Axis Ultra DLD spectrometer using a monochromatic aluminum source (AlKα; 1486.6 eV) operating at 150 W. Composition was first analyzed with survey scans acquired with a pass energy of

160 eV, while a pass energy of 20 eV was used in acquiring high resolution scans. All analyses were obtained under a Hybrid lens mode, which permitted a wider collection angle of the emitted photoelectrons to increase the signal-to-noise of the data. Data were collected from an analysis area of 700 μm by 300 μm, and analysis of this data was performed using Vision 2.2.7 Processing software. The S_{2p} XPS signals were fit with doublets that had a separation of 1.18 eV and an area ratio of 2:1 between $S_{2p3/2}$/$S_{2p1/2}$.[3] All background corrections were performed using a Shirley fit.

Testing the Stability of Monolayer Protected Gold Nanoparticles Against KCN Etching. The stability of MHDA modified gold nanoparticles with and without the addition of polysorbate 20 surfactants were tested by adding 100 µL of aqueous 1 M potassium cyanide (>97% pure; Alfa Aesar, Ward Hill, MA, USA) to a 2 mL purified solution of the modified gold nanoparticles (optical density 0.16, 0.18 nM AuNPs) in polystyrene cuvettes. *CAUTION: Potassium cyanide is extremely hazardous. It can cause adverse health effects when inhaled or absorbed through the skin. Handle and dispose of appropriately.* Extinction spectra were recorded (400 to 700 nm on a Cary 300-Bio UV-Visible spectrophotometer) immediately following addition of KCN to the nanoparticle solutions. The extinction spectra were acquired at 0.5 min intervals for a period of up to 30 min while incubating the nanoparticles with KCN.

2.3. Results and Discussion

The quality of molecular coatings on nanoparticles directly influences their long-term physicochemical stability. Defects in these molecular coatings will influence their ability to resist changes in size, composition and colloidal stability at elevated temperatures or under harsh chemical environments. The ability of nanoparticles to resist these changes will depend on the composition, uniformity and integrity of these coatings. This interface between the nanoparticles and their surroundings determines how these particles interact with each other, as well as with molecules or ions dissolved in the solution. It has been demonstrated previously that a key factor in determining the quality of molecular coatings on gold surfaces are the methods used to prepare these molecular coatings.[3-5,20,22,39] Our goal was to assess the long-term physicochemical stability of gold colloids modified with molecular coatings. Knowledge learned from these

studies can be used to guide the improvement of the quality of molecular coatings on nanoparticles.

One method to monitor the colloidal stability of AuNPs and to indirectly assess the stability of their molecular capping layers is through measuring changes in their extinction spectra. Faraday's gold colloidal suspensions on display at the Royal Institution in London still exhibit a brilliant red coloration after >150 years.[40] The localized surface plasmon resonance (LSPR) of a gold colloid that gives rise to this coloration is an indication of the particle's shape, size and composition.[41] We monitored the extinction spectra over a period of up to a month to assess changes in stability of the suspended particles. The intensity of the particles' extinction spectra was also monitored as an indication of changes in concentration of suspended nanoparticles.[42,43] During these month-long studies, the composition and temperature of the solutions were kept constant. Particles were suspended in a buffered solution at pH 7.2 and maintained at 22, 37 or 45°C. This study compared the colloidal stability of particles with molecular coatings prepared from MHDA either in the presence or absence of the polysorbate 20 (or P20) co-surfactants, but the results could have implications for the long-term stability of other nanoparticles.

This extinction maximum shifted from 521 nm for the as synthesized citrate-capped AuNPs to 523 nm upon modification of the nanoparticles with MHDA, due to change in the dielectric constant of the nanoparticle surrounding the surfaces of gold nanoparticles. The intensity of the LSPR peaks at 523 nm gradually decreased over the one month period for all suspensions of AuNPs, suggesting that some particles precipitated out of solution. A large decrease in spectral intensity was observed for those gold colloids held at 45°C (Figure 2.4) in comparison to those suspensions maintained at 22°C (Figure 2.2) and 37°C (Figure 2.3). There was, however, no increase in spectral scattering or shift in position at the maximum intensity of the LSPR peaks for any of these solutions of gold colloids. It is possible that the increase in the temperature at 45°C increases the mass transport of solutes to and from the surfaces of the colloids. This increased mass transport could result in removal of adsorbed species from the surfaces of the nanoparticles, which promotes destabilization of the nanoparticles. These destabilized gold particles would likely irreversibly precipitate from the phosphate

53

buffered solution. The impact of the increased mass transport was detrimental to samples held at 45°C, but the destabilization of the colloids manifests itself slowly over the period of 1 month. There was a negligible change in spectral intensity from 24 to 72 h in most samples, but a more substantial decrease in the LSPR intensity was observed after 1 week. The concentration of nanoparticles in solution continued to decrease over time (Figure 2.4). The fastest decrease in concentration of colloidal gold was observed for those nanoparticles whose molecular coatings of MHDA were prepared over the shortest period of time (Figure 2.4a). In general, the colloidal stability of the MHDA capped AuNPs increased in proportion to the time allowed for the assembly of these molecular coatings. The same trend was observed at all temperatures studied here (i.e. 22, 37 and 45°C). All suspensions of AuNPs capped with MHDA formed over a relatively short period of time exhibited the most dramatic decrease in colloidal stability irrespective of solution temperature over the month long studies. Each study was performed in quadruplicate with the same trends observed as those reported herein. Significant variations were observed when comparing particles whose capping layers were prepared either in the presence or absence of the P20 co-surfactant. For example, the particles prepared without the co-surfactant were most stable at 45°C over the period of 1 month, but those prepared with the co-surfactant exhibited more stability at 22 and 37°C over the same period of time. These observed differences will be discussed in further detail below. These different trends are sometimes obvious when comparing the extinction spectra, but more subtle changes in each of the observed trends are difficult to discern. This data was converted to percent change in relative concentration of colloidal AuNPs to provide a more quantitative measure of changes in their long-term stability.
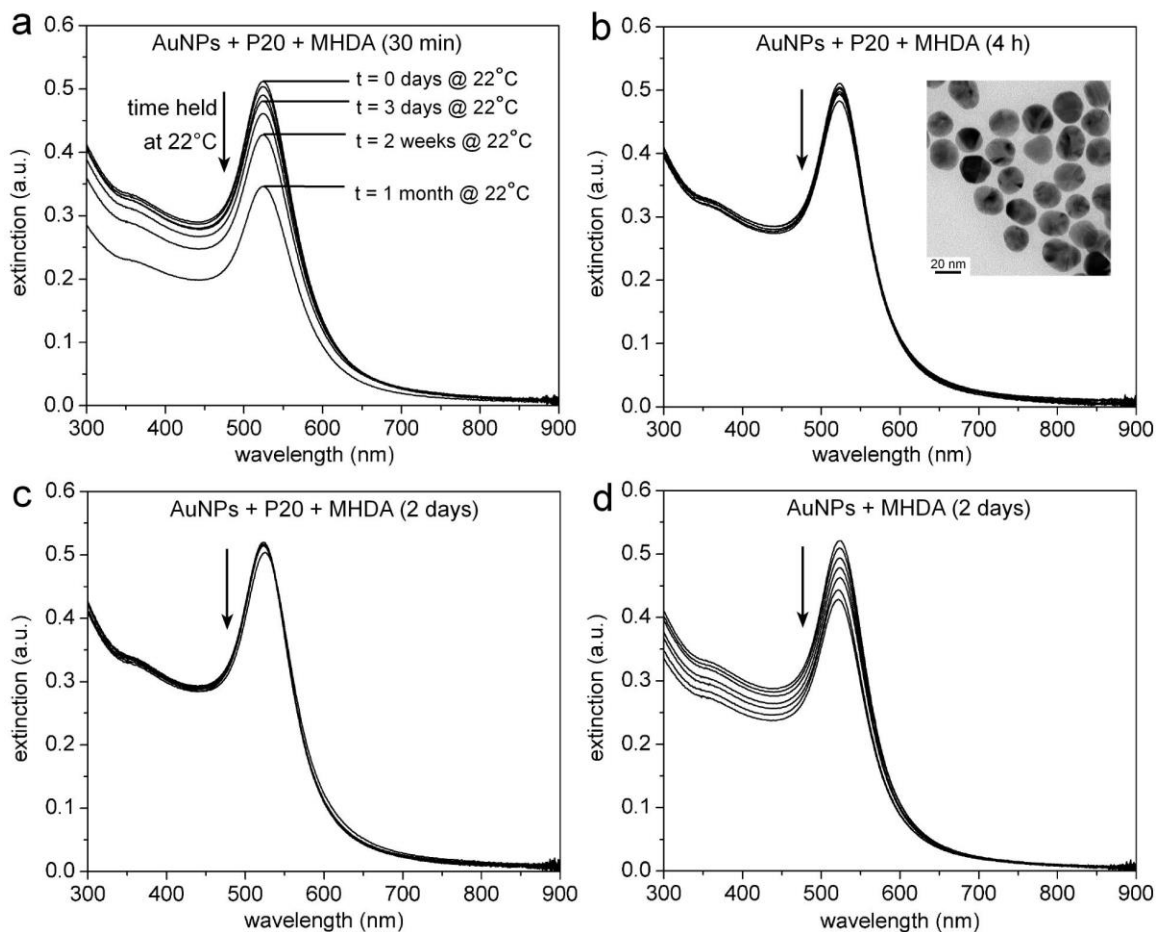
Figure 2.2. **Stability of AuNPs solutions with capping layers that were prepared by immersing the gold nanoparticles (AuNPs) in 16-mercaptohexadecanoic acid (MHDA) for either 30 min, 4 h, or 2 days (as indicated by the labels on each spectrum). These particles were held at 22°C and stability was assessed as a function of change in their extinction spectra. These AuNPs were capped with a molecular coating of MHDA prepared either in the (a-c) presence or (d) absence of a polysorbate 20 (P20) co-surfactant. Inset is a representative transmission electron microscopy (TEM) image of AuNPs stabilized with a mixture of MHDA and P20.**
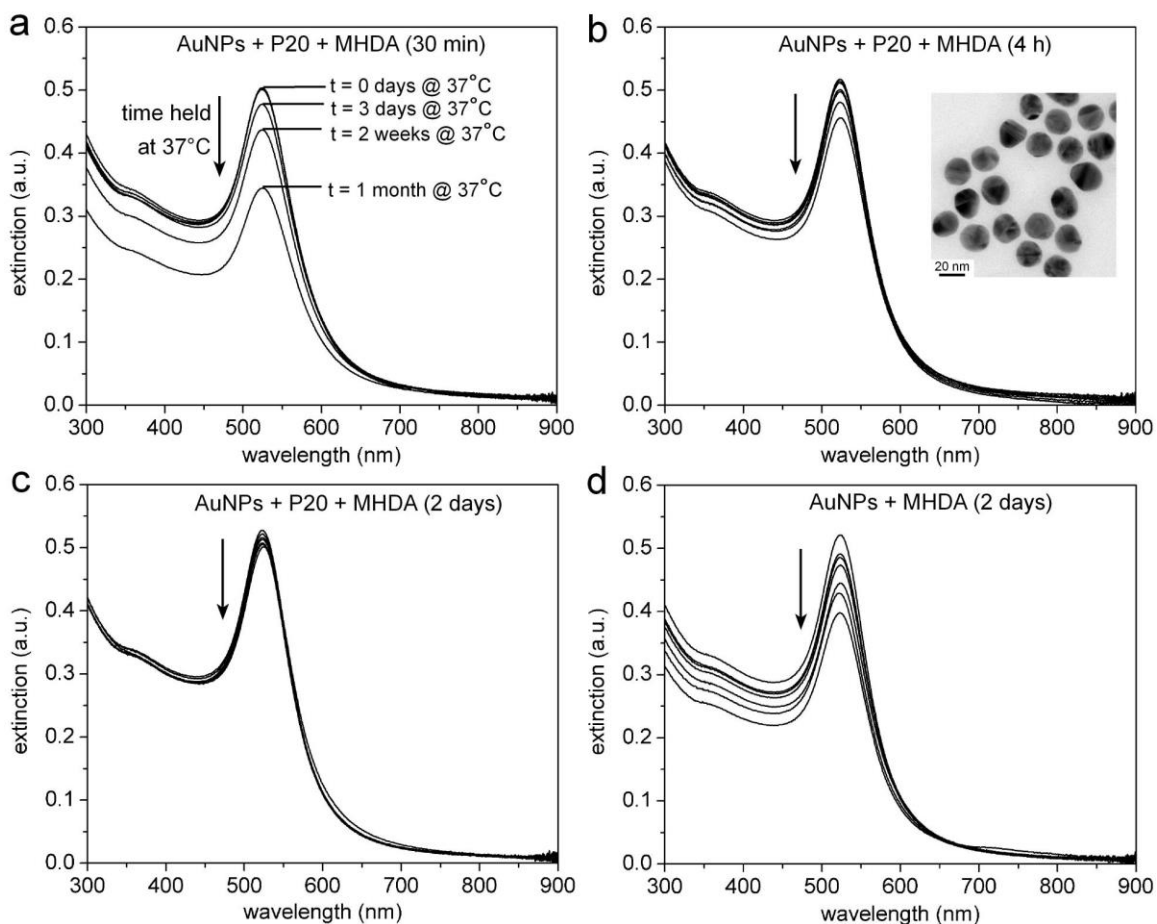
Figure 2.3. Stability of gold nanoparticles (AuNPs) solutions that were prepared by immersing AuNPs in MHDA for 30 min, 4 h, or 2 days. Stability was monitored by obtaining extinction spectra at regular intervals over a period of 1 month for these solutions held at 37°C. These gold nanoparticles were capped with a mixture of MHDA and P20 (a-c) or with only MHDA (d). The inset shows a representative TEM image of the as-made AuNPs capped with MHDA and P20.
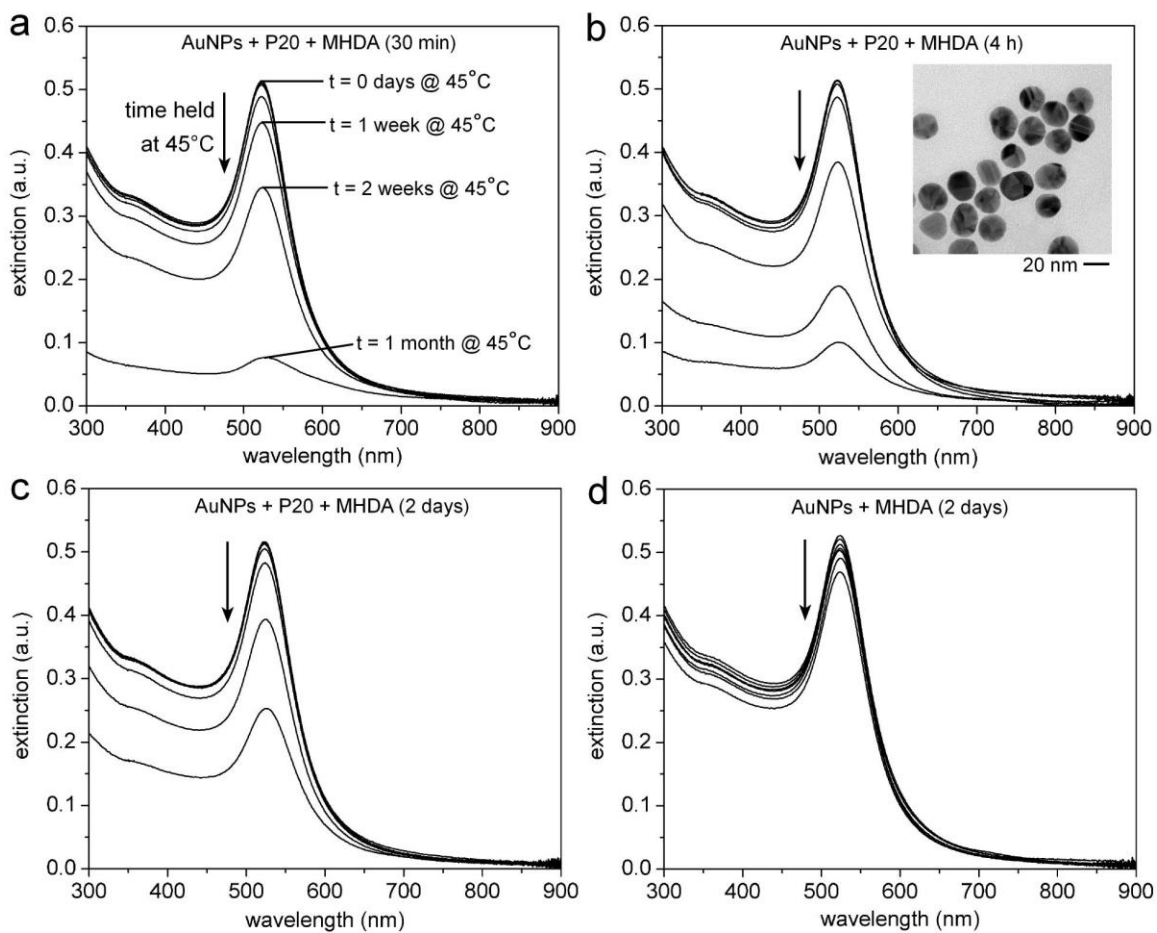
Figure 2.4. **Stability of colloidal AuNPs solutions that were prepared by immersing AuNPs in MHDA for either 30 min, 4 h, or 2 days. Stability was monitored by obtaining extinction spectra at regular intervals over a period of 1 month for these solutions held at 45°C. These AuNPs were capped with MHDA and P20 (a-c) or with only MHDA (d). The inset shows a representative TEM image of the as-made AuNPs capped with MHDA and P20.**

A simple method is needed to compare the relative rates of change in colloidal stability. One approach is to plot the relative percent change in maximum LSPR intensity recorded at specific time intervals for the same nanoparticle solution. These relative changes can be correlated to the concentrations of suspended particles, which will be discussed in more detail below. In this study, the LSPR peak associated with the MHDA capped AuNPs is consistently centered at 523 nm, but the intensity of this peak decreases at different rates depending on the method used to prepare the coating layers and the conditions of each experiment. Distinct differences are observed when comparing the changes in maximum LSPR intensity at 523 nm for gold colloids capped with MHDA and polysorbates that are held at 22, 37 and 45°C for a period of up to 1 month (Figure 2.5a-c). Error bars on these plots indicate the reproducibility of each trend as determined by one standard deviation from the mean of four independent experiments.

Solutions of AuNPs capped with a mixture of MHDA and polysorbates or with only MHDA over these 1 month studies exhibited variations in the relative change of their colloidal stability that depended on both the initial time allowed for the formation of the molecular coatings and the solution temperature throughout the course of the study (Figure 2.5). The concentration of particles capped with coatings formed over 30 min decreased by ~19±4%, 40±1% (or 0.20 nM) and ~85±2% after being held for 1 month at 22, 37, and 45°C, respectively (Figure 2.5a). Those particles capped with molecular layers formed over 4 h decreased by 7±2%, 15±8% (or 0.08 nM), and 75±9% when held for one month under the same conditions (Figure 2.5b). The most stable colloids of this series were those capped with monolayers formed over a period of 2 days. These solutions had a decrease of ~7±0.3%, ~2±2%, and ~50±0.1% in their maximum LSPR intensity when held for 1 month at 22, 37 and 45°C, respectively (Figure 2.5c). The AuNPs immersed in MHDA over shorter periods of time (e.g., 30 min and 4 h) most likely have less MHDA bound to the gold surfaces and a higher relative number of polysorbate molecules covering their surfaces due to an insufficient amount of time allowed for the displacement of P20 and formation of a complete monolayer of MHDA molecules. It could be that the lower quality of these monolayers leads to a greater particle instability over the month-long experiments. Particles stabilized with more densely packed

monolayers of MHDA, such as those with coatings prepared by the immersion of AuNPs in MHDA over a period of 2 days, were more stable and exhibited slower rates of spectral change. When prepared without addition of polysorbates, these particles also had an increased stability while stored over the 1 month at 45°C. The concentration of particles, capped with molecular coatings formed over 2 days in the absence of polysorbates, decreased by ~16±4%, 21±4%, and ~16±6% after being held for 1 month at 22, 37 and 45°C, respectively (Figure 2.5d). Table 2.1 summarizes the percent relative change in extinction maxima (at 523 nm) for AuNPs held at 22, 37 and 45°C for 1 month. The presence of P20 during preparation of the MHDA monolayers improves initial colloidal stability of gold during this capping procedure; ~10% of the particles precipitated from solution when MHDA capping layers were formed in the absence of P20. However, an incomplete displacement of P20 by MHDA would lead to a higher relative number of defects in the MHDA monolayer. It could be that the higher temperature (45°C) is necessary to desorb the remaining P20 from the AuNPs. In addition to an increased mass transport between the surfaces of the gold colloids and the suspending medium, the higher temperature could also initiate an increase in the oxidative damage of the surfactants. Hydrodynamic diameters were measured to further assess the stability of the AuNPs when held for 1 month at 22, 37 and 45°C (Figure 2.7). These measurements indicated an increase in hydrodynamic diameter for AuNPs capped with a mixture of MHDA and P20. The results also indicated an increase in hydrodynamic diameter and particle instability due to aggregation or flocculation for AuNPs stabilized by MHDA and P20 when heated to 45°C. Surface potentials for AuNPs prepared in the presence of P20 increased from −30 to −40 mV over 1 month while incubated at 45°C (Figure 2.8). The elevated temperature increases mass transport to and from the surfaces of the AuNPs, and accelerates degradation of P20. These processes could decrease shielding of a particle's surfaces by P20 surfactants, which would increase the apparent charge density on these particles and the solution pH might also change as a result of the added ions. The similarities in particle and surfactant instabilities observed at 45°C could be due to thermally initiated degradation of polysorbates.[44-46] Degradation of the P20, dissolved molecular oxygen, and the high concentrations of salt in solution result in an oxidizing environment.[6,29,44] Oxidation of the sulfur headgroups of MHDA would lead to its subsequent desorption and the consequent destabilization of the AuNPs. The observed differences between particles

prepared in the presence and absence of P20, and the relatively high rates of precipitation for those co-stabilized with P20, suggest that degradation of P20 could be a major contributor to particle instabilities at 45°C. Further insight into the observed differences in colloidal stability and its correlation to the quality of the MHDA monolayers was obtained using additional analytical techniques.
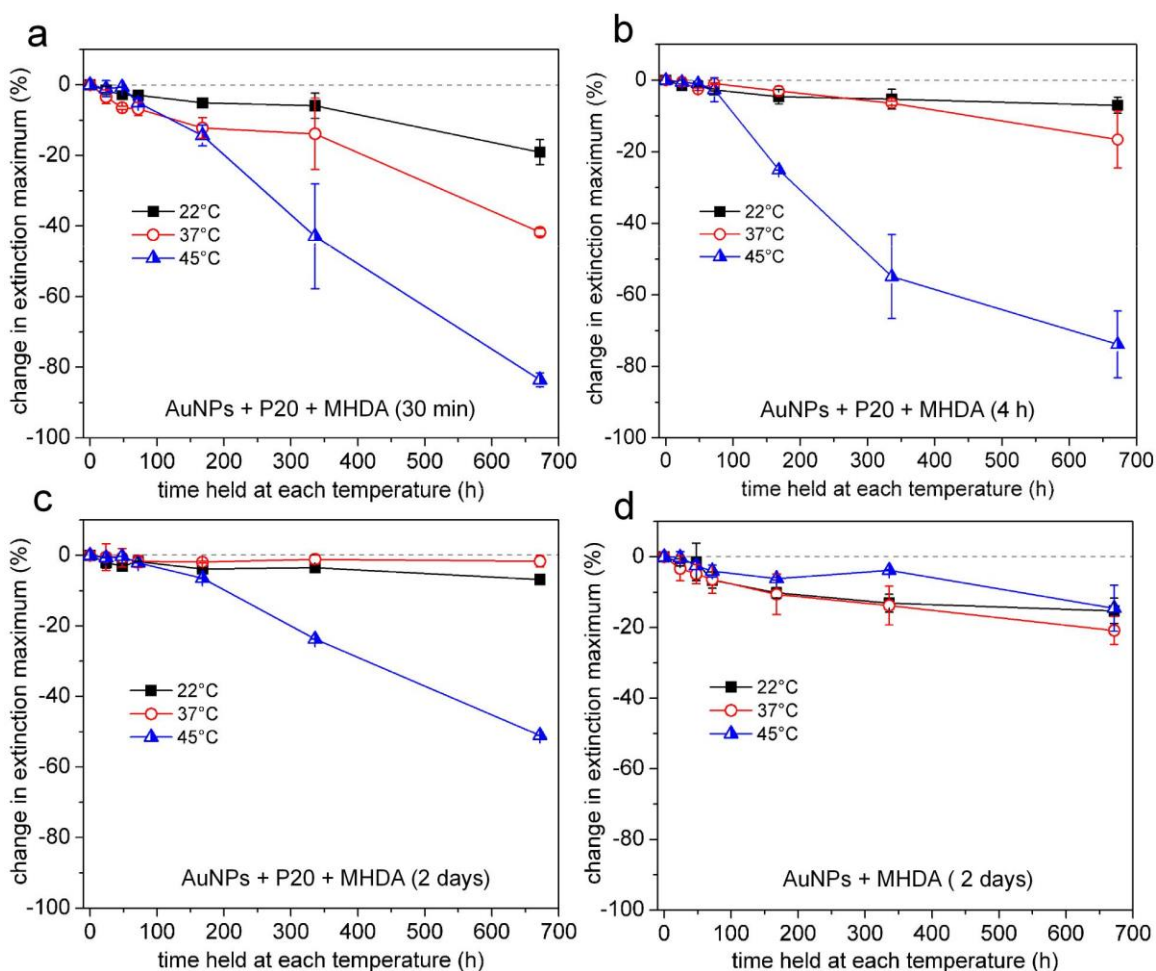
Figure 2.5. Changes in extinction maximum at 523 nm (relative to t=0 days) for suspensions of AuNPs as a function of time (e.g., 1 day, 1 week, or 1 month) held at 22, 37, or 45°C.

Table 2.1.   Comparison of Gold Colloid Stability After One Month

composition of nanoparticle and it's surface chemistry	change in extinction maximum at 523 nm after 1 month		
	22°C	37°C	45°C
AuNPs + P20 + MHDA (30 min)	− 19 ± 4 %	−40 ± 1 %	−85 ± 2 %
AuNPs + P20 + MHDA (4 h)	−7 ± 2 %	−15 ± 8 %	−75 ± 9 %
AuNPs + P20 + MHDA (2 days)	−7 ± 0.3 %	−2 ± 2 %	− 50 ± 0.1 %
AuNPs + MHDA (2 days)	−16 ± 4 %	−21 ± 4 %	−16 ± 6 %

Degradation of the MHDA and polysorbates protecting the colloidal gold can lead to flocculation and aggregation of these particles. Flocculation of nanoparticles would increase their hydrodynamic diameter as measured by dynamic light scattering analysis. All solutions of gold nanoparticles had a consistent hydrodynamic diameter of ~35 nm while suspended in a phosphate buffer solution for ~1 month at 22°C (Figure 2.7). Error bars in these plots are calculated as one standard deviation from the mean of four independent experiments. This distribution in the measured hydrodynamic diameters is most likely attributable to variations in the diameters of gold nanoparticles in solution, as well as a non-uniform distribution of adsorbed polysorbate 20 surfactants between different nanoparticles. Average diameter of the as-prepared gold nanoparticles is 21±2 nm by TEM analysis (Figure 2.6). The larger diameters reported from the PSA measurements are attributed to both the electrostatic double layer on the alkanethiolate-capped gold nanoparticles and the adsorbed polysorbate 20 surfactants. The majority of particle diameters, whether measured by PSA or TEM analysis, are consistent throughout the month-long experiments (Figures 2.2 and 2.7). Solutions of nanoparticles held at both 22°C and 37°C had consistent hydrodynamic diameters of ~35 nm and ~33 nm, respectively, throughout these studies. The smaller hydrodynamic diameter at 37°C could be associated with a temperature dependent redistribution and/or degradation of the molecules stabilizing these particles (Figures 2.7a, 2.7c). A slight deviation from this trend was observed for nanoparticles capped with SAMs formed over 4 h after being held at 37°C for 1 month (Figure 2.7b). In addition, the hydrodynamic diameter increased to ~47 nm for particles stabilized with SAMs formed over either 4 h or 2 days when held at 45°C. A significantly larger increase in hydrodynamic diameter is observed for particles stabilized with SAMs prepared over 30 min and stored at 45°C over the course

of 1 month (Figure 2.7a). Aggregates were not observed in the TEM analysis for samples stored at 45°C for one month, although black precipitates were observed at the bottom of these solutions. The presence of precipitates and the increased hydrodynamic diameters of the particles held at 45°C indicate a degradation of the capping layers on the surfaces of the gold. Another indication of the quality of this stabilizing layer, although an indirect measurement of stability, is the surface potential of the nanoparticles.
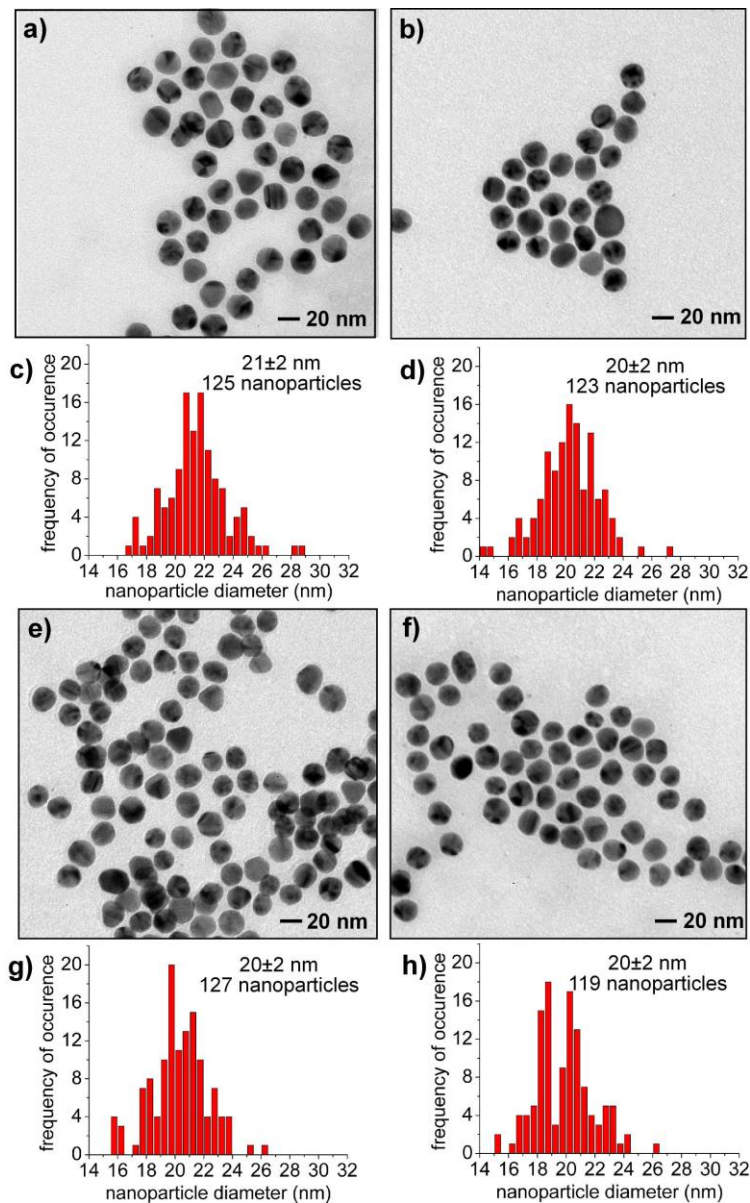
Figure 2.6. **(a) Transmission electron microscopy (TEM) images of gold nanoparticles stabilized with monolayers of 16-mercaptohexadecanoic acid (MHDA) and polysorbate 20 (P20) surfactants formed over 2 days. These particles were reanalyzed by TEM after suspension in a phosphate buffered solutions for 1 month at (b) 22°C, (e) 37°C, and (f) 45°C. Each average diameter of the particles was calculated from measurements made from over 100 nanoparticles in a given sample. Histograms and the mean diameters are reported for (c) as prepared nanoparticles, as well as those particles held for one month at (d) 22°C, (g) 37°C, and (h) 45°C.**
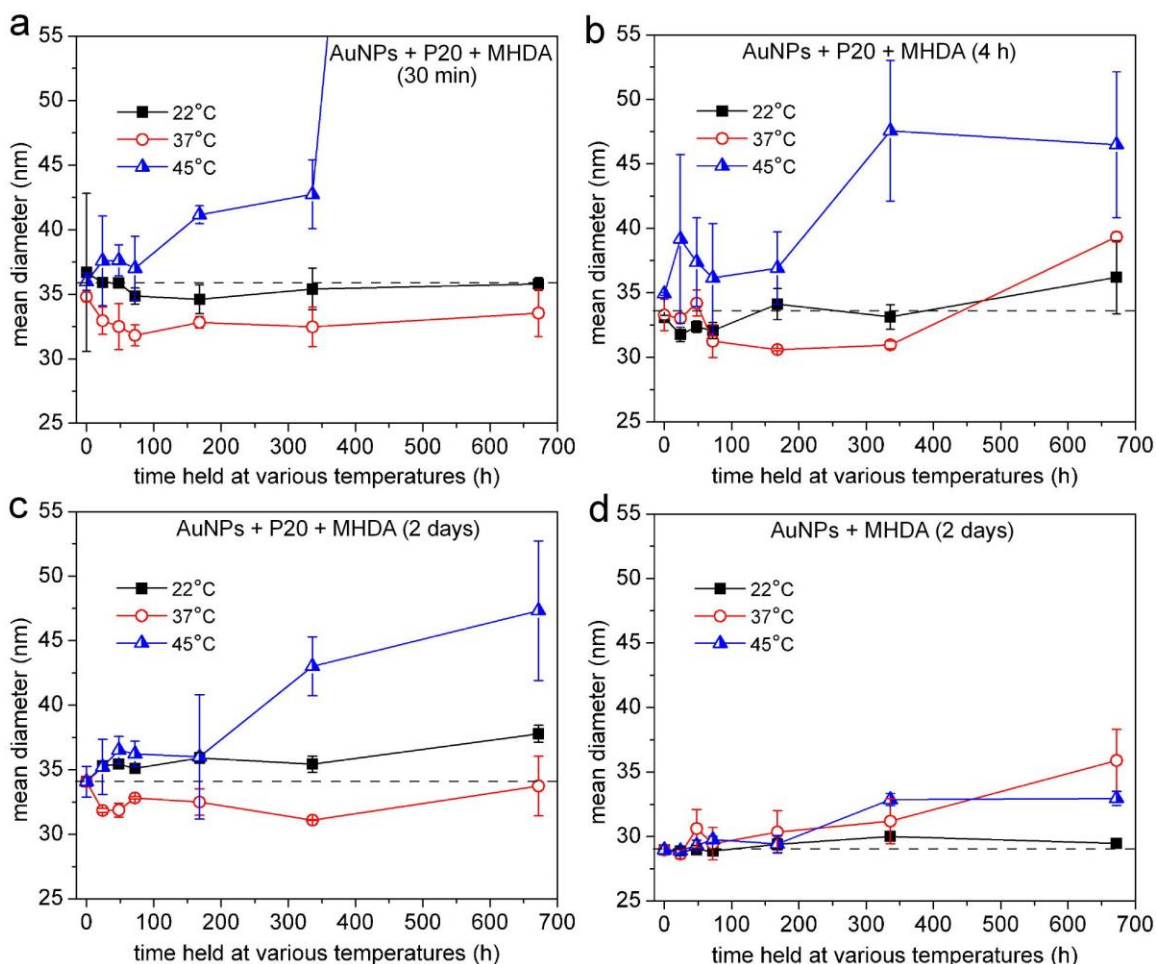
Figure 2.7. **Hydrodynamic diameters of AuNPs measured by dynamic light scattering measurements. Particle size was monitored over a period of 1 month for particles prepared by their immersion in MHDA in the presence of polysorbate surfactants for (a) 30 min, (b) 4 h, (c) 2 days, or for (d) 2 days in the absence of polysorbate surfactants. A portion of each type of sample was held at 22°C, 37°C, or 45°C for the period of 1 month. Error bars in these plots are calculated as one standard deviation from the mean of four independent experiments.**

A simple technique to measure surface potential of the nanoparticles is through zeta potential analysis. Nanoparticles decorated with MHDA and polysorbate 20 surfactants in phosphate buffered solution at pH 7.2 have an average ZP of –30 mV. This value is in the range of acceptable values for stable dispersions of nanoparticles, but a deviation from this value could indicate instability of the colloidal particles. The ZP value progressively changes over the course of a month for the colloids stored at 22, 37

or 45°C (Figure 2.8). Those nanoparticles stabilized with MHDA monolayers assembled in the presence of polysorbate 20 over either 30 min or 4 h have a ZP value of –9 mV after ~1 month (Figures 2.8a and 2.8b). In contrast, the ZP for particles capped with SAMs formed over 2 days changed to –18 mV after one month (Figures 2.8c and 2.8d). These results, in combination with the observation that these solutions exhibit little precipitation or flocculation, suggest that the observed changes in ZP values are due to alterations of the surface chemistry or double layer of the gold colloids. One possibility for these observed changes is a decreased density of the SAMs on the surfaces of the nanoparticles due to oxidative damage and loss of alkanethiolates. Another possibility is a re-distribution of the loosely adsorbed polysorbate 20 surfactants, or its degradation products, over the surfaces of the colloids.[30] Polysorbate 20 surfactants degrade by oxidative damage as a function of pH and temperature.[54-56] Increasing the solution temperature to 45°C promotes further degradation of polysorbate 20 surfactants, as well as an increase in mass transport to and from the surfaces of the nanoparticles. Both processes decrease the shielding of the surface potential by the polysorbate 20 surfactants. This change is most dramatically observed for the nanoparticles capped with polysorbate 20 and MHDA SAMs formed over 30 min, which exhibit an increase in ZP to –40 mV after 1 week at 45°C (Figure 2.8a). The ZP for these particles continued to change to –22 mV over the course of 1 month at 45°C. The most likely mechanism for the change in ZP values is the reorganization and potential degradation of polysorbate 20 surfactants. It is likely that the particles protected with SAMs prepared over 2 days had less polysorbate 20 surfactants adsorbed on their surfaces because of more densely packed monolayers and, therefore, exhibited a smaller change in ZP values over the course of 1 month.
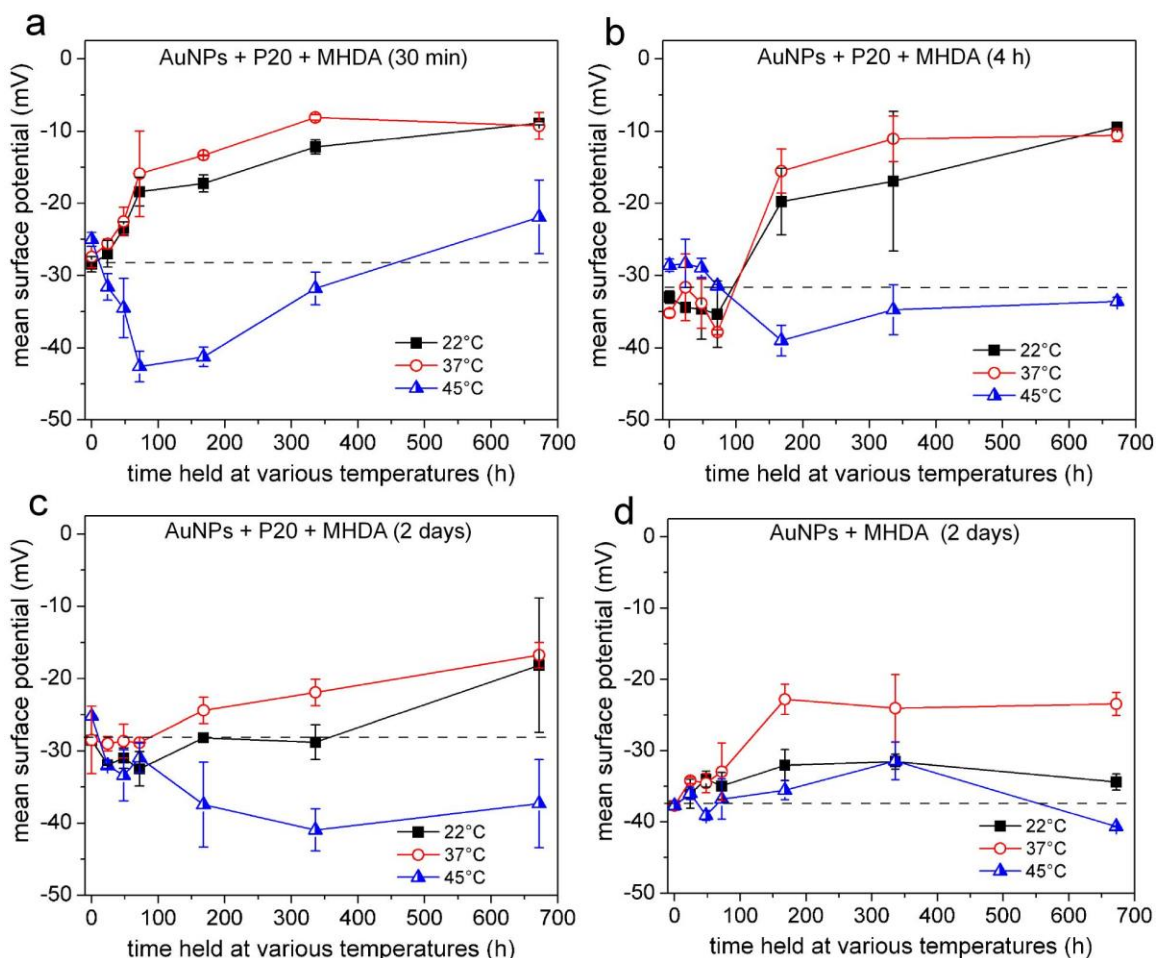
Figure 2.8. **Mean surface potentials for gold nanoparticles suspended in phosphate buffered solutions that are held at 22°C, 37°C, or 45°C for 1 month. The MHDA monolayers capping these nanoparticles were formed either in the presence of polysorbate surfactants over (a) 30 min, (b) 4 h, or (c) 2 days or in the absence of P20 over 2 days (d). Error bars in these plots are calculated as one standard deviation from the mean of four independent experiments.**

Mercaptohexadecanoic acid (MHDA)-modified nanoparticles were further analyzed by XPS. Survey scans for both freshly prepared gold nanoparticles and 1 month-aged nanoparticles showed the presence of C, O, Si, S, Au, Na, and P (Figures 2.9 and 2.10). The S is from the capping MHDA. The Au is from the nanoparticles. The Si and O signals are from the silicon substrate, on which the samples were drop casted for XPS analysis. Possible sources of C are the capping MHDA and polysorbates. The signals of Na and P are due to the sodium phosphate buffer solution, in which gold

nanoparticles are suspended. The N peak in freshly prepared nanoparticles is likely due to the presence of adsorbed nitrogen gas.

Further information about the composition of the monolayers stabilizing the AuNPs was obtained by high resolution X-ray photoelectron spectroscopy (HRXPS). These studies provided a relative assessment of the density of the capping molecules as determined from the relative amount of bound and unbound MHDA. Freshly prepared solutions of AuNPs were purified of excess alkanethiols and P20 as detailed in the experimental section. The high resolution S_{2p} spectra for all samples consisted of 3 chemical species, which are assigned to bound alkanethiolates (binding energies of 161.9-163 eV), unbound sulfur or disulfides (163.5-165 eV) and oxidized sulfur (>166 eV).[47,48] Nanoparticles with coatings formed over 30 min or 4 h both had a high percentage of free and oxidized sulfur species, although the 4 h sample contained a higher relative amount of bound sulfur (Figures 2.11a and 2.11b; Table 2.2). Monolayers formed on AuNPs over 2 days had a higher density of MHDA as evidenced by the higher levels of bound sulfur (Figures 2.11c and 2.11d). These particles, conversely, also contained the least amount of oxidized sulfur (Table 2.2). Nanoparticles prepared in the presence of P20 over periods of 2 days contained less bound or oxidized sulfur and more free sulfur when compared to those particles prepared without addition of P20. The latter sample contains a higher density of alkanethiolates versus unbound thiols possibly due to a lack of competition between MHDA and P20 for adsorption onto the gold surfaces. These samples were, however, less stable over 1 month at 22 and 37°C than those prepared with P20, presumably due to additional stabilization provided by P20 co-adsorbed onto the AuNPs (Figure 2.6).
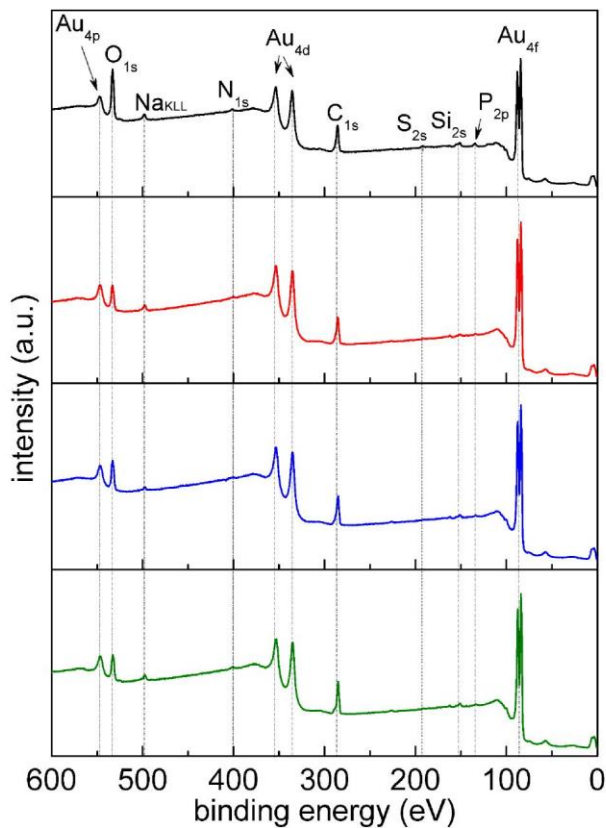
Figure 2.9. X-ray photoelectron spectra of gold nanoparticles stabilized by immersion in MHDA along with addition of P20 surfactants for 30 min (black line), 4 h (red line), 2 days (blue line), or immersed in MHDA for 2 days in the absence of P20 (green line). These spectra are from freshly prepared nanoparticles that were purified of excess MHDA and P20 surfactants.
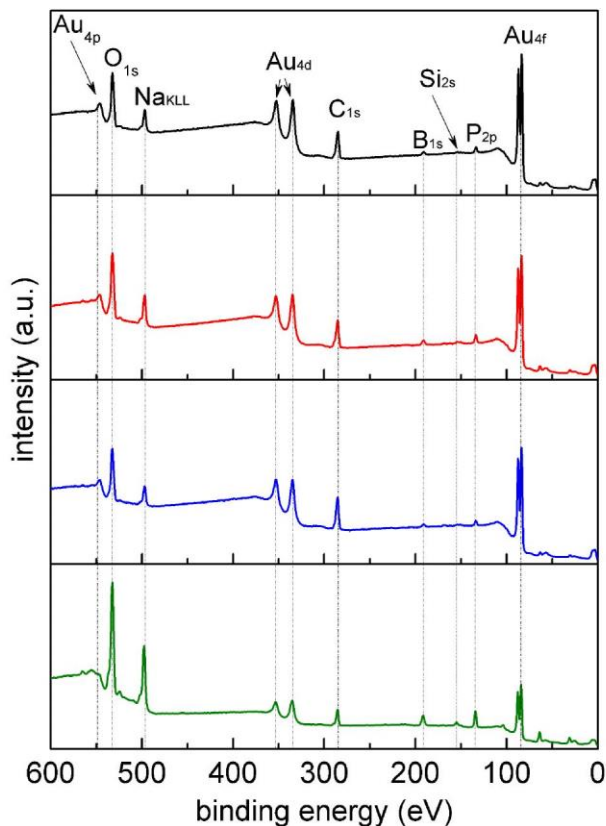
Figure 2.10. **X-ray photoelectron spectra of gold nanoparticles capped with a mixture of MHDA and P20 prepared by their immersion in excess surfactants for 30 min (black line), 4 h (red line), or 2 days (blue line), or capped with only MHDA monolayers prepared over 2 days in the absence of polysorbate surfactants (green line). These spectra were acquired from solutions of nanoparticles (purified of excess surfactants) after aging each sample for 1 month at 22°C. Composition of these samples is largely consistent with their freshly prepared equivalent (Figure 2.9), but the presence of boron is possibly a contribution from the glass vials in which the samples were stored during the month long experiments.**

Composition of the monolayer protected AuNPs was also assessed by XPS after storing purified samples in phosphate buffer at 22°C for 1 month. This analysis provided further insight into the integrity of the monolayers capping the AuNPs. The S_{2p} high resolution XPS (HRXPS) spectra for these samples (Figure 2.12) and the integrated results (Table 2.2) indicate that the relative amount of bound sulfur to unbound and oxidized sulfur species increased in most samples except those prepared without P20. The samples with the highest level of oxidized sulfur species were AuNPs initially prepared by immersion in MHDA and P20 for 30 min. The relative amount of oxidized

69

thiol in the each sample decreased in proportion to the time allowed for the assembly of the monolayers. The samples stabilized with monolayers prepared over a period of 2 days either with or without the addition of P20 exhibited similar ratios for all sulfur species (Table 2.2). Both of these samples exhibited a significant increase in the relative amount of oxidized sulfur after 1 month. The density of MHDA monolayers was not equivalent in these two samples, which was estimated from the ratio of bound sulfur species to Au (using the Au_{4f} intensities). These ratios were ~0.027 and ~0.040 for samples prepared with and without P20, respectively. The ratios suggest a significant amount of P20 stabilizes the AuNPs. Those samples without P20 had a larger overall increase in the portion of their capping layer that was oxidized and dissolved into solution after the 1 month period. This loss of capping molecules presumably led to the loss of colloidal stability in these samples. The instability observed in this sample is progressive over the 1 month period (Figure 2.6d). It is possible that the oxidized species were still strongly interacting with and stabilizing the AuNPs. Oxidized thiol (SS, SO_3^-, SO_4^-) could still interact with the surfaces of the particles due to van der Waals interactions with MHDA bound to the gold. These oxidized species could slowly dissolve from the surfaces and likely has a major contribution to the observed progressive destabilization of the particles. There was, however, little variation observed in the rate of particle destabilization with increase in temperature (Figure 2.6d). The rate limiting step leading to particle instability is most likely oxidation of the thiol molecules.
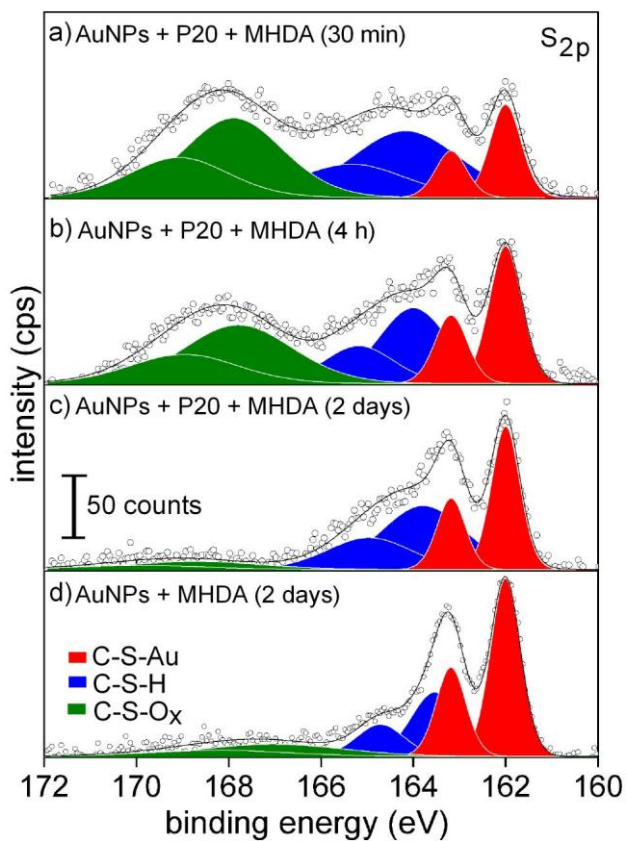
Figure 2.11. High resolution S_{2p} X-ray photoelectron spectra (XPS) of AuNPs stabilized with either (a-c) a mixture of MHDA and P20, or (d) only MHDA. These samples were analyzed directly after their preparation and purification.
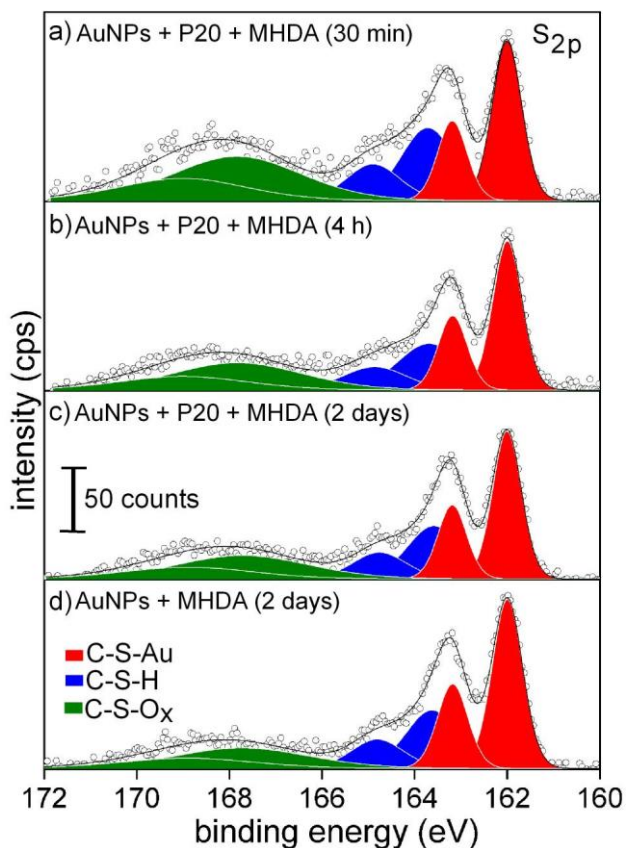
Figure 2.12. High resolution S_{2p} XPS spectra of AuNPs. All these samples were purified of excess surfactants and subsequently held at 22°C for 1 month before performing this XPS analysis.

Table 2.2. Sulfur Composition of MHDA Modified Gold Nanoparticles as Determined by XPS

composition of nanoparticle and it's surface chemistry	freshly prepared AuNPs			AuNPs after 1 month		
	bound sulfur	unbound sulfur	oxidized sulfur	bound sulfur	unbound sulfur	oxidized sulfur
AuNPs + P20 + MHDA (30 min)	16%	40%	44%	33%	27%	40%
AuNPs + P20 + MHDA (4 h)	28%	33%	39%	40%	27%	33%
AuNPs + P20 + MHDA (2 days)	39%	51%	10%	41%	28%	31%
AuNPs + MHDA (2 days)	55%	30%	15%	47%	28%	25%

The presence of P20 and the relative change in the amount of P20 on the surfaces of the stable colloidal gold over the course of 1 month is further confirmed by additional XPS analysis. High resolution C_{1s} XPS spectra for these samples had 5 peaks centered at binding energies of 285.0 eV, 285.6 eV, 286.8 eV, 287.9 eV, and 289.8 eV, which are assigned to **C**-C, **C**-COOH, **C**-O, **C**OOH, and carbonate, respectively (Figure 2.13).[49,50-51] Both the MHDA and the P20 contribute to the **C**-C, **C**-COOH, **C**-O and **C**OOH signals. The **C**-O peak is predominately associated with the presence of P20 (Figure 2.13a-c). The relative intensities of **C**-O to **C**-C in samples with P20 decreased after 1 month. This change could be due to the degradation and dissolution of P20 from the nanoparticles' surfaces. After a one month period, those gold colloids remaining in these solutions had a similar relative amount of P20 or P20 fragments as indicated by the relative intensities of the **C**-O and **C**-C XPS peaks. The particles capped with both MHDA and P20 also had a very similar ratio of bound sulfur to gold (~0.027) after the one month period. The colloids remaining in solution at the end of the 1 month study could be a result of both a specific ratio of surfactants that impart stability to the particles and an equilibrium ratio of surfactants associated with the surfaces of the nanoparticles.
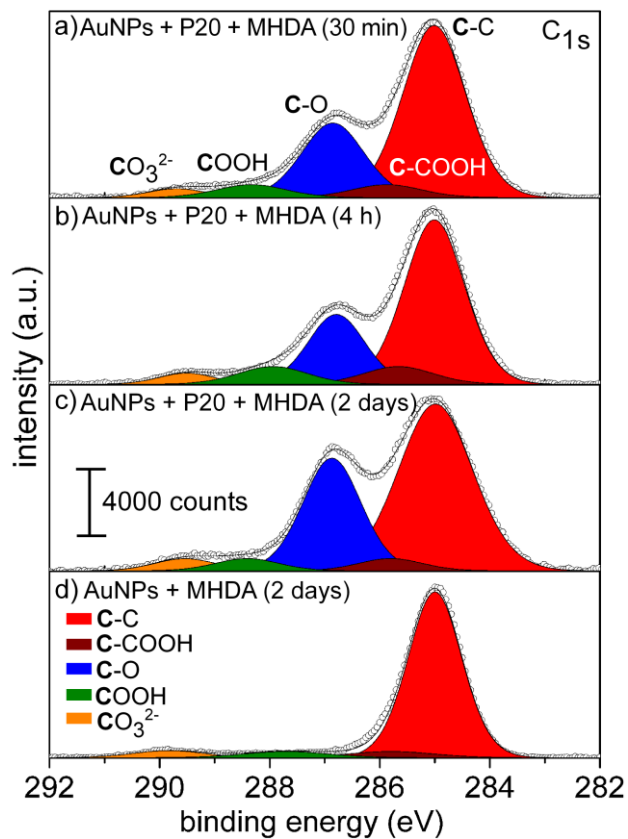
Figure 2.13. High resolution C_{1s} XPS spectra of freshly prepared and purified solutions of AuNPs. Particles were modified by immersion in MHDA and P20 for (a) 30 min, (b) 4 h, (c) and 2 days, or only MHDA for (d) 2 days.
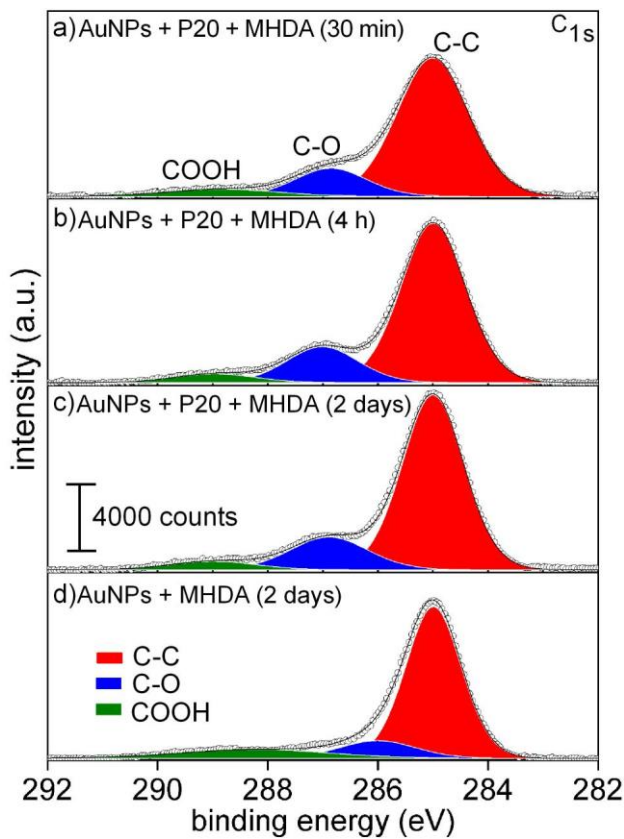
Figure 2.14. High resolution C_{1s} XPS spectra of gold nanoparticles after being held in buffered solutions for 1 month at 22°C. These particles were capped with a mixture of MHDA and P20 (a-c), or only with MHDA (d).

Quality of the monolayers capping the gold colloids was also evaluated by testing the ability of the monolayers to passivate the gold during treatment with potassium cyanide. Cyanide is known to etch gold even in the presence of protective monolayers, and has been previously utilized to investigate relative differences in passivation by different monolayers.[29,36,37] Observed differences in the rates of etching the gold cores were attributed to the steric hindrance, packing density and chain length of molecules within these monolayers. Other studies have used similar etching techniques to remove the gold core and quantify the presence of some capping molecules.[13,52,53] In the current study, changes in the physicochemical stability of gold colloids was monitored over 30 min in the presence of KCN (Figure 2.15). In contrast to the results of most of the prior studies little change was observed in particle concentration over this period of time. Insight into these differences could be found in a previous study on AuNPs capped with

a mixture of thiols and lipids. Stability of lipids on the surfaces of the nanoparticles increased with surface coverage of thiol molecules (serving as anchors for the coating of lipids) as inferred from observed differences in the rate of change in particle concentration during cyanide etching.[54] These results should extend to other passivation layers. Other changes to the physicochemical stability of our gold colloids also correlated to the quality of the MHDA monolayers both with and without the addition of P20. Peak position of the LSPR for the gold colloids progressively red-shifted over time after addition of cyanide in proportion to the quality of the MHDA monolayers (Figures 2.15 and 2.16). Those colloids with the lowest quality MHDA monolayers had the greatest shift in position of the LSPR peak and a simultaneous increase in polydispersity of particle size and shape as indicated by the increase in the peak width (Figure 2.17). A progressive increase in light scattering between 600 and 700 nm is also correlated with the observed changes to the samples. Collectively, these results suggest the nanoparticles flocculate and/or aggregate as the etching process likely destabilizes their surface passivation.
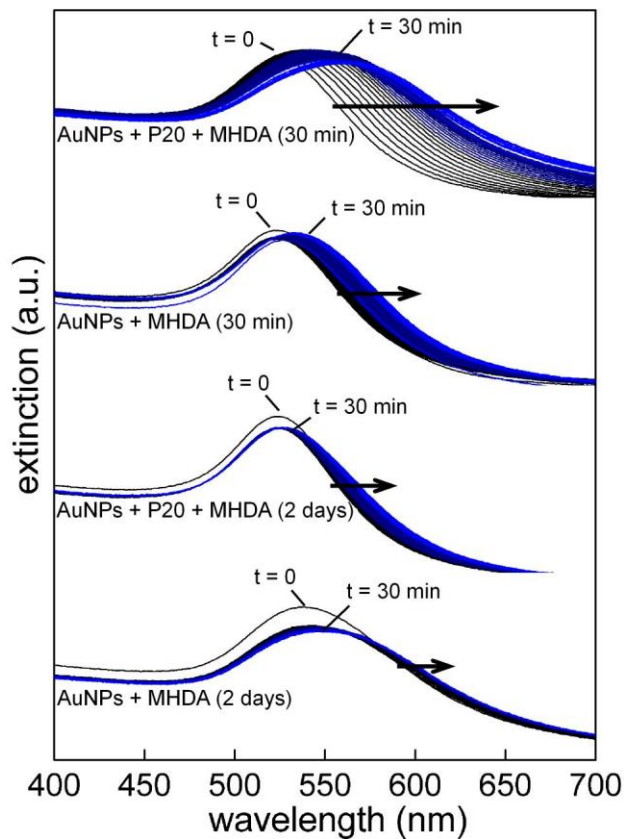
Figure 2.15. Stability of AuNPs against potassium cyanide etching assessed by changes in their extinction spectra. These nanoparticles were capped with MHDA and P20 or with only MHDA. Changes in extinction spectra included an increase in light scattering (vertical offset in baseline between 600 and 700 nm) and a red shift in the position of the surface plasmon band. The capping layers on the gold were prepared over a period of either 30 min or 2 days in the presence or absence of P20 co-surfactants as indicated below each set of spectra.
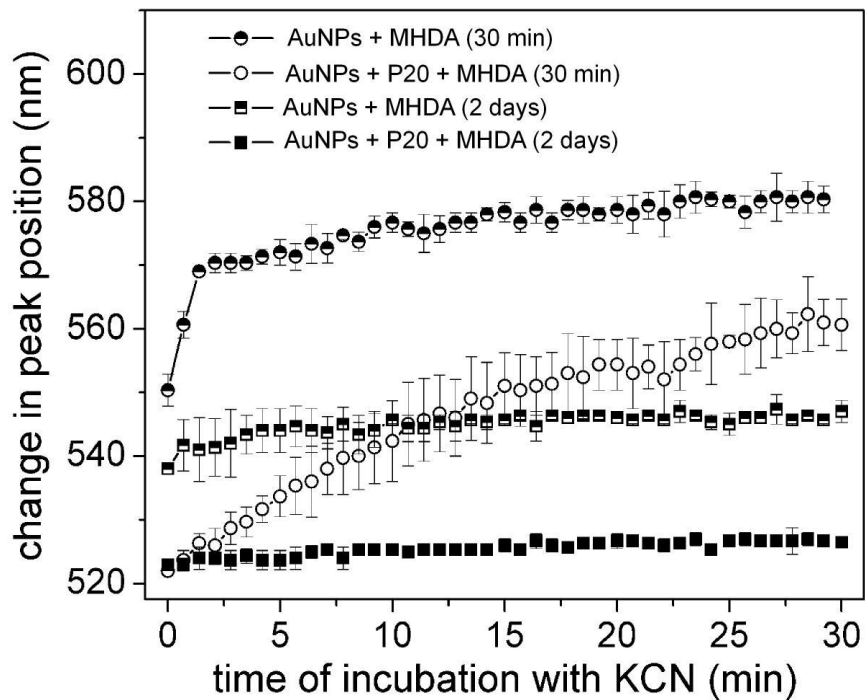
Figure 2.16. Change in position of the LSPR peak for AuNPs treated with KCN as a function of time. These particles were stabilized with either a mixture of MHDA and P20 or only MHDA, which were assembled over a period of either 30 min or 2 days as noted in the legend. The error bars represent one standard deviation from the mean derived from three independent experiments.
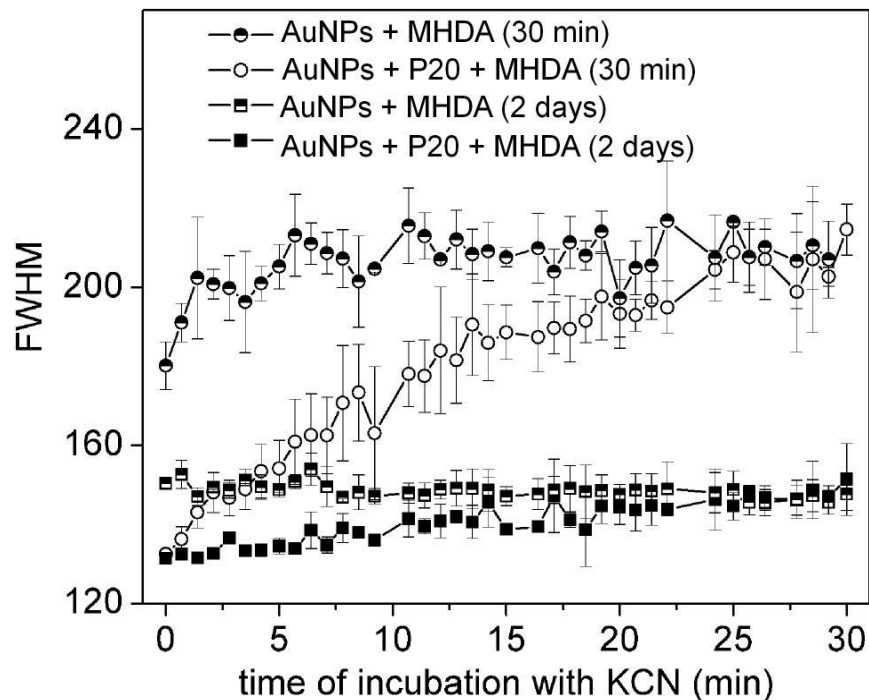
Figure 2.17. **Stability of gold nanoparticles against potassium cyanide (KCN) etching as assessed by changes in full width at half maximum (FWHM) of the localized surface plasmon resonance (LSPR) peaks plotted in Figure 2.15. The colloidal solutions of AuNPs were stabilized either with monolayers MHDA and P20 or with only MHDA. These stabilizing layers were prepared either over a period of 30 min or 2 days as noted in the legend. The error bars represent one standard deviation derived from the mean for three independent experiments.**

Analysis of the samples by TEM following exposure to KCN for 30 min reveals changes to the physical properties of the particles. Particle shape is largely retained after the etching process (Figure 2.18). However, the diameter decreases by ~4 nm and ~2 nm for those particles passivated with low quality monolayers of MHDA and P20 or only with MHDA, respectively. The TEM analysis also indicated a number of particles in both samples had formed aggregates. Commonly observed aggregates were two particles joined together at one interface (Figure 2.19). This fusion of gold particles is likely due to the removal of some capping molecules, creating unstable facets that can bond to the exposed gold surfaces of other particles.
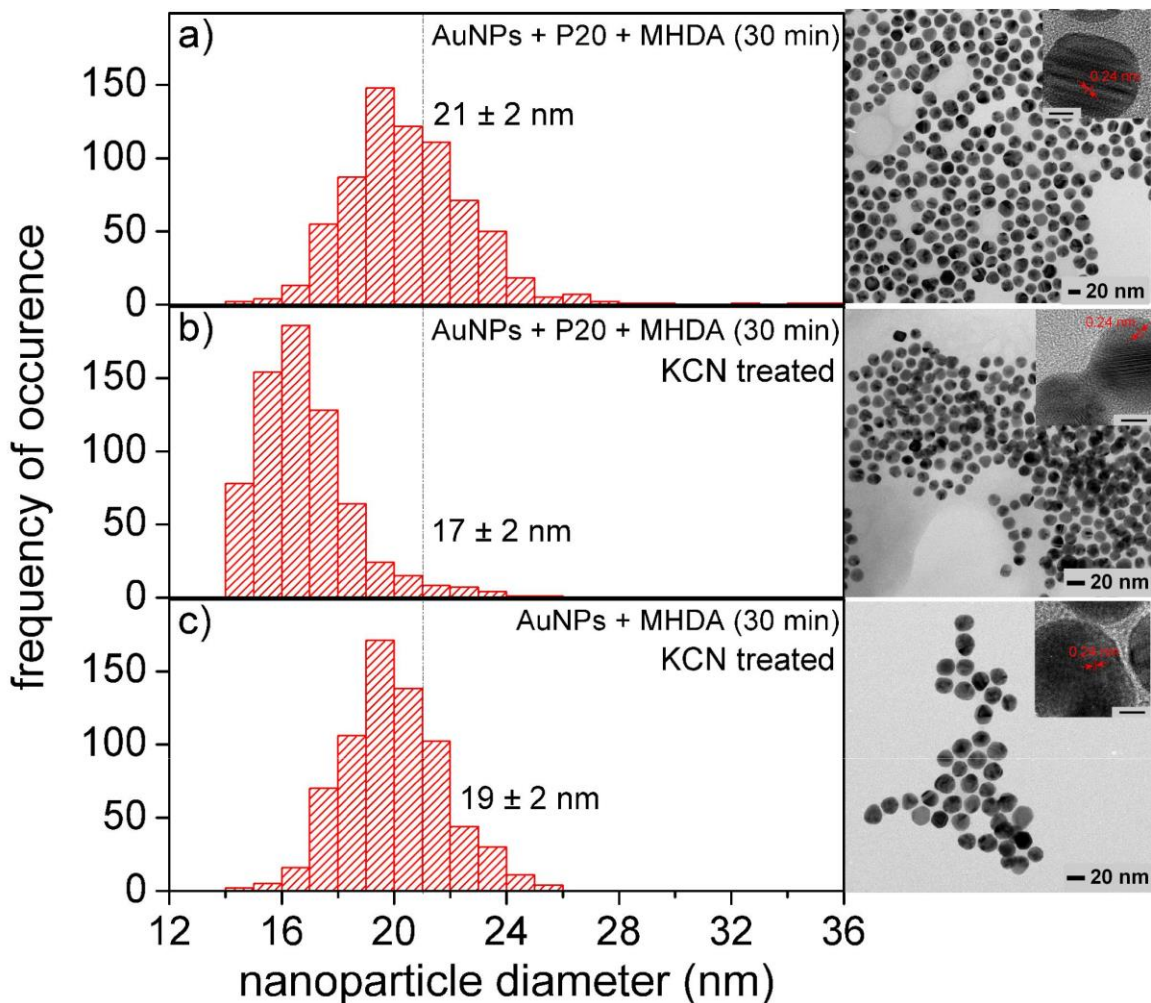
Figure 2.18. Histograms of particle diameters as determined by TEM analysis for: (a) as prepared nanoparticles modified with coatings of MHDA and P20 assembled over 30 min; (b) the same nanoparticles capped with MHDA and P20 surfactants after reacting with 50 mM KCN for 30 min; and (c) nanoparticles coated with only MHDA after being exposed to a solution of KCN. At least 700 nanoparticles were counted to prepare each histogram. Representative TEM images are included for each sample, including inset pictures with a scale bar 5 nm.
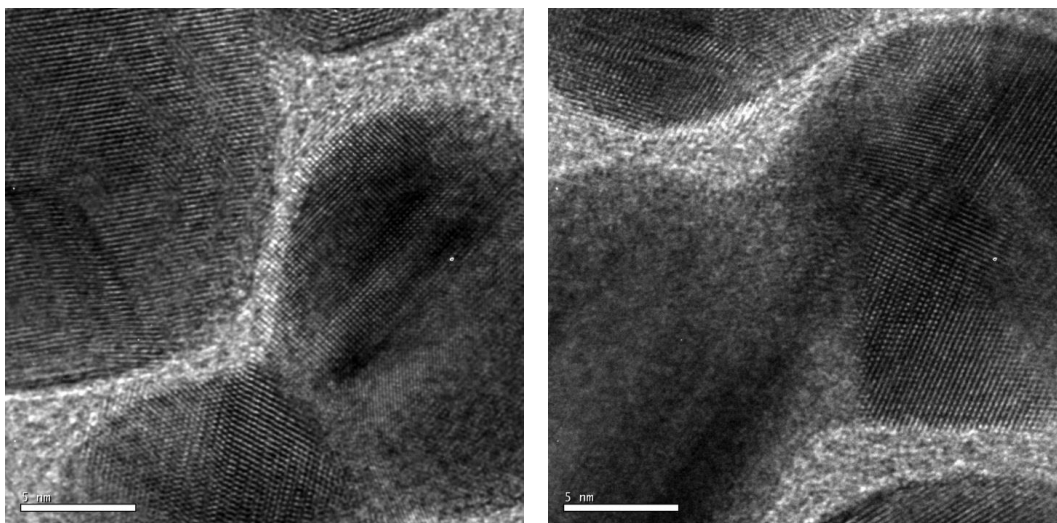
Figure 2.19. High resolution TEM images of gold nanoparticles stabilized with: (a) monolayers of MHDA and P20 surfactants formed over 30 min; (b) only MHDA coatings formed over 30 min. These particles were each incubated with 50 mM KCN over a period of 30 min. Although the particles retained their spherical shapes, many of the particles became fused together following treatment with KCN.
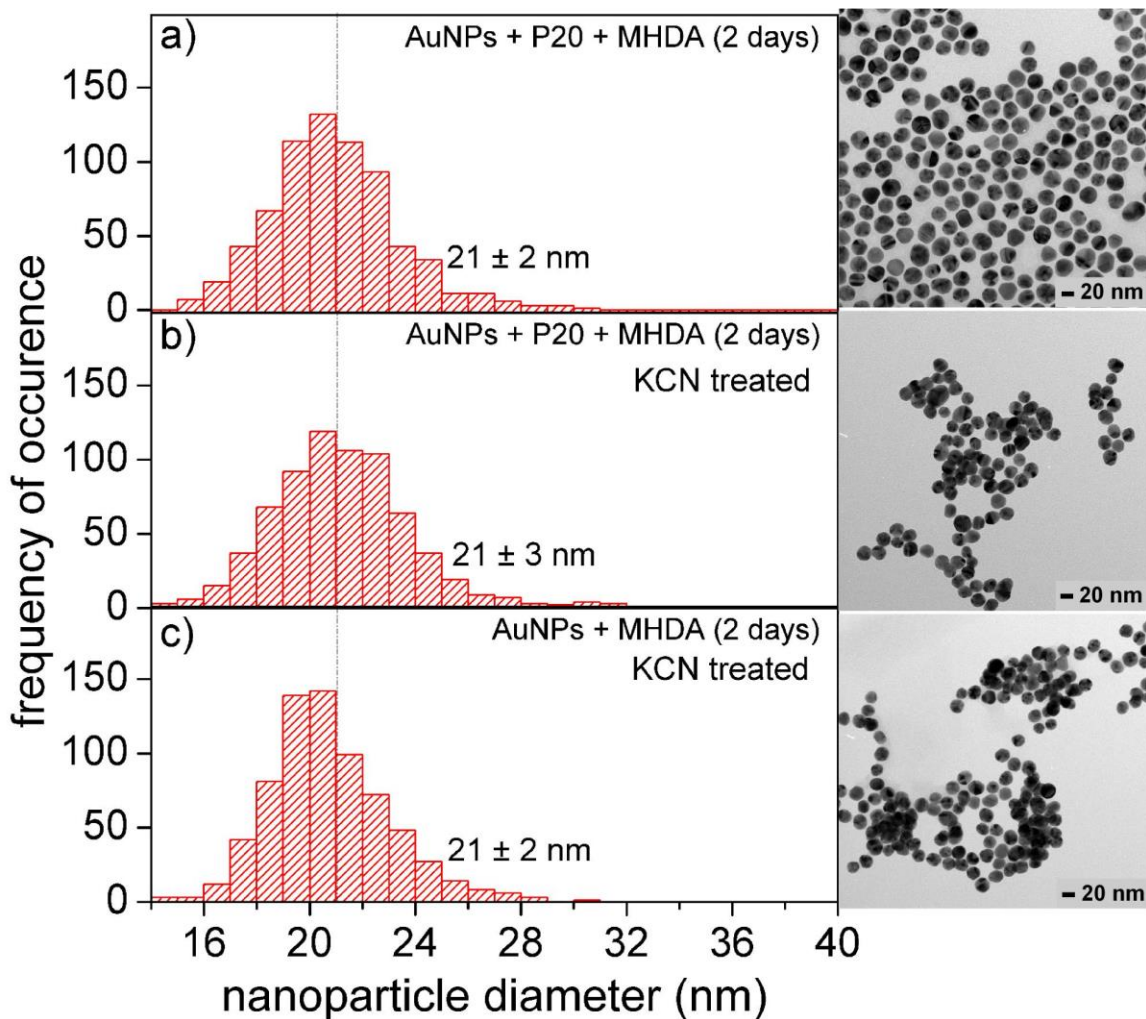
Figure 2.20. Histogram of diameters for **(a)** as prepared nanoparticles capped with coatings of MHDA and P20 surfactants formed over 2 days, or **(b)** the same nanoparticles capped with MHDA and P20 after reacting with 50 mM KCN for 30 min and **(c)** nanoparticles coated with only MHDA after being exposed to a solution of KCN. At least 700 nanoparticles were counted to prepare each histogram. Representative TEM images are included for gold nanoparticles before or after incubation with potassium cyanide (KCN, final concentration of 50 mM) for a period of 30 min.
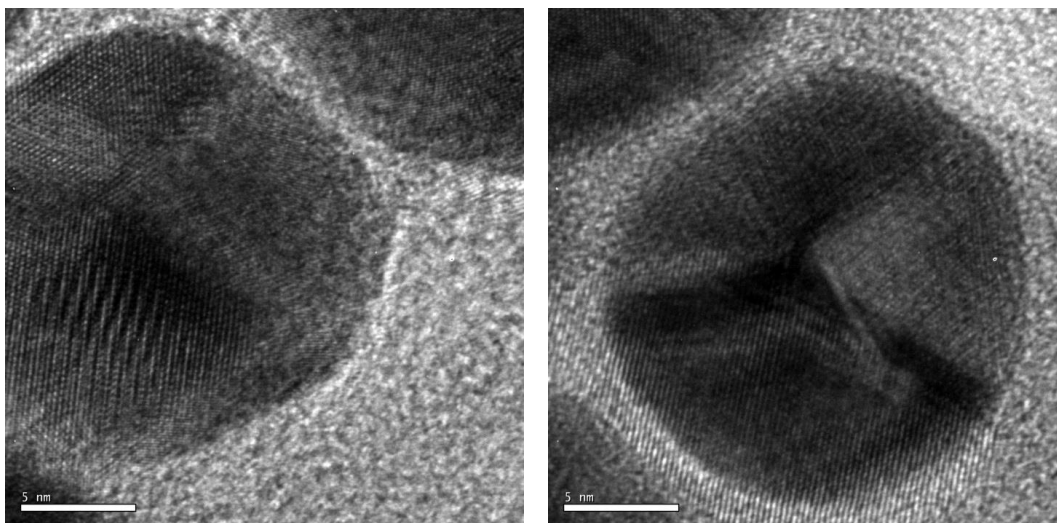
Figure 2.21. High resolution TEM images of gold nanoparticles stabilized with either (a) monolayers of MHDA and P20 surfactants formed over 2 days, or (b) only monolayers of MHDA formed over 2 days. These particles were each incubated with 50 mM KCN. The nanoparticles retained their spherical shapes and sizes following treatment with KCN for 30 min.

The effective increase in particle size due to this aggregation leads to both the observed increase in light scattering and red shift in the extinction spectra. A significantly smaller change in the position of the LSPR peak was observed for colloids stabilized with a higher quality monolayers assembled over 2 days (Figures 2.15 and 2.16). Although spectral differences were observed between these higher quality samples passivated either with or without the presence of P20 (Figure 2.16), their particle shape and size were not significantly changed by the addition of KCN (Figure 2.20 and 2.21). The higher quality monolayers passivating the surfaces of these gold colloids minimized etching and destabilization of the gold cores over the course of the experiment. Similar trends were observed for those particles passivated both with and without P20. A faster initial rate of spectral change was, however, observed for the particles capped with only MHDA than for the particles also stabilized with P20. The presence of P20 minimized aggregation of the gold colloids during the etching process, preventing a red-shift and broadening of the LSPR peak in their extinction spectra. Differences observed by TEM analysis suggest the decreases in size of the particles could be correlated with the quality of the monolayers. The spectral change for all samples, irrespective of the quality of the monolayers, appears to reach a steady rate after 30 min. The nonlinear change in

physicochemical stability of the AuNPs during this process in combination with the presence of excess cyanide ions ($CN^-/Au^- = 2.6 \times 10^6$) in solution suggest a time dependent change in the surface passivation of the gold colloids. It is possible that the surfaces of the colloids become passivated by the formation of adsorbed aurocyanide complexes that form during the etching of gold particles.[55] The addition of metal impurities or the use of alternative gold etchants[56-57] could be pursued to develop a process that further differentiates the quality of monolayers prepared with and without the addition of a co-surfactant. Future studies will also pursue other molecular coatings and co-surfactants, and their influence on the long-term physicochemical stability of these gold colloids.

The stability of the suspended nanoparticles can be correlated to the composition of the solution. For example, gold nanoparticles capped only with MHDA and suspended in a 1x Tris borate EDTA (TBE) buffered solution at pH 8.3 only had a small decrease in maximum UV-Vis absorbance over a period of 1 month at 22, 37, and 45°C. In comparison, those nanoparticles capped with MHDA and polysorbate 20 surfactants in phosphate buffered (PB) solution at pH 7.2 are more stable at 22°C, but less stable at 45°C (Figure 2.22). The phosphate buffer was chosen for the studies discussed herein because of its high affinity to the gold surfaces and its ability to destabilize the nanoparticles. The phosphate buffered solution at pH 7.2 was also chosen for its physiological relevance. The colloids capped with polysorbate 20 surfactants and MHDA are more stable than those without polysorbate surfactants over the course of one month when held at either 22 or 37°C in pH 7.2 phosphate buffered solutions. The stabilization of gold nanoparticles by the polysorbate 20 surfactants is further supported by varying the pH of the solution. A series of solutions were prepared with gold nanoparticles capped with SAMs formed over 2 days in either the absence or presence of polysorbate surfactants. These solutions were each partitioned into five equal volumes, each mixed with a specific buffer to establish solutions with pH values of ~3, ~5, ~7, ~9 and ~11. Particle stability at different pH's was characterized by both extinction spectroscopy and PSA measurements. An increase in the extinction intensities at wavelengths greater than 600 nm can indicate flocculation of nanoparticles in solution.[58-59] The flocculation parameter was calculated from the intergrated extinction between 600-800 nm for these solutions of gold nanoparticles suspended in the various buffers. Of all nanoparticles

prepared in the absence of polysorbate surfactants the solutions at pH 7.2 and 9.1 were the most stable with the least increase in flocculation (Figure 2.23a). Those colloids with SAMs formed in the presence of polysorbate 20 surfactants are relatively more stable at all pH values. The polysorbate 20 surfactants stabilize the gold colloids from pH values of 3.0 to 9.1. Some flocculation is observed for particles at pH 11.2, which is attributed to the instability of polysorbate surfactants under basic conditions.[44] Similar trends were observed for the hydrodynamic diameters of these particles at the various pH values (Figure 2.23b). These results further support the stabilization of the gold colloids by adsorbed polysorbate 20 surfactants at 22°C. It is important that nanoparticles and the quality of their capping groups be investigated under conditions relevant to the intended use of the nanoparticles. It is also important to study the long-term stability, and the stability under extreme conditions that might also be relevant for the intended use of the nanoparticles.
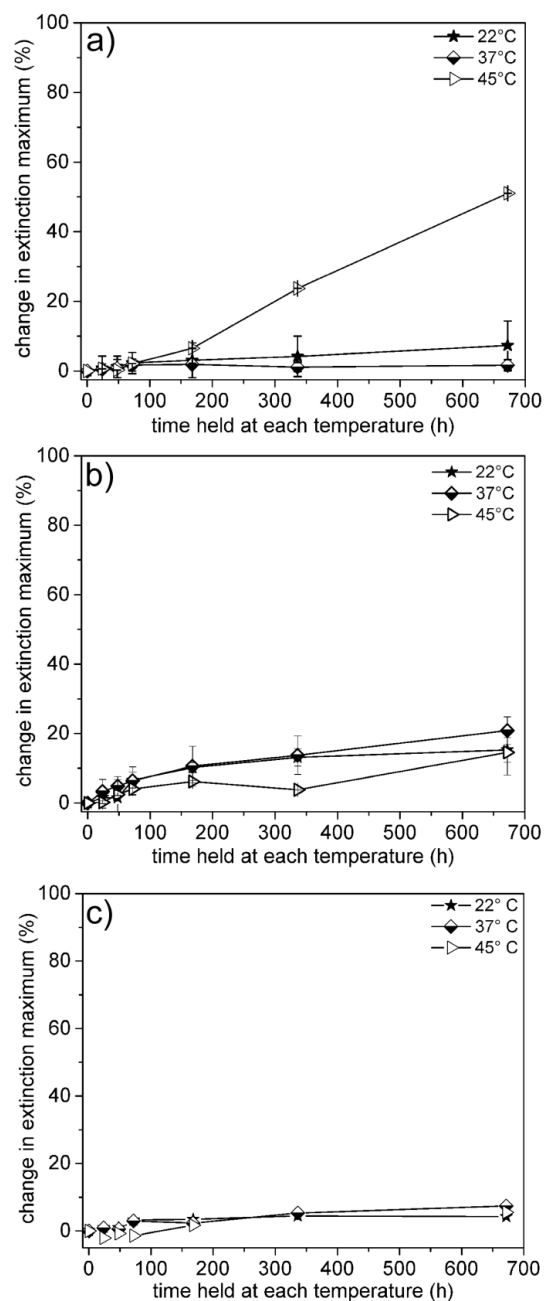
Figure 2.22. Change in extinction maximum at 523 nm for gold nanoparticles suspended in (a) 10 mM phosphate buffered (PB) solutions at pH 7.2 *with* polysorbate 20 surfactants, (b) 10 mM phosphate buffered solutions at pH 7.2 *without* polysorbate 20 surfactants, or (c) 1x tris borate EDTA (TBE) buffered solutions at pH 8.3 *without* polysorbate 20 surfactants. These changes in extinction maximum were plotted as a function of time over which the solutions had been held at 22, 37, or 45°C. In these studies, all nanoparticles are capped with monolayers of MHDA formed over 2 days.
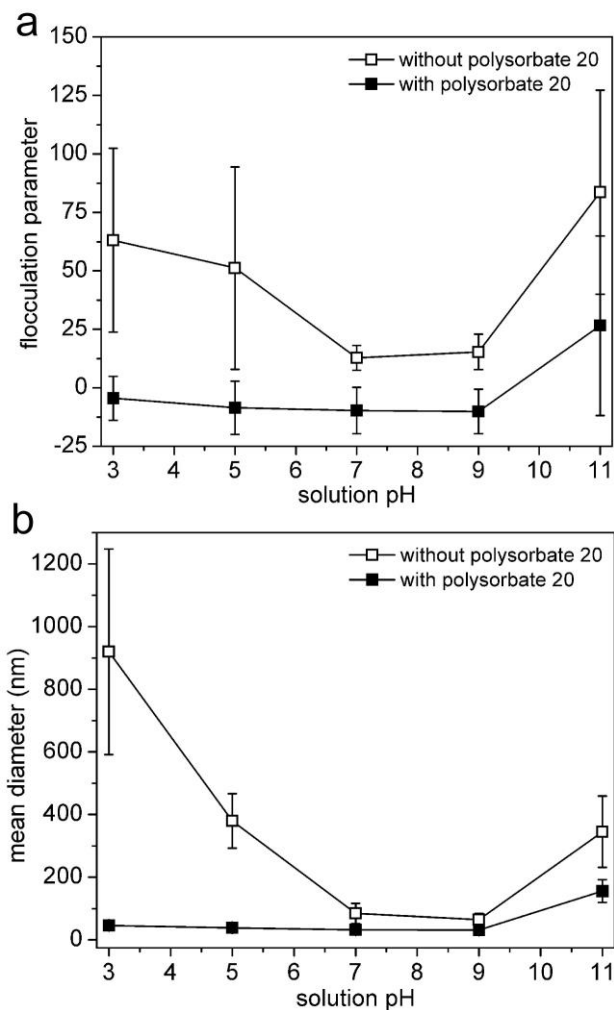
Figure 2.23. **Colloidal stability of gold nanoparticles assessed as a function of change in solution pH. These particles are capped with coatings of MHDA prepared either in the presence or absence of the polysorbate 20 surfactant. These monolayers were formed over a period of 2 days, and the purified particles were suspended in various buffers to achieve a solution pH from 3.0 to 11.2. Colloidal stability of the suspended nanoparticles is measured by their (a) flocculation parameter, and (b) mean hydrodynamic diameter. The flocculation parameter is calculated from the integrated extinction between 600 and 800 nm in the extinction spectra.[58,59] The particle size is measured by dynamic light scattering. The associated error bars are derived from the standard deviations of these measurements**

87

2.4. Summary and Conclusions

In summary, the colloidal and chemical stability of monolayer capped gold nanoparticles was evaluated as a function of temperature, solution composition and resistance to cyanide etching. These gold colloids were coated with monolayers of 16-mercaptohexadecanoic acid (MHDA) and some particles were also stabilized with the addition of a co-surfactant. Stability of the gold colloids was monitored by comparing changes in the relative concentration of the nanoparticles, their hydrodynamic size, and surface potential over the course of one month at 22, 37 and 45°C. These results were correlated to changes in the composition of the molecular coatings stabilizing the gold colloids over the course of one month as determined by X-ray photoelectron spectroscopy. Most of the particles were stable over the course of a few hours and even up to a period of one day, but the colloids displayed a dramatic difference in their longer-term stability. Stability over the month-long experiments depended primarily on the quality of the coatings on the surfaces of the gold nanoparticles. The higher quality coatings of alkanethiolates on the gold increased the chances that the particles would remain stable over the course of the month. The highest quality monolayers capping gold colloids resulted from the formation of self-assembled monolayers prepared over 2 days. Chemical stability of the gold colloids was further assessed by comparing changes in concentration, shape, size, and polydispersity of the gold colloids following their incubation with potassium cyanide. Those gold colloids modified with coatings of higher quality were better at protecting the underlying gold cores during these cyanide etching experiments, evident in both the extinction spectra and the preserved shape and dimensions of these particles. The initial formation of SAMs follows a Langmuir process, suggesting monolayers form within 30 min, but the rearrangement of molecules in a densely packed layer with the proper orientation takes a significantly longer time and is ultimately thermodynamically controlled and kinetically slow. We, therefore, conclude that sufficient time is necessary for the formation of densely packed monolayers of alkanethiolates on the surfaces of gold colloids to adequately stabilize these particles against aggregation and other unwanted changes.

2.5. References

(1)   Srisombat, L.; Jamison, A. C.; Lee, T. R. *Colloids Surf., A* **2011**, *390*, 1-19.

(2)   Stewart, M. H.; Susumu, K.; Mei, B. C.; Medintz, I. L.; Delehanty, J. B.; Blanco-Canosa, J. B.; Dawson, P. E.; Mattoussi, H. *J. Am. Chem. Soc.* **2010**, *132*, 9804-9813.

(3)   Flynn, N. T.; Tran, T. N. T.; Cima, M. J.; Langer, R. *Langmuir* **2003**, *19*, 10909-10915.

(4)   Johnson, S. R.; Evans, S. D.; Brydson, R. *Langmuir* **1998**, *14*, 6639-6647.

(5)   Paulini, R.; Frankamp, B. L.; Rotello, V. M. *Langmuir* **2002**, *18*, 2368-2373.

(6)   Herdt, A. R.; Drawz, S. M.; Kang, Y. J.; Taton, T. A. *Colloids Surf., B* **2006**, *51*, 130-139.

(7)   Sandhyarani, N.; Pradeep, T. *Chem. Phys. Lett.* **2001**, *338,* 33-36.

(8)   Ansar, S. M.; Arneer, F. S.; Hu, W. F.; Zou, S. L.; Pittman, C. U.; Zhang, D. M. *Nano Lett.* **2013**, *13*, 1226-1229.

(9)   Kang, J. S.; Taton, T. A. *Langmuir* **2012**, *28,* 16751-16760.

(10)   Kairdolf, B. A.; Nie, S. M. *J. Am. Chem. Soc.* **2011**, *133*, 7268-7271.

(11)   Love, J. C.; Estroff, L. A.; Kriebel, J. K.; Nuzzo, R. G.; Whitesides, G. M. *Chem. Rev.* **2005**, *105*, 1103-1169.

(12)   Zhang, S. S.; Leem, G.; Srisombat, L. O.; Lee, T. R. *J. Am. Chem. Soc.* **2008**, *130*, 113-120.

(13)   Liu, X.; Yu, M.; Kim, H.; Mameli, M.; Stellacci, F. *Nat. Commun.* **2012**, *3*, 1-9.

(14)   Vericat, C.; Vela, M. E.; Salvarezza, R. C. *Phy. Chem. Chem. Phys.* **2005**, *7*, 3258-3268.

(15)   Noh, J.; Hara, M. *Langmuir* **2001**, *17*, 7280-7285.

(16)   Vericat, C.; Vela, M. E.; Benitez, G. A.; Gago, J. A. M.; Torrelles, X.; Salvarezza, R. C. *J. Phys. Condens. Matter* **2006**, *18*, R867-R900.

(17)   Dederichs, T.; Moller, M.; Weichold, O. *Langmuir* **2009**, *25*, 10501-10506.

(18)   Merrill, N. A.; Sethi, M.; Knecht, M. R. *ACS Appl. Mater. Interfaces* **2013**, *5*, 7906-7914.

(19)   Schrodle, S.; Richmond, G. L. *J. Am. Chem. Soc.* **2008**, *130*, 5072-5085.

(20)   Schulz, F.; Vossmeyer, T.; Bastus, N. G.; Weller, H. *Langmuir* **2013**, *29*, 9897-9908.

(21)   Badia, A.; Gao, W.; Singh, S.; Demers, L.; Cuccia, L.; Reven, L. *Langmuir* **1996**, *12*, 1262-1269.

(22)   Wang, H.; Chen, S. F.; Li, L. Y.; Jiang, S. Y. *Langmuir* **2005**, *21*, 2633-2636.

(23)   Boschkova, K.; Stalgren, J. J. R. *Langmuir* **2002**, *18*, 6802-6806.

(24)   Geissler, M.; Schmid, H.; Bietsch, A.; Michel, B.; Delamarche, E. *Langmuir* **2002**, *18*, 2374-2377.

(25)   Lee, L. Y. S.; Lennox, R. B. *Phys. Chem. Chem. Phys.* **2007**, *9*, 1013-1020.

(26)   Schwartz, D. K. *Annu. Rev. Phys. Chem.* **2001**, *52*, 107-137

(27)   Cui, X. L.; Jiang, D. L.; Diao, P.; Li, J. X.; Tong, R. T.; Wang, X. K. *J. Electroanal. Chem.* **1999**, *470*, 9-13.

(28)   Dasog, M.; Scott, R. W. J. *Langmuir* **2007**, *23*, 3381-3387.

(29)   Hou, W. B.; Dasog, M.; Scott, R. W. J. *Langmuir* **2009**, *25*, 12954-12961.

(30)   Storhoff, J. J.; Elghanian, R.; Mucic, R. C.; Mirkin, C. A.; Letsinger, R. L. *J. Am. Chem. Soc.* **1998**, *120*, 1959-1964.

(31)   Yamada, R.; Wano, H.; Uosaki, K. *Langmuir* **2000**, *16*, 5523-5525.

(32)   Aslan, K.; Perez-Luna, V. H. *Langmuir* **2002**, *18*, 6059-6065.

(33)   Zhao, Y.; Wang, Z.; Zhang, W.; Jiang, X. *Nanoscale* **2010**, *2*, 2114-2119.

(34)   Duy, J.; Connell, L. B.; Eck, W.; Collins, S. D.; Smith, R. L. *J. Nanopart. Res.* **2010**, *12*, 2363-2369.

(35)   Cho, T. J.; Zangmeister, R. A.; MacCuspie, R. I.; Patri, A. K.; Hackley, V. A. *Chem. Mater.* **2011**, *23*, 2665-2676.

(36)   Lanterna, A. E.; Coronado, E. A.; Granados, A. M. *J. Phys. Chem. C* **2012**, *116*, 6520-6529.

(37)   Zopes, D.; Stein, B.; Mathur, S.; Graf, C. *Langmuir* **2013**, *29*, 11217-11226.

(38)   Agasti, S. S.; You, C.-C.; Arumugam, P.; Rotello, V. M. *J. Mater. Chem.* **2008**, *18*, 70-73.

(39)   Agonafer, D. D.; Chainani, E.; Oruc, M. E.; Lee, K. S.; Shannon, M. A*J. Nanotech. Eng. Med.* **2012***, 3,* 031006-1.

(40)   Faraday, M. Philos. Trans. R. Soc. London **1857**, 147, 145–181.

(41)   Eustis, S.; El-Sayed, M. A. *Chem. Soc. Rev.* **2006**, *35*, 209-217.

(42)   Liu, X. O.; Atwater, M.; Wang, J. H.; Huo, Q. *Colloids Surf. B* **2007,** *58*, 3-7.

(43)   Oh, E.; Susumu, K.; Maekinen, A. J.; Deschamps, J. R.; Huston, A. L.; Medintz, I. L. *J. Phys. Chem. C* **2013**, *117*, 18947-18956.

(44)   Kerwin, B. A. *J. Pharm. Sci.* **2008**, *97*, 2924-2935.

(45)   Donbrow, M.; Azaz, E.; Pillersdorf, A. *J. Pharm. Sci.* **1978**, *67*, 1676-1681.

(46)   Kishore, R. S. K.; Pappenberger, A.; Dauphin, I. B.; Ross, A.; Buergi, B.; Staempfli, A.; Mahler, H. C. *J. Pharm. Sci.* **2011**, *100*, 721-731.

(47)   Vericat, C.; Vela, M. E.; Benitez, G.; Carro, P.; Salvarezza, R. C. *Chem. Soc. Rev.* **2010**, *39*, 1805-1834.

(48)   Ishida, T.; Hara, M.; Kojima, I.; Tsuneda, S.; Nishida, N.; Sasabe, H.; Knoll, W. *Langmuir* **1998**, *14*, 2092-2096.

(49)   Techane, S. D.; Gamble, L. J.; Castner, D. G. *J. Phys. Chem. C* **2011**, *115*, 9432-9441.

(50)   Cecchet, F.; Marcaccio, M.; Margotti, M.; Paolucci, F.; Rapino, S.; Rudolf, P. *J. Phys. Chem. B* **2006**, *110*, 2241-2248.

(51)   Gelius, U.; Hedén, P. F.; Hedman, J.; Lindberg, B. J.; Marine, R.; Nordberg, R.; Nordling, C.; Siegbahn, K. *Phys. Scr.* **1970**, *2*, 70-80.

(52)   Xia, X. H.; Yang, M. X.; Wang, Y. C.; Zheng, Y. Q.; Li, Q. G.; Chen, J. Y.; Xia, Y. N. *ACS Nano* **2012**, *6*, 512-522.

(53)   Jiang, W.; Hibbert, D. B.; Moran, G.; Akter, R. *J. Anal. Atom. Spectrom.* **2012**, *27*, 1465–1473.

(54)   Sitaula, S.; Mackiewicz, M. R.; Reed, S. M. *Chem. Commun.* **2008**, *26*, 3013–3015.

(55)   Marsden, J. O.; House C. L. *The Chemistry of Gold Extraction*, 2nd ed.; Society for Mining, Mettallurgy, and Exploration, Inc. Littleton: USA, 2006; p 238-239.

(56)   Jeffrey, M. I.; Ritchie, I. M. *J. Electrochem. Soc.* **2000**, *147*, 3272-3276.

(57)   Zou, R. X.; Guo, X.; Yang, J.; Li, D. D.; Peng, F.; Zhang, L.; Wang, H. J.; Yu, H. *CrystEngComm.* **2009**, *11*, 2797-2803.

(58)   Mayya, K. S.; Patil, V.; Sastry, M. *Langmuir* **1997**, *13*, 3944-3947.

(59)   Gao, D. J.; Tian, Y.; Liang, F. H.; Ding, L.; Bi, S. Y.; Chen, Y. H.; Zhang, H. Q.; Yu, A. M. *Colloids Surf., B* **2006,** 47, 71-77

Chapter 3.

Stability of Gold Nanorods During Photothermal Processes

3.1. Introduction

The generation of heat at surfaces of gold nanoparticles during laser irradiation i.e., the photothermal effect (PTE) is useful for triggering molecular release or activating molecular reactions. The influence of the PTE on the surface chemistry of the particles and their long-term colloidal stability remains largely unknown. The increase in temperature during photothermal processes can lead to breakage of chemical bonds between the nanoparticles and their capping molecules (e.g., the Au-S bond)[1,2,3] or lead to significant transformations in the shapes and sizes of anisotropic nanoparticles.[4-10] The dissociation of the Au-S bond between nanoparticles and alkanethiolate coatings could lead to a loss of capping molecules, which could subsequently lead to the destabilization of these laser irradiated nanoparticles. In addition, previous studies have shown that cylindrical gold nanorods can be transformed into dumbbell-shapes or ɸ-shapes,[4,5,6] melt into spheres,[4,5,6] fragment into shorter nanorods,[7] or fuse into larger structures [8,9] as a result of irradiation with intense laser powers whose wavelengths overlap with the longitudinal or transverse surface plasmon bands of the nanorods. These anisotropic nanostructures are transformed into more thermodynamically stable spherical particles of smaller sizes as a result of the PTE.[4,5,6,10]

It is, however, of interest (for some applications) to preserve the shape, dimensions, aspect ratio, and ultimately the surface chemistry of these nanorods during photothermal-triggered release of a molecular payload. A major concern of the reshaping of nanoparticles during photothermal processes is the likely unwanted changes in both the optical properties (LSPR band position shifting)[10,11,12] and their surface chemistry, which could lead to destabilization of the particles and a mismatch between the incident laser wavelength and the maximum peak absorbance of nanoparticles. This non-overlap of the excitation wavelength and LSPR band would lower the subsequent heating efficiency of these nanostructures and limit their use for further molecular release and/or activation of molecular reactions.[12] The reshaping of nanoparticles could also lead to a generation of nanoparticles with undesired surface plasmon resonance properties and unknown surface chemistry.[13] It is, therefore, important to carefully choose irradiation parameters during photothermal applications, such as during photothermal-triggered release of molecules from nanoparticles, while preserving the desirable optical properties of the nanoparticle carriers. Maintaining these properties is crucial for the successful use of the nanorods in a prolonged delivery of localized heat by the PTE, which could ensure an accurately delivered dose of molecules, as well as enhanced mass transfer and diffusion of the released payloads into the surrounding environment (e.g., tissues).

For most photothermal applications that involve the use of nanoparticle solutions, a careful choice of surface coatings and solution composition is required to maintain the stability of these nanoparticles during photothermal processes.[14,15,16,17] The surface chemistry and the quality of molecular coatings is directly related with the physicochemical stability of these surface modified nanoparticles during photothermal processes.[14,15,16] Solution composition affects the dynamics of binding and releasing of molecules from the surfaces of nanoparticles.[18,19,20,21] When added into solutions of nanoparticles, excess capping molecules could repair defects in the nanoparticle coatings [22] created by the photothermal desorption of ligands. The surface coating also influences energy transfer from the nanoparticle to its surroundings.[16,23,24] For example, bilayers of cetyltrimethylammonium bromide (CTAB) on gold nanorods accelerated their photothermal reshaping due to low heat diffusion constants of the CTAB layer, whereas polyethylene glycol (PEG) and polysodium stryrenesulfonate (PSS) coated gold

nanorods retained their shapes due to a high heat diffusion constant, which was attributed to the presence of water contained within the PEG and PSS layers that readily absorbs heat.[23] In addition to the surface chemistry, the surrounding environment (composition of the solutions in which nanoparticles are suspended) also plays a critical role in their stability. The critical role of the surrounding medium during heating processes was demonstrated for CTAB coated nanorods.[24] For example, an optimal concentration of excess free CTAB in solution was required to favor the release of octadecyl rhodamine B chloride, intercalated into the CTAB bilayers.[24] Very low concentrations of CTAB in the solutions of nanorods led to nanorod aggregation during photothermal-initiated release of rhodamine, whereas higher concentrations of CTAB (~10 mM) drove the desorption of rhodamine molecules from CTAB-coated nanorods into free CTAB micelles present in solution. The goal of our study was to assess the influence of the surface chemistry, as well as additives in the surrounding medium, on changes to the nanorods following laser irradiation. Gold nanorods were chosen in part because it is easy to follow changes in their shape resulting from photothermal processes through analysis by extinction spectroscopy and transmission electron microscopy (TEM). Changes in their shape would imply a significant potential for alteration to the surface chemistry of these nanomaterials, which could impact the colloidal stability and ability to activate molecular processes as discussed above. The primary aim of this study is to address the question: how do different surface chemistries (or composition of coating molecules) and chemical environments (e.g., composition and concentration of additives in solution) influence the physicochemical stability of gold nanorods during photothermal processes?

It is important to understand the effects of photothermal heating on nanoparticles in order to appropriately select the operating parameters for activating molecular release from these nanoparticles, while also minimizing any lateral damage to molecular payloads. It is also important to manipulate the surface chemistry of nanoparticles in order to minimize desorption of stabilizing molecules. Poon *et al.* demonstrated that photothermal-triggered melting of double-stranded DNA bound to gold nanoparticles can also induce cleavage of the Au-S bond (10 Hz, 4 ns, 100 mW, 35.4 mJ/cm^2, 532 nm).[1] By tuning the ionic strength of the solution and the applied laser fluence, the heating process could favor denaturation of the complementary single standed DNA over

cleavage of the Au-S bond. A loss of thiolated DNA strands capping the gold particles would otherwise lead to aggregation of the nanoparticles. Bakhtiari *et al.* demonstrated the release of fluorescein tethered to the surfaces of gold nanoparticles through a photothermally initiated reverse diels-alder reaction.[2] This molecular release was initiated by heat released from the surfaces of AuNPs during laser irradiation, while the thiolated ligand remained attached to the surfaces of the AuNPs. If uncontrolled, loss of capping molecules from nanoparticles would lead to colloidal instability, formation of radical species, and morphological changes of the nanoparticles.[25] Colloidal instabilities of gold nanorods following photothermal heating would decrease the concentration of nanorods in the solution through aggregation and/or precipitation of these particles.[3,8,10]

Payloads such as DNA,[25,26,27] polyethylene glycol (PEG),[28,29] and chemical drugs[30,31] have been released from gold nanoparticles through photothermal activation. However, in each of these studies the shapes and surface chemistry of the nanoparticles were not preserved during the photothermal process. We aim to minimize such morphological changes and to attempt to preserve the surface chemistry of gold nanorods following the PTE. Our approach to controlling the photothermal response of AuNRs was to precisely control the composition of the solutions in order to identify the influence of solution-based additives on the resulting changes in morphology (and possibly surface chemistry) of the AuNRs. The retention of structural shape implies a minimal restructuring of the atoms within the nanoparticle.[5] By probing the photothermal response as a function of the type of surface chemistry and the solution composition, we probed the dynamics of damage versus repair of the surface coatings and, indirectly, the rate of damage to capping groups as a function of surface chemistry and conditions for repair. In this fundamental study, gold nanorods capped with a bilayer of cetyltrimethylammonium bromide (CTAB) or with self-assembled monolayers of 11-mercaptoundecanoic acid (MUDA) were irradiated and their physicochemical stability assessed as a function of excess ligands in solution. A correlation of the photothermal response of these nanorods capped with either CTAB or MUDA will be discussed as it relates to their surface chemistries and the presence (or lack there in) of excess capping molecules. Our goal is to use gold nanorods as a platform for delivery of heat through the photothermal effect (PTE) while preserving the morphology, colloidal stability, and

surface chemistry of the nanorods, which is of particular importance in the prolonged delivery of heat or release of molecules from these nanorods.

3.2. Experimental Methods

Synthesis of Gold Nanorods. Gold nanorods were synthesized using a published seed-mediated method.[32] This synthesis was carried out at 30°C and the solution temperature was controlled by heating reactants contained within a flask in a water bath Briefly, a seed solution was prepared in a clean round bottom flask by mixing together 5 mL of an aqueous solution of 0.5 mM $HAuCl_4 \cdot 3H_2O$ and 5 ml of an aqueous solution of 0.2 M cetyltrimethyl ammonium bromide (CTAB) under stirring. Next, 0.6 mL of ice-cold 0.01 M $NaBH_4$ dissolved in water was quickly added to the round bottom flask, resulting in the formation of brown colored gold seeds. This solution was further stirred for 30 min at 30°C.

To prepare the gold nanorod growth solution, the following reagents were added into a polystyrene container with gentle mixing, listed in order of sequence of addition:

50 mL of an aqueous solution of 0.1 M CTAB,
316 µL of an aqueous solution of 10 mM $AgNO_3$,
2.1 mL of an aqueous solution of 10 mM $HAuCl_4 \cdot 3H_2O$,
336 µL of an aqueous solution of 0.1 M ascorbic acid (the solution changed color from deep yellow to colorless upon the addition of ascorbic acid),
and 420 µL of the seed solution prepared earlier.

This growth solution was then transferred to a water bath heated to 30°C. The color of the solution changed gradually from colorless to dark brown to brownish red within 1 h. This gold nanorod growth solution was left undisturbed at 30°C overnight.

Glass flasks and Teflon® coated stir bars used in this synthesis were cleaned with a solution of aqua regia and piranha, for 15 min in each solution. An 8 mL solution of aqua regia [3:1 (v/v) solution of 37% hydrochloric acid and 70% nitric acid] was prepared and used for cleaning a 50 mL round bottom flask and stir bar. A round bottom

flask and a magnetic stir bar were soaked with the freshly prepared solution of aqua regia over a period of 15 min. After 15 min, the aqua regia solution was disposed of. The flask and stir bar were then rinsed with at least 500 mL of 18 MΩ•cm deionized water produced using a Barnstead NANOpure DIamond Life Science water filtration system. *CAUTION: Aqua regia solutions are extremely corrosive. This solution should be handled with extreme care and disposed of appropriately.* Next, 9 mL of piranha solution [7:2 (v/v) mixture of concentrated 97% sulfuric acid and a 30% hydrogen peroxide] was prepared and used to further clean the 50 mL round bottom flask and stir bar. These were soaked with 9 mL of freshly prepared piranha for 15 min. After 15 min, the piranha solution was discarded before rinsing the flask and stir bar with at least 500 mL of of 18 MΩ•cm deionized water. NOTE: *Use caution when working with aqua regia and piranha solutions as they are corrosive.*

Purification of Gold Nanorods and Varying the Concentration of CTAB in Solution. The as-synthesized gold nanorods capped with CTAB surfactant were purified to remove excess CTAB by centrifugation (10 mL per centrifuge tube) at 8500 rpm for 25 min. The CTAB-capped nanorods were washed two times with a 1 mM CTAB solution through repeated steps of centrifugation and decantation of supernatants. The nanorods were further centrifuged, supernatants decanted and the nanorods were re-suspended in either: deionized water, or a 50 µM, 1.0 mM, or 5.0 mM CTAB solution. In total, these solutions of CTAB-coated nanorods were purified 3 times. These solutions with added CTAB were left in a water bath at 30°C overnight prior to performing photothermal studies. Following purifications and incubation at 30°C, these nanorods had the longitudinal surface plasmon resonance band centered at 751 nm.

Surface Modification of Gold Nanorods with 11-Mercaptoundecanoic Acid. A previously published ligand exchange procedure was used to displace the CTAB capping with 11-mecaptoundecanoic acid (MUDA)[33]. The as-synthesized CTAB-capped gold nanorods were used for a ligand exchange with an intermediate capping layer (dodecanethiol) without purification. In a 20 mL glass vial, 4 mL of the as-synthesized gold nanorods, 4 mL dodecanethiol (DDT) and 12 mL acetone were mixed together. The glass vial was swirled thoroughly to mix these solutions. A phase separation immediately occurred, with the DDT-capped gold nanorods observed as a purple colored organic

phase on top of a clear aqueous layer in the glass vial. Next a portion of the organic layer (~4 mL) was carefully collected and transferred into a 50 mL centrifuge tube. In addition, 4 mL of toluene and 22 mL of methanol were also added to the centrifuge tube containing the DDT-capped gold nanorods. The well mixed solution of DDT-capped nanorods were centrifuged at 8500 rpm for 30 min, the supernatant decanted and the nanorods re-suspended in 1 mL of toluene. In a clean round bottom flask with a stir bar and condenser attached to it, 9 mL of 0.05 M MUDA solution (dissolved in toluene) was heated to 70°C for ~15 min. This step is for thiol exchange, and it is anticipated that there may be some residual DDT left on the surfaces of gold nanorods after completion of this process. After 15 min, the 1 mL DDT-capped nanorods were added into the round bottom flask and the solution temperature increased to 120°C. Heating continued until the solution begun refluxing. After refluxing begun, the solution was refluxed further for 10 min until visible aggregates (small black particles) could be seen in the solution. This MUDA-capped gold nanorod solution was allowed to cool to room temperature, before being transferred into a 15 mL centrifuge tube. The solution was centrifuged at 8500 rpm for 20 min and the supernatant decanted. The MUDA capped nanorods were washed twice with toluene and once with isopropanol through repeated centrifugation, decantation of supernatants and suspension in the respective solvent. These nanorods were finally re-suspended in 1x TBE buffer (~2 mL buffer). The solutions were deep-blue colored immediately after adding TBE buffer, but the solution color changed to a deep-brown color after a few hours due to charge repulsion resulting from deprotonation of the carboxylates within the MUDA capping layers. These gold nanorods had the NIR surface plasmon resonance peak centered at 773 nm.

Varying the Concentration of MUDA in Solution. The MUDA-capped gold nanorods were diluted with more TBE buffer to a final OD of less than 1. These nanorods were then divided into three separate solutions and MUDA solutions dissolved in ethanol were added to final concentrations of: 0 (ethanol only, to keep the final volume, and hence the concentration, of each solution the same), 0.05 mM, 1.0 mM and 5.0 mM. These solutions were then left to mix on a vortex overnight. These solutions, containing either no excess MUDA or varying amounts of excess MUDA (0.05 mM, 1.0 mM, 5.0 mM), were used in subsequent photothermal studies without further purification.

Laser Irradiation of Gold Nanorods. Two milliliter solutions of gold nanorods were used for each irradiation experiment. These solutions of nanorods were prepared as detailed above and suspended in a known concentration of excess surfactants (MUDA or CTAB). A Neodymium-YAG laser (Spectra Physics) set to a wavelength of 800 nm was used to irradiate the nanorods. The pulsed light had pulse width was 120 fs, producing 1.24 mJ/cm^2 energy fluence per pulse at a repitition rate 1000 Hz. The diameter of the laser beam was 0.6 cm and the corresponding area of beam was 0.28 cm^2. The gold nanorods were irradiated in 4 mL polystyrene cuvettes and the laser beam was directed from the top-down directly to the samples. Samples were irradiated at 1 min intervals and UV-Vis spectra immediately acquired following their photothermal heating. The samples were each irradiated for a total of 10 min. Irradiated solutions were sampled for TEM analyses after 10 min irradiation without further purification. Gold nanorods capped with either CTAB or MUDA were also irradiated at 0.177 mJ/cm^2, 0.531 mJ/cm^2, and at 0.884 mJ/cm^2 energy fluences using neutral density filters. Each energy fluence was verified using a power meter.

Characterization. The extinction spectra were acquired using a Varian Cary 300 Bio spectrophotometer. Bright field TEM images were obtained with a Tecnai G2 STEM operating at 200 kV. The TEM samples were prepared by drop-casting solutions of nanorods onto a copper grid (300 mesh size) coated with Formvar/carbon (SPI Supplies Canada, ON, Canada). Samples were aliquoted for TEM analysis before irradiation and after 10 min irradiation. Samples collected for TEM analysis post-irradiation were immediately drop-cast onto TEM grids in order to avoid potential time-dependent changes to the nanorods' shape and/or size. The hydrodynamic diameters of the particles were acquired using a Malvern Zetasizer Nano ZS system. For each measurement, 1 mL of gold nanorod sample was used for analysis. The particle size analyses were performed on the samples before and after their laser irradiation. The XPS analyses were performed using a Kratos Analytical Axis Ultra DLD spectrometer using a monochromatic aluminum source (AlKα; 1486.6 eV) operating at 150 W. Composition was first analyzed with survey scans acquired with a pass energy of 160 eV, while a pass energy of 20 eV was used in acquiring high resolution scans. All analyses were obtained under a Hybrid lens mode, which permitted a wider collection angle of the emitted photoelectrons to increase the signal-to-noise of the data. Data

were collected from an analysis area of 700 μm by 300 μm, and analysis of this data was performed using Vision 2.2.7 Processing software.

3.3. Results and Discussion

Surface plasmon resonance (SPR) is a useful property of gold nanoparticles, and it can be exploited for enabling the photothermal effect and subsequently heat initiatied processes. The as-synthesized gold nanorods had a longitudinal SPR band centered at 769 nm. Gold nanoparticles can strongly absorb and scatter light due to a collective oscillation of the conduction band electrons. When the frequency of the incident light is the same as the frequency of oscillation of the surface conduction electrons, a resonance condition is reached (due to the absorption of electromagnetic waves by the electrons in gold nanoparticles), giving rise to a strong peak in the extinction spectra of gold nanoparticles. This peak is referred to as the localized surface plasmon resonance (LSPR) band.[6,34] The position of the LSPR band of gold nanorods depends on their size and shape[35]. Interestingly, anisotropic gold nanoparticles have two surface plasmon bands corresponding to light absorption and scattering along the long and short axes of the nanoparticles. When gold nanoparticles are irradiated with laser beams at wavelengths corresponding to the nanoparticles' LSPR band, the nanoparticles absorb the light and convert it into heat by a process known as the photothermal effect. This photothermal effect of gold nanoparticles can activate chemical processes (e.g., Au-S bond cleavage) associated with coating molecules bound to their surfaces[1,2,28,36], or lead to destabilization of the nanoparticles. In this study, changes in stability, shape and size of the gold nanorods during their photothermal heating were assessed by extinction spectroscopy, and transmission electron microscopy (TEM). Any changes to the LSPR band would imply a change in size or shape of the nanorods as well as destabilization of the nanorods due to the photothermal heating. TEM is used to analyze changes in the size of the gold nanorods following laser irradiation. The long-term goal was to preserve the shape, size and optical properties of these nanoparticles when used towards delivery/release of a molecular payload, such as a therapeutic agent. Preservation of these properties could be essential for prolonged, quantitiative release of a therapeutic

molecular payload, but changes in these properties would imply a chang in the surface chemistry, and thus impact the long-term stability, of these particles.

Desorption of capping molecules during photothermal processes could lead to instabilities of the nanoparticles by creating gaps in the monolayer coverage (where coatings are desorbed), which leads to Au-Au aggregation. It is, therefore, important to manipulate the surface chemistry of nanoparticles in order to minimize deprotection of the surfaces through desorption of stabilizing molecules. The aim of this study was to minimize the structural and chemical damage to gold nanorods upon photothermal treatment, in an attempt to preserve their shape, size and surface chemistry. Instabilities in the AuNRs during PT heating were probed by tuning the concentrations of additives in solution (e.g., excess stabilizing molecules) during photothermal treatment. Maintaining these properties is crucial for the successful use of AuNRs in a prolonged delivery of localized heat by the PTE. When added into solutions of nanoparticles, excess capping molecules could repair any 'hole' defects created by the photothermal desorption of molecular coatings (Figures 3.1 and 3.2). We monitored the extinction spectra over a period 10 min to assess changes in stability of the suspended particles. These spectra were acquired at 1 min intervals of laser irradiation up to a total of 10 min, in order to assess the progressive change of nanoparticle stability during the photothermal treatment. Integrated peak areas from the particles' extinction spectra were also monitored and proportional to changes in concentration of suspended nanoparticles. This study presents an initial comparison of the photothermal response as a function of the type of surface chemistry on the AuNRs and composition of additives in solution. By tuning the solution composition, we seek to tune the photothermal response of gold nanorods during their photothermal heating. Additionally, the strength of interaction between molecular coatings and the nanorods (e.g., covalent versus ionic interacations) will be indirectly compared by studying gold nanorods with two different surface chemistries. These results will help in assessing the influence of surfactants on the physicochemical stability of AuNRs during their potential use in photothermal applications, which can include triggered molecular release and/or activation of molecular reactions.

no excess CTAB in solution

800 nm, 120 fs, 350 mW

A.

← CTAB bilayer

excess CTAB in solution

B.
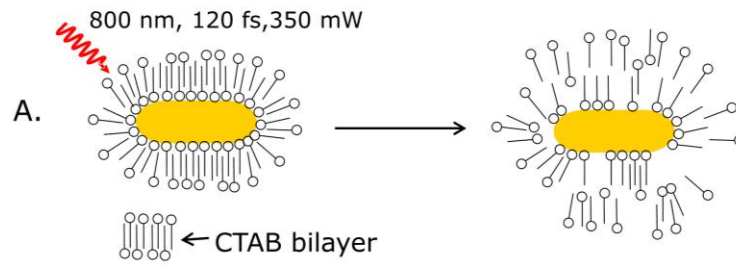
free CTAB   CTAB micelle
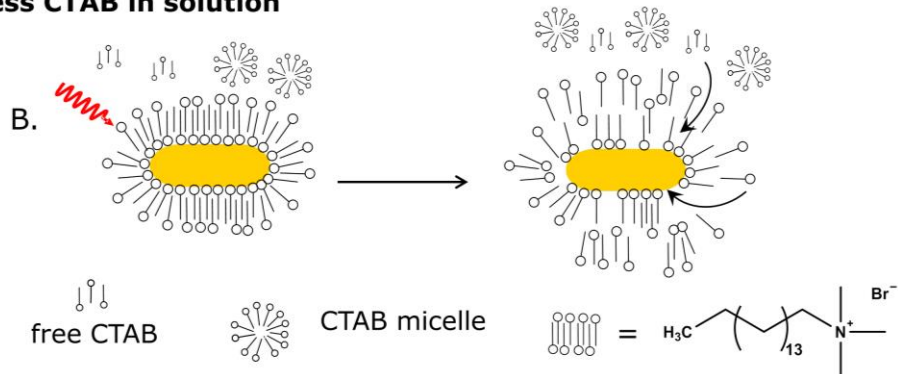
Figure 3.1.   Gold nanorods capped with cetyltrimethylammonium bromide (CTAB). CTAB coatings form a bilayer on gold nanorod surfaces. The bilayer is in dynamic equilibrium with free CTAB molecules and micelles in solutions of nanorods.

no excess MUDA in solution

800 nm, 120 fs, 350 mW

A.

excess MUDA in solution

excess MUDA

B.

$\sim\!\sim\!\sim$ = OH $\left(\right)_8$ SH MUDA
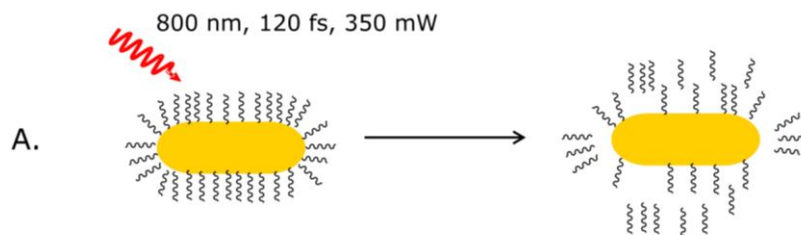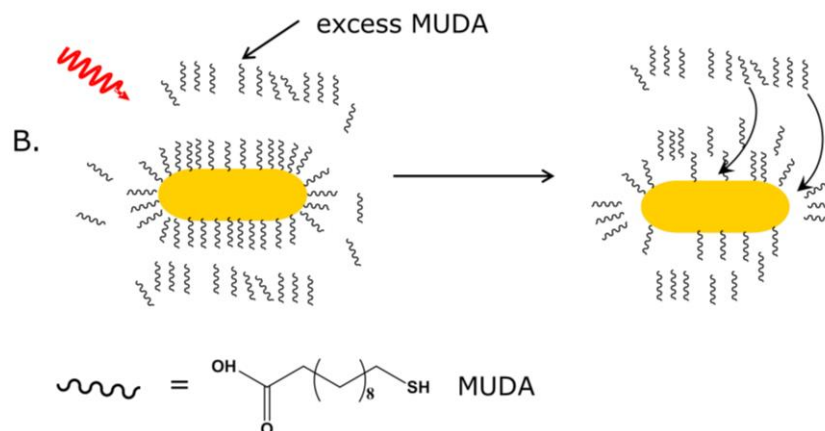
Figure 3.2.   Gold nanorods capped with 11-mercaptoundecanoic acid (MUDA). MUDA forms a monolayer around gold nanorods.

A red-shift in the longitudinal LSPR of CTAB-capped gold nanorods following their modification with MUDA by 3 nm confirmed a change in surface chemistry of these gold nanorods,. These nanorods were further analyzed by XPS to assess the exchange of capping layers for the MUDA-modified nanorods. Survey scans for both types of nanorods were analyzed for the presence of C, S, Au, Ag, N, O, Br, Si (Figure 3.3). The Au and Ag contributions are from the nanoparticles prepared by the seed-mediated method. The Si_{2s} and Si_{2p} signals are from the polished silicon substrate on which the samples were drop cast for XPS analysis. Possible sources of C_{1s} are the molecular coatings (CTAB or MUDA) on the nanorods. The Br_{3p} signal is characteristic of the counterion associated with the CTAB molecules, and S_{2p} is from the thiolate of the MUDA capping layers. The presence of a Br_{3p} signal in the MUDA-capped gold nanorods suggests that there is some residual bromide ion remaining on the surfaces of these nanorods after the ligand exchange. The N_{1s} signal is also from CTAB, which has a quaternary amine. The Cl_{2s} and Cl_{2p} peaks in the MUDA-capped nanorods is likely

from the salts in the buffer solution. Further information about the composition of the coatings stabilizing the AuNPs was obtained by high resolution X-ray photoelectron spectroscopy (HRXPS) in the N_{1s} and S_{2p} regions (Figure 3.4). The high resolution S_{2p} spectra had peaks only for the MUDA-capped nanorods centred at 168.1 eV and 162 eV, and none for the CTAB-capped nanorods as expected (Figure 3.4b). The S species is from the bound sulfur headgroup of alkanethiolates (161.9-163 eV), and oxidized sulfur (>166 eV) species on gold nanorods.[37-38] High resolution N_{1s} XPS spectra for these samples had two peaks centered at binding energies of 401.9 eV and 404.6 eV which is associated with CTAB bound to gold nanorods and unbound or free CTAB, respectively (Figure 3.4a).[39] These further confirmed the successful exchange of CTAB-coatings for MUDA-coatings on gold nanorods. The XPS analysis provides a qualitative analysis of the surface composition, but other techniques were necessary to characterize other properties of the particles. Extinction spectroscopy was used in conjunction with these studies to analyze the colloidal stability of nanorods following the photothermal heating processes.

Changes in the optical properties of gold nanorods were initially assessed by the changes in intensity and shifts in position of the LSPR band following laser irradiation. Following their photothermal treatment, a number of changes were observed for the gold nanorods modified with CTAB. The rate of decrease of the longitudinal surface plasmon band is fastest for those gold nanorods in pure water (no excess CTAB, Figure 3.5a) and this rate gradually decreases as the amount of CTAB in solution increases (Figures 3.5c, 3.5e, 3.5g). The nanorods containing no added CTAB were destabilized during irradiation most likely due to desorption of capping molecules from the nanorod surfaces during their photothermal treatment. The photothermal-initiated desorption of molecular coatings has been previously observed for AuNPs.[3,10] This loss of spectral intensity continues throughout the experiment, such that at 10 min of irradiation the spectrum was almost at a baseline value (Figure 3.5a). Additional surfactants in solution should replace the desorbed and/or thermally damaged molecules, thereby minimizing chemical changes to irradiated nanorods. As little as 0.05 mM excess CTAB in solutions of gold nanorods slowed the rate of their destabilization during PT heating (Figure 3.5c), in comparison to those nanorods suspended in only deionized water. After 1 min of irradiation, the extinction spectra of the nanorods suspended without excess CTAB (or

water only) and 0.05mM excess CTAB, decreased in intensity by ~71% and ~31%, respectively. Those nanorods suspended in 1.0 mM and 5.0 mM CTAB exhibited a progressive blue shift in their LSPR band throughout the duration of laser irradiation. These samples also exhibited a sharpening of their extinction spectra (Figures 3.5e and 3.5g), which could be attributed to a decrease in the polydispersity of the particle dimensions within the population of nanorods during photothermal treatments. This effect has been observed in previous studies.[40] The extinction spectra of these nanorods suspended in 5.0 mM and 1.0 mM CTAB blue-shifted from 751 nm (for non-irradiated nanorods) to 738 nm and 726 nm, respectively, following their laser irradiation at 800 nm for 10 min, which could be attributed to a change in the aspect ratios of the nanorods.
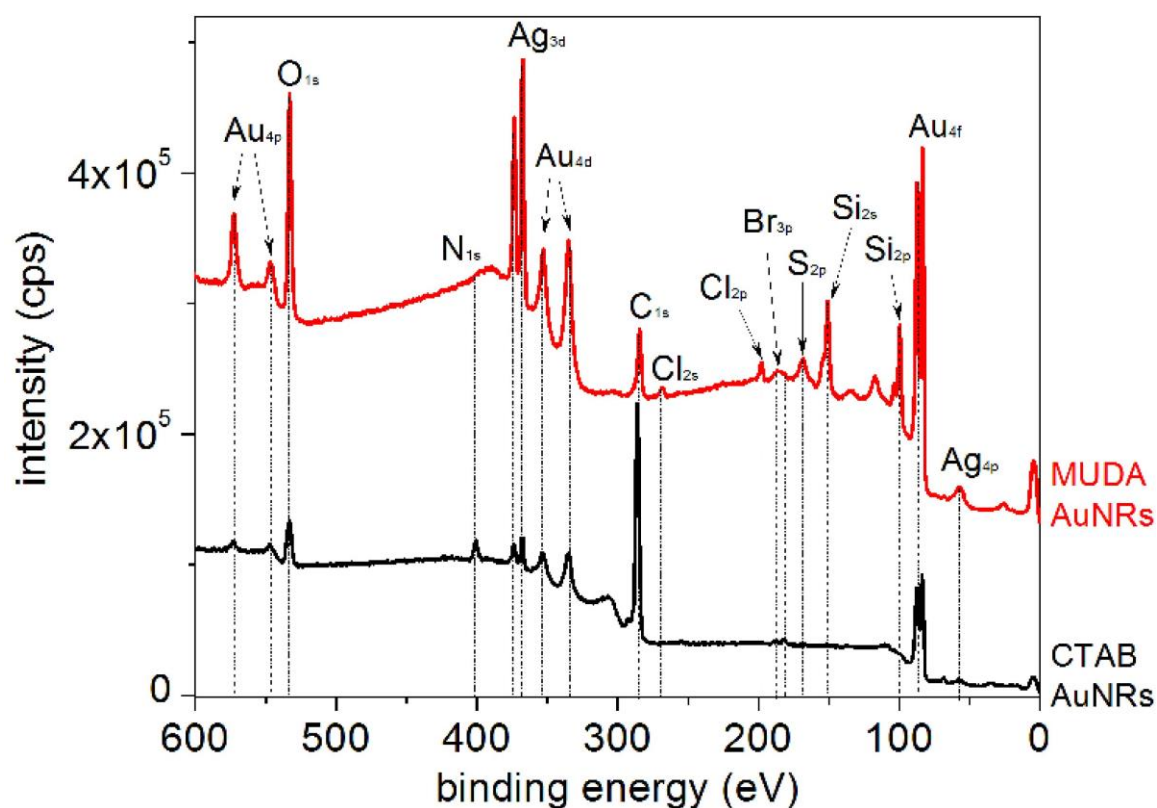
Figure 3.3.   Survey X-ray photoelectron spectroscopy (XPS) scans of as-made MUDA- and CTAB-capped gold nanorods. The MUDA-capped gold nanorods were cast from a suspension in TBE buffer and the CTAB-capped nanorods were cast from a solution in deionized water.
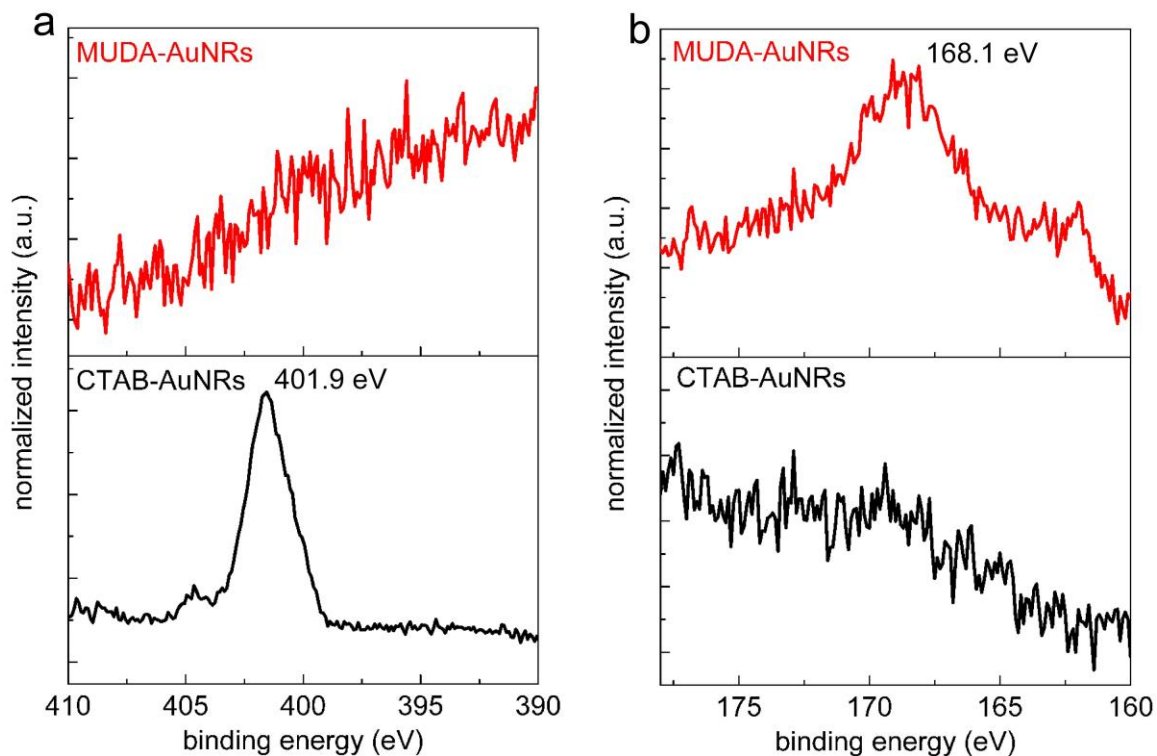
Figure 3.4. High resolution X-ray phototelectron spectroscopy (XPS) of MUDA and CTAB-capped gold nanorods. a) N_{1s} region b) S_{2p} region for the as-prepared nanorods. The MUDA-capped gold nanorods were cast from a suspension in TBE buffer and the CTAB-capped nanorods were cast from a solution in deionized water.

The analysis of the samples by TEM was used to further monitor morphological changes to the nanorods following the photothermal treatment. Gold nanorods, in solutions without any excess CTAB or with 0.05 mM excess CTAB, fused together (Figure 3.5b and 3.5d) after 10 min of laser irradiation, indicating instability of these nanostructures. These nanorods likely suffered from desorption and/or thermal damage of CTAB molecules and a consequent aggregation of the nanorods. There was slight restructuring of gold nanorods suspended in millimolar concentrations of CTAB, as they transformed into peanut shaped structures (Figures 3.5f and 3.5h). Such structural changes can be minimized by using lower laser fluence energies, or by changing surface chemistry of gold nanoparticles. It has been previously demonstrated that differences in heat diffusion is caused by the types of molecular coatings on gold nanoparticles.[23] The corresponding TEM images of these AuNRs suspended in 1.0 mM and 5.0 mM CTAB also indicated these particles were well dispersed after 10 min laser irradiation with no

evidence of Au-Au fusion between separate nanorods (Figures 3.5f and 3.5h). The relatively higher concentrations of excess CTAB in solution replaces any molecules desorbed during photothermal heating processes, thereby greatly improving the photothermal stability of those nanorods suspended in millimolar concentrations of excess CTAB. These different trends are sometimes obvious when comparing the extinction spectra, but more subtle changes in each of the observed trends are difficult to discern. This data was converted to a change in relative integrated peak areas of gold nanorods to provide a more quantitative measure of changes in their physicochemical stability.

Physicochemical stability of gold nanorods during photothermal processes was further assessed by changes in peak areas of nanoparticles in solution, as well as the position of the plasmon band during irradiation. The rate of decrease in nanorod peak areas during photothermal treatment gives an indication of the stability of the nanorods and was found to depend on the amount of excess surfactants in solutions of gold nanorods. The nanorods irradiated in the absence of excess capping molecules had the largest decrease in peak areas as comparison to those irradiated in the presence of excess surfactants, confirming the importance of added surfactants during photothermal irradiation (Figure 3.6). The gold particles suspended with no excess CTAB or with 0.05 mM CTAB decreased in relative peak area of nanorods from 0.35 to 0.02 or 0.04, respectively, after 3 min of laser irradiation. At least 1.0 mM of excess CTAB was required in solution to significantly reduce the loss of particles during irradiation (Figure 3.6a). Those nanorods suspended with a millimolar excess CTAB dropped in peak areato 0.25 nanorods after 10 min of irradiation. These results indicate that the destabilization of the gold nanorods suspended in little or no excess CTAB was due to desorption and/or damage of capping CTAB molecules, triggered by the photothermal treatment. All irradiated nanorods exhibited a blue spectral shift, but those nanorods suspended with little or no excess CTAB had a resulting longitudinal LSPR band that approached the baseline of their spectra within ~3 min of laser irradiation. The position of the longitudinal LSPR band could, therefore, not be further assessed for these solutions of gold nanorods (Figure 3.6b).The critical micellar concentration of CTAB to maintain a bilayer on nanorods is ~1 mM[41,42], which would explain the similarity in the observed stability for the nanorods suspended in 1.0 mM and 5.0 mM excess CTAB.

Therefore, no significant difference in the photothermal response was expected for those nanorods suspended in CTAB concentrations greater than 1.0 mM, when compared with nanorods suspended in 1.0 mM excess surfactants.
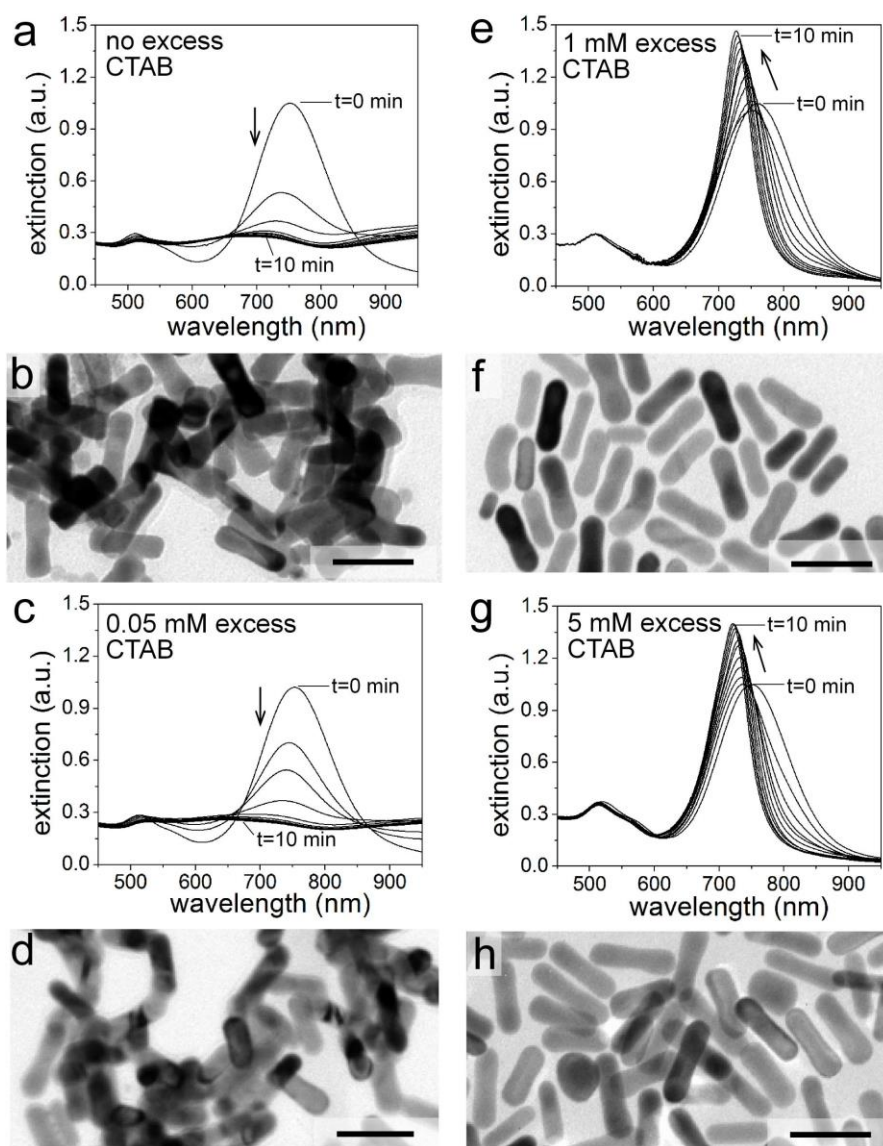
Figure 3.5. Photothermal stability of cetyltrimethylammonium bromide (CTAB) capped gold nanorods following laser treatment. Particle stability determined by extinction spectroscopy and transmission electron microscopy (TEM). Samples were irradiated at 1 min intervals with a 120 fs pulsed laser (1 kHz) operating with an output of 1.24 mJ/cm^2 at 800 nm. A spectrum of the nanorods prior to irradiation (t=0 min) is included for comparison. The nanoparticles were suspended in deionized water containing varying amounts of CTAB: (a-b) no excess CTAB; (c- d) 0.05 mM CTAB; (e-f), 1 mM CTAB; and (g-h) 5 mM CTAB. Electtron microscopy images correspond to the nanoparticles after irradiation for 10 min. Coalescence of nanorods is apparent in the samples suspended without excess CTAB or with only 0.05 mM CTAB. Scale bars in the TEM images are 50 nm.
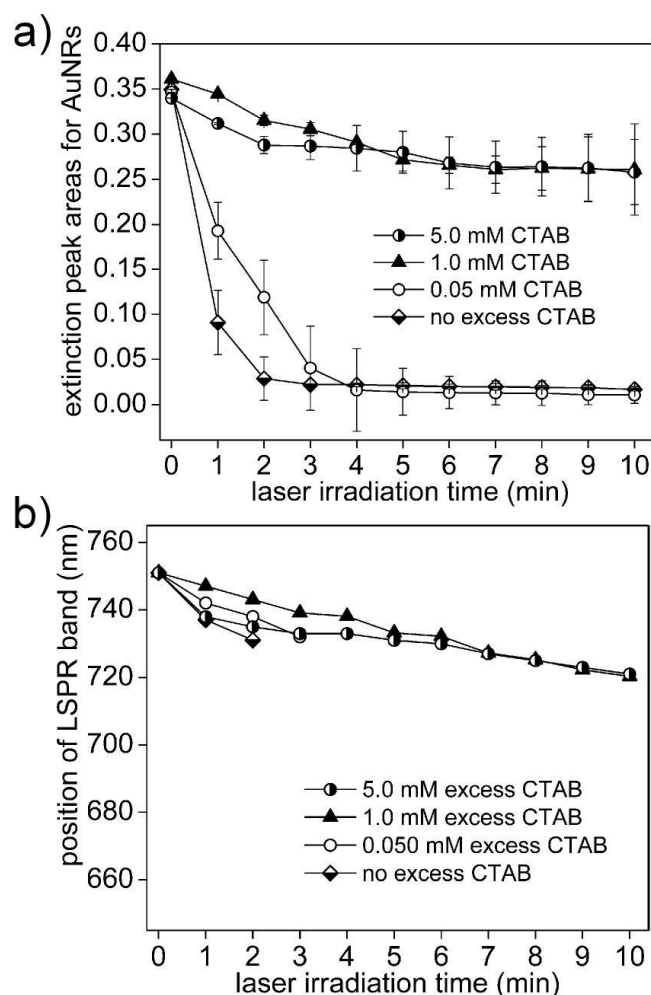
Figure 3.6. **(a) Time dependent change in relative peak areas of gold nanorods (AuNRs) suspended in solutions of varying concentrations of CTAB during laser irradiation. Error bars in this plot are calculated as one standard deviation from the mean of two independent experiments (b) Dependence of the position of the longitudinal localized surface plasmon resonance (LSPR) band position on the duration of laser irradiation for these CTAB capped nanorods.**

Figure 3.7 shows extinction spectra and electron microscopy images of MUDA-modified nanorods irradiated for a total of 10 min at a fixed laser fluence of 1.24 mJ/cm^2. The decrease LSPR band intensities was fastest for those nanorods suspended in only TBE buffer (Figure 3.7a). In contrast, the addition of 0.05 mM excess MUDA to the solutions of MUDA-capped gold nanorods helped stabilize their stability as seen in the minimized rate of spectral decrease following photothermal treatment (Figure 3.7c). The excess MUDA could help stabilize the gold nanorods in solution by influencing the

111

equilibrium between desorbed thiols and the free thiols in solution.[43] A further increase in concentration of excess MUDA in solutions of gold nanorods during irradiation resulted in a gradual sharpening of the longitudinal LSPR bands (Figures 3.7e and 3.7g), similar to those nanorods capped with CTAB and suspended in millimolar concentrations of excess CTAB (Figures 3.5e and 3.5g). This stability trend correlates with the amount of excess surfactants added to each solution of gold nanorods during photothermal treatments and indicates the stabilizing role of surfactants in solution. Heat from photothermal processes could increase mass transfer to and from the surfaces of the nanorods, which could anneal the surfaces (and defects therein) of the nanorods. This thermal treatment could also induce the oxidation of MUDA, which would consequently lead to its dissolutionfrom surfaces of gold nanorods, producing defect sites on these gold nanostructures. The dissolution of bound alkanethiolates may lead to oxidation of the desorbed thiols, which could form disulfides that have lower kinetics of binding (re-adsorption) to gold when compared to alkanethiols.[44] The excess surfactants, therefore, result in lower defect sites on surfaces of nanoparticles, or otherwise increase the density of the molecular coatings by repairing (or filling gaps created by the desorbed thiols) within molecular coatings during photothermal processes.
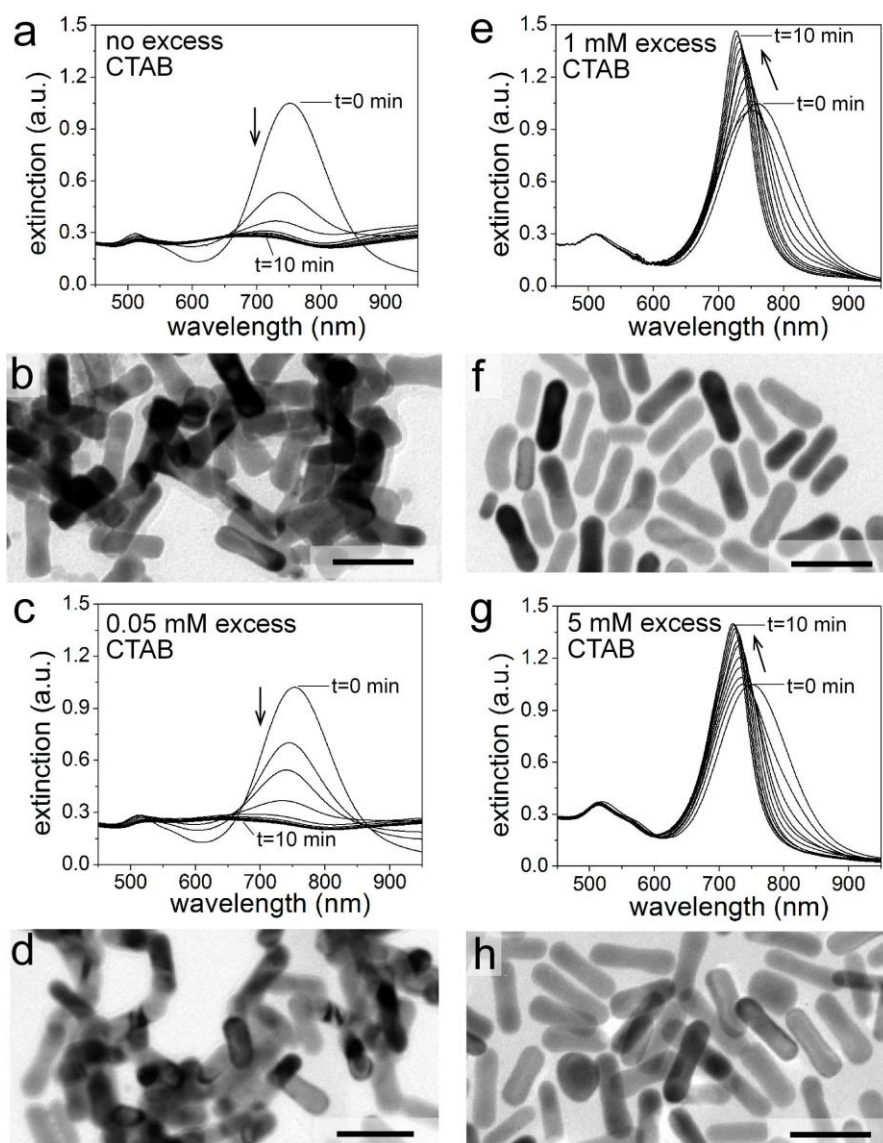
Figure 3.7. **Photothermal stability of 11-mercaptoundecanoic acid (MUDA) capped AuNRs after laser irradiation as assessed by extinction spectroscopy and TEM analysis. Solutions were irradiated at 1 min intervals with a 120 fs pulsed laser (1 kHz and an output of 1.24 mJ/cm^2 at 800 nm). The nanorods were suspended in a 1× TBE buffer containing varying amounts of MUDA: (a-b) no excess MUDA; (c-d) 0.05 mM MUDA; (e-f), 1.0 mM MUDA; and (g-h) 5.0 mM MUDA. Electron microscopy images show dispersion and morphology of nanorods that have been irradiated for 10 min. Scale bars for the TEM images are 50 nm.**

The physicochemical stability of MUDA-modified nanorods was additionally assessed by electron microscopy. The MUDA-capped nanorods nanorods suspended in

0.05 mM excess MUDA were more stable against aggregation, as compared with those suspended in no excess CTAB. The former showed a good dispersity following irradiation, with no evidence of particle-particle fusion (Figure 3.7d). There was, however, some formation of peanut-shaped nanorods for these nanorods suspended in 0.05 mM excess MUDA. The nanorods suspended in millimolar concentrations of excess MUDA had the least extent of aggregation or reshaping, and we could, therefore, reasonably conclude that MUDA is a more robust coating. The alkanethiolate coatings likely form more ordered coating layers due to both the dative bond formed between the sulfur headgroup and the gold surfaces, as well additional van der Waals forces between neighboring alkanethiolate chains.[45,46] Gold nanorods stabilized with CTAB are stabilized by non-covalent and ionic interactions between the quaternary amine headgroup, as well as with van der Waals forces between the hydrophobic tails of the CTAB molecules.[47] The energy of adsorption of an alkanethiolate and a CTAB molecule on gold is ~50 kcal/mol[48] and ~26 kcal/mol (or 108.8 kJ/mol) [49], respectively. It is, therefore, expected that the MUDA coatings will form stronger stabilizing interactions with gold surfaces, as compared to less strongly binding CTAB. These interactions will also dictate the kinetics of the photothermal desorption of molecular coatings from gold nanoparticles during the process of their photothermal heating. Both the extinction data and electron microscopy results indicate the greatest destabilization of those nanorods with least amounts of excess surfactants. Monitoring the change in peak areas of the suspended nanoparticles during the process of laser irradiation can be used to quantify these time-dependent changes in colloidal stability of the CTAB or MUDA capped particles.

The peak area calculated from the extinction spectra of gold nanorods modified with MUDA dropped gradually during photothermal treatments for those nanorods suspended in excess MUDA (Figure 3.8a). The rate of loss of peak area of AuNRs was, however, significantly higher for solutions of gold nanorods without any excess MUDA (Figure 3.8). The peak areas of nanorods dropped to ~12%, ~46%, ~83%, and ~77% of their original values after 10 min of laser irradiation for those nanorods suspended in no excess, 0.05 mM, 1.0 mM and 5.0 mM excess MUDA, respectively. The nanorods suspended in only TBE buffer (no excess MUDA) likely had the most desorption of the MUDA capping molecules. This desorption of capping molecules can lead to the

formation of defects (due to missing molecules), which cause instabilities to the AuNRs during photothermal processes. These results highlight the impact of defects within molecular capping layers on the observed stabilities of AuNRs.[18] It is, however, not clear why the nanorods suspended in 1.0 mM excess MUDA were more stable than those suspended in 5.0 mM excess MUDA. It is possible that the excess surfactants are saturated in solution above 1.0 mM concentrations. The position of the LSPR band blue-shifted with increasing times of exposure of the MUDA-modified gold nanorods to laser irradiation (Figure 3.8b), which corresponded to a decrease in nanorod aspect ratio. The rate of blue shifting was fastest for gold nanorods suspended in TBE buffer, without any excess MUDA. The longitudinal LSPR blue-shifted by 47 nm for these nanorods suspended without any excess MUDA (Figure 3.8b) after 1 min of laser irradiation and by 85 nm after 10 min of irradiation. The rates of shifting of the LSPR band was much slower for the nanorods suspended in some excess amount of MUDA, which shifted by 11 nm or 4 nm for nanorods in 0.05 mM and 1.0 mM excess MUDA, respectively, after 1 min of laser irradiation. The photothermal annealing of the nanorods could result in reshaping of these structures. These structural changes were quantified by measuring the dimensions of the nanorods following photothermal treatment by electron microscopy.

We measured the dimensions of the gold nanorods before and after laser irradiation in order to assess any structural changes resulting from the laser irradiation of these nanostructures. There were interesting changes observed in dimensions of both CTAB- and MUDA-modified nanorods. At least 400 particles per sample were measured in order to compute the average dimensions of the nanorods. These subtle changes in dimensions of the anisotropic gold structures could only be identified through a statistical analysis of the changes in dimensions of a large quantity of nanorods following the photothermal treatment. As-synthesized AuNRs CTAB-capped nanorods had dimensions of 41 nm × 15 nm (length × width). These gold nanorods elongated to 46 nm when irradiated either in the presence of 5.0 mM CTAB or in the absence of excess CTAB . The elongation of nanorods could be due to photofragmentation of the gold, leading to a high presence of small gold nanoparticles in solution that could be readily adsorbed onto the end facets of the gold nanorods. The lengths were, however, preserved for intermediate concentrations of excess CTAB (Figure 3.9). The widths

increased in all cases of irradiated samples, whether with or without excess CTAB, with the greatest increase in width (to 17 nm), observed for those nanorods suspended in no excess excess CTAB. There is no clear trend in change of nanorod dimensions, but the nanorods suspended in 0.05 mM to 1.0 mM excess CTAB largely retained their dimensions following the photothermal processes. It is noteworthy that all those nanorods suspended in no excess CTAB or in 0.05 mM CTAB decreased in aspect ratios, while the nanorods suspended in either 1.0 mM or 5.0 mM excess CTAB had slight increases in their aspect ratios upon laser irradiation. The changes in dimensions of nanorods could be attributed to the desorption of CTAB coatings from high energy (100) and (110) facets, which results in the exposure of these facets and subsequent shape change of these anisotropic nanostructures.[50]

Structural transformations of MUDA-capped nanorods were also analyzed by measuring the lengths and diameters of these nanostructures (from TEM micrographs) following laser irradiation. The MUDA-modified nanorods were 49 nm in length and 18 nm in width before laser irradiation. The average lengths of the nanorods decreased to 40 nm and 43 nm for those particles suspended in the absence of excess MUDA and 5.0 mM MUDA, respectively (Figure 3.10). Those nanorods suspended in 0.05 mM or 1.0 mM excess MUDA had lengths of 446 nm and 48 nm, respectively, following 10 min of laser irradiation. The width of nanorods suspended in 5.0 mM excess MUDA increased by 2 nm. The relatively high concentrations of excess MUDA are likely stabilizing small particles formed from photofragmentation of the nanorods, increasing the presence of colloidally stable nanoparticles that can add back onto the high energy end facets of the gold nanorods, which leads to an increase in their overall length. The nanorods suspended in no excess or 0.05 mM excess MUDA changed to 14 nm or 17 nm, respectively, in their widths after the photothermal processes. Gold nanorods suspended in 1.0 mM excess MUDA best preserved their dimensions following photothermal treatments, similar to those suspended in 1.0 mM excess CTAB. The high concentrations of excess surfactants stabilize smaller particles formed from photofragmentation of gold, which can be seen as an increased distribution of lengths and widths post-irradiation for those nanorods suspended in either 5.0 mM excess CTAB or 5.0 mM excess MUDA. It may be that there is an optimal concentration of excess

116

molecular additives in solution to shift the equilibrium to favor the adsorption of molecules, replacing those that are desorbed in the process of photothermal treatments.

Lower laser energy fluences (Appendix A) were also applied to these nanorods modified with varying amounts of excess surfactants, in order to compare the stabilities of AuNRs during irradiation with lower energies. Colloidal stability of these materials was assessed as a function of the type of capping molecules and concentrations of excess stabilizing molecules in solution. Both types of nanorods (CTAB- or MUDA-coated) had similar trends in their stabilities. The nanorods irradiated in the absence of excess capping molecules had largest decrease in concentrations as compared to those irradiated in the presence of excess surfactants, further confirming the importance of added surfactants during photothermal irradiation. The rates of destabilization of nanorods increased with increasing energy fluences as expected, due to the increased loss of molecules as a function of the applied energy. Through these studies, we show that stability of nanoparticle systems is greatly improved by increasing the concentrations of excess stabiliizing molecules during laser irradiation. In addition, irradiation parameters (e.g., energy fluence and irradiation time) can be tuned to optimize the use of the PTE, while maintaining the desirable optical properties of AuNPs, as well as their colloidal stability.
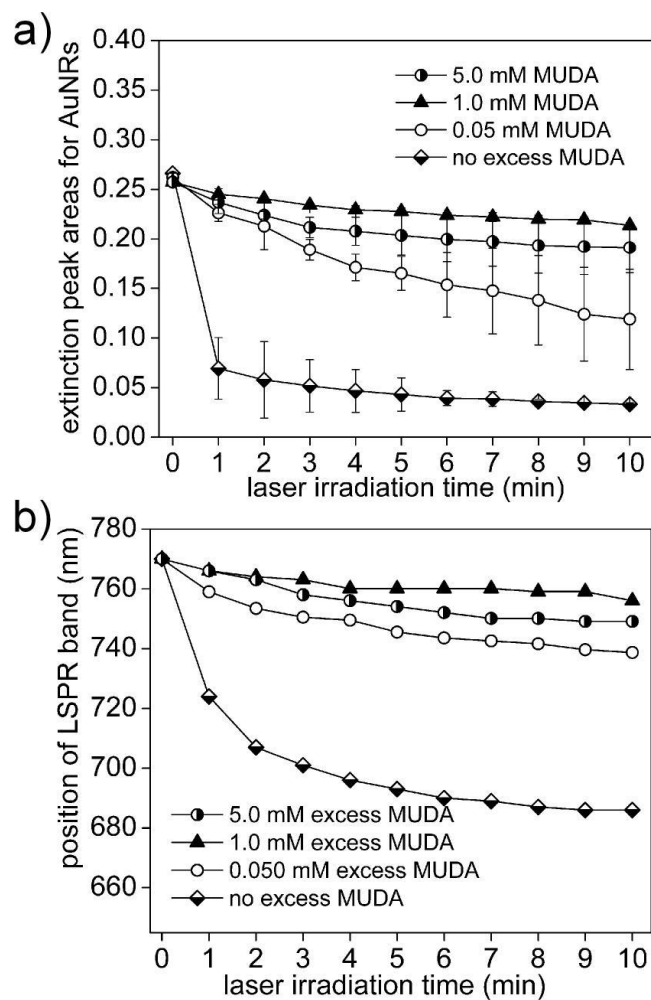
Figure 3.8. **(a) Time dependent change in the relative peak areas of MUDA capped AuNRs during irradiation with a pulsed laser. Error bars in this plot are calculated as one standard deviation from the mean of two independent experiments (b) Time dependent shifts in the position of the longitudinal LSPR band during this laser irradiation of the MUDA-capped AuNRs.**
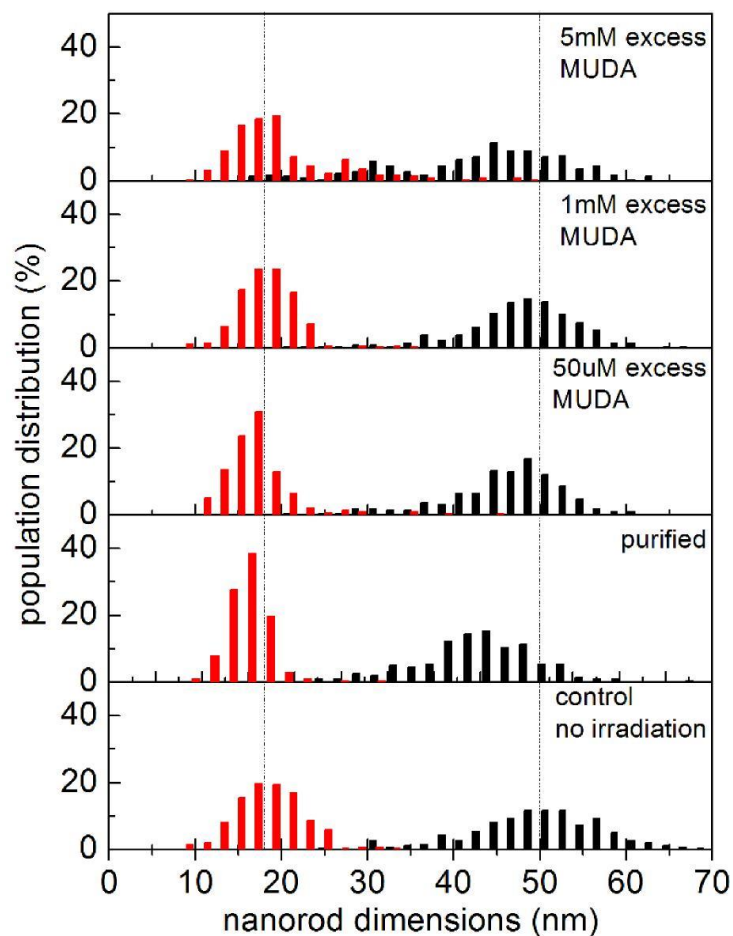
Figure 3.9. Histograms of measured diameters and lengths of CTAB capped AuNRs as determined by TEM analysis before and after irradiation with a pulsed laser. Irradiation studies used a 120 fs laser at 800 nm, overlapping with the longitudinal LSPR band of the AuNRs.
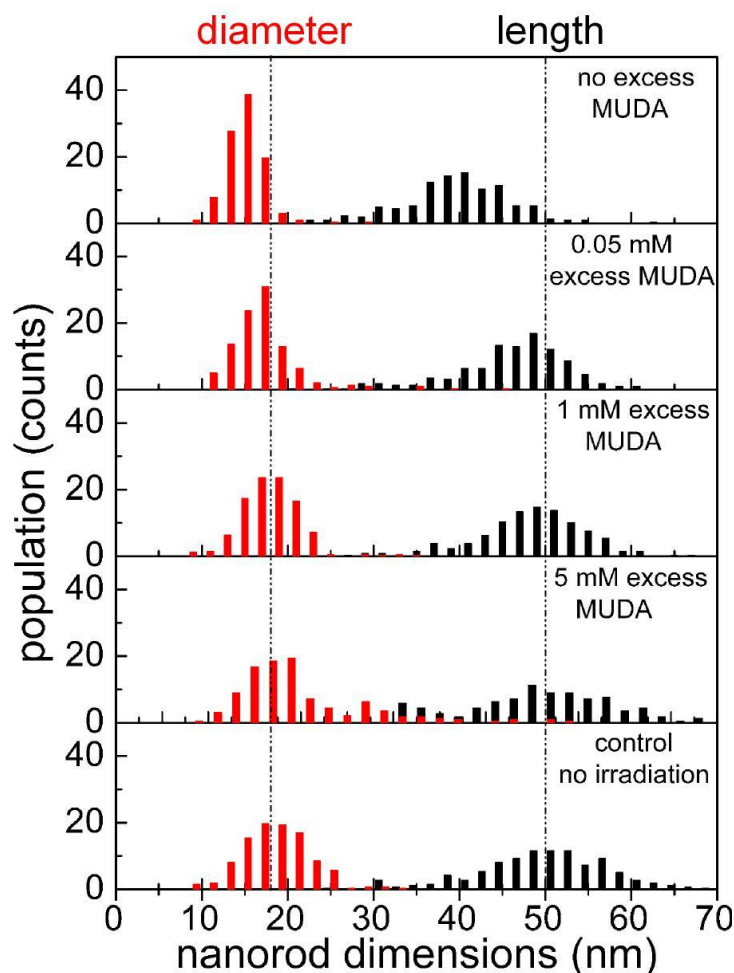
Figure 3.10. **Histograms of measured diameters and lengths of AuNRs capped with MUDA as determined by TEM analysis before and after irradiation with a pulsed laser. Irradiation was performed at a laser fluence of 1.24 mJ/cm² at 800 nm for a total of 10 min.**

3.4. Summary and Conclusions

In summary, the photothermal response of gold nanorods following their irradiation with a pulsed laser has been tuned by varying concentrations and the type of excess stabilizing molecules in solution. Addition of excess surfactants to the solutions of gold nanorods during photothermal processed improved the physicochemical stability of the nanorods by repairing defects within molecular coatings on the nanorod surfaces. Otherwise the nanorods suspended without any excess surfactants had relatively higher

rates of destabilization due to desorption of the molecular coatings. Changes to the physicochemical stabilites of gold nanorods were reflected in the change in their optical properties, as assessed by extinction spectroscopy. MUDA-capped gold nanorods were more robust capping layers when little or no surfactant was added in solution due to both the strong Au-S bond on AuNPs and strong intermolecular forces between alkyl chains of MUDA. The forces of interaction between nanoparticles and surfactants, or intermolecular forces between surfactants adsorbed onto or bound to the surfaces of the particles influence the quality of coatings on the nanoparticles and their resistance to desorption following PT processes. The CTAB coatings bind less strongly to surfaces of gold and would, therefore, be dissolved from surfaces of gold at a faster rate when compared to MUDA coatings. The CTAB capping layers do, however, provide a better protection against structural (e.g., size) changes when the concentrations of excess CTAB in solution were in the millimolar range. This study demonstrates that both surfactants on the surfaces of nanoparticles, as well the excess surfactants in solution play an important role of stabilizing these nanoparticles during photothermal processes. Knowledge learned from these studies could be used to prepare plasmonic nanoparticles as a platform for the controlled, time dependent release of heat and molecular payloads (e.g., chemotherapeutics) while simultaneously maintaining a high degree of control over the desired properties of the nanorods. This controlled release is achievable by tuning the energy that is applied to trigger the release of molecules from nanoparticles. Preliminary results also indicate that there might be an optimal laser fluence that minimizes the structural damage to the nanoparticles and their surface chemistry during the photothermal processes. Further work is necessary to identify the balance between heat triggered release of a molecular payload while minimizing or avoiding structural damage to the nanostructures. In addition, other additives must also be sought / explored to improve the stability of nanoparticles during photothermal processes. This will include a detailed analysis of molecular species (e.g., peptide fragments and proteins) that might be present in solution in more physiologically relevant solutions.

3.5. References

(1)   Poon, L.; Zandberg, W.; Hsiao, D.; Erno, Z.; Sen, D.; Gates, B. D.; Branda, N. R. *ACS Nano* **2010**, *4*, 6395-6403.

(2)   Bakhtiari, A. B. S.; Hsiao, D.; Jin, G.; Gates, B. D.; Branda, N. R. *Angewandte Chemie-International Edition* **2009**, *48*, 4166-4169.

(3)   Jain, P. K.; Qian, W.; El-Sayed, M. A. *Journal of the American Chemical Society* **2006**, *128*, 2426-2433.

(4)   Chang, S. S.; Shih, C. W.; Chen, C. D.; Lai, W. C.; Wang, C. R. C. *Langmuir* **1999**, *15*, 701-709.

(5)   Link, S.; Wang, Z. L.; El-Sayed, M. A. *Journal of Physical Chemistry B* **2000**, *104*, 7867-7870.

(6)   Link, S.; El-Sayed, M. A. *International Reviews in Physical Chemistry* **2000**, *19*, 409-453.

(7)   Link, S.; Burda, C.; Mohamed, M. B.; Nikoobakht, B.; El-Sayed, M. A. *Journal of Physical Chemistry A* **1999**, *103*, 1165-1170.

(8)   Gordel, M.; Olesiak-Banska, J.; Matczyszyn, K.; Nogues, C.; Buckle, M.; Samoc, M. *Physical Chemistry Chemical Physics* **2014**, *16*, 71-78.

(9)   Werner, D.; Hashimoto, S.; Uwada, T. *Langmuir* **2010**, *26*, 9956-9963.

(10)   Link, S.; El-Sayed, M. A. *Journal of Chemical Physics* **2001**, *114*, 2362-2368.

(11)   Warshavski, O.; Minai, L.; Bisker, G.; Yelin, D. *Journal of Physical Chemistry C* **2011**, *115*, 3910-3917.

(12)   Ungureanu, C.; Kroes, R.; Petersen, W.; Groothuis, T. A. M.; Ungureanu, F.; Janssen, H.; van Leeuwen, F. W. B.; Kooyman, R. P. H.; Manohar, S.; van Leeuwen, T. G *Nano Letters* **2011**, *11*, 1887-1894.

(13)   Abdelhamid, S.; Saleh, H.; Abdelhamid, M.; Gohar, A.; Youssef, T. *Journal of Biomedical Optics* **2012**, *17*, 068001-068007.

(14)   Song, J. B.; Pu, L.; Zhou, J. J.; Duan, B.; Duan, H. W. *ACS Nano* **2013**, *7*, 9947-9960.

(15)   Kirui, D. K.; Krishnan, S.; Strickland, A. D.; Batt, C. A. *Macromolecular Bioscience* **2011**, *11*, 779-788.

(16)   Li, J.; Han, J. S.; Xu, T. S.; Guo, C. R.; Bu, X. Y.; Zhang, H.; Wang, L. P.; Sun, H. C.; Yang, B. *Langmuir* **2013**, *29*, 7102-7110.

(17)   Becker, R.; Liedberg, B.; Kall, P. O. *Journal of Colloid and Interface Science* **2010**, *343*, 25-30.

(18)   Merrill, N. A.; Sethi, M.; Knecht, M. R. *ACS Applied Materials & Interfaces* **2013**, *5*, 7906-7914.

(19)   Sethi, M.; Joung, G.; Knecht, M. R. *Langmuir* **2009**, *25*, 317-325.

(20)   Rostro-Kohanloo, B. C.; Bickford, L. R.; Payne, C. M.; Day, E. S.; Anderson, L. J. E.; Zhong, M.; Lee, S.; Mayer, K. M.; Zal, T.; Adam, L.; Dinney, C. P. N.; Drezek, R. A.; West, J. L.; Hafner, J. H. *Nanotechnology* **2009**, *20*, 43005.

(21)   Kah, J. C. Y.; Zubieta, A.; Saavedra, R. A.; Hamad-Schifferli, K. *Langmuir* **2012**, *28*, 8834-8844.

(22)   Sidhaye, D. S.; Prasad, B. L. V. *Chemistry of Materials* **2010**, *22*, 1680-1685.

(23)   Alpert, J.; Hamad-Schifferli, K. *Langmuir* **2010**, *26*, 3786-3789.

(24)   Huang, J. Y.; Jackson, K. S.; Murphy, C. J. *Nano Letters* **2012**, *12*, 2982-2987.

(25)   Wijaya, A.; Schaffer, S. B.; Pallares, I. G.; Hamad-Schifferli, K. *ACS Nano* **2009**, *3*, 80-86.

(26)   Chen, C. C.; Lin, Y. P.; Wang, C. W.; Tzeng, H. C.; Wu, C. H.; Chen, Y. C.; Chen, C. P.; Chen, L. C.; Wu, Y. C. *Journal of the American Chemical Society* **2006**, *128*, 3709-3715.

(27)   Yamashita, S.; Fukushima, H.; Akiyama, Y.; Niidome, Y.; Mori, T.; Katayama, Y.; Niidome, T. *Bioorganic & Medicinal Chemistry* **2011**, *19*, 2130-2135.

(28)   Yamashita, S.; Fukushima, H.; Niidome, Y.; Mori, T.; Katayama, Y.; Niidome, T. *Langmuir* **2011**, *27*, 14621-14626.

(29)   Niidome, T.; Ohga, A.; Akiyama, Y.; Watanabe, K.; Niidome, Y.; Mori, T.; Katayama, Y. *Bioorganic & Medicinal Chemistry* **2010**, *18*, 4453-4458.

(30)   Kuo, T. R.; Hovhannisyan, V. A.; Chao, Y. C.; Chao, S. L.; Chiang, S. J.; Lin, S. J.; Dong, C. Y.; Chen, C. C. *Journal of the American Chemical Society* **2010**, *132*, 14163-14171.

(31)   Zhang, Z. J.; Wang, J.; Chen, C. Y. *Theranostics* **2013**, *3*, 223-238.

(32)   Sau, T. K.; Murphy, C. J. *Langmuir* **2004**, *20*, 6414-6420.

(32)   Wijaya, A.; Hamad-Schifferli, K. *Langmuir* **2008**, *24*, 9966-9969.

(34)   Qin, Z. P.; Bischof, J. C. *Chemical Society Reviews* **2012**, *41*, 1191-1217.

(35)   Lu, X. M.; Rycenga, M.; Skrabalak, S. E.; Wiley, B.; Xia, Y. N. *Annual Review of Physical Chemistry* **2009**, *60*, 167-192.

(36)   Huschka, R.; Neumann, O.; Barhoumi, A.; Halas, N. J. *Nano Letters* **2010**, *10*, 4117-4122.

(37)   Park, J. W.; Shumaker-Parry, J. S. *Journal of the American Chemical Society* **2014**, *136*, 1907-1921.

(38)   Bastus, N. G.; Comenge, J.; Puntes, V. *Langmuir* **2011**, *27*, 11098-11105.

(39)   Pekcevik, I. C.; Poon, L. C. H.; Wang, M. C. P.; Gates, B. D. *Analytical Chemistry* **2013**, *85*, 9960-9967.

(40)   Resta, V.; Siegel, J.; Bonse, J.; Gonzalo, J.; Afonso, C. N. *Journal of Applied Physics* **2006**, *100*, 084311.

(41)   Dubey, N. *Journal of Molecular Liquids* **2013**, *184*, 60-67.

(42)   Pashley, R. M.; McGuiggan, P. M.; Horn, R. G.; Ninham, B. W. *Journal of Colloid and interface Science* **1988**, *126*, 569-578.

(43)   Schulz, F.; Vossmeyer, T.; Bastus, N. G.; Weller, H. *Langmuir* **2013**, *29*, 9897-9908.

(44)   Shon, Y. S.; Lee, T. R. *Journal of Physical Chemistry B* **2000**, *104*, 8192-8200.

(45)   Love, J. C.; Estroff, L. A.; Kriebel, J. K.; Nuzzo, R. G.; Whitesides, G. M. *Chemical Reviews* **2005**, *105*, 1103-1169.

(46)   Hinterwirth, H.; Kappel, S.; Waitz, T.; Prohaska, T.; Lindner, W.; Lammerhofer, M. *ACS Nano* **2013**, *7*, 1129-1136.

(47)   Hu, X. G.; Gao, X. H. *Physical Chemistry Chemical Physics* **2011**, *13*, 10028-10035.

(48)   Love, J. C.; Estroff, L. A.; Kriebel, J. K.; Nuzzo, R. G.; Whitesides, G. M. *Chemical Reviews* **2005**, *105*, 1103-1169.

(49)   Meena, S. K.; Sulpizi, M. *Langmuir* **2013**, *29*, 14954-14961.

(50)   Liu, Y.; Mills, E. N.; Composto, R. J. *Journal of Materials Chemistry* **2009**, *19*, 2704-2709.

Chapter 4.

Tunable Loadings of DNA on Gold Nanorods

4.1. Introduction

Gold nanoparticles decorated with DNA could be useful for a number of applications, such as biological sensing,[1-4] gene therapy,[5,6] and drug delivery.[7,8] These DNA-nanoparticle conjugates can also serve as building blocks in the formation of self-assembled nanostructures.[9-11] Density of the DNA and other biofunctional molecules coating gold nanoparticles could influence their colloidal stability and their utility in these and other applications. For example, coupling the tunable optical properties of gold nanoparticles[12-14] with the photothermal effect,[15-18] is a simple method of releasing either thiolated DNA[15] or its complementary DNA strand[16-19] from these nanoparticles for gene therapy. The number of DNA molecules attached to the nanoparticles will determine either the corresponding concentration of molecules that can be released as a result of the photothermal activation, or the number of functional groups that can be attached to the surfaces of the gold nanorods. We present a new approach to optimize the loading of thiol-functionalized single-stranded DNA (ss-DNA) monolayers onto gold nanorods in order to fine tune (and maximize) the number of DNA molecules capping these particles.

* Synthesis and surface modifications of nanoparticles, as well as detailed analysis of the modified particles were carried out by Idah C. Pekcevik. Lester C. H. Poon, working as a research associate with Dr. Gates after graduating from SFU, trained Idah C. Pekcevik in proper handling of DNA, functionalization of particles with ss-DNA and in running gel electrophoresis. Michael C. P. Wang performed XPS characterization of the prepared samples. The "Tunable Loading of Single-Stranded DNA on Gold Nanorods through the Displacement of Polyvinylpyrrolidone" manuscript was co-written by Idah C. Pekcevik, and Dr. Byron D. Gates. The contents of this publication were reproduced with the permission of the American Chemical Society and co-authors.[65] Note that some aspects of this work have not been published elsewhere at this time.

One of the most widely pursued syntheses of gold nanorods relies on the use of cetyltrimethylammonium bromide (CTAB) surfactants.[13,20-22] These seed mediated syntheses produce gold nanorods capped with a bilayer of CTAB surfactants. Complete displacement of the CTAB bilayer by ss-DNA can be hindered as the CTAB bilayer impedes the formation of the sulfur-gold bond between the thiolated DNA and the gold nanorod. These molecules can non-specifically interact through electrostatic forces between the positively charged ammonium of CTAB and the negatively charged phosphate backbone of the DNA to create non-uniform multi-layered DNA-CTAB coatings. It is essential to avoid these unwanted interactions in order to achieve reliable and well-packed self-assembled monolayers (SAMs) of ss-DNA on the surfaces of these gold nanorods.

There are a number of methods that have been developed to displace CTAB from the surfaces of gold nanorods, or to otherwise control the electrostatic interactions between CTAB and DNA. One approach is to harness the electrostatic interactions between DNA and positively charged surfaces through the layer-by-layer deposition of polyelectrolytes onto the CTAB coated gold nanorods.[12,23-25] A second approach is through the encapsulation of the nanorods with a thin film of silica.[26] The outer surfaces of this sol-gel derived silica layer are further modified to bind amine- or thiol-functionalized DNA.[27] In a third approach, ss-DNA is decorated onto the gold nanorods through a process of ligand exchange.[15,16,28-30] In this approach, the CTAB bilayers are initially replaced with a short chain alkanethiol (e.g., dodecanethiol). This short thiol-functionalized molecule forms SAMs on the nanorods that are subsequently replaced by ss-DNA through a ligand exchange process.[15,16,29,30] In each of these techniques, the packing density of DNA relies on the ability to uniformly control electrostatic interactions in multilayered films, or to uniformly functionalize a layer of silica, or to completely displace alkanethiol-based SAMs (stabilized by van der Waals interactions) with thiolated ss-DNA. We sought an alternative method to affix a high density of ss-DNA onto the surfaces of gold nanorods.

We have developed a modified approach to decorating the surfaces of the gold nanorods with ss-DNA SAMs by introducing a new intermediate step. This new step replaces the CTAB stabilizing layer on the gold nanorods with a water-soluble mixture of

127

small molecules (sodium dodecylsulfate, or SDS) and polymers (polyvinylpyrrolidone, or PVP) (Figure 4.1). This mixture of surfactants stabilize the nanorods by weakly associating with the gold surfaces,[31,32,33] but can be easily displaced with more strongly binding thiol-functionalized molecules.[34] Polyvinylpyrrolidone forms coordinate bonds between the pyrrolidone sub-units and the surfaces of noble metals.[35-42] These interactions form through electron donation from either the nitrogen or oxygen on a pyrrolidone sub-unit to the metal surfaces. The more dominant interaction is between the carbonyl of the PVP and the surfaces of noble metal nanoparticles.[36,41] Gold particles modified with PVP are stable over a range of pH values,[43] which is useful for dispersing these nanoparticles in a range of media for further decoration. After decoration of the gold nanorods with a mixture of PVP and SDS, we demonstrate the exchange of these weakly coordinated surfactants with thiolated ss-DNA molecules.

CTAB   PVP + SDS   ss-DNA
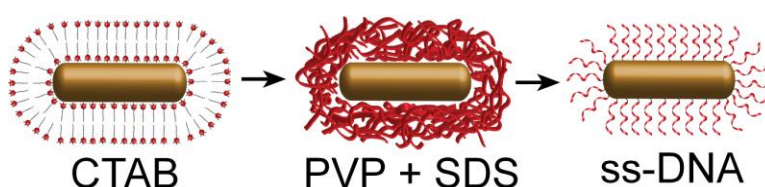
Figure 4.1. **Schematic representations of as-synthesized gold nanorods capped with cetyltrimethylammonium bromide (CTAB), which is exchanged for a mixture of polyvinylpyrrolidone (PVP) and sodium dodecylsulfate (SDS) as an intermediate step before capping these nanorods with thiol-functionalized single-stranded DNA (ss-DNA).**

4.2. Experimental Methods

Materials and Supplies: Surfactants used in the synthesis and preparation of gold nanorods were all obtained from Sigma-Aldrich (St. Louis, MO, USA). These reagents included cetyltrimethylammonium bromide or CTAB (≥96.0%), polyvinylpyrrolidone or PVP (average molecular weight 10,300), and sodium dodecylsulfate or SDS (≥98.5%). The gold salt, $HAuCl_4 \cdot 3H_2O$ (99.0%), silver salt, $AgNO_3$ (≥99.0%), tris (2-carboxyethyl) phosphine hydrochloride or TCEP (≥99.0%), and L-ascorbic acid (≥99.0%), were also obtained from Sigma-Aldrich (St. Louis, MO, USA). The sodium borohydride, $NaBH_4$ (98.0%) was purchased from Fisher Scientific Canada (Ottawa, ON). The acids used in these procedures included acids from Anachemia Canada Inc. (Richmond, BC, Canada), such as hydrochloric acid (36.5 – 38.0% in

water), nitric acid (68 – 70% in water), and concentrated sulfuric acid. Other reagents included a 30% by volume aqueous solution of hydrogen peroxide (VWR International, Mississauga, ON, Canada) and an ethanol solution (95%; Brampton, ON, Canada). All reagents were used as received without further purification. Demineralized water (18 MΩ·cm, produced using a Barnstead NaNOpure DIamond water filtration system) was used to prepare all aqueous solutions described throughout this work.

Oligonucleotides were purchased from University of Calgary (UCDNA Synthesis Lab, Calgary, AB, Canada). The sequence of the oligonucleotide used in optimizing the loading of thiol-functionalized single-stranded monolayers onto gold nanorods was 5′ HS-spacer-TTT AGT CGA CCT CT 3′ terminated with Quasar 670. The spacer segment contains a C6 linker connecting the terminal thiol to the 5′ phosphate of the oligonucleotide through an ether linkage. The complementary sequences of oligonucleotides used in the formation of core-satellite assemblies were 5' HS-spacer- TCA ACA TCA GTC TGA TAA GCT A (AS2a) and 5' HS-spacer- TAG CTT ATC AGA CTG ATG TTG A (AS2b). Dithiothreitol (DTT) was purchased from Pierce Biotechnology, Inc. (Rockford, IL) and Sephadex G-25 Microspin Columns used for DNA purification were purchased from VWR International, Mississauga, ON, Canada. Clear bottom 384-well plates (Greiner non-binding microplate were purchased from VWR International, Mississauga, ON, Canada). Boric acid (≥99.5%), tris(hydroxymethyl)aminomethane (tris base), sodium phosphate monobasic and sodium phosphate dibasic were each purchased from Caledon Laboratories Ltd. (Georgetown, ON, Canada). Ethylenediaminetetraacetic acid (EDTA) (99.5%) and Agarose A (Biotechnology grade) were purchased from Bio Basic Inc. (Markham, ON, Canada).

Synthesis of Gold Nanorods: An aqueous solution of 0.2 M CTAB (5 mL total volume) was stirred at 30°C for 1 h. To this heated solution, 5 mL of 0.5 mM $HAuCl_4·3H_2O$ was added under stirring, followed by 0.6 mL of an ice-cold aqueous solution of freshly prepared 0.01 M $NaBH_4$. This reaction mixture was stirred for another 1 h. The resulting solution of gold nanoparticles was used as seed particles in the synthesis of the gold nanorods.

The gold nanorods were synthesized in 100 mL polystyrene vials (Dynalab Corp., Rochester, NY, USA. Catalog number 2637-0001). To each vial was added 50 mL of 0.1 M CTAB and 315.7 µL of 0.01 M AgNO$_3$. The solution was gently swirled to mix these reagents. To this polystyrene vial, 2.1 mL of 0.01 M HAuCl$_4\cdot$3H$_2$O was added under gently swirling of the solution, followed by 336 µL of 0.1 M L-ascorbic acid with continual gentle mixing of the solutions. The solution changed from orange to colorless during this process. To this mixture, 420 µL of the seed particles (prepared as described above) were added with gentle swirling. The solution changed from clear to dark brown within 1 h of this final step. This solution was maintained at 30°C for 15 h without further stirring or mixing. The resulting gold nanorods were analyzed by extinction spectroscopy and transmission electron microscopy (TEM). The extinction spectra were acquired using a Varian Cary 300 Bio spectrophotometer. These spectra had two characteristic peaks, one centered at 514 nm and the other at 767 nm. Bright field TEM images were obtained with a Tecnai G2 STEM operating at 200 kV. These TEM samples were prepared by drop-casting solutions of nanorods onto a copper grid (300 mesh size) coated with Formvar/carbon (SPI Supplies Canada, ON, Canada). The gold nanorods had an average length of 38.2 ± 3.4 nm and width of 11.0 ± 1.2 nm as measured by TEM analysis of ~200 nanorods.

Preparation of PVP and SDS Stabilized Gold Nanorods: Gold nanorods were synthesized by a seed-mediated synthesis as discussed above. The as-synthesized gold nanorods were purified to remove excess CTAB. This process included centrifugation (Thermo IEC Microlite Microcentrifuge) at 17k rcf for 30 min, followed by decanting the supernatant. The precipitate was subsequently dispersed in 10 mM phosphate buffer at pH 8.0 containing 0.3% w/v SDS. This process of centrifugation, decanting, and suspension of the precipitate in a buffered solution was repeated two more times. A 10 mL aliquot of the purified gold nanorods, suspended in a solution of phosphate buffer and 0.3% SDS, was mixed in a clean round bottom glass flask with a 10 mL solution of PVP (10% w/v in ethanol). The addition of SDS was necessary to prevent aggregation of the purified nanorods and adhesion of these particles to the walls of the centrifuge tubes during the subsequent process of surfactant exchange. This mixture was heated at 40°C with stirring for 18 h. After this period of time, the PVP and SDS modified nanorods were purified by the process described above for centrifugation, decanting and suspension of

the precipitate in a solution of phosphate buffer with 0.3% SDS. The concentration of the PVP and SDS stabilized nanorods was determined using the Beer-Lambert law ($\varepsilon = 4.4 \times 10^9$ M^{-1} cm^{-1} at 767 nm) to be 0.32 nM.[44] The extinction spectra for these PVP and SDS modified nanorods had characteristic peaks centered at 513 nm and 760 nm. These nanorods were further modified with the addition of single-stranded DNA that had one end functionalized with a thiol-containing linker.

Deprotection of DNA: DNA was purchased in a lyophilized form and re-dissolved in tris-EDTA (TE) buffer (pH 7.4) to prepare a 1 mM stock solution of ss-DNA. The 1x TE buffer solution was prepared using 10 mM of the HCl salt of tris(hydroxymethyl)aminomethane (or tris) and 0.1 mM ethylenediaminetetraacetic acid (or EDTA). The oligonucleotide sequence is 5′ HS-spacer-TTT AGT CGA CCT CT 3′ terminated with Quasar 670 (excitation maximum at 644 nm, emission maximum at 670 nm). The spacer segment contains a C6 linker. The as-purchased DNA also contains a dimethoxytrityl protecting group. This protecting group is removed from the thiol-functionalized single-stranded DNA using tris(2-carboxyethyl)phosphine (TCEP) followed by column filtration.[16] Briefly, 50 μL of 1 mM ss-DNA (50 nmol) containing the 5′-thiol and a 3′ Quasar 670 dissolved in 1×TE buffer was added to 50 μL of 100 mM TCEP dissolved in 1 M phosphate buffer (pH 8.0). This mixture of ss-DNA and deprotecting solution were left at room temperature for 1 h. The deprotected ss-DNA was purified through GE G-25 Microspin columns as per manufacturer instructions. The concentration of deprotected, purified ss-DNA was measured to be 182 μM using a micro-volume UV-Vis spectrophotometer (Thermo Scientific NanoDrop 2000). The concentration of the purified ss-DNA was calculated from the measured absorbance of ss-DNA, which was monitored at 260 nm using a molar absorptivity provided by the manufacturer ($\varepsilon_{260} = 125{,}600$ M^{-1} cm^{-1}).

Preparation of Gold Nanorods Modified with Thiol-Functionalized Single-Stranded DNA (ss-DNA): Solutions of de-protected and purified ss-DNA were added to the PVP and SDS modified gold nanorods (details of the de-protection and purification procedures as outlined above). Various concentrations of ss-DNA were prepared by performing serial dilutions of the initial 182 μM ss-DNA with 1×TE buffer to make a total of 8 different samples. The samples were prepared to have a final molar ratio of thiol-

DNA-Quasar to gold nanorods ranging from 250 to 40,000. Briefly, 10 µL of ss-DNA solution in a 1×TE buffer was added to 200 µL of 0.23 nM gold nanorods modified with PVP and SDS suspended in 10 mM phosphate buffer (pH 8.0) with 0.3% SDS. These mixtures of gold nanorods and ss-DNA were sonicated (Branson Ultrasonic Cleaner, Model 1510) for 5 s and left at room temperature for 16 h before the addition of salt. A salt shielding strategy was used to assist in maximizing the loading of ss-DNA on to the gold nanorods.[45] Briefly, 20 µL of a salting solution—containing 10 mM phosphate (pH 8.0), 300 mM NaCl, 4 mM $MgCl_2$ and 0.3% SDS—was added in a dropwise manner to the mixture of the nanorods and ss-DNA. After addition of the salting solution, the mixtures were sonicated for 5 s. This salting procedure was repeated every 30 min for a total of 10 separate additions of salting solution to achieve a final salt concentration of 10 mM phosphate (pH 8.0), 150 mM NaCl, 2 mM $MgCl_2$ and 0.3% SDS. The salted samples were left at room temperature for a total of 16 h before subsequent purification.

Samples were purified of excess ss-DNA by a series of successive steps that included centrifugation, supernatant removal and suspension of the purified nanorods in a fresh phosphate buffered solution. The samples were centrifuged at 9.3k rcf (Eppendorf 4515 D) for 30 min while held at 4°C. The supernatant was removed and the ss-DNA-nanorod pellet suspended with 200 µL of 10 mM phosphate buffer (pH 8.0) containing 0.3% SDS. The ss-DNA decorated nanorods were suspended into this solution with the aid of 10 s to 1 min of sonication. This purification process was repeated an additional 3 times for a total of 4 supernatant removal steps. Four repetitions of this purification process were sufficient to remove all detectable traces of unbound oligonucleotides from the supernatant (Figure 4.2). The extinction spectra for these ss-DNA modified gold nanorods had two characteristic LSPR peaks centered at 510 nm and 767 nm. Decanted solutions from this purification process were analyzed for the presence of Quasar 670 by fluorescence spectroscopy. These wash solutions were excited at 644 nm and emission detected at 670 nm with a Cary Eclipse Fluorometer.

The number of ss-DNA decorating the gold nanorods was quantified by treating these samples (measured out in 40 µL aliquots) with 10 µL of 500 mM DTT to achieve a final concentration of 100 mM DTT. The DTT treated samples were left at room temperature for 16 h. After this period of time, both the DTT treated and untreated

(control) samples were heated at 90°C for 30 min. All samples were centrifuged at 9.3k rcf (Eppendorf 4515 D) for 30 min while held at 4°C. The supernatant of all samples were removed for subsequent analysis. For the untreated samples, 4 µL of 500 mM DTT was added to 36 µL of the supernatant. The fluorescence of all the treated and untreated samples, negative controls, standards (Figure 4.9a), and blank solutions [prepared from 10 mM phosphate buffer (pH 8.0) with 0.3% SDS and 100 mM DTT] were measured using a fluorescence microplate reader (Molecular Devices Spectra Max M5) operating at an excitation wavelength of 600 nm while monitoring emission at 670 nm. An excitation wavelength of 600 nm was chosen (as opposed to 644 nm) in order to easily decouple the excitation from the detected emission because the detector was in line with the excitation source within the plate reader. A single standard of Quasar 670 at a concentration of 100 µM was used as a reference to relate the fluorescence readings between each 384 well plate.

Preparation of Negative Controls to Investigate Alternative Mechanisms for Thiol-Containing DNA to Bind to Nanorods*:* Negative control samples were prepared using a protocol similar to that outlined above, except replacing the thiol-functionalized single-stranded DNA with a DNA strand lacking the thiol modification. This control was used to assess the necessity of the thiol-functionality in obtaining high density ss-DNA SAMs. Briefly, 3′-Quasar 670 modified DNA with a 5′-dodecanol modification in place of a hexanethiol modification was used to prepare the negative control samples. This control DNA was not treated with TCEP. An aliquot (measuring 19 µL) of 1 mM control DNA dissolved in 1×TE was added to 2 mL of 0.32 nM gold nanorods modified with PVP and SDS suspended in 10 mM phosphate buffer (pH 8.0) with 0.3% SDS. These solutions were prepared with a molar ratio of 40,000 times of the control DNA to gold nanorods. The samples were subsequently salted, purified, treated with DTT and analyzed as described in the previous section with minor adjustments. The volumes were scaled as necessary in order to obtain the same concentrations of reagents used for preparation and the analysis of the gold nanorods modified with thiol-functionalized DNA. In addition, after the final purification step, these control DNA-gold nanorod samples were resuspended in 2 mL of 10 mM phosphate buffer (pH 8.0) with 0.3% SDS. Fluorescence spectroscopy indicated the absence of DNA in the purified particles. A portion of these control samples were also incubated with DTT and heated at 90°C for

133

30 min, but the lack of fluorescence emission further indicated an absence of the Quasar 670 labeled DNA in the purified nanorods.

Preparation of Standard Curves for the Quantification of Quasar Modified ss-DNA*:* Solutions of ss-DNA, prepared as described above, were used to make standard solutions in order to quantify the amount of ss-DNA conjugated to the gold nanorods (Figure 4.3a). Standards of ss-DNA were prepared between 0.04 nM and 1000 nM (100 µL total volume) in 10 mM phosphate (pH 8.0), 150 mM NaCl, 2 mM $MgCl_2$ and 0.3% SDS. Standards for the control DNA were prepared in the same manner as those of the thiol-functionalized single-stranded DNA standards. Dithiothreitol (10 µL of 500 mM DTT) was added to each of the standards (40 µL) before measuring the standard fluorescence curves. The DTT treated standards were heated at 90°C for 30 min and cooled to room temperature. The fluorescence emission of the DTT treated samples at 670 nm (excitation at 600 nm) was measured with a fluorescence microplate reader (Molecular Devices Spectra Max M5).

Analysis of Particle Size and Surface Potential by Dynamic Light Scattering Techniques*:* Particle sizes and zeta potential values were acquired by a Malvern Zetasizer Nano ZS system. The dynamic light scattering measurements were performed on the same samples used for extinction analysis (optical density of gold nanorod solutions was ~1.4). The temperature of the solution was 22°C. Folded capillary cells (Malvern, Westborough, MA, USA) were used for the measurements. The volume of the cells is 0.75 mL. The capillary cells were cleaned by injection of 0.6 mL of ethanol through the cell using a 10 mL syringe. Ethanol solution was flushed through the cells 5 times. These cleaned capillary cells were rinsed with either water (for use with the CTAB-capped nanorods) or 10 mM phosphate buffer at pH 8.0 (for use with the PVP/SDS and ss-DNA modified gold nanorods). The rinsing solutions were removed prior to loading the nanorod solutions. Intensity of the back-scattered light was measured at an angle of 173° from the incident He-Ne laser (633 nm).

Analysis of ss-DNA-Gold Nanorod Conjugates by Gel Electrophoresis*:* The ss-DNA-gold nanorod conjugates were prepared as described above with minor adjustments. Instead of using 200 µL of 0.32 nM gold nanorods, 2 mL of 0.32 nM gold

nanorods was used to prepare all of the samples. These solutions of nanorods were mixed with various amounts of ss-DNA to achieve a range of ss-DNA concentrations that reflected the ratios of ss-DNA to gold nanorods prepared in the previous sections. All volumes were scaled relative to the protocol described above. After four washes to remove excess ss-DNA, the samples were redispersed in 2 mL of 10 mM phosphate buffer (pH 8.0) with 0.3% SDS and briefly sonicated (10 to 30 s). The samples were split into two 1 mL aliquots. One aliquot was concentrated by 50-fold to prepare samples for gel electrophoresis. This aliquot was concentrated by centrifuging 1 mL samples at 9.3k rcf for 30 min while held at 4°C. The majority of the supernatant was removed, leaving 20 μL of 10 mM phosphate buffer (pH 8.0) with 0.3% SDS to resuspend the pellet of ss-DNA-gold nanorod conjugates. In order to help disperse the pellet of ss-DNA modified gold nanorods, the samples were sonicated between 10 to 30 s. In preparation for loading the samples in an agarose gel, 2 μL of glycerol was added to each of the concentrated samples. Gel electrophoresis plates were prepared from a 3% agarose gel in 0.5X TBE at pH 8.0. (TBE: Tris base, boric acid and EDTA). A 10X TBE solution was prepared using 108 g tris base, 55 g boric acid, and 40 mL of EDTA solution (0.5 M) mixed in 1 L of water. Each well in the 3% agarose gel was loaded with a 10 μL solution of either the ss-DNA modified gold nanorods or the PVP and SDS stabilized gold nanorods. Samples were electrophoresed at 120 V (or 7.5 V/cm) for 2 h. Gels were imaged by transmission illumination with a HP scanner.

Analysis of ss-DNA-Gold Nanorod Conjugates by Inductively Coupled Mass Spectrometry (ICP-MS)*: Gold nanorods capped with ss-DNA were dissolved in aqua regia to a volume of 12.5 mL and analyzed by ICP-MS (ALS Geochemistry, North Vancouver BC, Canada). A 7% solution of nitric acid was used to rinse the instrument between analyses to ensure no carryover. A standard five-point calibration curve was prepared and used to quantify the amount of gold in each sample analyzed. In order to determine the average number of gold nanorods in solution, it was assumed that each gold nanorod could be approximated by a cylinder that is capped at each end with half of a sphere. These nanorods had an average length of 41 nm and an average diameter of 11 nm. From the stated assumptions and these dimensions, we calculated the average volume of a gold nanorod. The concentration of gold determined by ICP-MS analysis of the ss-DNA coated gold nanorods was converted into the average number of gold

nanorods per milliliter of solution using this calculated volume of a gold nanorod and the density of Au.[28] To calculate the surface area of each ss-DNA molecule on a nanorod, we proposed a model which assumes that a gold nanorod is made up of a cylinder and two semi-circles at its ends. The semi-circles at the ends were estimated to be slightly larger in diameter than the central diameter of the nanorods to mimic the dumbbell like shapes observed for the gold nanorods. The total surface area of a nanorod is the sum of the surface areas of the cylinder and the sphere. The estimated average surface area per nanorod was ~1645 nm^2. Our modeling and surface area calculations were performed using 3D CAD software from Dassault Systèmes SolidWorks Corporation.

Analysis of Gold Nanorods by X-ray Photoelectron Spectroscopy (XPS): Chemical composition of the gold nanorods was investigated by XPS. These studies were conducted using a Kratos Analytical Axis ULTRA DLD system with a monochromatic aluminum source (AlKα of 1486.7 eV) operating at 150 W. Survey scans (0 to 600 eV) were acquired using a pass energy of 160 eV, a dwell time of 100 ms, and an average of 2 scans. High resolution spectra (0.05 eV step size with a spectral resolution of 0.1 eV) were obtained using a pass energy of 20 eV, a dwell time of 1000 ms, and an average of 5 scans.

Preparation of Gold Nanorod-Gold Nanoparticle Assemblies: Spherical gold nanoparticles were prepared for assembly onto the DNA decorated gold nanorods. These ~10-nm diameter gold nanoparticles were synthesized with modifications to a previously published procedure.[63] Briefly, a 20 mL aqueous solution of 0.34 mM HAuCl$_4$·3H$_2$O was refluxed while continuously stirring. A 2 mL portion of a 38.8 mM solution sodium citrate was quickly added to this boiling solution of gold salts. The combined solutions were further refluxed for at least 10 min.

Citrate-capped gold nanoparticles (2 mL; optical density, OD, of 1) were mixed together with 70 μL of purified and de-protected AS2b ss-DNA. The final molar ratio of ss-DNA to spherical gold nanoparticles is 1000:1. This mixture of nanoparticles and ss-DNA were shaken gently on a vortexer for 42 h. After 42 h, 200 μL of a salting solution— containing 10 mM phosphate (pH 8.0), 300 mM NaCl, 4 mM MgCl$_2$ and 0.3% SDS—was added in a drop wise manner to the mixture of gold nanoparticles and ss-DNA. After

136

addition of the salting solution, the mixtures were sonicated for 5 s. This salting procedure was repeated every 30 min for a total of 10 separate additions of salt solution to achieve a final salt concentration of 10 mM phosphate (pH 8.0), 150 mM NaCl, 2 mM MgCl$_2$ and 0.3% SDS. The salted sample was shaken under ambient conditions on a vortexer for a total of 18 h before subsequent purification.

The following procedure was adapted from the work of Xu et al.[10] Assemblies of spherical gold nanoparticles on gold nanorods were prepared by mixing the two types of particles (DNA decorated nanorods and DNA decorated spherical nanoparticles). A 200 µL solution of gold nanorods modified with ss-DNA (final molar ratio of AS2b ss-DNA to nanorods was 40,000:1; OD of 1 at 767 nm) was mixed with 50 µL of spherical gold nanoparticles decorated with a complementary ss-DNA (final molar ratio of AS2a ss-DNA to nanorods 1000:1; OD of 2 at 521 nm). These ss-DNA modified gold particles were suspended in a solution of 10 mM phosphate (pH 8.0), 150 mM NaCl, 2 mM MgCl$_2$ and 0.3% SDS. The mixture of ss-DNA modified nanorods and spherical nanoparticles were vortexed for 20 h. After this period of time, 50 µL of a salt solution—containing 10 mM phosphate (pH 8.0), 180 mM NaCl, 40 mM MgCl$_2$ and 0.3% SDS—was added in a dropwise manner to the mixture of the gold particles. After addition of this salt solution, the mixtures were sonicated for 5 s. This salting procedure was repeated every 30 min for a total of 5 separate additions of salt solution. The salted sample was left shaking on a vortexer under ambient conditions for a total of 52 h before taking aliquots of the sample for TEM analysis. No further purification was performed on the assemblies of spherical nanoparticles on gold nanorods. Analysis by electron microscopy was performed as described above.

Testing the Stability of gold nanorods modified with varying loading of ss-DNA. The stability of ss-DNA-gold nanorod conjugates (modified with a low, medium and high DNA loading) were tested by adding 100 µL of aqueous 0.01 M potassium cyanide (>97% pure; Alfa Aesar, Ward Hill, MA, USA) to a 2 mL purified solution of the modified gold nanorods (optical density 0.16, 0.18 nM) in polystyrene cuvettes (CN$^-$/Au$^-$ = 3.6×10^7). The loadings of ss-DNA per nanorod were ~150, ~400 and >800 for the nanorods with a low, medium, and high loadings, respectively, as determined by methods described above. *CAUTION: Potassium cyanide is extremely hazardous. It can*

137

cause adverse health effects when inhaled or absorbed through the skin. Handle and dispose of appropriately. Extinction spectra were recorded (400 to 900 nm on a Cary 300-Bio UV-Visible spectrophotometer) immediately following addition of KCN to the nanoparticle solutions. The extinction spectra were acquired at 0.5 min intervals for a period of up to 30 min while incubating the nanoparticles with KCN.

Testing the Stability of gold nanorods modified with varying loading of ss-DNA at 37°C. The stability of gold nanorods with a low, medium and high DNA loading were also tested at 37°C over the period of ~1 month. These solutions were maintained at 37.0±0.5°C using a microprocessor controlled Precision 280 water bath from ThermoScientific. Extinction spectra were recorded regularly (400 to 900 nm on a Cary 300-Bio UV-Visible spectrophotometer) for each sample of gold nanorods modified with varying loadings of ss-DNA.

4.3. Results and Discussion

The process of exchanging surfactants and forming SAMs of ss-DNA on the gold nanorods was initially monitored by changes in localized surface plasmon resonance (LSPR). The extinction spectra of gold nanorods suspended in phosphate buffer display a shift in the LSPR associated with each exchange of the dielectric coating. The CTAB coated nanorods had two LSPR peaks centered at 514 nm and 775 nm (Figure 4.2) that shifted to 512 and 753 nm, respectively, after stabilizing the nanorods with PVP and SDS. Intensity of the LSPR bands also decreased slightly, corresponding to a minimal loss of gold nanorods during this surfactant exchange process. The observed spectral blue shift after this surfactant exchange is attributed to the increased water permeability and decreased thickness of the dielectric coating on the nanorods,[46] which was supported by dynamic light scattering measurements. Subsequent decoration of the nanorods with ss-DNA SAMs resulted in a red-shift of the longitudinal LSPR to 761 nm (Figure 4.2), confirming a further change in the surface chemistry and a possible increase in the thickness of the dielectric coating. An absorption shoulder at ~665 nm indicates the presence of Quasar 670 labeled ss-DNA attached to the gold nanorods (Figure 4.3). These spectral shifts suggest changes have taken place in the surface

chemistry on the particles, but complementary measurements were required to determine the nature of these changes.
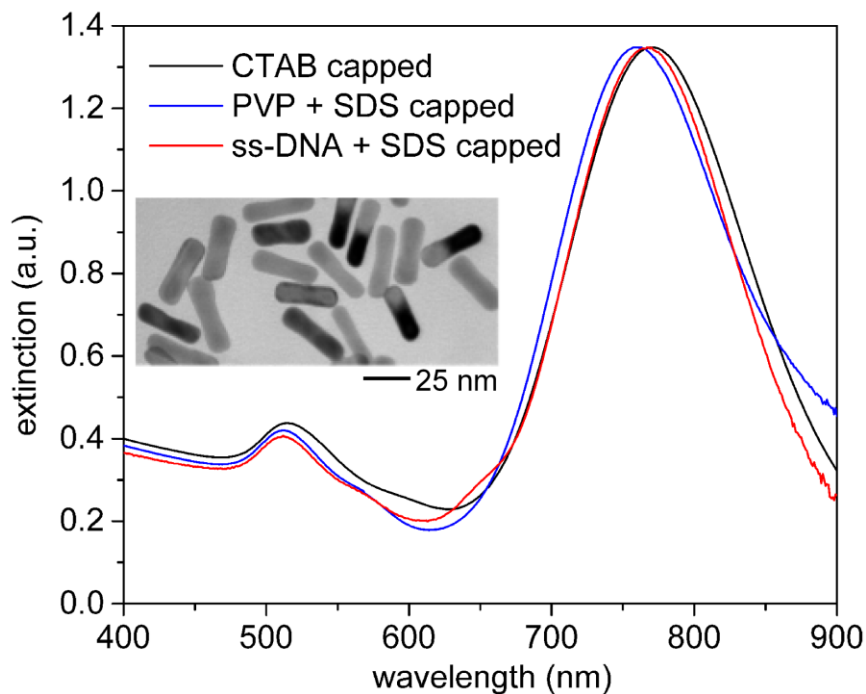
Figure 4.2. **Extinction spectra of solutions containing CTAB (black), PVP and SDS (blue), or ss-DNA (red) capped gold nanorods. The CTAB modified gold nanorods were suspended in water, while both the PVP and SDS modified and the ss-DNA modified gold nanorods were suspended in 10 mM phosphate buffered solution (pH 8.0) containing 0.3% SDS. The inset is a representative transmission electron microscopy (TEM) image of ss-DNA modified gold nanorods.**
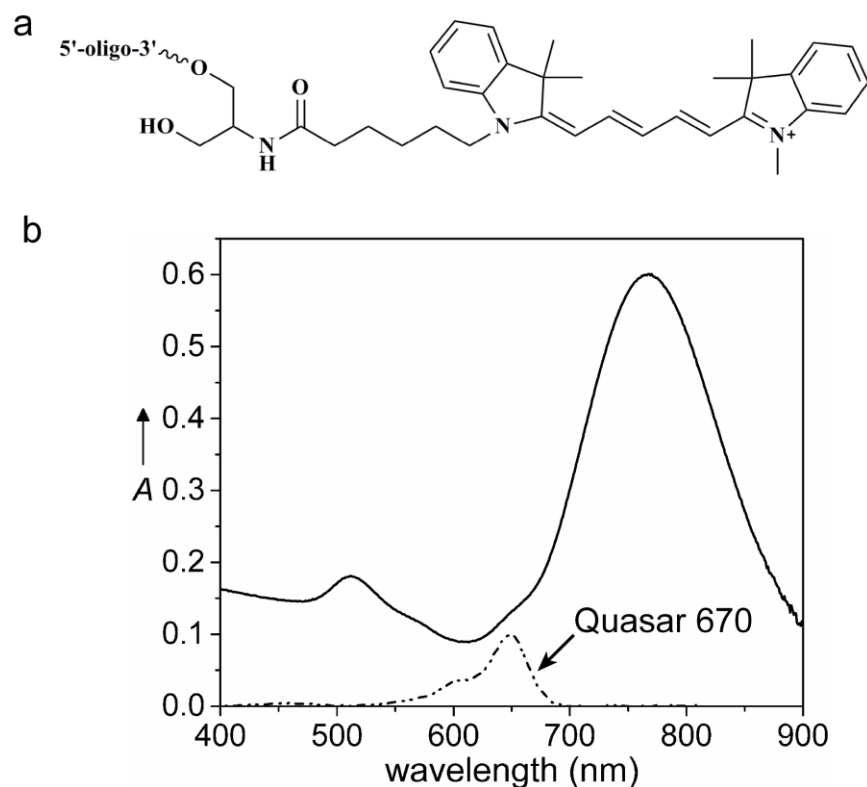
Figure 4.3. **(a) Chemical structure of Quasar 670 conjugated to the 3'-end of an oligonucleotide. (b) Absorbance spectrum of Quasar 670 (dashed line) and extinction spectrum of gold nanorods capped with Quasar modified thiol-functionalized single-stranded DNA (solid line).**

Stable colloidal suspensions are achieved after each surfactant exchange. Changes to the dielectric coating of these colloidal particles were monitored to assess the success of exchanging the surfactants from CTAB to PVP/SDS to ss-DNA. The as-synthesized gold nanorods had a surface potential of +46 mV as determined by zeta potential measurements (Table 4.1). This zeta potential value is consistent with other reports for CTAB stabilized gold nanorods.[47] Replacement of CTAB with a mixture of PVP and SDS shifted the surface potential to –57 mV. A negative surface potential (–50 mV) is also observed after decoration of the nanorods with ss-DNA. The negative surface potentials are attributed to the surfactants adsorbed onto or bound to the surfaces of the gold nanorods (i.e. PVP/SDS and SDS/ss-DNA, respectively).[35,36,42] Changes to the dielectric coating of the nanorods during the surfactant exchange process were also determined by monitoring changes in the average particle size. Average dimensions of the nanorods were monitored by dynamic light scattering (DLS)

techniques (Table 4.1) and transmission electron microscopy (TEM) measurements (Figure 4.4). The increase in average lengths of the gold nanorods (as measured from TEM micrographs) following their decoration with ss-DNA could be attributed to etching and deposition of gold atoms at the ends of nanorods due to the reactions of thiols with the surfaces of gold. Differences in the lengths of the nanorods determined from the DLS and TEM measurements were divided by two in order to determine the thickness of the dielectric layer. Observed changes in the thickness of the dielectric coating of the nanorods with each subsequent replacement of the surfactants suggested a change in the surface chemistry of gold nanorods at each step of surfactant exchange. The average thickness of the dielectric layer for the CTAB capped nanorods after purification was ~1.5 nm, which is consistent with other literature.[48] Exchange of the CTAB layer for a mixture of PVP and SDS decreased the average thickness of the dielectric coating to ~0.5 nm, which correlates with the observed shift in LSPR mentioned above. Average thickness of the dielectric coating increased to ~3 nm after decorating the nanorods with ss-DNA. This increased thickness of the capping layer is attributed to the formation of 14-mer ss-DNA SAMs on the surfaces of the particles. The thickness of this capping layer is slightly less than the estimated length of the fully extended ss-DNA strand (~4.5 nm). It is most likely that the thickness of the ss-DNA capping layer is less than this theoretical thickness due to the flexibility of the ss-DNA and limitations in accurately determining thickness of the dielectric layer coating on the curved surfaces of the particles.[49] Another possibility is that the dielectric coating on the nanorods is non-uniform due to an incomplete surfactant exchange. The extent of the surfactant exchange was further assessed through a series of spectroscopic measurements.

Table 4.1. **Mean hydrodynamic length (L$_h$), lengths measured from TEM micrographs, estimated dielectric layer thickness (T$_{dl}$), and mean zeta potentials determined by dynamic light scattering techniques for gold nanorods (AuNRs) modified with CTAB, PVP and SDS, or ss-DNA and SDS.**

| gold nanorods (or AuNRs)	L$_h$ (nm)	length (nM)	T$_{dl}$ (nm)	zeta potential (mV)
AuNRs + CTAB in water	41 ± 3	38 ± 3	~1.5	+46 ± 19
AuNRs + PVP in phosphate buffer with SDS	40 ± 3	39 ± 3	~0.5	−57 ± 23
AuNRs + ss-DNA in phosphate buffer with SDS	47 ± 5	41 ± 4	~3	−50 ± 26
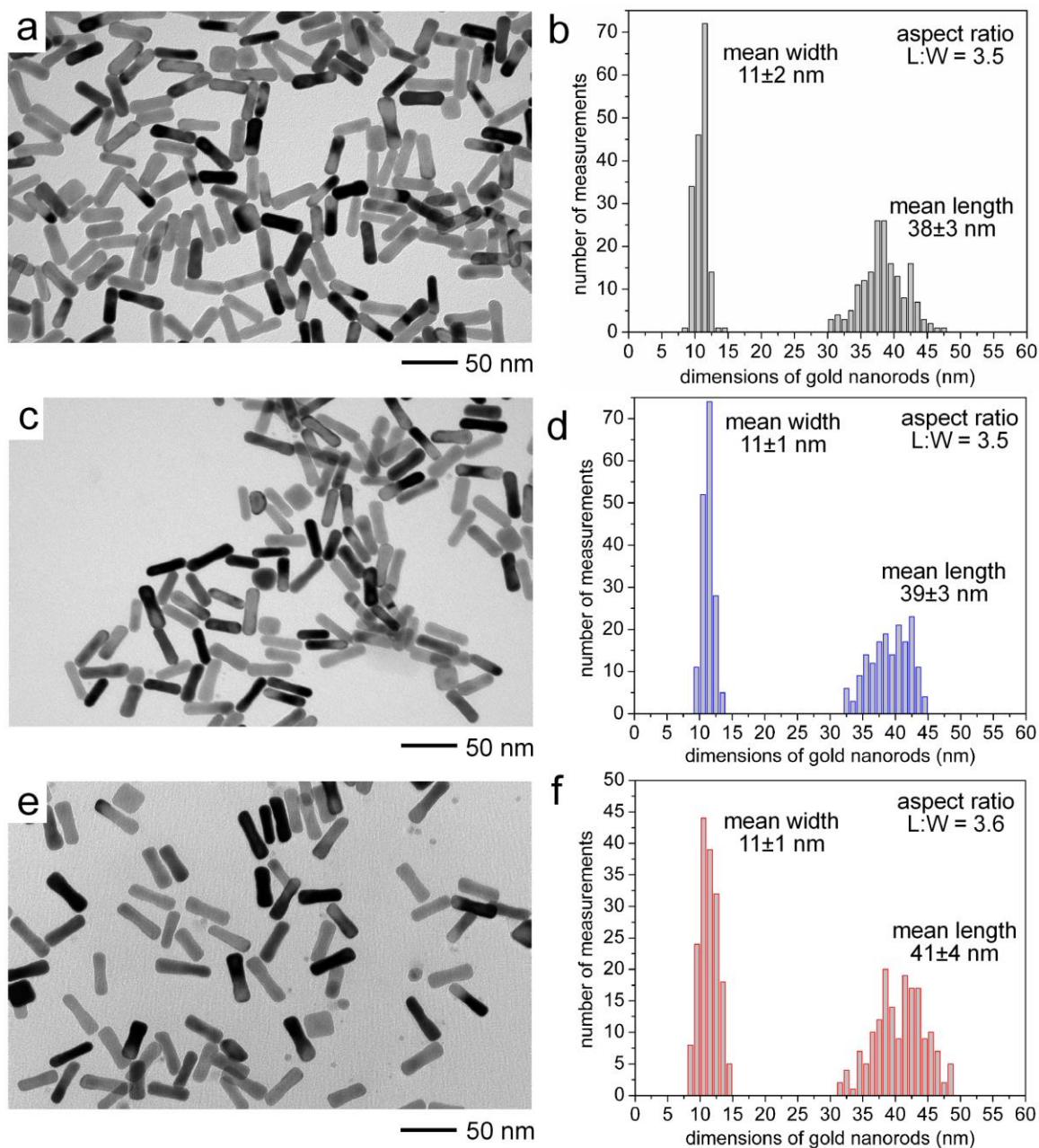
Figure 4.4. Representative transmission electron microscopy (TEM) images of gold nanorods and corresponding histograms for their measured dimensions. The gold nanorods were capped with (a,b) CTAB, (c,d) a mixture of PVP and SDS, or (e,f) a mixture of ss-DNA and SDS. Each histogram contains measurements from ~200 gold nanorods and also contains the calculated aspect ratio for each sample.

Completeness of the surfactant exchange process at each step was also monitored by infrared (IR) spectroscopy and X-ray photoelectron spectroscopy (XPS). Infrared spectroscopy confirmed the association of PVP with the nanorods during the intermediate step of this process to cap the nanorods with ss-DNA. Polyvinylpyrrolidone has a strong absorption band centered at 1666 cm^{-1} due to a v(C=O) stretching vibration.[35,36] This absorption band shifts to 1660 cm^{-1} for the PVP coated nanorods, which is attributed to the coordination of the carbonyl to the gold surfaces.[35,40] Infrared spectroscopy on the DNA decorated nanorods was inconclusive as to whether PVP has been completely displaced , which was attributed to the structural similarities of PVP and ss-DNA. Analysis by XPS confirmed the presence of gold and silver in the nanorods and the exchange of the capping layers that stabilize these nanoparticles (Figure 4.5). Bromide ions in the CTAB sample are exchanged for chloride ions associated with sodium salts in the buffer solution used to disperse the PVP and ss-DNA capped particles. The relatively high ratio of C_{1s} to Au_{4f} in the CTAB sample relative to that observed in the other samples is attributed excess CTAB in solution. In addition to these differences observed in the XPS of the three different types of samples, significant differences were also observed in the high-resolution XPS spectra (Figure 4.6). The carbon species expected from the CTAB samples were hydrocarbons (C-C and C-H) and carbon bound to nitrogen (C-N). These species had characteristic binding energies (BEs) of ~285, and ~287 eV, respectively. The signal also includes carbon bound to oxygen (C-OH) in the form of oxidized adventitious carbon.[50] The carbon species anticipated for the PVP stabilized samples included the addition of amide carbon (N-C=O) with a characteristic binding energy of ~288 eV. The ss-DNA stabilized samples included further species associated with nucleobases, nucleosides, and nucleotides, such as carbon bound to nitrogen (C-N and N-C-N), and urea carbon (N-(C=O)-N). These species have characteristic BEs of approximately ~287 and ~289 eV, respectively.[51,52] The large quantity of unbound CTAB and the compositional differences between the three types of samples is further supported from analysis of the high resolution N_{1s} spectrum (Figure 4.6b). There is a 3.1 eV shift between the N_{1s} peaks associated with the CTAB molecules that are free in solution (i.e. referred to as unbound CTAB) and those in proximity to the surfaces of the gold nanorods (i.e. referred to as bound CTAB). Distinct N_{1s} spectra were observed when comparing the CTAB and PVP stabilized samples in connection with quaternary and tertiary amines, respectively, within

144

these surfactants. High resolution XPS analysis of the N_{1s} spectral region for ss-DNA capped nanorods also indicated the presence of heterocylic amines, primary amines, and amides.[52] The ss-DNA samples contain amines and amides associated with the bases found in DNA, and Quasar 670 (fluorescent label on ss-DNA). The latter sample also contained sulfur with a binding energy of 168.8 eV attributed to the presence of SDS (Figure 4.7).[53] We were unable to confirm the presence of S_{2p} peaks at either 162.0 or 163.3 eV due to the poor signal-to-noise ratio of this signal from these samples. These peaks were anticipated to be present in association with the terminal sulfur of the ss-DNA from either the formation of a gold-sulfur bond or the adsorption of thiol onto the surfaces of the nanorods, respectively.[54] Insufficient levels of SDS were present in the PVP stabilized samples for detection by XPS (Figure 4.7), which is attributed to the fact that these samples were extensively purified prior to XPS analysis and that the SDS was primarily used to prevent unwanted adhesion of the nanorods to the centrifuge tubes during purification. In summary, the IR and XPS analyses provide further evidence that the CTAB molecules were successfully displaced during the surfactant exchange process. There is insufficient evidence from these results to draw a conclusion on the success of decorating the surfaces of the nanorods with ss-DNA including if PVP was still present in the capping layers of the ss-DNA stabilized particles. Separate control experiments were performed by gel electrophoresis and fluorescence spectroscopy to further assess the presence of the ss-DNA on nanorods and to address the potential for residual PVP on these nanorods.
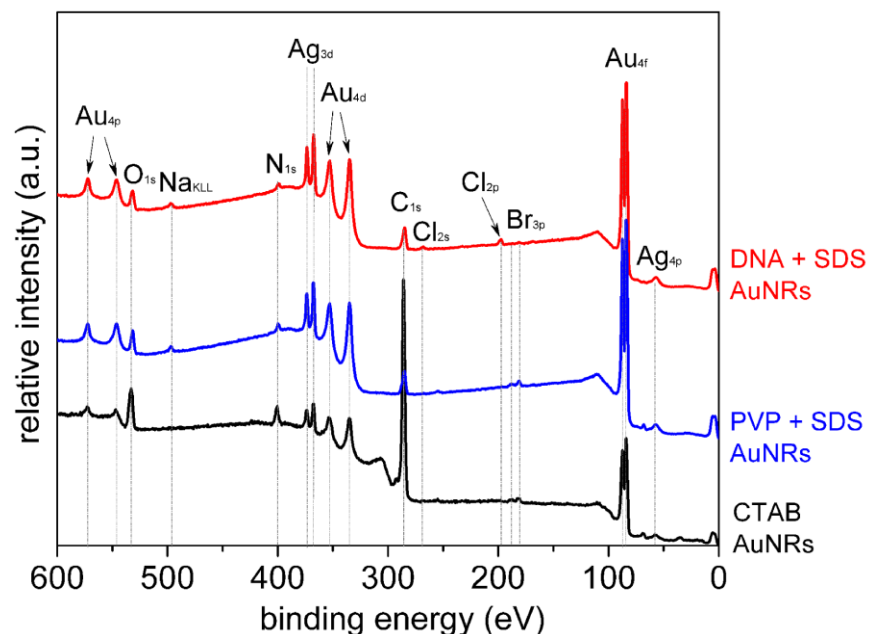
Figure 4.5. X-ray photoelectron spectra of gold nanorods either capped with CTAB (black line), after exchange with a mixture of PVP and SDS (blue line), or after exchange with a mixture of ss-DNA and SDS (red line).
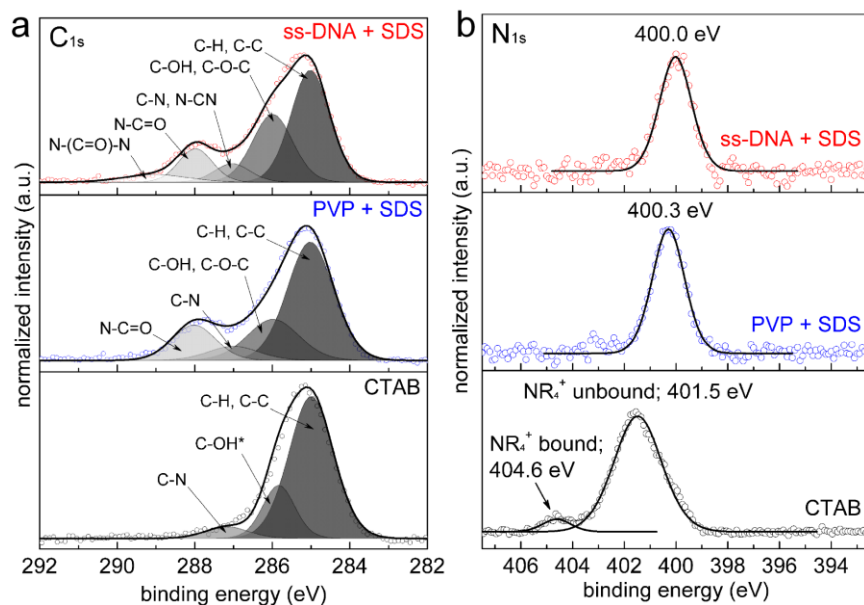
Figure 4.6. High resolution (a) C_{1s} and (b) N_{1s} XPS spectra of gold nanorods either capped with CTAB, or exchanged for a mixture of PVP and SDS or a mixture of ss-DNA and SDS. Note that C-OH* is most likely an oxidized form of adventitious carbon.[50]
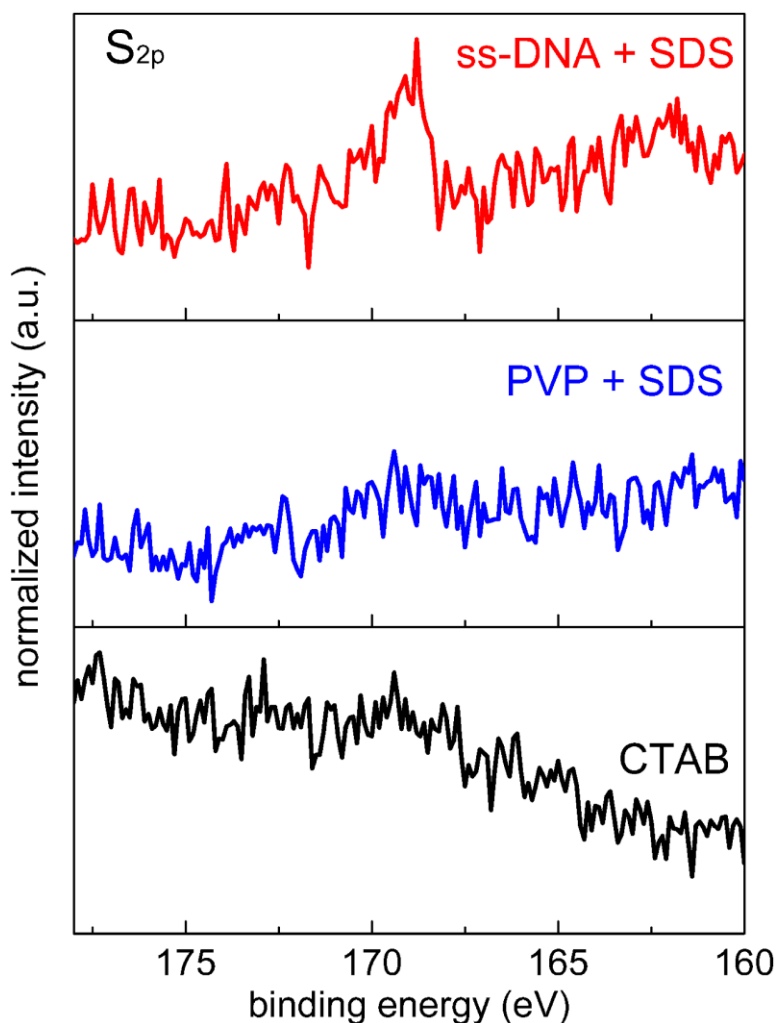
Figure 4.7. **High resolution S$_{2p}$ XPS spectra of gold nanorods either capped with CTAB, or exchanged for a mixture of PVP and SDS or a mixture of ss-DNA and SDS.**

Gel electrophoresis is used to investigate the relative density of charges bound to the surfaces of the gold nanorods. The distance that colloidal particles migrate through a gel under an applied potential is proportional to the number of surface charges and the size of the particles.[29,55] The top row of dark bands in Figure 4.8 corresponds to the wells in an agarose gel into which the particles were loaded. A solid band is present that spans all the wells corresponding to a blue line drawn below the wells during the preparation of the gels (Figure 4.8). The red colored bands within the gels below each of the wells indicate the positions of nanorods migrating through each lane in the gel. The red coloration of the nanoparticles corresponds to their surface plasmon resonance

147

properties as observed under white light illumination. This gel electrophoresis of the nanorods indicated that nanorods modified with a mixture of PVP and SDS in phosphate buffer (without additional NaCl and $MgCl_2$) move towards the cathode (Figure 4.8, lane 1). A significant difference was observed when comparing the nanorods stabilized with a mixture of PVP and SDS to those capped with ss-DNA when analyzed by gel electrophoresis under high salt concentrations. The addition of 150 mM NaCl and 2 mM $MgCl_2$ prevented the migration of the PVP and SDS coated nanorods in the gel due to salt induced aggregation (lane 2). In contrast, movement of purified ss-DNA capped nanorods through the gel was not hindered by addition of these salts (lanes 3-10). The distance migrated by a band of nanorods and the concentration of particles within that band (i.e. spatial distribution of particles within a lane) could be related to the number of charge groups (e.g., ss-DNA) bound to the surfaces of the gold particles. This density of thiolated DNA on the nanorods should be proportional to the initial concentration of ss-DNA added to the PVP and SDS stabilized gold nanorods. A series of different particles were prepared by varying the initial ratio of ss-DNA to nanorods (lane 3, particles prepared from an initial ratio of ss-DNA molecules per Au nanorod of 200:1; lane 4, 400:1; lane 5, 800:1; lane 6, 1600:1; lane 7, 3200:1; lane 8, 6400:1; lane 9, 12800:1; lane 10, ~25600:1). Gold particles restricted to the wells or to the start of the lane in the agarose gel (e.g., particles prepared from ratios of ss-DNA to Au nanorod of 200:1) are attributed to a low charge to mass ratio associated with relatively fewer strands of ss-DNA bound to the particles. A further increase in the initial ratio of ss-DNA to nanorods produced diffuse bands of particles in the gel as indicated by the dark streaks in some of the lanes (e.g., lanes 6 to 9). These diffuse bands could be the result of a population of gold nanorods that are non-uniformly coated with ss-DNA. Nanorods that moved more uniformly through the gel, such as the relatively tight single band observed in lane 10 (i.e. particles prepared from a ratio of ss-DNA:Au nanorod of ~25600:1) is, by comparison, attributed to a more dense layer of ss-DNA coating the nanorods. Relative positions of the gold nanorods in each lane of the gel may indicate their colloidal stability and density of surface charges (e.g., ss-DNA coverage), but further analysis was required to determine the average number of ss-DNA decorating these particles.

148
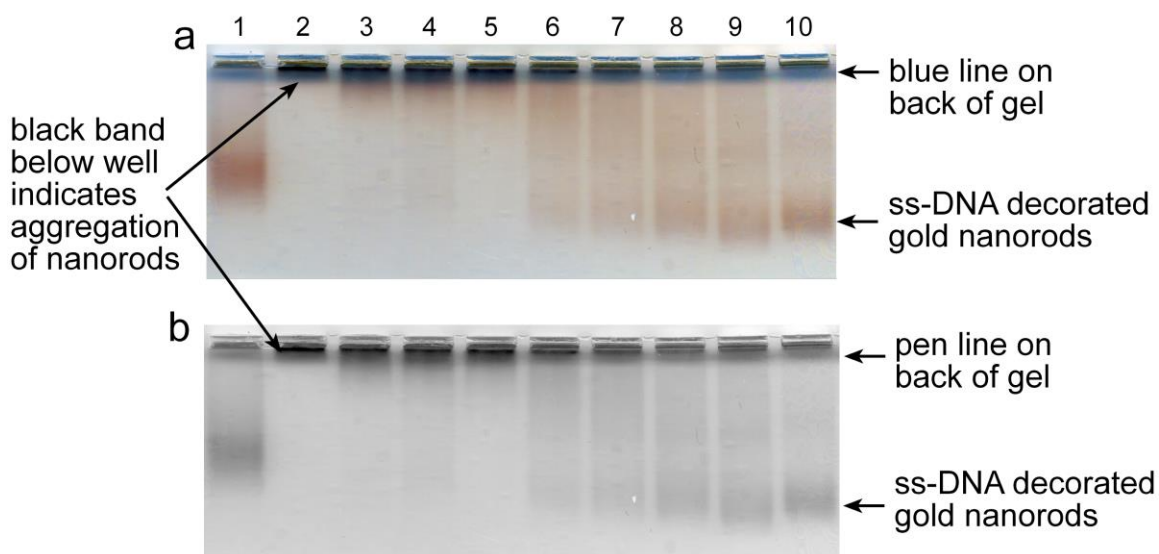
Figure 4.8. (a,b) Digital images of an agarose gel after electrophoresis (0.5×TBE buffer and 3% agarose gel) of gold nanorods modified with PVP and SDS (lanes 1 and 2) or modified with various concentrations of ss-DNA (lanes 3 to 10). The purified gold nanorods were suspended in 10 mM phosphate buffered solution (pH 8.0) containing 0.3% SDS prior to loading into the agarose gel. Lanes 2 through 10 contained samples treated with 150 mM NaCl and 2 mM $MgCl_2$ prior to loading into the gel. Lane 1 corresponds to nanorods that were not treated with these salts. The ss-DNA coated nanorods were prepared from solutions containing an increasing ratio of ss-DNA to gold nanorods (lane 3 to 10, ss-DNA/Au nanorod from ~200 to ~25600). This gel is identical to that in Figure 4.8a, but shown here in (a) color, and (b) black-and-white to highlight the differences between the blue guide line and aggregation of the gold nanorods at the start of lanes 2, 3, 4, 5 and 6.

The quantity of ss-DNA conjugated through sulfur-gold linkages to each nanorod was determined by fluorescence spectroscopy using Quasar 670 labeled ss-DNA. Solutions of ss-DNA, prepared as described in the experimental section, were used to make standard solutions in order to quantify the amount of ss-DNA conjugated to the gold nanorods (Figure 4.9a). Briefly, ss-DNA with a Quasar 670 label was released from the surfaces of the purified DNA-gold nanorods by adding dithiothreitol (DTT),[56] and heating the suspension at 90°C for 30 min. Four repetitions of the purification process were sufficient to remove all detectable traces of unbound oligonucleotides from the supernatant (Figure 4.10). Fluorescence emission spectra were collected from the supernatant of the DTT treated samples after removing the gold nanorods by

149

centrifugation (Figure 4.9b). In addition, a separate experiment was performed to assess the amount of DNA that was potentially non-specifically adsorbed to the DNA-gold nanorod conjugates (e.g., through association with the gold or DNA bound to the surfaces of the nanorods). In this experiment, samples of the DNA-gold nanorod solutions were separately heated at 90°C for 30 min (Figure 4.9c). Any observed fluorescence from these latter measurements was attributed to non-specifically adsorbed DNA on the nanorods, although these molecules could also be attributed to desorption of thiolated oligonucleotides from the surfaces of the nanorods during their heating. The concentrations of this non-specifically adsorbed DNA (<3% of total fluorescence; see Figure 4.11) were subtracted from samples treated with DTT and heat in order to remove any potential contribution from DNA bound through non-specific electrostatic interactions when determining the amount of DNA bound to the gold nanorods through sulfur-gold bonds. In order to further evaluate our proposed mechanism of DNA attachment through displacement of PVP and SDS followed by sulfur-gold bond formation, we replaced the thiol functional group with an alcohol functional group on the Quasar 670 labeled DNA. This control investigated the potential interactions between non-thiol-functionalized DNA and the PVP and SDS capped gold nanorods. Fluorescence spectroscopy indicated the absence of DNA within this sample of particles purified by centrifugation and re-dispersed in 10 mM phosphate buffer in (pH 8.0) with 0.3% SDS (Figure 4.12). These results suggest that the DNA is not simply intertwined or otherwise strongly interacting with the PVP and SDS, and that the thiol functionality is required for a high loading of DNA onto the surfaces of the gold nanorods.
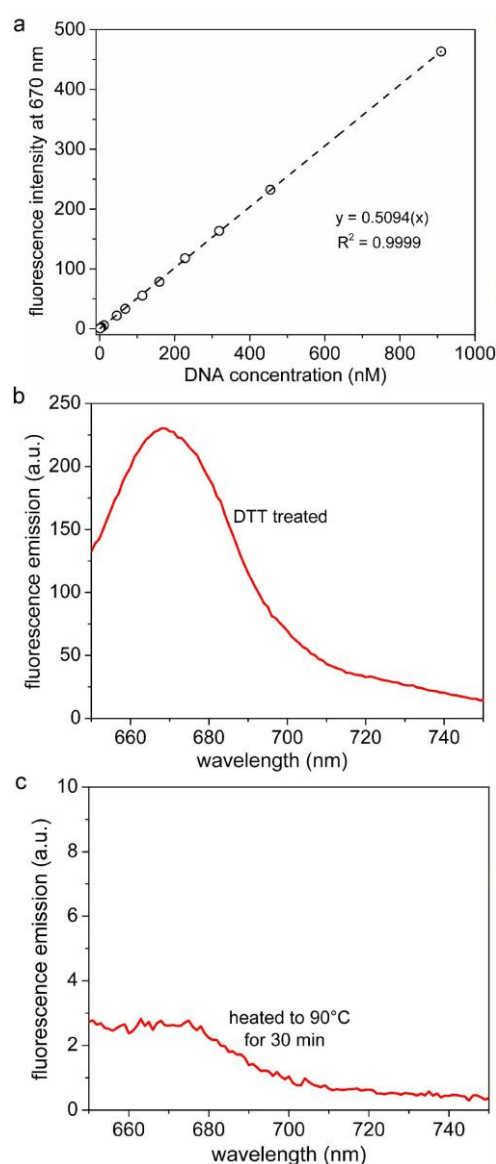
Figure 4.9. (a) Fluorescence calibration curve (λ_{ex} = 600 nm; λ_{em} = 670 nm) of single-stranded DNA modified with Quasar 670 treated with dithiothreitol (DTT) and heated at 90°C for 30 min and cooled to room temperature as described in the Experimental Methods section. (b) Representative fluorescence emission spectra (λ_{ex} = 600 nm) of the supernatants collected from ss-DNA modified gold nanorods after treatment with DTT and heated at 90°C. (c) Representative fluorescence emission spectra (λ_{ex} = 600 nm) of the supernatants collected from ss-DNA modified gold nanorods after heating these samples at 90°C without addition of DTT.

151
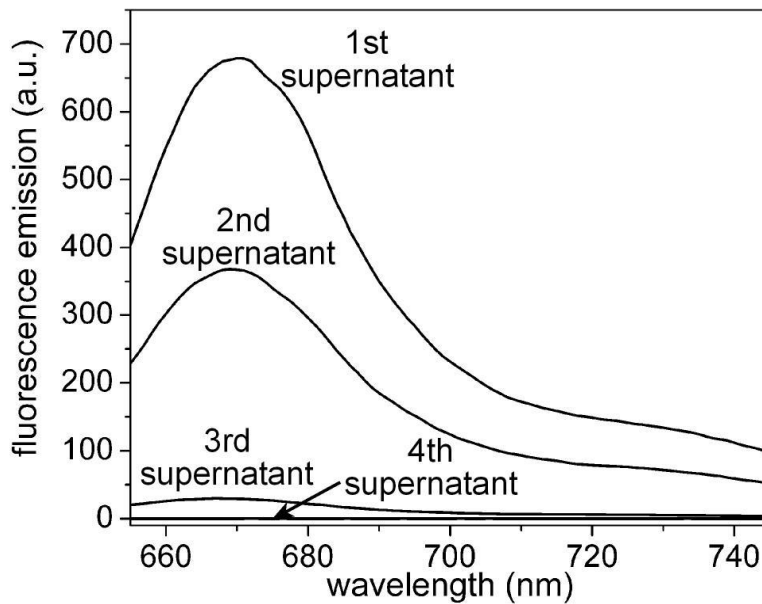
Figure 4.10. Fluorescence emission spectra (λ_{ex} = 644 nm) of the supernatants retrieved after centrifugation of solutions containing gold nanorods that were incubated with thiol-functionalized single-stranded DNA modified with Quasar 670. Emission spectra correspond to the first, second, third and fourth supernatant solutions decanted from the particles during the sequential wash procedures used to purify the ss-DNA decorated gold nanorods.
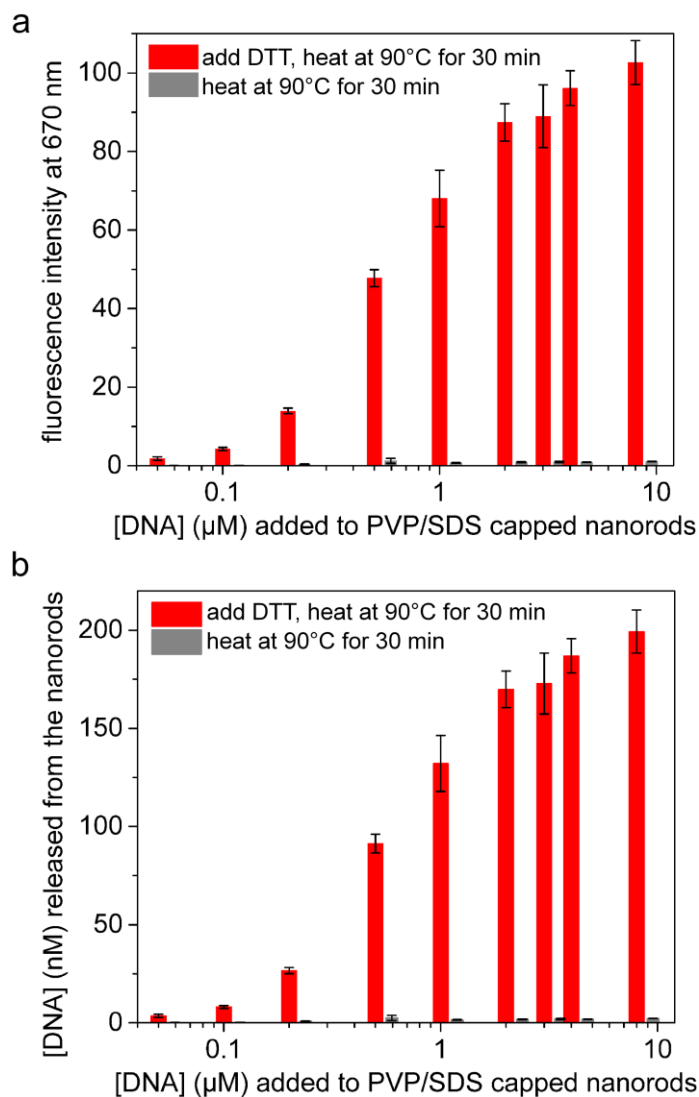
Figure 4.11. **(a) Maximum fluorescence intensities (λ_{ex} = 600 nm; λ_{em} = 670 nm) of the supernatants collected from samples of gold nanorods capped with ss-DNA. These supernatants were collected after treating the samples by either the addition of DTT and heating at 90°C for 30 min, or heating without the addition of DTT at 90°C for 30 min. The maximum fluorescence intensities are reported as a logarithmic function of the initial concentration of ss-DNA added to 0.32 nM PVP and SDS capped gold nanorods. (b) Concentrations of ss-DNA released into the supernatant from samples of gold nanorods capped with ss-DNA. These supernatants were collected after treating the samples by either the addition of DTT and heating at 90°C for 30 min, or heating without the addition of DTT at 90°C for 30 min. The concentrations of ss-DNA released are reported as a function of the initial concentration of ss-DNA added to 0.323 nM PVP and SDS capped gold nanorods.**
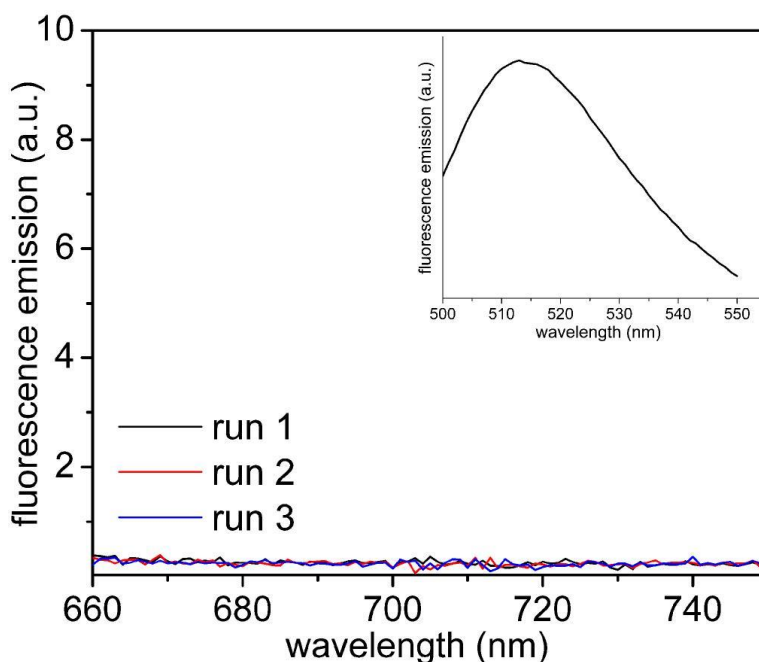
153

Figure 4.12. Fluorescence emission spectra (λ_{ex} = 600 nm) of the supernatants retrieved after centrifugation of solutions containing PVP and SDS capped gold nanorods that were incubated with alcohol-functionalized single-stranded DNA modified with Quasar 670. Three repeats are shown for this experiment. The inset shows a fluorescence emission spectrum (λ_{ex} = 520 nm) for a fluorescein isothiocyanate dye, used as an internal reference in the experiment. This result validates the response of the spectrometer.

The number of ss-DNA molecules loaded onto each gold nanorod was proportional to the initial concentration of thiol-functionalized ss-DNA used to form these oligonucleotide-based monolayers and the concentration of gold nanorods in solution. A large excess of ss-DNA was added relative to the number of DNA bound to each nanorod. The concentration of ss-DNA stabilized gold nanorods in solution was determined by inductively coupled plasma mass spectrometry (ICP-MS). The details of this determination are provided in Appendix B. The concentration of gold nanorods was further confirmed through calculations using the Beer-Lambert law and an extinction coefficient of 4.4×10^9 M^{-1}cm^{-1} at 767 nm.[44] These analyses confirmed a concentration of $\sim 1.25 \times 10^{11}$ gold nanorods per mL of solution. The number of thiol-functionalized ss-DNA initially added to each suspension of PVP/SDS stabilized gold nanorods was confirmed by fluorescence spectroscopy, monitoring the Quasar 670 label on each ss-DNA. The number of ss-DNA strands bound to the nanorods was determined after removing

excess DNA from the samples followed by DTT treatment and fluorescence spectroscopy (as described above). The results of these spectroscopic measurements were divided by the corresponding concentration of gold nanorods in solution to assess the number of ss-DNA strands bound to each nanorod. The amount of ss-DNA bound to each nanorod steadily increased in proportion to an increase in concentration of thiol-functionalized oligonucleotides added to the nanorods stabilized by a mixture of PVP and SDS (Figure 4.13). The number of ss-DNA molecules bound to each gold nanorod reached a plateau for samples prepared from ratios ≥25600:1 (mole ratios) of thiol-functionalized ss-DNA to PVP/SDS stabilized nanorods. This study revealed that the method of displacing the PVP/SDS stabilizing layer with oligonucleotides reached a maximum loading of 870±60 ss-DNA molecules per gold nanorod.
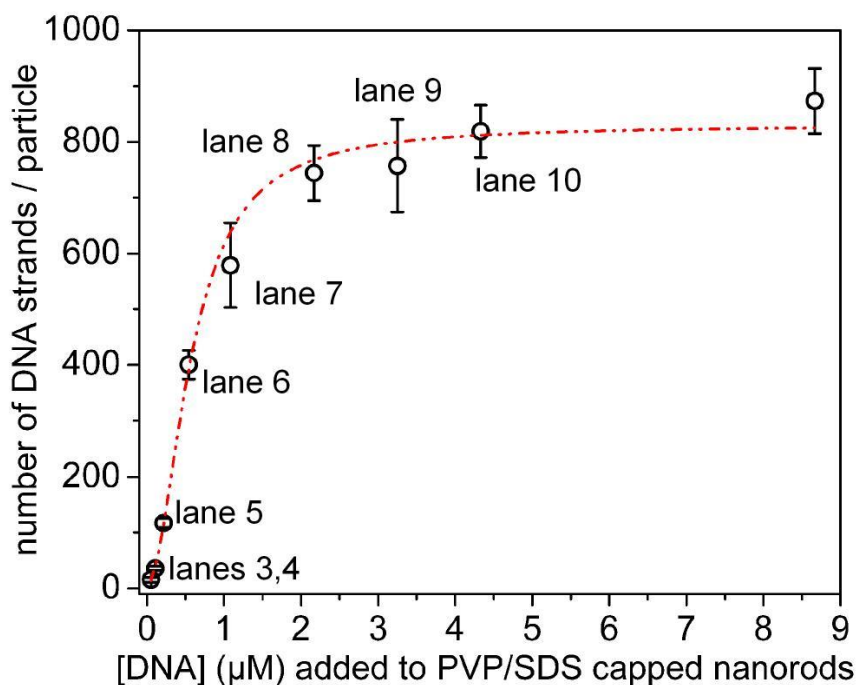
Figure 4.13.   A plot showing the relationship between the initial concentrations of ss-DNA added to a 0.23 nM solution of PVP/SDS stabilized gold nanorods, and the resulting average number of ss-DNA strands bound to each nanorod in the purified samples. All experiments were run in triplicate and error bars are equivalent to one standard deviation from the mean associated with the variance for these measurements.

One method to assess the utility of using PVP and SDS as an intermediate stabilizing layer is to compare the surface coverage achieved herein to prior literature. The minimum surface area (or footprint) per ss-DNA molecule was calculated by dividing the total surface area of a nanorod by the maximum loading of ss-DNA molecules. This footprint per ss-DNA molecule is ~2.0 nm^2 for the highest loading achieved in these studies. Previous studies report a footprint of >4 nm^2 per ss-DNA on gold nanorods.[45,57] The density of ss-DNA molecules on the surfaces of the gold nanorods achieved in our studies is close to the maximum loading of ss-DNA achieved on the surfaces of gold films.[49,58,59] In these previous studies, the packing densities of ss-DNA on polycrystalline gold films approached a surface coverage proportional to that of a densely packed monolayer of thiolated oligonucleotides; the effective diameter of the area occupied by each ss-DNA in these studies was between 1.2 and 1.4 nm. The diameter of single-stranded DNA is ~1.2 nm.[49,58] In our studies, the effective diameter of the area occupied by each ss-DNA is estimated to be ~1.5 nm corresponding to a circular footprint with an area of 2.0 nm^2. This improved loading of thiolated ss-DNA on gold nanorods in comparison to the prior literature could be attributed in part to: i) the ease of displacing the PVP and SDS layers relative to displacing other capping molecules (e.g., CTAB, alkanethiol) on the gold nanorods;[60] and ii) the use of multivalent cations (i.e. Mg^{2+}) in solution to stabilize the interactions between the nucleic acids on the gold surfaces.[61,62] The increased density of ss-DNA bound to the gold nanorods in our study could also be due to the differences in the assumed shape of the nanorods used to calculate the surface area (we assumed a dumbbell shape to match the results of our TEM analysis; further details are provided in the Experimental Methods, section 4.2), as well as the curvature and surface roughness for our gold nanorods prepared in the presence of CTAB in contrast to those prepared by previous studies through electrodeposition.[45,57] A more accurate comparison would require a detailed, systematic study of nanorods synthesized by the same method and capping layers of ss-DNA assembled under the same conditions, which is beyond the scope of this current study. Our studies demonstrate the ease of exchanging a mixed stabilizing layer of PVP and SDS on gold nanorods with a layer of thiolated ss-DNA. This method avoids potential interference from CTAB molecules through electrostatic interactions that could impede a maximum and uniform loading of ss-DNA onto the gold nanorods.

We also evaluated the ability of the gold nanorods capped with a high loading of ss-DNA to hybridize with complementary probes attached to spherical particles. The success of the hybridization process was evaluated by the ability of these nanorods to form core-satellite assemblies.[9-11] Probe ss-DNA molecules were bound to the surfaces of ~10-nm diameter spherical gold particles. The hybridization process was performed by mixing the spherical and nanorod particles, each decorated with a different ss-DNA molecule that is complementary to each other. The resulting core-satellite assemblies contained an average of 8±2 spherical particles for every nanorod (Figure 4.14 and Figure 4.15). The formation of core-satellite assemblies required the presence of complementary ss-DNA molecules on the nanorods and the nanoparticles (Figure 4.16).
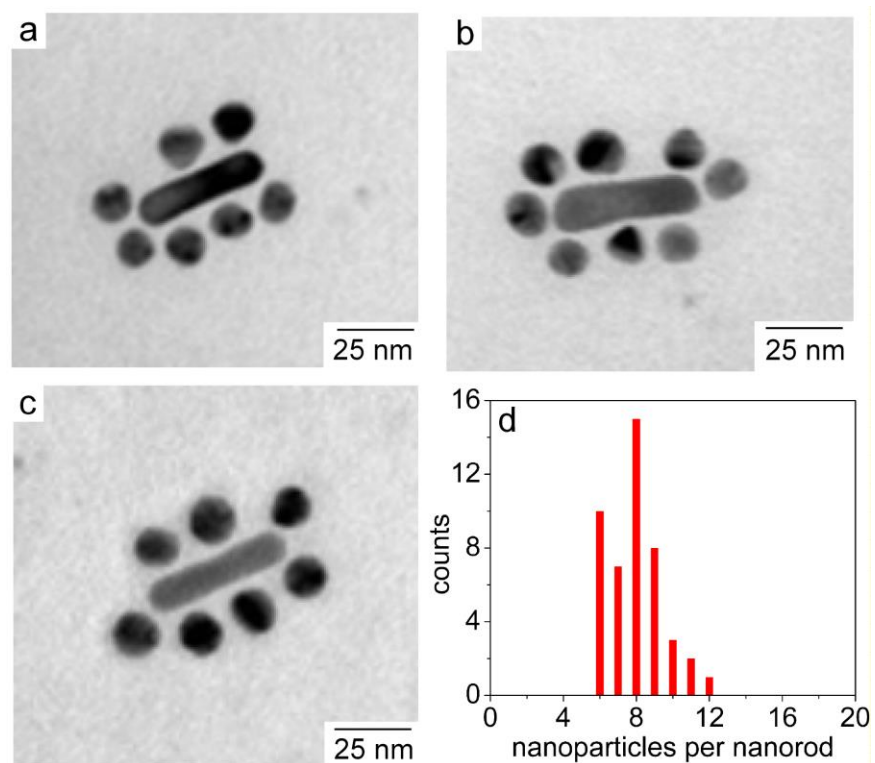
Figure 4.14. **(a-c) Representative TEM images of core-satellite assemblies of gold nanorods decorated with spherical gold nanoparticles. These assemblies form through the hybridization of complementary ss-DNA bound to each type of nanoparticle. (d) A corresponding histogram of satellite particles assembled onto the nanorod cores within a population of ~50 nanorods.**
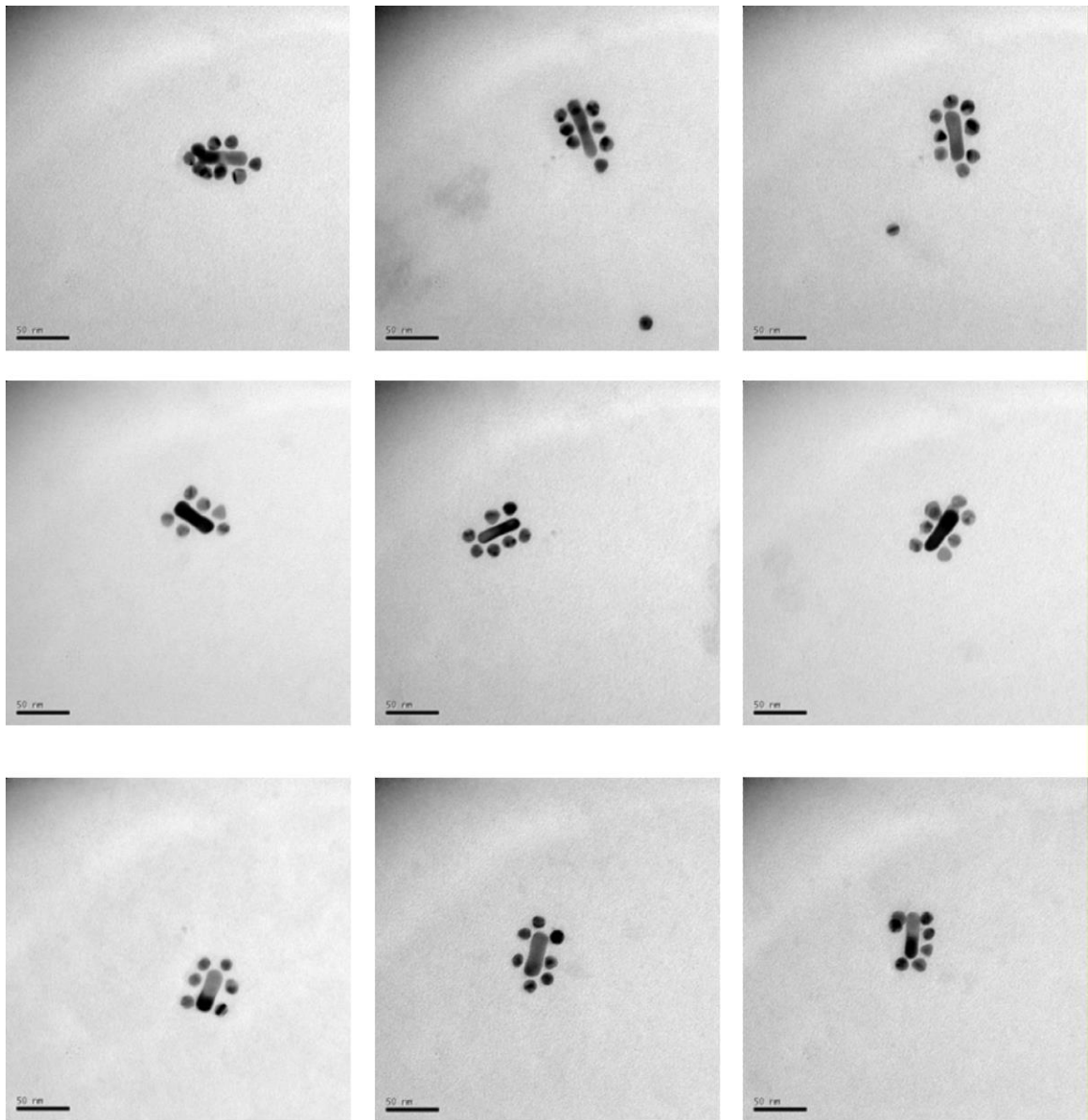
50 nm

Figure 4.15. Additional representative transmission electron microscopy (TEM) images of core-satellite assemblies of gold nanoparticles on gold nanorods.
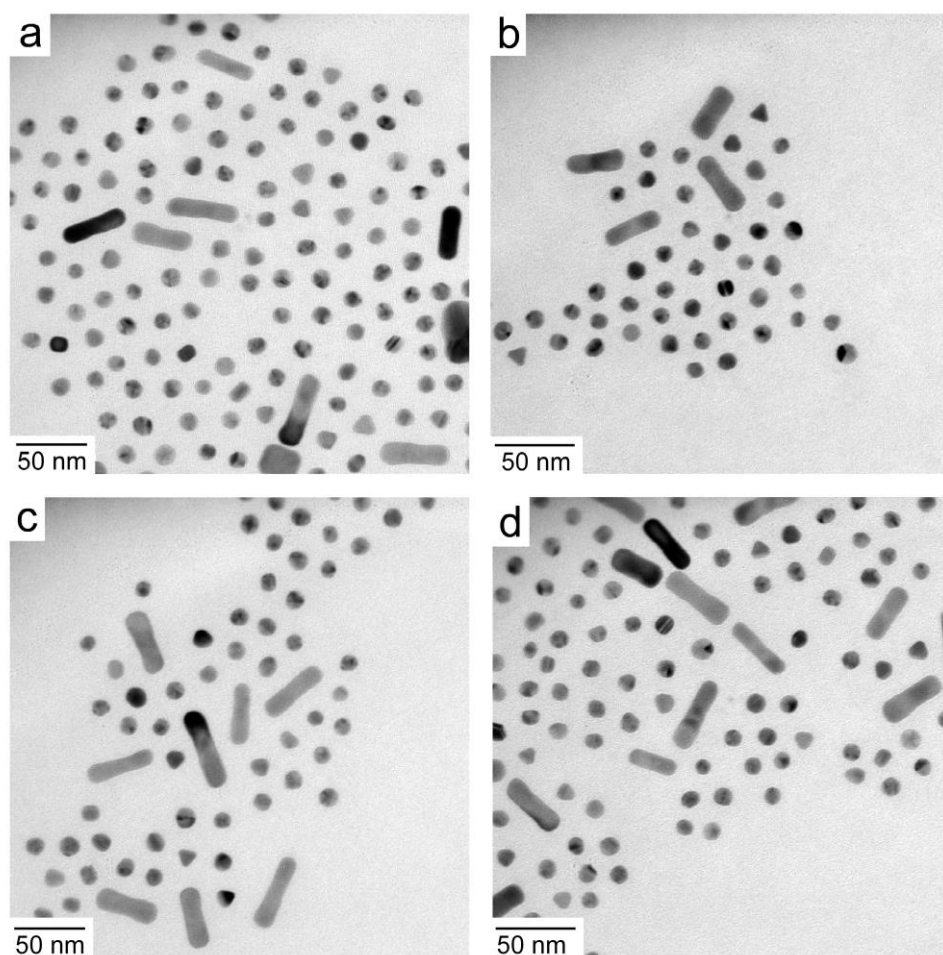
Figure 4.16. **(a-d) Representative transmission electron microscopy (TEM) images of non-assembling gold nanorods and gold nanoparticles. The nanorods are capped with monolayers of ss-DNA, and the nanoparticles are stabilized with sodium citrate.**

159

The colloidal stability of, ss-DNA decorated AuNRs was further analyzed at elevated temperatures or with the addition of chemical etchants for gold nanorods decorated with a low loading (~150 DNAs per nanorod), medium loading (~400 DNAs per nanorod) and a high loading (>800 DNAs per nanorod). Particles decorated with a higher loading of ss-DNA had least change in concentration at 37°C over a period of a few weeks, indicating relatively high thermal stability of these nanorods in comparison to those capped with medium and low densities of ss-DNA. The observed changes in concentration of nanorods decorated with lower densities of ss-DNA could be attributed to the aggregation of these particles, as observed in the loss of LSPR intensities (Figure 4.17). During the KCN etching studies, the rates of dissolution of the gold cores were fastest for those nanorods decorated with the relatively lower density of ss-DNA as observed in the respective extinction spectra (Figure 4.18). There was also an observed decrease in intensity of the LSPR bands, which is due to a decreased concentration of particles in solution due to cyanide-induced etching of these nanorods. Another observed change was blue shifts in the extinction spectra, which could be attributed to a change in aspect ratios of the nanorods. Change in dimensions of nanorods were quantified by electron microscopy analyses and will be discussed in more detail below. The results of these studies indicate that the chemical and thermal stability of the ss-DNA capped nanoparticles depends on density of these capping ligands or, in other words, it depends on the presence of defects within the molecular coatings. These results provide further important insights into the correlation between the quality of the capping layers decorating the surfaces of nanoparticles and their resulting colloidal stability.
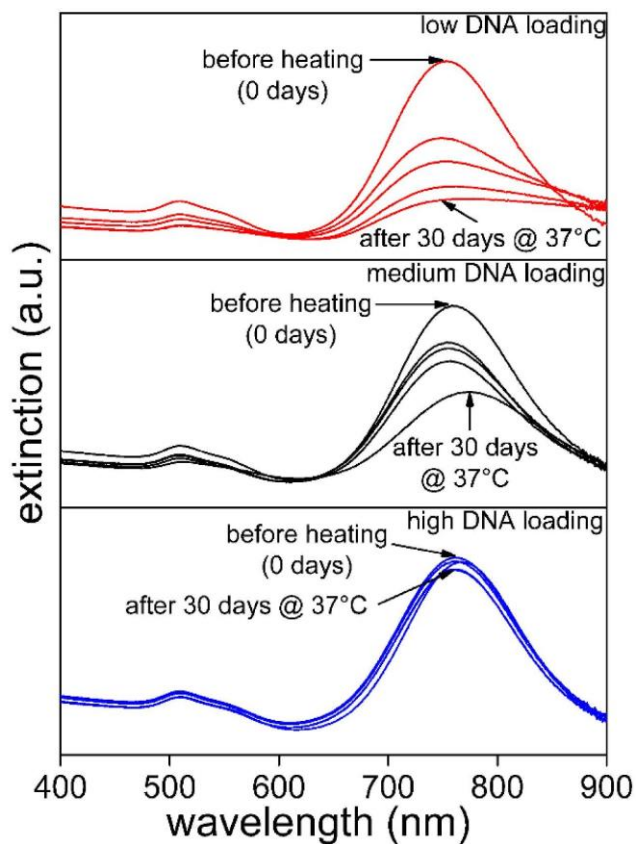
Figure 4.17. Thermal stability of AuNRs capped with varying loadings of ss-DNA as indicated in each set of spectra. The rate of decrease in intensity of extinction spectra for each sample of ss-DNA modified nanorods depended on their loading of DNA.
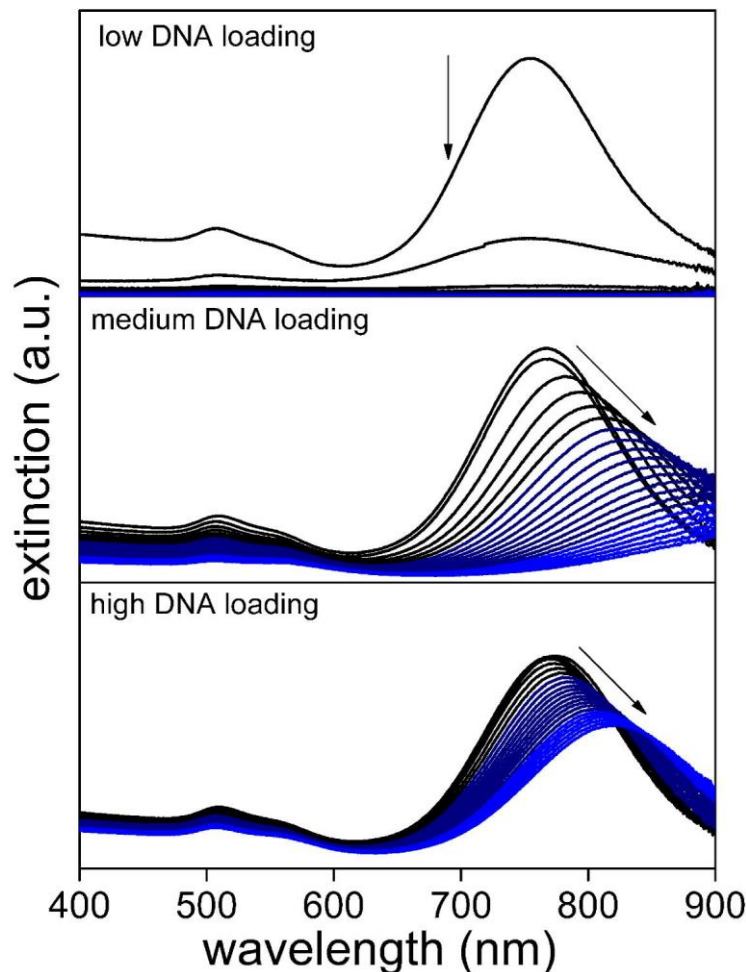
Figure 4.18. Chemical stability of gold nanorods capped with varying loadings of ss-DNA as indicated in each set of spectra. These samples were incubated with 0.01 M KCN for a period of 30 min, during which the extinction spectra were acquired every 1 min. Those nanorods with a high loading of ss-DNA were the most resistant to etching.

The samples with a medium and high loading of ss-DNA were analyzed by TEM following exposure to KCN for 30 min. Prior to TEM analysis, the samples were centrifuged and rinsed once with water, in order to stop the KCN reaction. Those samples with a low loading of ss-DNA (~150 ss-DNA per gold nanorod) were completely etched after 30 min incubation with KCN, and their solutions turned colorless as observed previously when complete metal oxidation occurs.[64] These nanorods with ~150 ss-DNA per gold nanorod could, therefore, not be further analyzed by electron microscopy. There was a morphological transformation of nanorods modified with either a medium or high ss-DNA loading after 30 min incubation with KCN (Figures 4.19 and

4.20). In addition, TEM analysis revealed an increase in aspect ratios from 4.0 to 4.4, and from 3.9 to 5.2 for the nanorods with a high and medium ss-DNA loading, respectively. Nanorods modified with a medium and high loading of DNA became shorter and significantly narrower after the KCN etching experiment when compared to their dimensions before etching. The nanorods with a medium loading of ss-DNA were more adversely etched, suggesting that the ss-DNA coatings were less protective against chemical etching as compared to those nanorods with high ss-DNA loadings. The difference in DNA loadings is confirmed by the increased rates of gold etching for those samples modified with medium loadings of ss-DNA relative to the nanorods with a high ss-DNA loading (Figure 4.18).
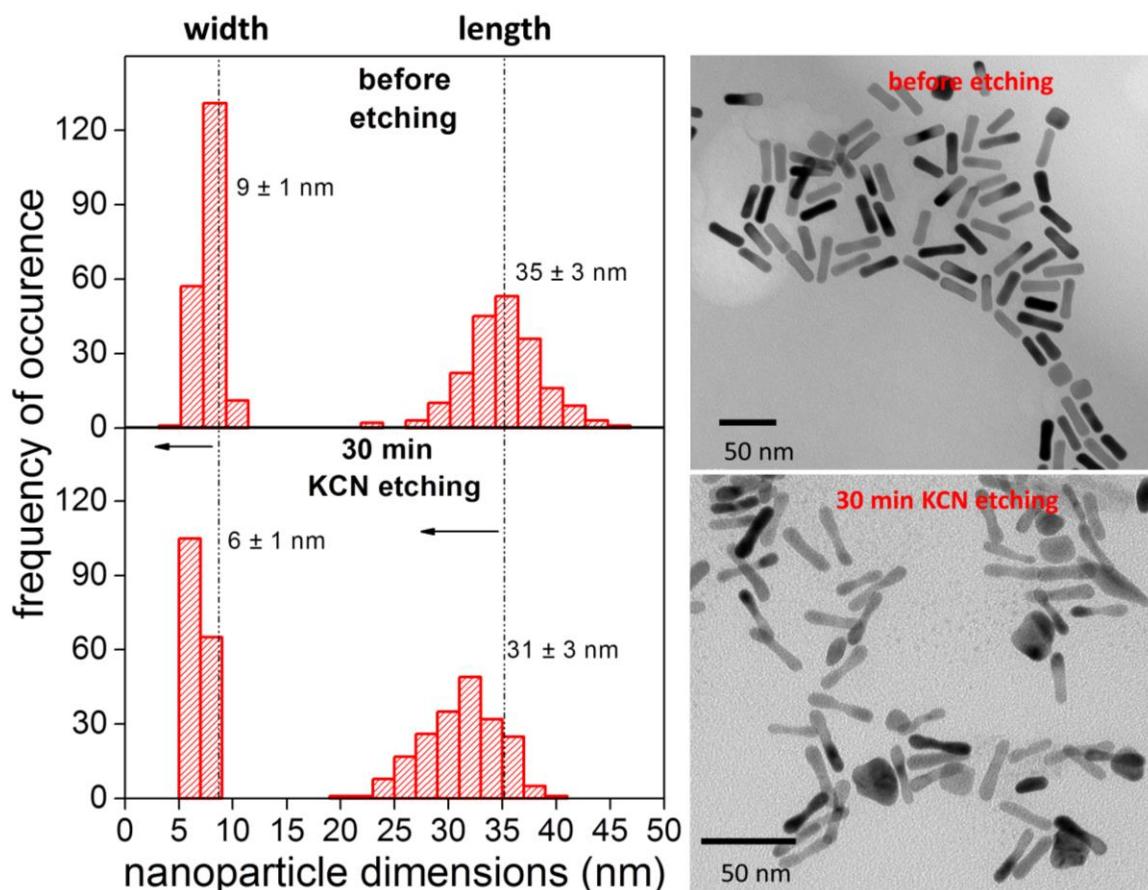
Figure 4.19. Histograms of particle lengths and widths as determined by TEM analysis for nanorods with ~400 ss-DNA molecules per gold nanorod.
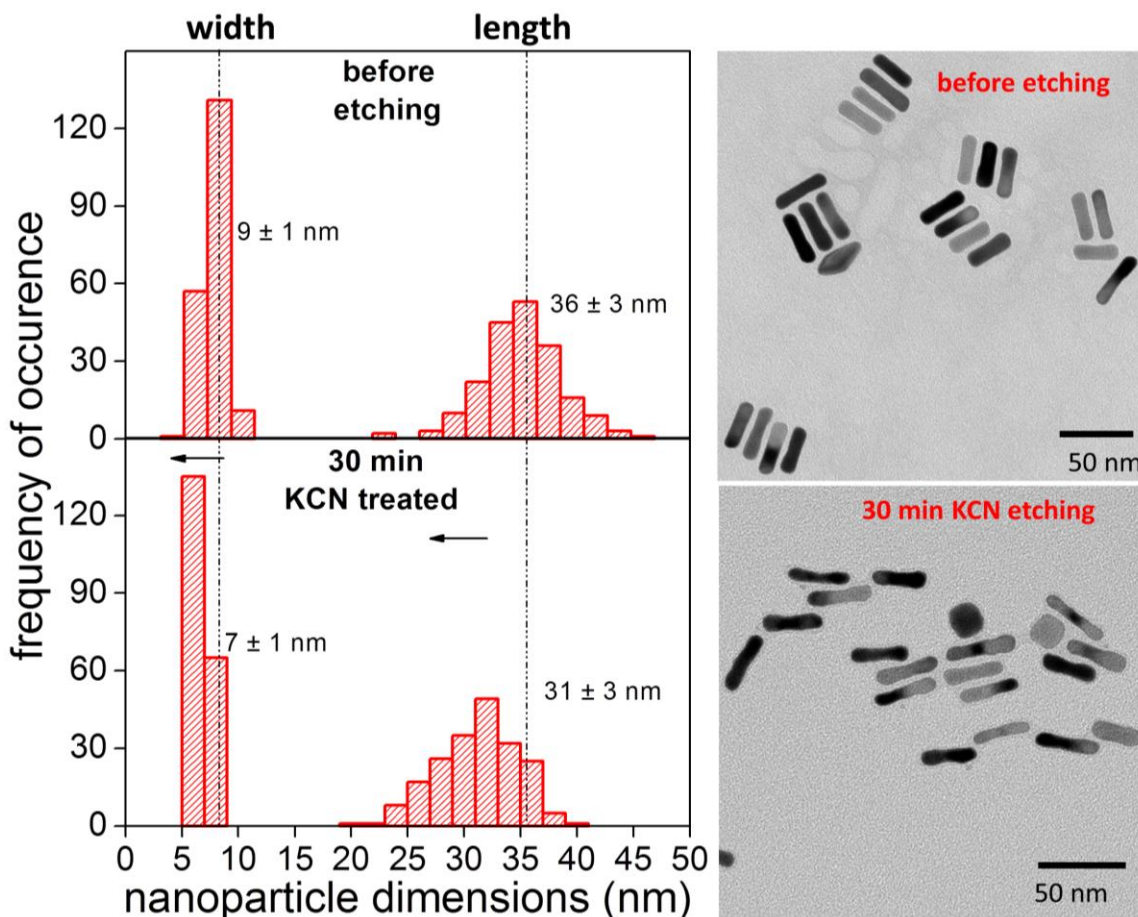
Figure 4.20. Histograms of particle lengths and widths as determined by TEM analysis for nanorods with >800 ss-DNA molecules per gold nanorod.

4.4. Summary and Conclusions

We have demonstrated a versatile strategy for decorating CTAB capped gold nanorods with oligonucleotides, and demonstrated the ability to fine tune the number of oligonucleotides per nanorod. A mixture of PVP and SDS is used as an intermediate stabilizing layer for the gold nanorods before capping these particles with thiol-functionalized ss-DNA. The quality of molecular coatings was found to depend on the density of ss-DNA on these nanorods, as seen in their relative physicochemical stabilities and ability to resist degradation by chemical etchants. The packing of ss-DNA was further improved by using the salts to screen charges between DNA backbones. This study highlights the importance of the choice of intermediate coatings when

modifying nanoparticles through the ligand exchange process as well as other interactions in solution to maximize the loading of coatings on nanoparticles. The methodology of using a weakly binding coating (e.g., a mixture of PVP and SDS), allowed controllable decoration of the surfaces of AuNRs with DNA, and this could be extended to other molecular coatings.

Analysis by fluorescence spectroscopy demonstrated a reproducible process of decorating the gold nanorods with a well-defined number of oligonucleotides. The physicochemical stability of these ss-DNA decorated nanorods in concentrated salt solutions, at the physiological temperature and in the presence of a chemical etchant is proportional to the density of oligonucleotides coating their surfaces as further assessed by electrophoretic mobilities of the nanorods, and their extinction spectra and dimensions as observed by electron microscopy. Dense layers of ss-DNA capping the nanorods were prepared with an average footprint down to ~2.0 nm^2. These particles were used to successfully prepare core-satellite assemblies by a hybridization assay. This new methodology of surfactant exchange could be universally adapted for the uniform and high yielding decoration of gold nanoparticles with other capping groups of interest. The method may also be of use to modify gold nanoparticles with a well-defined number of functional groups in preparation for a variety of applications that include use in drug delivery, photothermal or photodynamic therapies.

4.5. References

(1) Nam, J. M.; Park, S. J.; Mirkin, C. A. *J. Am. Chem. Soc.* **2002**, *124*, 3820-3821.

(2) Elghanian, R.; Storhoff, J. J.; Mucic, R. C.; Letsinger, R. L.; Mirkin, C. A. *Science* **1997**, *277*, 1078-1081.

(3) Yu, C. X.; Irudayaraj, J. *Anal. Chem.* **2007**, *79*, 572-579.

(4) Cheng, Y. N.; Stakenborg, T.; Van Dorpe, P.; Lagae, L.; Wang, M.; Chen, H. Z.; Borghs, G. *Anal. Chem.* **2011**, *83*, 1307-1314.

(5) Rosi, N. L.; Giljohann, D. A.; Thaxton, C. S.; Lytton-Jean, A. K. R.; Han, M. S.; Mirkin, C. A. *Science* **2006**, *312*, 1027-1030.

(6) Bardhan, R.; Lal, S.; Joshi, A.; Halas, N. J. *Acc. Chem. Res.* **2011**, *44*, 936-946.

(7) Dhar, S.; Daniel, W. L.; Giljohann, D. A.; Mirkin, C. A.; Lippard, S. J. *J. Am. Chem. Soc.* **2009**, *131*, 14652-14653.

(8) Luo, Y. L.; Shiao, Y. S.; Huang, Y. F. *ACS Nano* **2011**, *5*, 7796-7804.

(9) Xu, X. Y.; Rosi, N. L.; Wang, Y. H.; Huo, F. W.; Mirkin, C. A. *J. Am. Chem. Soc.* **2006**, *128*, 9286-9287.

(10)   Xu, L. G.; Kuang, H.; Xu, C. L.; Ma, W.; Wang, L. B.; Kotov, N. A. *J. Am. Chem. Soc.* **2012**, *134*, 1699-1709.

(11)   Shi, D. W.; Song, C.; Jiang, Q.; Wang, Z. G.; Ding, B. Q. *Chem. Commun.* **2013**, *49*, 2533-2535.

(12)   Choi, W. I.; Sahu, A.; Kim, Y. H.; Tae, G. *Ann. of Biomed. Eng.* **2012**, *40*, 534-546.

(13)   Ye, X. C.; Jin, L. H.; Caglayan, H.; Chen, J.; Xing, G. Z.; Zheng, C.; Vicky, D. N.; Kang, Y. J.; Engheta, N.; Kagan, C. R.; Murray, C. B. *ACS Nano* **2012**, *6*, 2804-2817.

(14)   Alkilany, A. M.; Thompson, L. B.; Boulos, S. P.; Sisco, P. N.; Murphy, C. J. *Adv. Drug Delivery Rev.* **2012**, *64*, 190-199.

(15) Wijaya, A.; Schaffer, S. B.; Pallares, I. G.; Hamad-Schifferli, K. *ACS Nano* **2009**, *3*, 80-86.

(16) Huschka, R.; Zuloaga, J.; Knight, M. W.; Brown, L. V.; Nordlander, P.; Halas, N. J. *J. Am. Chem. Soc.* **2011**, *133*, 12247-12255.

(17) Yamashita, S.; Fukushima, H.; Akiyama, Y.; Niidome, Y.; Mori, T.; Katayama, Y.; Niidome, T. *Bioorg. Med. Chem.* **2011**, *19*, 2130-2135.

(18) Thibaudau, F. *J. Phys. Chem. Lett.* **2012**, *3*, 902-907.

(19) Poon, L.; Zandberg, W.; Hsiao, D.; Erno, Z.; Sen, D.; Gates, B. D.; Branda, N. R. *ACS Nano* **2010**, *4*, 6395-6403.

(20) Nikoobakht, B.; El-Sayed, M. A. *Chem. Mater.* **2003**, *15*, 1957-1962.

(21) Sau, T. K.; Murphy, C. J. *Langmuir* **2004**, *20*, 6414-6420.

(22) Jana, N. R.; Gearheart, L.; Murphy, C. J. *Adv. Mater.* **2001**, *13*, 1389-1393.

(23) Pastoriza-Santos, I.; Pérez-Juste, J.; Liz-Marzán, L. M. *Chem. Mater.* **2006**, *18*, 2465-2467.

(24) Gole, A.; Murphy, C. J. *Chem. Mater.* **2005**, *17*, 1325-1330.

(25) Huang, H. C.; Barua, S.; Kay, D. B.; Rege, K. *ACS Nano* **2009**, *3*, 2941-2952.

(26) Hauck, T. S.; Ghazani, A. A.; Chan, W. C. W. *Small* **2008**, *4*, 153-159.

(27) Sendroiu, I. E.; Warner, M. E.; Corn, R. M. *Langmuir* **2009**, *25*, 11282-11284.

(28) Grabinski, C.; Schaeublin, N.; Wijaya, A.; D'Couto, H.; Baxamusa, S. H.; Hamad-Schifferli, K.; Hussain, S. M. *ACS Nano* **2011**, *5*, 2870-2879.

(29) Wijaya, A.; Hamad-Schifferli, K. *Langmuir* **2008**, *24*, 9966-9969.

(30) Vigderman, L.; Manna, P.; Zubarev, E. R. *Angew. Chem. Int. Ed.* **2012**, *51*, 636-641.

(31) Hou, W. B.; Dehm, N. A.; Scott, R. W. J. *J. Catal.* **2008**, *253*, 22-27.

(32) Pastoriza-Santos, I.; Gomez, D.; Perez-Juste, J.; Liz-Marzan, L. M.; Mulvaney, P. *Phys. Chem. Chem. Phys.* **2004**, *6*, 5056-5060.

(33)   Caschera, D.; Federici, F.; Zane, D.; Focanti, F.; Curulli, A.; Padeletti, G. *J. Nanopart.Res.* **2009**, *11*, 1925-1936.

(34)   Tsunoyama, H.; Nickut, P.; Negishi, Y.;Al-Shamery, K Matsumoto, Y.; Tsukuda, T. *J. Phys. Chem. C* **2007**, *111*, 4153-4158.

(35)   Kan, C. X.; Cai, W. P.; Li, C. C.; Zhang, L. D. *J. Mater. Res.* **2005**, *20*, 320-324.

(36)   Kedia, A.; Kumar, P. S. *J. Phys.Chem. C* **2012**, *116*, 23721-23728.

(37)   Liu, H.; Zhang, B.; Shi, H. Q.; Tang, Y. J.; Jiao, K.; Fu, X. *J. Mater. Chem.* **2008**, *18*, 2573-2580.

(38)   Mdluli, P. S.; Sosibo, N. M.; Revaprasadu, N.; Karamanis, P.; Leszczynski, J. *J. Mol. Struct.* **2009**, *935*, 32-38.

(39)   Behera, M.; Ram, S. *Appl. Nanosci.* **2013**, DOI: 10.1007/s13204-013-0198-9.

(40)   Seoudi, R.; Fouda, A. A.; Elmenshawy, D. A. *Physica B* **2010**, *405*, 906-911.

(41)   Tu, W. X.; Zuo, X. B.; Liu, H. F. *Chin. J. Polym. Sci.* **2008**, *26*, 23-29.

(42)   Zhang, J. H.; Liu, H. Y.; Wang, Z. L.; Ming, N. B. *Chem. Eur. J.* **2008**, *14*, 4374-4380.

(43)   Lim, D. K.; Cui, M. H.; Nam, J. M. *J. Mater. Chem.* **2011**, *21*, 9467-9470.

(44)   Liao, H. W.; Hafner, J. H. *Chem. Mater.* **2005**, *17*, 4636-4641.

(45)   Hill, H. D.; Millstone, J. E.; Banholzer, M. J.; Mirkin, C. A. *ACS Nano* **2009**, *3*, 418-424.

(46)   Tagliazucchi, M.; Blaber, M. G.; Schatz, G. C.; Weiss, E. A.; Szleifert, I. *ACS Nano* **2012**, *6*, 8397-8406.

(47)   Hu, X. G.; Gao, X. H. *Phys. Chem. Chem. Phys.* **2011**, *13*, 10028-10035.

(48)   Gómez-Graña, S.; Hubert, F.; Testard, F.; Guerrero-Martínez, A.; Grillo, I.; Liz-Marzán, L. M.; Spalla, O. *Langmuir* **2012**, *28*, 1453-1459.

(49)   Steel, A. B.; Levicky, R. L.; Herne, T. M.; Tarlov, M. J. *Biophys. J.* **2000**, *79*, 975-981.

(50)   Barr, T. L.; Seal, S. *J. Vac. Sci. Technol. A* **1995**, *13*, 1239-1246.

(51)   May, C. J.; Canavan, H. E.; Castner, D. G. *Anal. Chem.* **2004**, *76*, 1114-1122.

(52)   Lee, C.-Y.; Gong, P.; Harbers, G. M.; Grainger, D. W.; Castner, D. G.; Gamble, L. J. *Anal. Chem.* **2006**, *78*, 3316-3325.

(53)   Terlingen, J. G. A.; Feijen, J.; Hoffman, A. S. *J. Colloid Interface Sci.* **1993**, *155*, 55-65.

(54)   Vericat, C.; Vela, M. E.; Benitez, G.; Carro, P.; Salvarezza, R. C. *Chem. Soc. Rev.* **2010**, *39*, 1805-1834.

(55)   Kim, J. Y.; Kim, H. B.; Jang, D. J. *Electrophoresis* **2013**, *34*, 911-916.

(56)   Hurst, S. J.; Lytton-Jean, A. K. R.; Mirkin, C. A. *Anal. Chem.* **2006**, *78*, 8313-8318.

(57)   Cederquist, K. B.; Keating, C. D. *ACS Nano* **2009**, *3*, 256-260.

(58)   Rekesh, D.; Lyubchenko, Y.; Shlyakhtenko, L. S.; Lindsay, S. M. *Biophys. J.* **1996**, *71*, 1079-1086.

(59)   Song, Y. H.; Liu, Y. Q.; Yang, M. L.; Zhang, B. L.; Li, Z. *Appl. Surf. Sci.* **2006**, *252*, 5693-5699.

(60)   Xia, X. H.; Yang, M. X.; Wang, Y. C.; Zheng, Y. Q.; Li, Q. G.; Chen, J. Y.; Xia, Y. N. *ACS Nano* **2012**, *6*, 512-522.

(61)   Russell, R.; Millett, I. S.; Doniach, S.; Herschlag, D. *Nat. Struct. Biol.* **2000**, *7*, 367-370.

(62)   Fang, X. W.; Littrell, K.; Yang, X.; Henderson, S. J.; Siefert, S.; Thiyagarajan, P.; Pan, T.; Sosnick, T. R. *Biochemistry* **2000**, *39*, 11107-11113.

(63)   Kimling, J.; Maier, M.; Okenve, B.; Kotaidis, V.; Ballot, H.; Plech, A. *J. Phys. Chem. B* **2006**, *110*, 15700-15707.

(64)   Fateixa, S.; Correia, M. R.; Trindade, T. *Phys. Chem. C* **2013**, *117*, 20343-20350.

(65)   Pekcevik, I. C.; Poon, L. C. H.; Wang, M. C. P.; Gates, B. D. *Analytical Chemistry* **2013**, *85*, 9960-9967.

Chapter 5.

Conclusions and Future Directions

A challenge with using most types of nanoparticles is that the colloids can be destabilized upon extended exposure to variable environmental conditions. Even the simplest conditions of exposure to an electrolyte can destabilize the nanoparticles. These instabilities can be the result of oxidative damage to molecular coatings on the nanoparticles, leading to unwanted changes (such as aggregation) of nanoparticles. This thesis work details the preparation of varying qualities of molecular coatings on AuNPs. The quality of molecular coatings is established through a series of analytical techniques, which are complementary to each other. Through these detailed analyses, we sought to establish a quality factor for the molecular coatings on the modified nanoparticles, as it relates to the observed physicochemical stability of the particles under varied environmental conditions (e.g., temperature). Many studies reported in the literature offer incomplete analyses of nanoparticle stability and often the modification procedures are irreproducible because of a lack of comprehensive stability testing. Many studies utilize the functionalized nanoparticles, for example, for drug delivery within a biological system without first analyzing the stability of these particles under the relevant conditions of study (i.e., biological environments). The goal of this thesis work was to create a methodology that can be implemented to quickly and comprehensively determine changes in the colloidal and chemical stability of AuNPs, especially under changing environmental conditions. Knowledge learned from these studies can be extended to other types of nanoparticles and a variety of surface chemistries.

This work details the preparation and surface modification of gold nanoparticles, using a variety of molecular coatings. Specifically, MUDA, MHDA, CTAB and thiolated ss-DNA coatings are used to decorate gold nanoparticles for enhanced stability under a variety of conditions employed in this thesis work. These nanoparticles were modified

through ligand exchange processes and the quality of the resulting coating layers was analyzed using methods commonly applied to characterize such particles. The physicochemical stability of these surface modified gold particles is examined under a variety of environmental conditions, mainly conditions that could destabilize these modified nanoparticles. These series of complementary stability tests enable a comprehensive study of the quality of the resulting molecular coatings. We found that both the nanoparticles' coatings, as well as surrounding media that includes additives such as co-surfactants, influence the stability of the colloidal particles. The nanoparticles could become partially unprotected if the molecular coatings are desorbed from their surfaces during exposure of these nanoparticles to various oxidative, chemical and physiological environments. It is, therefore, necessary to analyze the integrity of molecular coatings following their exposure to such harsh environments. Lessons learned from these analyses can be used to guide the preparation of modified particles that are more robust. In summary, the environment surrounding the particles (such as solvent composition and solution pH), as well as the nature of the interaction between molecular coatings and the nanoparticles are all factors that need to be carefully considered when preparing these nanoparticles for their intended applications. The research presented herein provides methods for analyzing the quality of molecular coatings on nanoparticles and could be useful to further improve the methodology used to prepare surface coatings on the particles.

Chapter 1 reviews some commonly used literature approaches to the synthesis and functionalization of AuNPs. There are numerous methods of nanoparticle synthesis and functionalization, each of which results in the formation of nanoparticles with pre-formed coatings. Depending on the type of molecular coating that is pre-formed on nanoparticles, some coatings may remain on the surfaces of nanoparticles (these are not completely exchanged) during subsequent surface modifications with alternative coatings. Incomplete displacement of coatings will result in the formation of non-uniform layers of molecular coatings or otherwise introduce potential defects, especially in cases where the pre-formed coatings are loosely bound to the surfaces of the nanoparticles and are easily displaceable at elevated temperatures. In addition, the quality of molecular coatings depends on the uniformity and density of molecular packing within these coatings on the nanoparticles, as well as the strength of interactions between

171

nanoparticles and their molecular coatings. Preparation conditions should, therefore, be tuned in order to improve the quality of molecular coatings on nanoparticles and ultimately, to improve the long-term stability of these particles under a wide variety of environmental conditions. Future directions that could be pursued include developing other methods to probe quality of molecular coatings on AuNPs. For example, exploring the use of alternative gold etchants such as Fe^{3+} and $Cu(I)$,[1-2] as well as exploring the interaction of nanoparticles with biomolecules, such as in the formation of protein coronas (as a function of the quality of molecular coatings).

In Chapter 2, AuNPs with varying qualities of molecular coatings were prepared by: i) varying the time allowed for the formation and organization of molecular coatings; ii) incorporation of a co-surfactant (Polysorbate 20 or P20), which under some circumstances can significantly improve the colloidal stability of the nanoparticles both during ligand exchange processes and throughout month-long studies. This improved stability included particles suspended at 37°C for prolonged periods. This study improved on previous methods for the functionalization of AuNPs using polysorbates as a co-surfactant during the ligand exchange processes.[3-5] These previous methods, however, did not comprehensively evaluate the long-term stability of the modified nanoparticles. For example, we found that the P20 surfactants degraded on the surfaces of nanoparticles when the particles were heated to 45°C. The long-term thermal stability of the particles in this work was also studied as a function of the quality of molecular coatings on the nanoparticles. Those nanoparticles with higher quality coatings were more resistant to changes, including improved stability against cyanide etching. Future studies could be expanded to investigate how other surfactants (e.g., CTAB, and fluorinated surfactants) that can interact with the nanoparticles, as well as extending the work to multidentate molecular coatings (e.g., bidentate thiols) that could significantly impact long-term stability of these AuNPs. The goal remains to identify a nanoparticle coating that offers superior physicochemical stability to the particles. Fluorinated surfactants have been reported to be resistant to heat, while CTAB coatings interdigitate with hydrocarbon chains of alkanethiols to improve the packing of molecular coatings on AuNPs.[6-7] A combination of these coatings may offer both improved thermal stability and colloidal stabilization. Multidentate thiols have been shown in some cases to improve the chemical and thermal stability when used as molecular coatings on

AuNPs.[8-11] Each of these capping layers should also be tested against additional changes in solvent conditions that are specific for the intended use of the nanoparticles. For example, the stability of nanoparticles in biologically relevant buffers and electrolytes should be assessed for those nanoparticles intended for use in *in vitro* and *in vivo* studies.

Chapter 3 presented a comparative study of the physicochemical stability of anisotropic AuNPs during photothermal processes. AuNRs coated with either cetyltrimethylammonium bromide (CTAB) or 11-mercaptoundecanoic acid (MUDA) were irradiated at fixed laser fluences. The stability of these nanorods was assessed as a function of the types of molecular coatings (CTAB or MUDA), as well as excess stabilizing surfactants in each solution of nanorods. This study highlights the importance of solution composition on the stability of nanoparticles. The excess added surfactants were shown to improve stability of the nanoparticles, with stability increasing in proportion to the increase in concentration of excess surfactants in solution. Improved stability of the nanorods during photothermal processes was attributed to the replacement of thermally desorbed molecules (or filling holes in the surface capping layers). The successful implementation of the photothermal effect using AuNPs to controllably release a molecular payload requires a better understanding of the threshold for damage to the nanoparticles and their molecular surface coatings. It is also important to preserve the desirable optical properties of these nanoparticles during the PT processes for a prolonged delivery of heat from these nanoparticles through the PTE, such as for PT induced localized hyperthermia used to treat cancer. Previous studies have pursued the PT-activated release of molecules from AuNPs, but ignored changes in size, shape and surface chemistry of these nanoparticles following their photothermal heating.[12] In this particular case, AuNRs were irradiated at energy fluences of up to 1.73 mJ/cm^2. By tuning the applied energy fluence (0.177−1.24 mJ/cm^2), controlling the surface chemistry and controlling the solution composition, we minimized damage to AuNRs during photothermal heating. Using similar conditions to those determined from our study, the PTE may be harnessed for an improved method of light-activated release of payloads (e.g., therapeutics) within cancerous tissues.

Chapter 4 focused on tuning densities of thiolated single-stranded DNA (ss-DNA) on AuNRs through a new process that we developed, and we also demonstrated improved chemical and colloidal stability of those nanorods with high loadings of DNA. The ability to tune the loading of ss-DNA and to achieve a high loading on AuNRs was attributed to the ease of displacing an intermediate PVP and SDS coating with the stronger binding coatings of thiolated DNA. The density of DNA molecules within these loadings define the quality of these coatings and, ultimately, the long-term physicochemical stability of the DNA-decorated nanoparticles. The number of ss-DNA molecules per nanorod increased in proportion to the concentration of DNA added to the nanorods, but reached a plateau at 870±60 ss-DNA molecules per AuNR. This coating corresponds to a footprint of ~2.0 nm^2 per ss-DNA, which is the highest achieved density of ss-DNA bound to AuNRs reported at this time. My work showed a 2-fold improvement in the loading of DNA (for similar sized nanorods) as compared to a previous study, which prepared ss-DNA coatings on AuNRs by the direct displacement of CTAB molecules.[13] In addition, our nanorods prepared with a high loading of ss-DNA had an improved uniformity between nanoparticles within the solution and an enhanced colloidal stability as seen in their uniform mobilities through an agarose gel. The nanorods with a higher quality coating of ss-DNA also exhibited the most colloidal stablility during heating (at 37°C) for 1 month and against attack during cyanide etching. The results of these studies indicate that the chemical and thermal stability of the nanoparticles depends on density of their capping ligands or, in other words, it depends on the presence of defects within the molecular coatings. These results provide important insights into the correlation between the quality of the capping layers on the surfaces of nanoparticles and their resulting physicochemical stability. In addition, nanorods coated with a high loading of ss-DNA were hybridized with complementary DNA probes attached to spherical particles to demonstrate the functionality of the ss-DNA coatings. This process of tuning the density of the molecular coatings could be extended to other payloads and bioactive molecules for preparing nanoparticles with a tunable quantity of each type of functional coating. Besides oligonucleotides, future research directions could focus on modifying AuNPs with other molecules, such as targeting moieties and a payload containing cancer therapeutics. The density of these biologically relevant molecules on the surfaces of nanoparticles directly influences the potential therapeutic dose that could be delivered via the nanoparticles when used as a platform for targeting and controlling

174

the release of these molecules. This methodology could alternatively be used to prepare multifunctional nanoparticles (e.g., particles decorated with double-stranded DNA for drug intercalation, PEG molecules for improved solubility of the nanoparticles and antibodies for targeting specific cancer cells) with a defined number of each of these functional molecules per nanoparticle, which I believe will have an important impact on their use in cancer management.

5.1. References

(1)   Jeffrey, M. I.; Ritchie, I. M. *J. Electrochem. Soc.* **2000**, *147*, 3272-3276.

(2)   Zou, R. X.; Guo, X.; Yang, J.; Li, D. D.; Peng, F.; Zhang, L.; Wang, H. J.; Yu, H. *CrystEngComm.* **2009**, *11*, 2797-2803.

(3)   Aslan, K.; Perez-Luna, V. H. *Langmuir* **2002**, *18*, 6059-6065.

(4)   Zhao, Y.; Wang, Z.; Zhang, W.; Jiang, X. *Nanoscale* **2010**, *2*, 2114-2119.

(5)   Duy, J.; Connell, L. B.; Eck, W.; Collins, S. D.; Smith, R. L. *Journal of Nanoparticle Research* **2010**, *12*, 2363-2369.

(6)   Wang, L.; Zhang, L.; Lu, C. *Trends in Analytical Chemistry*, **2014**, *54*, 45-55.

(7)   Swami, A.; Kumar, A.; Sastry, M. *Langmuir*, **2003**, *19*, 1168-1172.

(8)   Oh, E.; Susumu, K.; Maekinen, A. J.; Deschamps, J. R.; Huston, A. L.; Medintz, I. L. *Journal of Physical Chemistry C* **2013**, *117*, 18947-18956.

(9)   Zhang, S. S.; Leem, G.; Srisombat, L.-O.; Lee, T. R. *Journal of the American Chemical Society* **2008**, *130*, 113-120.

(10)   Mei, B. C.; Susumu, K.; Medintz, I. L.; Mattoussi, H. *Nature Protocols* **2009**, *4*, 412-423.

(11)   Shon, Y. S.; Lee, T. R. *Journal of Physical Chemistry B* **2000**, *104*, 8192-8200.

(12)   . Wijaya, A.; Schaffer, S. B.; Pallares, I. G.; Hamad-Schifferli, K. *ACS Nano* **2009**, *3*, 80-86.

(13)   Hill, H. D.; Millstone, J. E.; Banholzer, M. J.; Mirkin, C. A. *ACS Nano* **2009**, *3*, 418-424.

Appendix A.

# Control Experiments for Laser Irradiation at Varied Energy Fluences
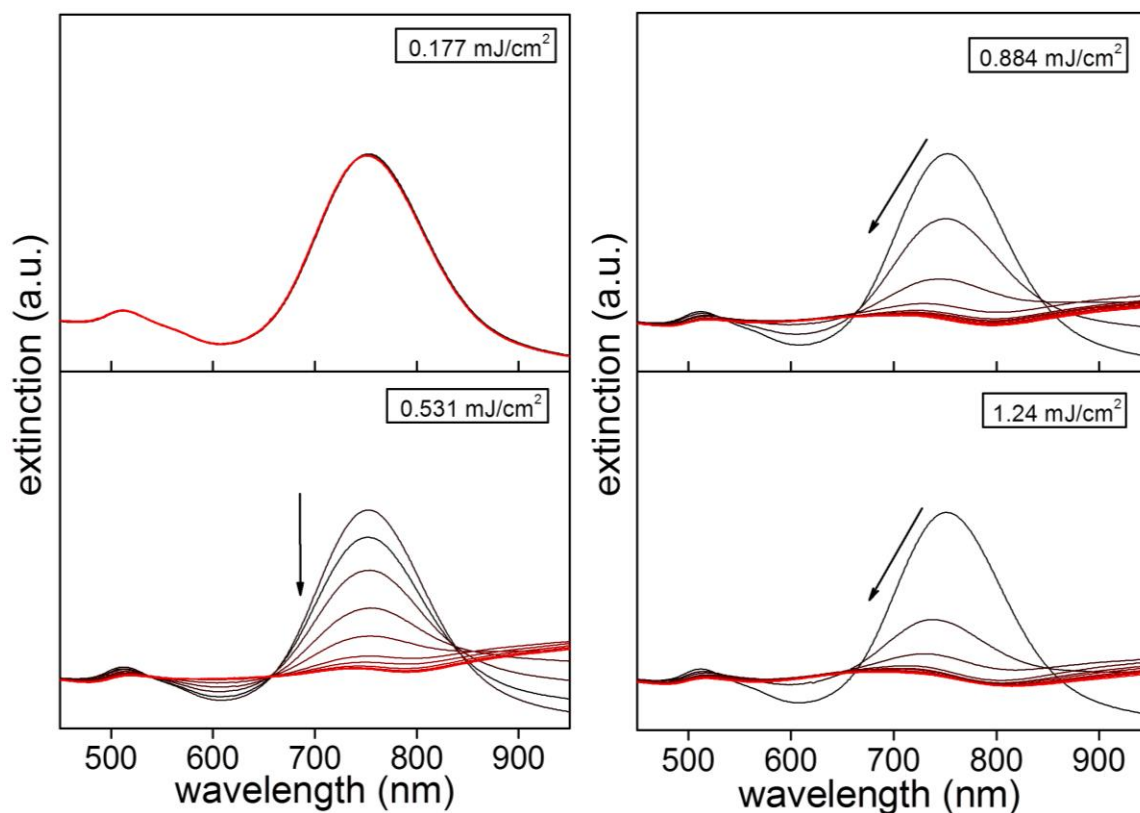
Figure A 1. **Photothermal stability of cetyltrimethylammonium bromide (CTAB) capped gold nanorods following laser treatment. Samples were irradiated at 1 min intervals up to 10 min irradiation with a 120 fs pulsed laser (1 kHz) operating at 800 nm and with varying laser fluences as indicated. The nanoparticles were suspended in deionized water containing <u>no excess CTAB</u>.**
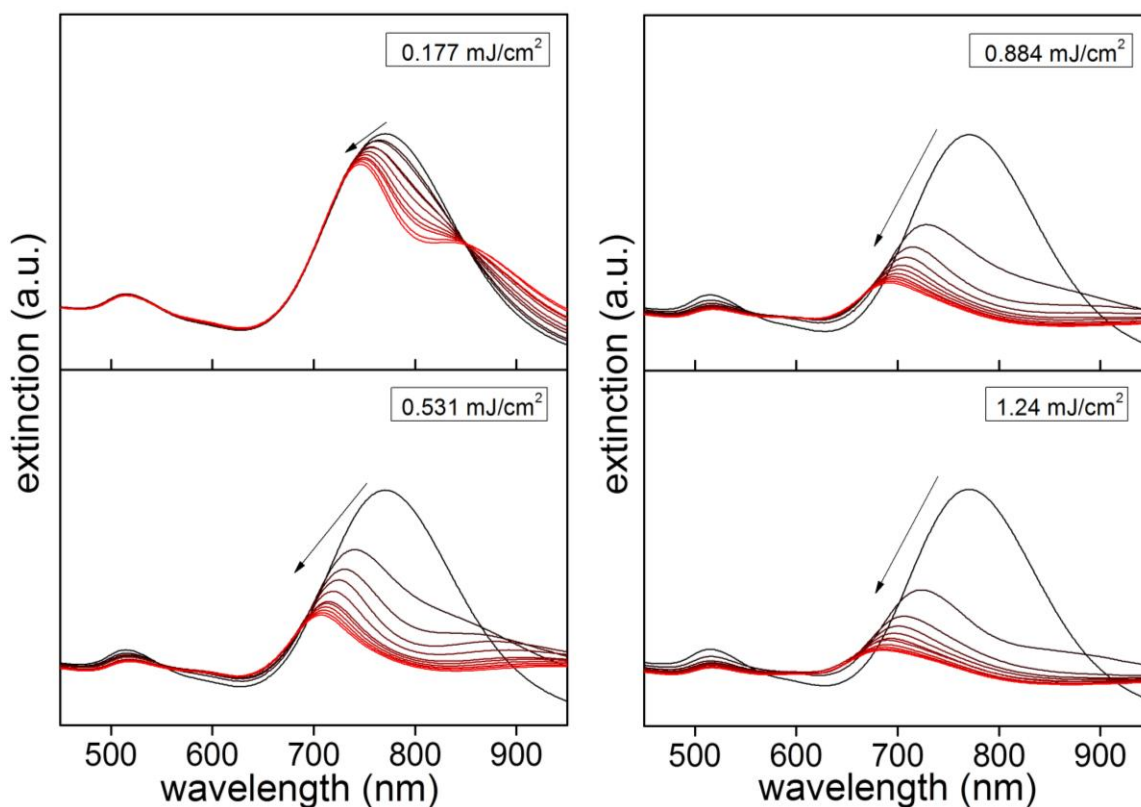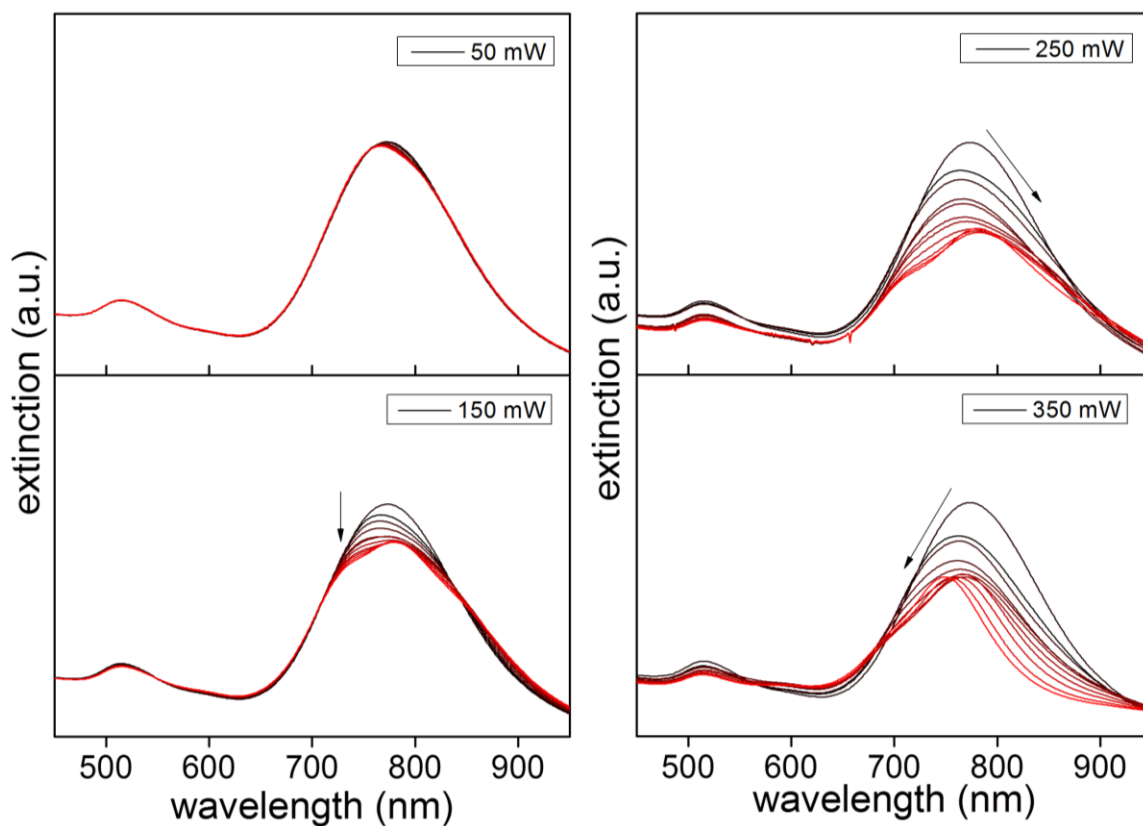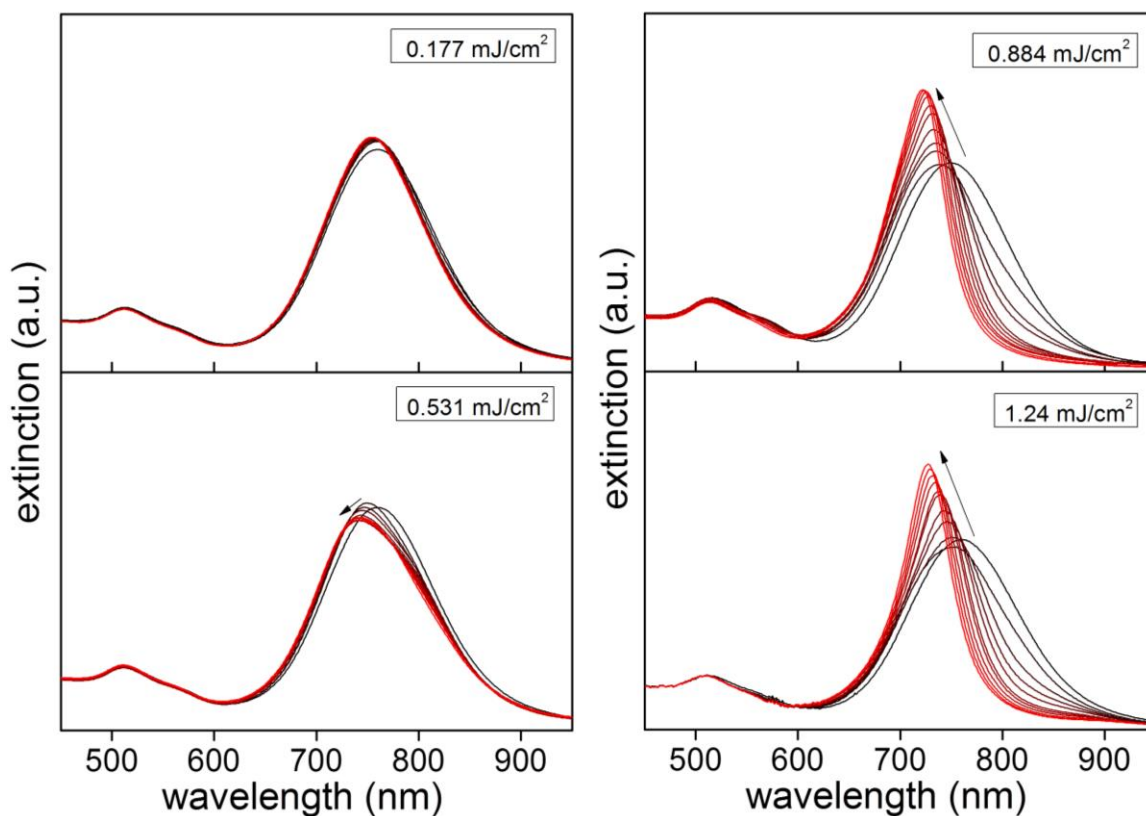
Figure A 2. **Photothermal stability of 11-mercaptoundecanoic acid (MUDA) capped gold nanorods following laser treatment. Samples were irradiated at 1 min intervals up to 10 min irradiation with a 120 fs pulsed laser (1 kHz) operating at 800 nm and with varying laser fluences as indicated. The nanoparticles were suspended in 1x TBE buffer <u>without any excess MUDA</u>.**
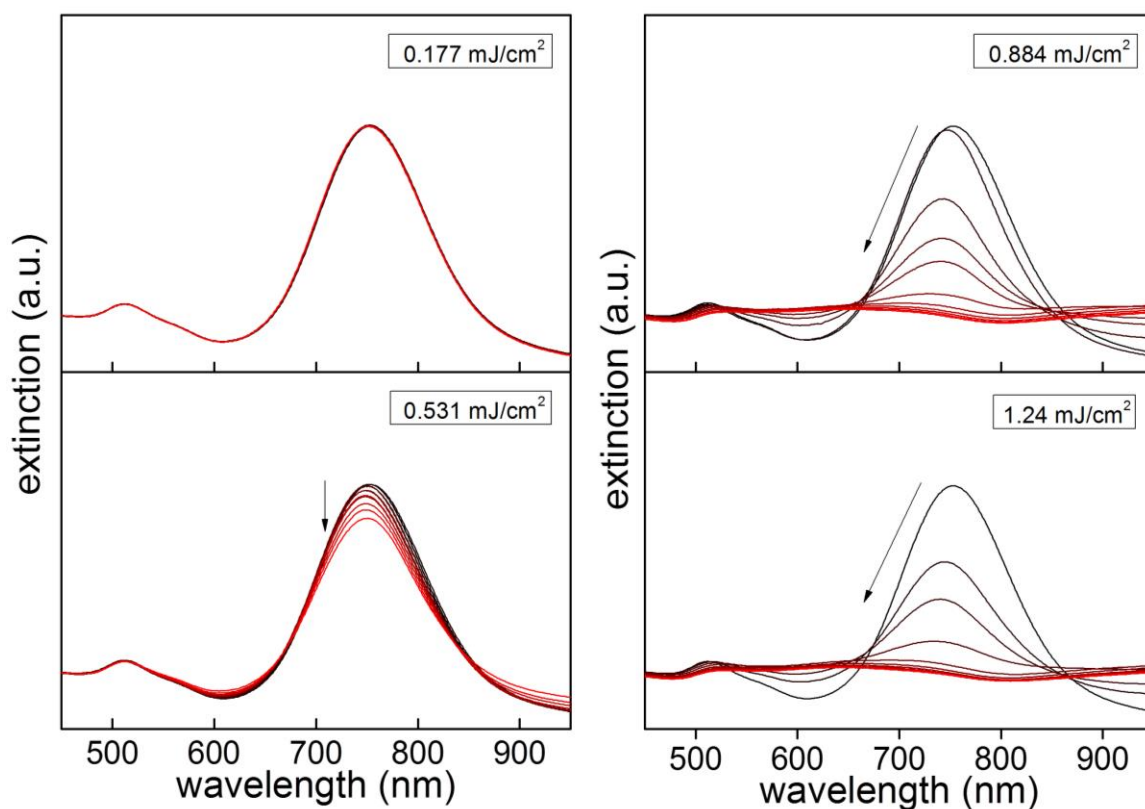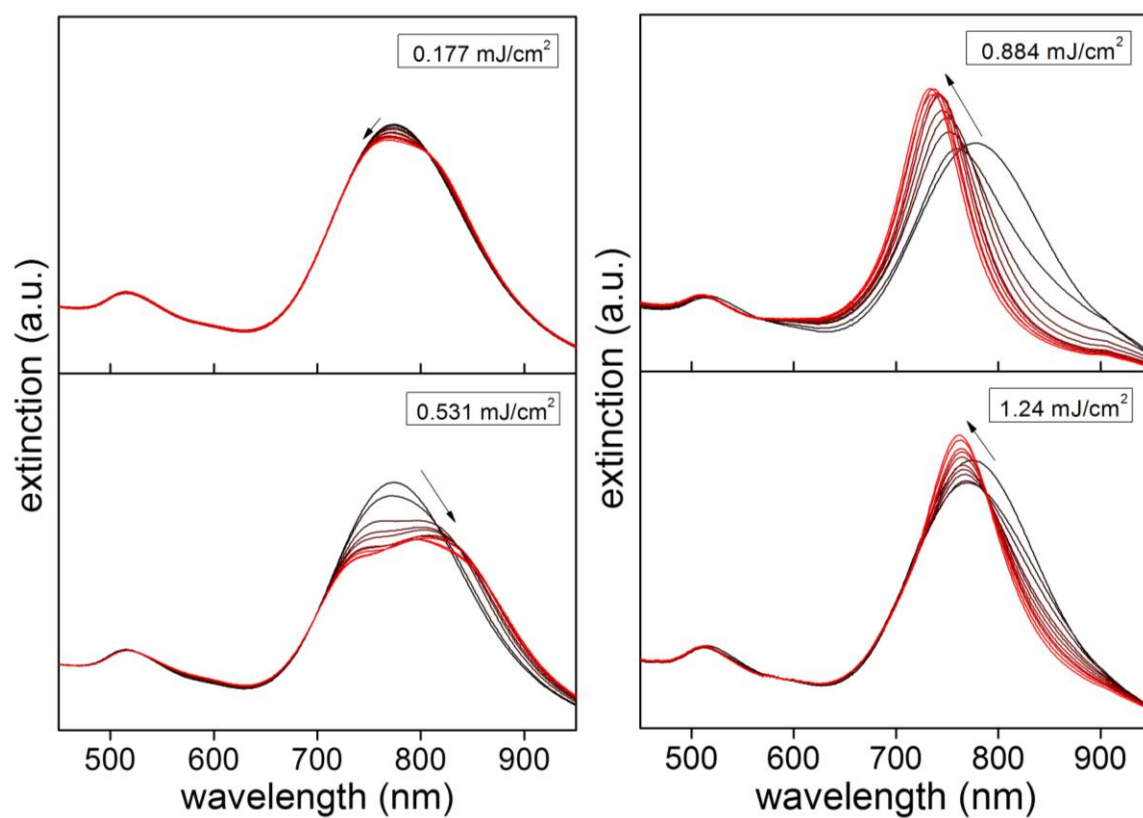
Figure A 3. **Photothermal stability of CTAB capped gold nanorods following laser treatment. Samples were irradiated at 1 min intervals up to 10 min irradiation with a 120 fs pulsed laser (1 kHz) operating at 800 nm and with varying laser fluences as indicated. The nanoparticles were suspended in deionized water containing 0.05 mM excess CTAB.**
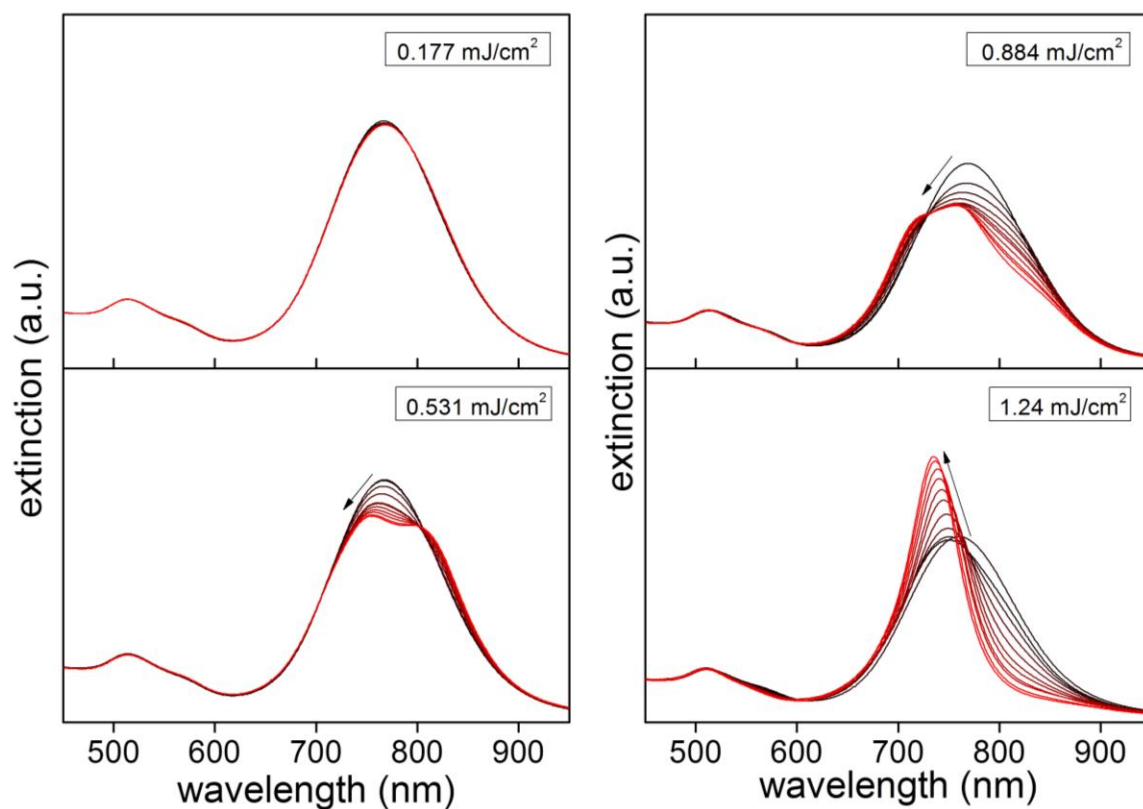
Figure A 4. **Photothermal stability of MUDA capped gold nanorods following laser treatment. Samples were irradiated at 1 min intervals for up to 10 min irradiation with a 120 fs pulsed laser (1 kHz) operating at 800 nm and with varying laser fluences as indicated. The nanoparticles were suspended in 1x TBE buffer containing <u>0.05 mM excess MUDA</u>.**
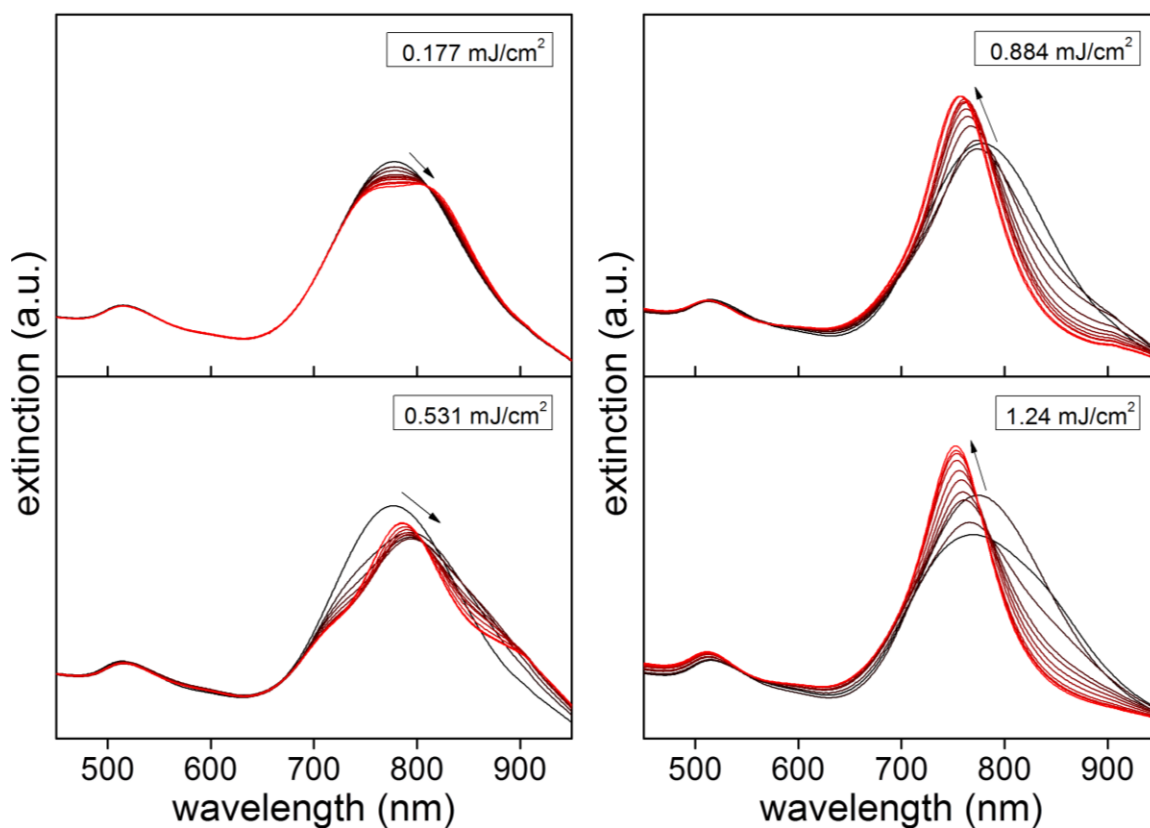
Figure A 5. **Photothermal stability of CTAB capped gold nanorods following laser treatment. Samples were irradiated at 1 min intervals for up to 10 min irradiation with a 120 fs pulsed laser (1 kHz) operating at 800 nm and with varying laser fluences as indicated. The nanoparticles were suspended in deionized water containing <u>1 mM excess CTAB</u>.**

Figure A 6. **Photothermal stability of MUDA capped gold nanorods following laser treatment. Samples were irradiated at 1 min intervals for up to 10 min irradiation with a 120 fs pulsed laser (1 kHz) operating at 800 nm and with varying laser fluences as indicated. The nanoparticles were suspended in 1x TBE buffer containing <u>1 mM excess MUDA</u>.**

Figure A 7. **Photothermal stability of CTAB capped gold nanorods following laser treatment. Samples were irradiated at 1 min intervals for up to 10 min with a 120 fs pulsed laser (1 kHz) operating at 800 nm and with varying laser fluences as indicated. The nanoparticles were suspended in deioinized water containing <u>5 mM excess CTAB</u>.**

Figure A 8. Photothermal stability of MUDA capped gold nanorods following laser treatment. Samples were irradiated at 1 min intervals for up to 10 min with a 120 fs pulsed laser (1 kHz) operating at 800 nm and with varying laser fluences as indicated. The nanoparticles were suspended in 1x TBE buffer containing 5 mM excess MUDA.
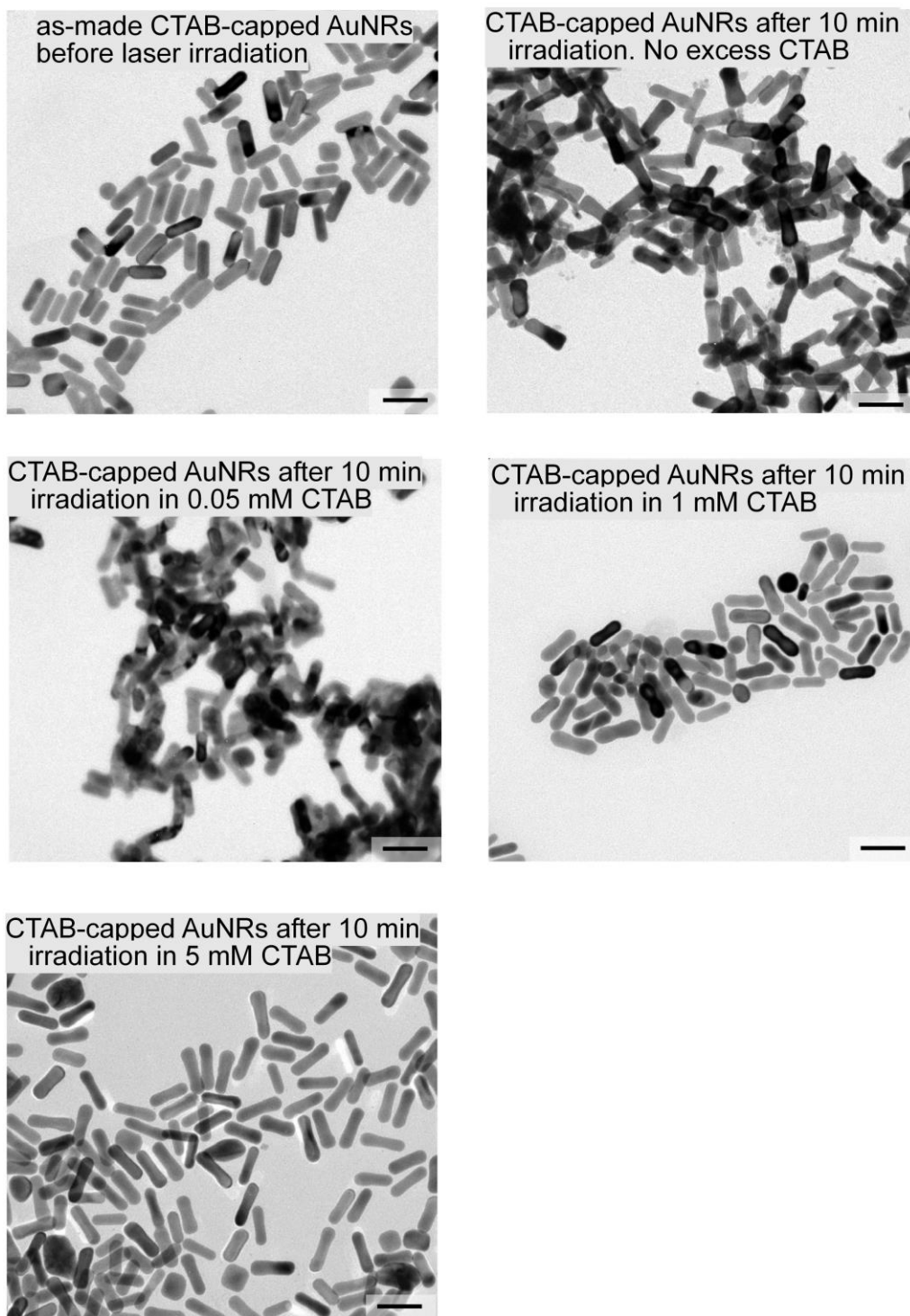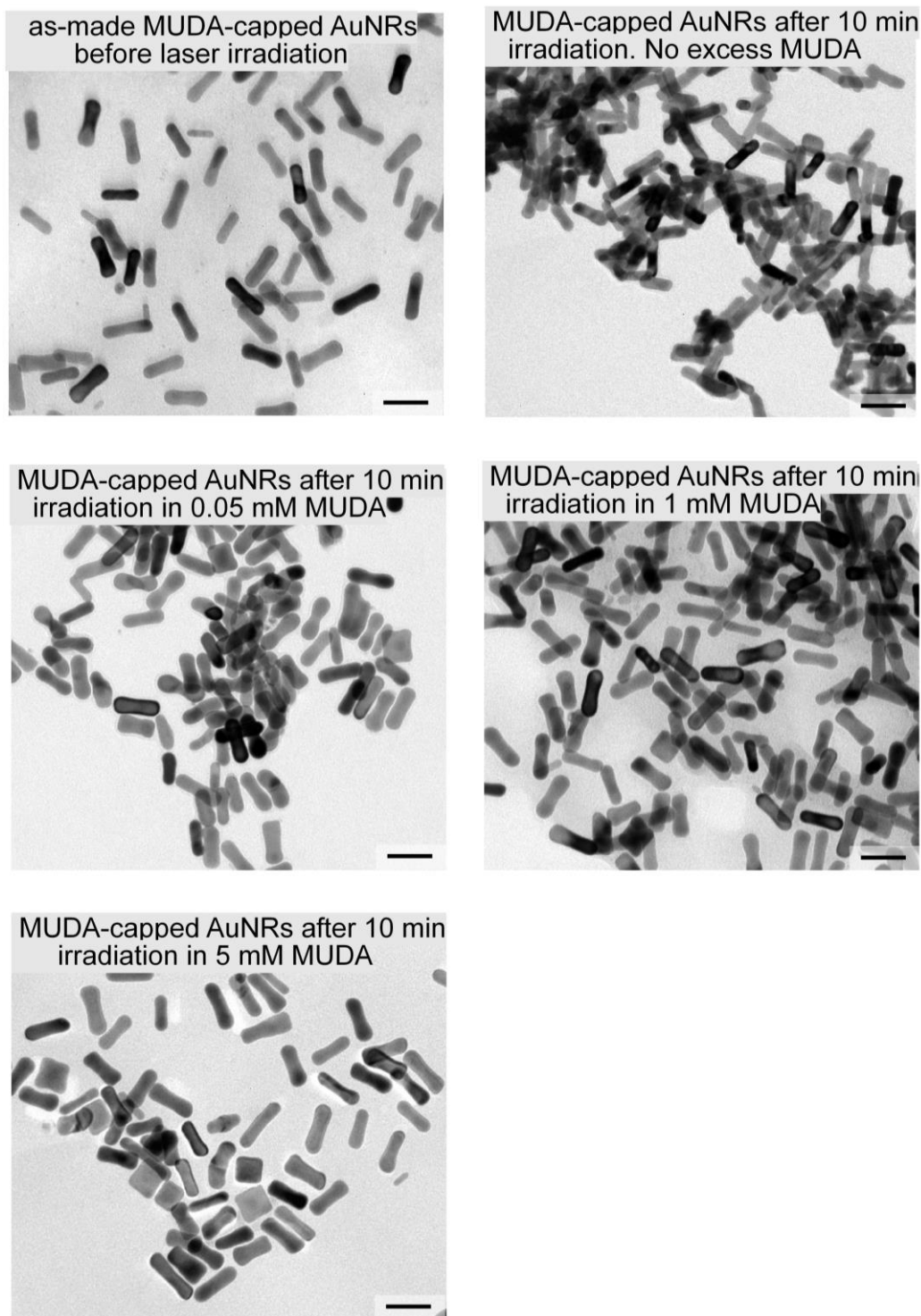
Figure A 9. **Transmission electron microscopy (TEM) of gold nanorods suspended in varying concentrations of CTAB before and after laser irradiation. Irradiation was performed at a fluence of 1.24 mJ/cm^2 for a total of 10 mins. The scale bars are 50 nm.**
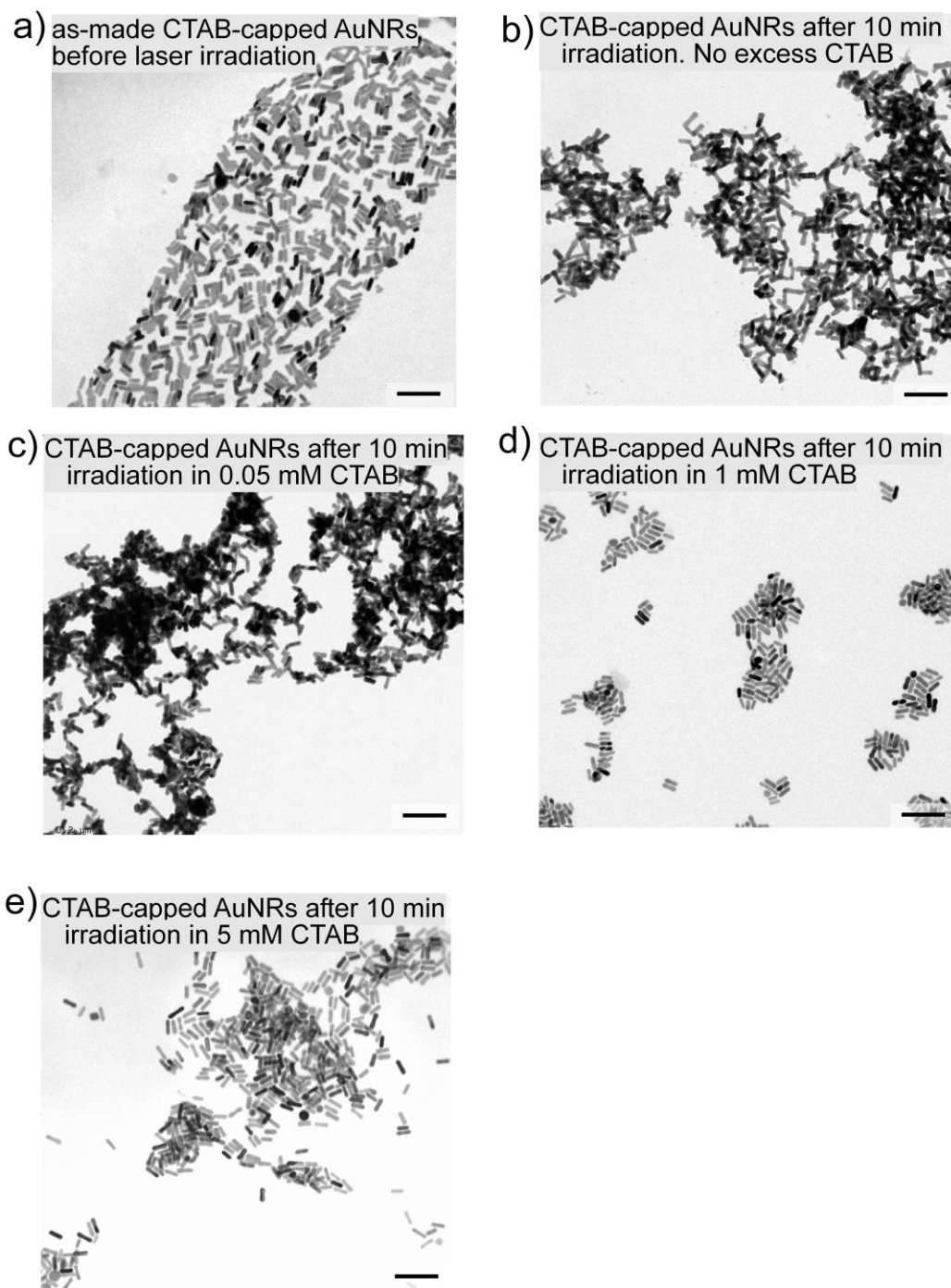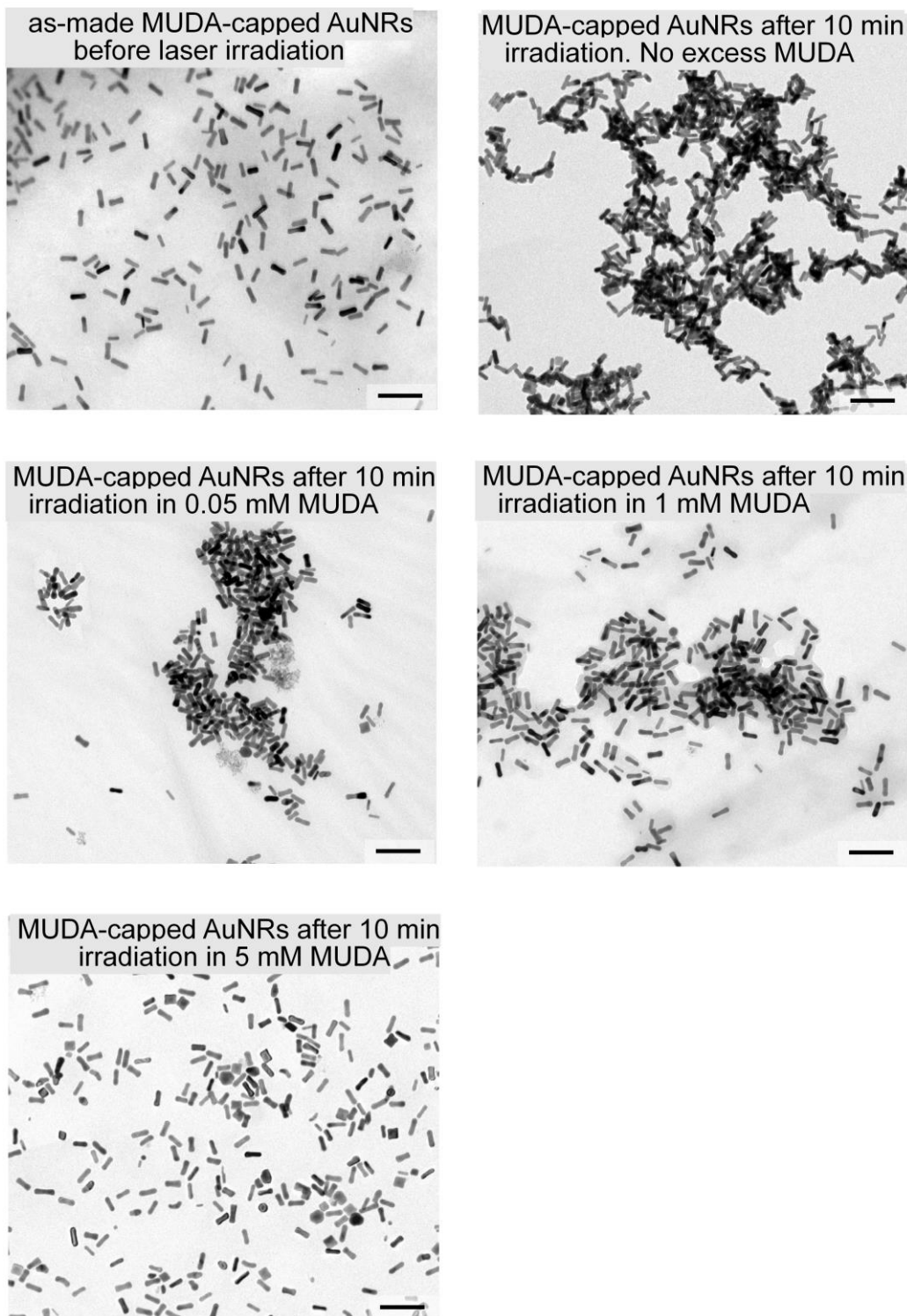
Figure A 10. More TEM images of gold nanorods suspended in varying concentrations of CTAB before and after laser irradiation. Irradiation was performed at a fluence of 1.24 mJ/cm^2 for a total of 10 mins. The scale bars are 140 nm.

Figure A 11. TEM images of gold nanorods suspended in varying concentrations of MUDA before and after laser irradiation. Irradiation was performed at a fluence of 1.24 mJ/cm^2 for a total of 10 mins. The scale bars are 50 nm.

as-made MUDA-capped AuNRs before laser irradiation

MUDA-capped AuNRs after 10 min irradiation. No excess MUDA

MUDA-capped AuNRs after 10 min irradiation in 0.05 mM MUDA

MUDA-capped AuNRs after 10 min irradiation in 1 mM MUDA

MUDA-capped AuNRs after 10 min irradiation in 5 mM MUDA

Figure A 12.   More TEM images of gold nanorods suspended in varying concentrations of MUDA before and after laser irradiation. Irradiation was performed at a fluence of 1.24 mJ/cm^2 for a total of 10 mins. The scale bars are 140 nm.

Appendix B

Calculation of the Molar and Number Concentration of Gold Nanorods

The concentration of gold determined by ICP-MS analysis of the ss-DNA coated gold nanorods was converted into the average number of gold nanorods per milliliter of solution using the calculated volume of a gold nanorod and the density of Au as detailed below:
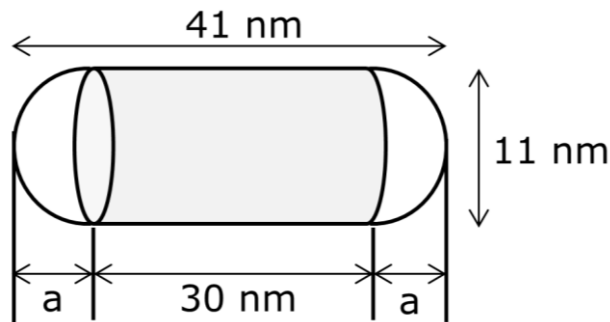
1) Determine the volume of a gold nanorod:

density of Au = 59 atoms/nm^3

density of Au = 19.3 g/cm^3 = 1.93 × 10^{-14} µg/nm^3

molecular weight of Au = 197 g/mol

Volume of a nanorod = (π/3) × (a) × ($3r^2 + a^2$) + πrh

where r is the radius of the nanorods, a is the radius of each semi-circle, and h is the length of the cylinder. These variables were determined from TEM measurements of >100 independent particles.

Volume of a nanorod = (3.14 / 3) × (5.5 nm) × (3 × 5.5^2 nm^2+ 5.5^2 nm^2) + 3.14 × 5.5 nm × 30 nm = **3546.1 nm^3**

2) Determine the number of gold atoms in nanorod:

Number of atoms of Au per nanorod = 3546 nm^3/nanorod × 59 atoms Au/nm^3 = **209220 atoms Au/nanorod**

Next, convert the number of atoms into moles by dividing with the Avogadro's number:

Moles of gold per nanorod = **$3.47 × 10^{-19}$ moles Au/Nanorod**

3) Determine the weight of Au in each nanorod:

molecular weight of Au = 197 g/mol

weight of each gold nanorod = $3.47 × 10^{-19}$ moles Au/Nanorod × 197 g/mol
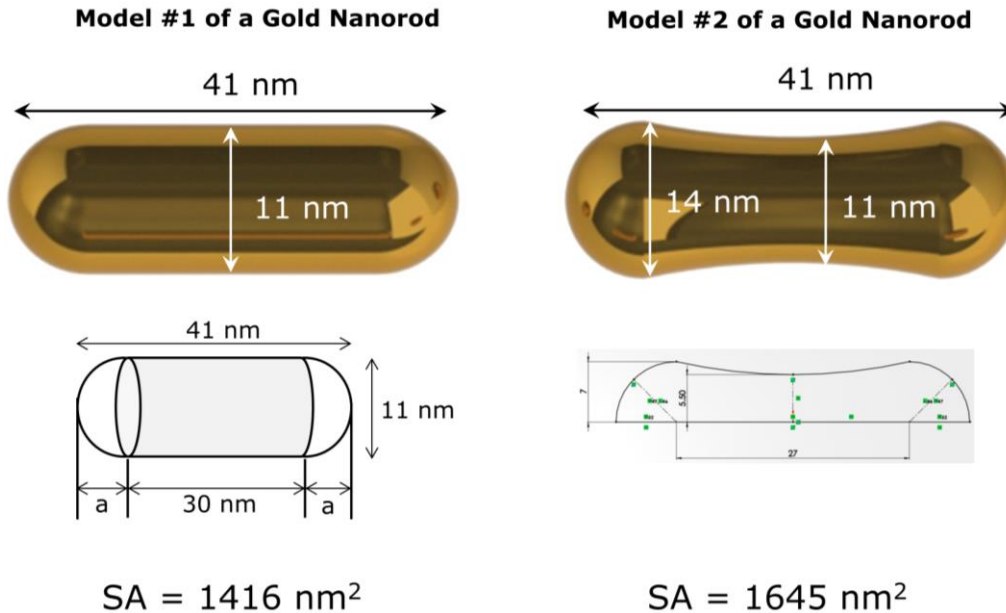
= **$6.84 × 10^{-11}$ µg Au/Nanorod**

4) The concentration of gold determined by ICP-MS analysis of the ss-DNA coated gold nanorods was **7.93 ppm** = **7.93 µg Au/ mL**

Therefore, the number of nanorods per mL of solution:

7.93 µg Au/ mL × 1/$6.84 × 10^{-11}$ µg Au/Nanorod = **$1.20 × 10^{11}$ gold nanorods/mL**

Appendix C

Determination of the Loading of DNA on Gold Nanorods

Model #1 of a Gold Nanorod

41 nm

11 nm

41 nm

11 nm

a   30 nm   a

SA = 1416 nm²

Model #2 of a Gold Nanorod

41 nm

14 nm   11 nm

SA = 1645 nm²

1) Assume that the nanorods are cylinders, with two semi-circles at each end for nanorod model #1:

Surface area of a nanorod = 2πrh + 2 π a^2 + 2 π a^2

where *a* is the length of one semi-circle; *h* is the width of the gold nanorod; and *r* is the radius of the nanorods (measured from TEM micrographs. See example in Appendix D).

Surface area of a nanorod = (2× 3.14 × 5.5 nm × 30 nm) + (2 × 3.14 × 5.5^2 nm) + (2 × 3.14 × 5.5^2 nm) = **1416.1 nm^2**

The surface area of nanorod model #2 above was derived from SolidWorks as stated in the Experimental Methods section in Chapter 4. The modeled surface area was ~**1645 nm^2**.

2) To determine the number of DNA strands on each nanorod, divide the molar concentration of DNA by molar concentration of gold nanorods.

(a) The concentration of DNA bound to gold nanorods was determined by detaching DNA from the nanorods, separating the detached DNA from the nanorods by centrifugation, and measuring fluorescence of the supernant in order to quantify the amount of released DNA (or the DNA that was bound to nanorods). Note that the DNA was labeled with a fluorescent dye (Quasar 670). Fluorescence values were then converted into concentrations of DNA from a calibration curve of fluorescence versus [DNA] initially added to PVP/SDS capped nanorods. The concentrations of non-specifically adsorbed DNA were subtracted from samples treated with DTT and heat (90°C) in order to remove any potential contribution from DNA bound through non-specific interactions when determining the amount of DNA bound to the gold nanorods through sulfur-gold bonds.

(b) Next, a plot of the number of the number of DNA strands per nanorod, versus the initial concentration of DNA added to the PVP/SDS capped nanorods. From this plot, determine the highest number of DNA strands loaded on the nanorods (or maximum DNA loading).

(c) The DNA footprint on the nanorods was calculated by dividing the total surface area of a nanorod by the maximum loading of ss-DNA molecules. The footprint per ss-DNA was 1.7 nm^2 for the highest DNA loading achieved as detailed in Chapter 4 of this thesis.
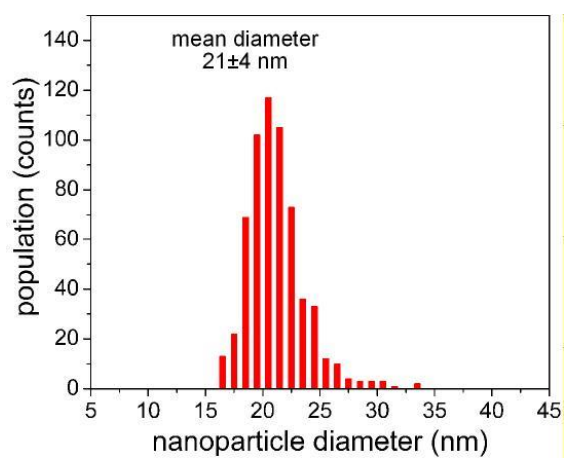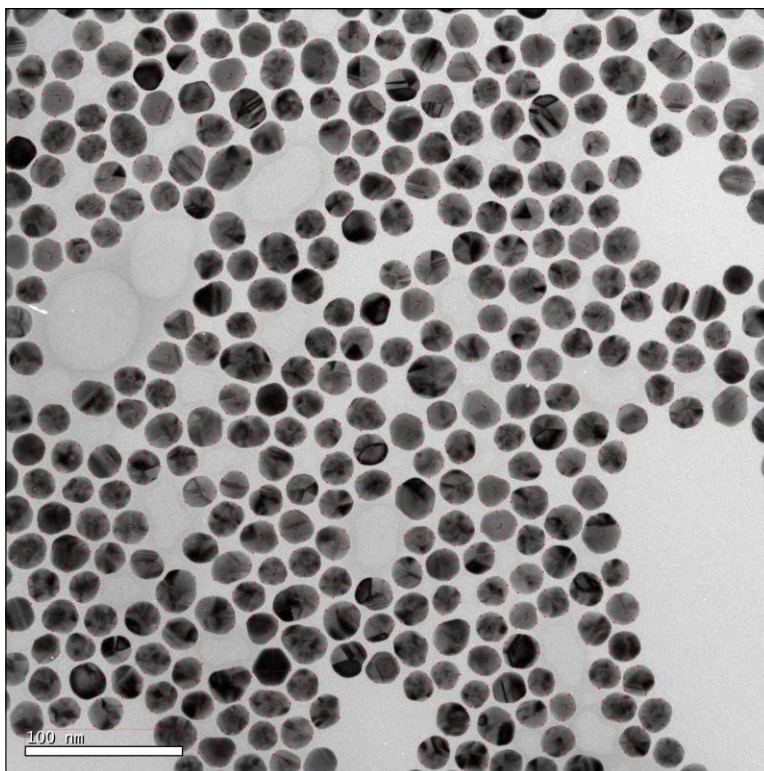
Appendix D

Size Analysis of Gold Nanorods and Nanoparticles
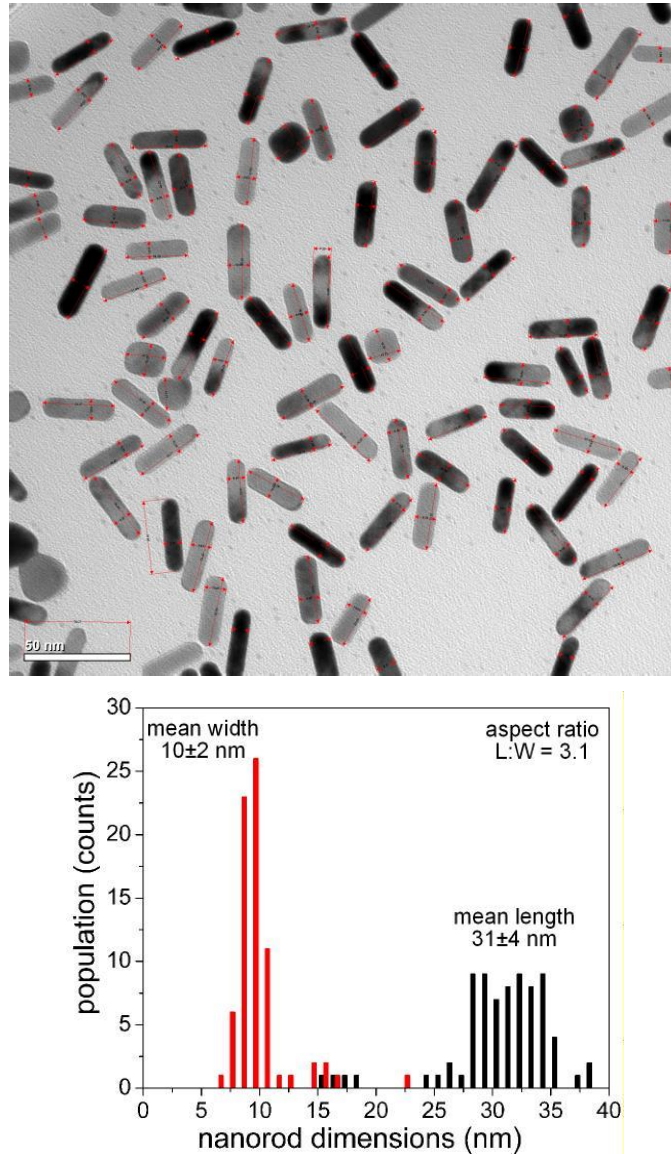
Figure D 1. Size analysis of gold nanorods measured from the TEM micrograph shown above. Greater than 100 particles were counted for this statistical analysis. These measurements were often performed with 2 or more independent assessments (i.e., 2 or more individuals made separate measurements to confirm each others results of the average particle dimensions).

Figure D 2. **Size analysis of spherical gold nanoparticles measured from the TEM micrograph shown above. Greater than 300 particles were counted for this statistical analysis. These measurements were often performed with 2 or more independent assessments (i.e., 2 or more individuals made separate measurements to confirm each others results of the average particle diameter).**